An Investigation of Ground-based GNSS Atmospheric Remote Sensing Techniques for Weather and Climate Monitoring in Nigeria

By

Olalekan Adekunle Isioye

A thesis submitted for examination in partial fulfillment of the requirements for the Degree of ***Doctor of Philosophy (Geoinformatics)***

Department of Geography, Geoinformatics and Meteorology
Faculty of Natural and Agricultural Sciences
University of Pretoria, South Africa

UNIVERSITEIT VAN PRETORIA
UNIVERSITY OF PRETORIA
YUNIBESITHI YA PRETORIA

February 2017

Declaration

I certify that the ideas, designs and experimental work, results, analysis and conclusions set out in this thesis are entirely my own effort, except where otherwise indicated and acknowledged. Additionally, Chapters 2 to 8 have been co-authored with my promoters and other colleagues, the conceptualization of all these chapters plus their scientific analysis and elucidations, article writings as well as the rebuttal during the peer-review processes were executed by me.

Finally, I certify that the entire work is original and has not been previously submitted for assessment in any other course or institution.

…… ……

Olalekan Adekunle Isioye **Date**

(Student No: u13390742)

Certification

I certify that I have read this thesis and that, in my opinion, it is fully adequate in scope and quality as a thesis for the degree of Doctor of Philosophy.

……..

[1, 2] Prof Ludwig Combrinck (Principal Supervisor)

[2]Hartebeesthoek Radio Astronomy Observatory (HartRAO),
P. O. Box 443, Krugersdorp 1740, South Africa

[1] Department of Geography, Geoinformatics and Meteorology,
University of Pretoria, Pretoria 0002, South Africa

I certify that I have read this thesis and that, in my opinion, it is fully adequate in scope and quality as a thesis for the degree of Doctor of Philosophy.

……..

[1, 3] Dr Joel O. Botai (Co- Supervisor)

[1] Department of Geography, Geoinformatics and Meteorology,
University of Pretoria, Pretoria 0002, South Africa

[3]South African Weather Service,
442 Rigel Avenue South, Erasmusrand,
Pretoria 0001, South Africa

Acknowledgement

I would like to express my profound gratitude to my supervisors, Prof. Ludwig Combrinck and Dr. Joel Ondego Botai, for their guidance and support throughout my doctoral studies at the University of Pretoria. Prof Combrinck is highly appreciated for his effort at making facilities at the Hartebeesthoek Radio Astronomy Observatory (HartRAO) accessible for my research.

I would like to thank the management of Ahmadu Bello University, Nigeria for the award of study fellowship which enabled me to take up of a full time PhD programme at the University of Pretoria in South Africa. Special appreciation goes the Tertiary Education Trust Fund of Nigeria and the Surveyors Registration Council of Nigeria (SURCON) for the financial support the provided.

Appreciation is also extended to Mr. Cilence Munghemezulu, Dr. Abiodun Adeola, and Mr. Adedayo Adeniyi all of the Department of Geography, Geoinformatics and Meteorology, University of Pretoria and other colleagues in the Space geodesy Group at HartRAO for creating an enjoyable working environment. I acknowledge the support of Mr. Moses Mefe, Mr. Ebenezer Akomolafe, Mr. Ifechukwu Nzelibe and all other colleagues at the Department of Geomatics in Ahmadu Bello University, Nigeria.

Finally, I am grateful to my family for their support and patience during my stay at the University of Pretoria in South Africa. Last, but not least, I thank Surveyor Winston Ayeni; the immediate past registrar of SURCON, Prof. Kabir Bala; the Dean of School of Post Graduate Studies, Ahmadu Bello University, Dr. Abdulmalik Wahab, and Prof. Ahmed Ibrahim Doko. I could not have done it without you all.

Abstract of the Thesis

An Investigation of Ground-based GNSS Atmospheric Remote Sensing Techniques for Weather and Climate Monitoring in Nigeria

Author: Olalekan Adekunle ISIOYE

Supervisors: [2,1]Ludwig COMBRINCK, [3,1]Joel BOTAI

Affiliations: [1] Department of Geography, Geoinformatics and Meteorology, University of Pretoria, Pretoria 0002, South Africa

[2]Hartebeesthoek Radio Astronomy Observatory (HartRAO), P. O. Box 443, Krugersdorp 1740, South Africa, ludwig@hartrao.ac.za

[3]South African Weather Service, 442 Rigel Avenue South, Erasmusrand, Pretoria 0001, South Africa, joel.botai@weathersa.co.za

Degree: Doctor of Philosophy (Geoinformatics)

ABSTRACT

Radio signals from Global Navigation Satellite Systems (GNSS) satellites suffer delay as they propagate through the atmosphere (neutral and non-neutral) and this delay is partially driven by the water vapour content in the atmosphere. The delay component due to the non-neutral atmosphere (ionosphere) is removed through the use of dual frequency GNSS receivers. The main tropospheric parameter is the zenith tropospheric (or total) delay (ZTD), which is a widely accepted parameter with which to express the total delay in the signal from all satellites due to the neutral atmosphere. The ZTD is a measure of the integrated tropospheric condition over a GNSS receiver station. Accordingly, the integrated water vapour or precipitable water vapour (PWV) can be obtained from a portion of the ZTD, if the atmospheric pressure and temperature at the station are known through a concept often referred to as GNSS meteorology. A number of GNSS receivers have been deployed for mapping and geodetic services in Nigeria under the African reference frame initiative, but unfortunately most of these receivers do not have co-located meteorological sensors for pressure and temperature measurements. The prospect of incorporating GNSS meteorology into weather monitoring and climate analysis in Nigeria was investigated and is reported in this thesis. During the first task of this research, the technical basis for ground-based GNSS meteorology was reviewed and the potentials and challenges

of the approach to meteorological activities in Africa (including Nigeria) were identified. Thereafter an in-depth analysis of the spatial and temporal variability of ZTD over Nigeria for the period of 2010-2014 was conducted; results revealed weak spatial dependence among the stations. Tidal oscillations (of the diurnal and semi-diurnal components) were observed at the GNSS stations of which the diurnal ZTD cycles exhibited significant seasonal dependence, affirming the prospective relevance of ground-based GNSS data to atmospheric studies. Also in this research, the accuracy and suitability of using reanalysis datasets (ERA-Interim and NCEP/NCAR) and a GPT2 neutral model in retrieving PWV from GNSS observations over Nigeria were investigated; results showed that PWV can be retrieved to within a precision of about 1 mm, provided GNSS-derived ZTD is of high precision. A fundamental issue for GNSS meteorology in the West African region was yet again addressed in this research; this is the development of a weighted tropospheric mean temperature model for use in current and future GNSS meteorology activities in the region. A multi-technique comparison of PWV estimates showed good agreement between GNSS estimates and other techniques (i.e. the atmospheric infrared sounder, and ERA-Interim reanalysis). This result is suggestive of the potential of assimilating GNSS atmospheric products into reanalysis and climate models. Diurnal and seasonal variability of GNSS PWV estimates exhibits strong correlation with weather events that influence the region (i.e. solar activity and rainfall events); this further demonstrated the immense contribution of the approach to efficient weather forecasting and climate monitoring for Nigeria.

Keywords: *GNSS Meteorology, Zenith Tropospheric Delay (ZTD), Precipitable Water Vapour (PWV), Nigerian GNSS Network (NIGNET), Nigerian Weighted Mean Temperature Equation (NWMTE), Total Electron Content (TEC), Reanalysis model, Blind tropospheric model, Atmopsheric Infrared Sounder (AIRS), Regional climate model (RCM)*

Author's literature and conference contributions

- **Refereed Journals**

1. **Isioye, O.A.,** Combrinck, L, Botai, J.O. & Munghemezulu, C. 2015. The Potential of observing African Weather with GNSS Remote Sensing, *Advances in Meteorology*, Volume 2015, Article ID 723071, http://dx.doi.org/~10/1155/2015/723071.

2. **Isioye, O.A.,** Combrinck, L. & Botai, J.O. 2015. Performance Evaluation of Blind Tropospheric Delay Correction Models over Africa, *South African Journal of Geomatics*, Vol. 4, No. 4, November 2015, http://dx.doi.org/10.4314/~sajg.v4i4.8.

3. **Isioye, O. A.,** Combrinck, L. & Botai, O. J. 2016. Modeling Weighted Mean Temperature in West African Region: Implication for GNSS Meteorology. *Meteorological Applications*, volume 23, issue 4, 614-632, http://dx.doi.org/~10.1002/met.1584 .

4. **Isioye O. A.,** Combrinck L. & Botai, J.O. 2016. Evaluation of Spatial and Temporal Characteristics of GNSS-Derived ZTD Estimates in Nigeria. *Theoretical and Applied Climatology* (**Revised**).

5. **Isioye O. A.,** Combrinck L. & Botai J.O. 2016. Retrieval and Analysis of Precipitable Water Vapour based on GNSS, AIRS, and Reanalysis Models over Nigeria. *International Journal of Remote Sensing* (**Revised**).

6. **Isioye O. A.,** Combrinck L., Botai, J.O., Luhunga, P. & Moses, M. 2016. Assessing the Meteorological Impact of Variations in Atmospheric Water Vapour Content over Nigeria from GNSS Measurements. *Advances in Meteorology* (**Revised**).

- **Refereed Conference Proceedings**

1. **Isioye O. A.** 2016. Evaluation of Surface Variables from Global Reanalysis Models and their application in Precipitable Water Vapour Retrieval from GNSS Observations over Nigeria. Proceedings of the 29th International Technical Meeting of the satellite division of the Institute of Navigation (ION GNSS + 2016), Portland, Oregon, USA, pp.1617-1641, September 12-16, 2016. (**Student Award Paper**, https://www.ion.org/publications/ abstract.cfm?~jp=p&articleID=14723.

- **Conference Presentations**

1. **Isioye, O.A.,** Combrinck, L. & Botai, J. O. 2014. *Modelling of Atmospheric Parameters over Nigeria based on GNSS Data*. A Presentation at the United Nations/Abdus Salam International Centre for Theoretical Physics Workshop on the use of Global Navigation Satellite Systems for Scientific Applications, Trieste, Italy, 1-5 December 2014. Available at http://www.unoosa.org/pdf/~sap/2014/trieste-gnss/23.pdf .

2. **Isioye O. A.,** Combrinck L. & Botai, J.O. 2015. *Performance Evaluation of the GPT2w and UNB3M Tropospheric Delay Correction Models over Africa*. A Presentation at the United Nations/Russian Federation Workshop on the Application of Global Navigation Satellite Systems, 18–22 May 2015, Krasnoyarsk, Russia Federation. Available at: *http://www.unoosa.org/oosa/en/SAP/act2015/russia-gnss/2015workshop-gnss.html* .

3. **Isioye O. A.,** Moses, M., Combrinck L. & Botai, J.O. 2016. *Characterisation of Atmospheric Responses during Solar Events from GNSS Measurements in Low Equatorial African Region*. A Presentation (Poster) at the 2016 Beacon Satellite Symposium at the Abdus Salam International Centre for Theoretical Physics, Trieste, Italy, 27 June- 1July 2016.

Table of Contents

Title Page ..... **i**

Declaration ..... **ii**

Certification ..... **iii**

Acknowledgement ..... **iv**

Abstract of the Thesis ..... **v**

Author's Literature and conference Contributions ..... **vii**

Table of Contents ..... **ix**

List of Figures ..... **xv**

List of Tables ..... **xxi**

List of Acronyms ..... **xxiv**

Chapter 1: Introduction **1**

1.1 Climate System and Water Vapour 1

1.2 Water Vapour Observing Systems 6

1.3 GNSS and its Scientific Applications 8

1.4 Research Objectives 12

1.5 Research Methodology 14

1.6 Scope and Limitation of Research 16

1.7 Organisation of Thesis 16

Chapter 2 : The Potential of Observing African Weather with GNSS Remote Sensing **18**

2.1 Introduction and Background 19

2.2 Operational Requirements and Standards for GNSS Meteorology 22

2.3 Status of the African GNSS Network 24

2.4 Preliminary Results on Monitoring of GNSS ZTD Variability on the African GNSS Network 28

2.4.1 GNSS Data Processing and Tropospheric Product Descriptions ……....28

2.4.2 GNSS ZTD Variability on the African GNSS Network ……..…33

2.5 Steps to Improve GNSS Meteorology within the African GNSS Network. ...37

2.5.1 Densification of GNSS Networks through Collaborative Initiatives..... ...37

2.5.2 Meteorological Parameter Modelling from Global/Regional Weather Models. 38

2.5.3 Filling the Gaps with GNSS Radio Occultation (RO)..... ...39

2.6 Concluding Remarks …….....43

Acknowledgment ……...……...…44

Chapter 3: Evaluation of Spatial and Temporal Characteristics of GNSS-Derived ZTD Estimates in Nigeria **45**

3.1 Introduction and Background……..….. 46

3.2 Material and Methods …….....…...48

3.2.1 GNSS Data Processing …….....…48

3.2.2 Spatial Auto-Correlation Analysis …….....……...49

3.2.3 Temporal Characteristics (Diurnal and Intra-seasonal Trends)……..…..51

3.2.3.1 The Mann Kendall Test …….....51

3.2.3.2 Spectral Analysis and Testing for White Noise …….....52

3.2.3.3 Test for Stationarity …….....53

3.3 Results and Discussions …….....…..….55

3.3.1 Spatial Characteristics …….....…..….55

3.3.2 Temporal Characteristics (Diurnal and Intra-seasonal Trends)……..….60

3.4 Concluding Remarks …….....75

Acknowledgment ……...……..77

Chapter 4: Performance Evaluation of Blind Tropospheric Delay Correction Models over Africa..... **78**

4.1 Introduction and Background …….....79

4.2 Description of Tropospheric Correction Models Adopted in This Study…...82

4.2.1 Saastamoinen Model ……...82

4.2.2 UNB3m Hydrostatic Delay Model……...83

4.2.3 Global Pressure Temperature wet (GPT2w) Model……....86

4.3 Assessment of the Accuracies of the UNB3m and GPT2w Models…….…...88

4.4 Concluding Remarks ……...97

Acknowledgment ……..……..... 98

Chapter 5: Evaluation of Surface Variables from Global Reanalysis Models and their Application in Precipitable Water Vapour Retrieval from GNSS Observations over Nigeria.....**99**

5.1 Introduction and Background……..….....100

5.2 Data and Methods……..….102

5.2.1 Reanalysis Datasets……...….102

5.2.2 Observational Data…….103

5.2.3 Validation of Reanalysis Dataset using AWOS Over Nigeria……..…….104

5.2.4 Application of Reanalysis Dataset in GNSS Atmospheric Precipitable Water Vapour Estimations……....107

5.3 Results and Discussions…….112

5.3.1 Results on the Validation of the ERAI and NCEP/NCAR Reanalysis Models…….…...112

5.3.2 Analysis of Derived PWV from GNSS and ECMWF/NCEP/GPT2 Dataset.....118

5.3.2.1 Comparison of ZHD from AWOS, ECMWF, NCEP, and GPT2 Dataset.....119

5.3.2.2 Comparison of T_m Estimated from T_s of AWOS, ECMWF, NCEP, and GPT2 Dataset.....119

5.3.2.3 Comparison of PWVs from AWOS, ECMWF, NCEP, and GPT2 Dataset...122

5.4 Concluding Remarks……..128

Acknowledgment ……..……...……130

Chapter 6: Modelling Weighted Mean Temperature in the West African Region: Implication for GNSS Meteorology.....131

6.1 Introduction and Background ……...….132

6.2 Materials and Methods ……..….136

6.2.1 Data and Location ……....136

6.2.1.1 Radiosonde Data ……...……136

6.2.1.2 NWP Data……...……138

6.2.2 Estimation of Tropopause Height from the NCEP/NCAR Reanalysis Model and Sounding Data …….....139

6.2.3 Determination of T_m from NCEP/NCAR Reanalysis Model and Sounding Data (Integral Method) …….....140

6.2.3.1 Harmonic Model from Global NCEP/NCAR Reanalysis Data……....….141

6.2.3.2 UNB3m Model…….....142

6.2.3.3 GPT2w Model …….....….142

6.2.4 Estimating Precipitable Water Vapour from GNSS Observations……....143

6.3 Results, Model Validation and Discussions…….....144

6.3.1 Results of the Models …….....….144

6.3.2 Validation of Models ……..…148

6.3.3 Spatiotemporal Variation of T_m Models …….....…153

6.4 Implication of T_m Modelling for GNSS Meteorology……....156

6.4.1 Precision of PWV from T_m Models…….…….....156

6.4.2 Analysis of Derived PWV from GNSS and the Various T_m Models…….157

6.5 Concluding Remarks …….....…161

Acknowledgment ……...……... 162

Chapter 7: Retrieval and Analysis of Precipitable Water Vapour based on GNSS, AIRS, and Reanalysis Models over Nigeria **163**

7.1 Introduction and Background ……..……..164

7.2 Overview of Data sets and PWV Retrieval Procedures ….....….167

7.2.1 GNSS Observations ….....….167

7.2.2 Atmospheric Infrared Sounder .....….....….....….171

7.2.3 ERA-Interim Reanalysis.....….....173

7.3 Methodology ….....….....174

7.4 Results and Discussions ….....…177

7.4.1 Diurnal Relations of GNSS PWV with other Retrievals (AIRS and ERAI) ….....…….....177

7.4.2 Monthly Relations of GNSS PWV with other Retrievals (AIRS and ERAI) ….....…….....182

7.5 Concluding Remarks..... ….....…187

Acknowledgment ……..……..188

Chapter 8 : Assessing the Meteorological Impact of Variations in Atmospheric Water Vapour Content over Nigeria from GNSS Measurements **189**

8.1 Introduction and Background ……... ……..……190

8.2 Data and Methodology …….....192

8.3 Variability of GNSS PWV over Nigeria ……..….196

8.4 Investigation of GNSS PWV and Rainfall Events over Nigeria.....202

8.5 Investigation of GNSS PWV and Solar Events over Nigeria.....208

8.6 Concluding Remarks …….....……217

Acknowledgment ……..……..221

Chapter 9 : Conclusion, Outlook and Recommendations..... **222**

9.1 Summary.....……..…….....222

9.2 Conclusion.....……...……..224

9.3 Outlook and Recommendations……...…….228

List of References.....**230**

List of Figures

Figure1.1	Vertical structure of the atmosphere	**2**
Figure 1.2	The climatic hydrological cycle at global scale	**3**
Figure 1.3	Flow chart of the research framework	**15**
Figure 2.1	Summary of requirements for GNSS Meteorology from IGS, GRUAN and EUREF	**24**
Figure 2.2	Map depicting the position of IGS and AFREF Stations in Africa	**25**
Figure 2.3	Daily variation of ZTD estimates over Africa in 2013 (DOY 1-365)	**33**
Figure 2.4	Plot of GNSS ZTD against station elevation	**34**
Figure 2.5	Periodogram graph of ZTD time series	**35**
Figure 2.6	Average two Hourly ZTD plots for 2010-2014	**36**
Figure 2.7	Distribution of IGS, AFREF stations and other GNSS stations/networks in Africa	**38**
Figure 3.1	Map depicting the location of NIGNET GNSS CORS in Nigeria	**47**
Figure 3.2	Chart showing weights matrix for GNSS stations	**56**
Figure 3.3	Area chart of mean, 2-hourly ZTD estimates over Nigeria from 2010–2014	**62**
Figure 3.4	Area chart of mean, monthly ZTD estimates over Nigeria from 2010–2014	**63**
Figure 3.5a	Periodograms illustrating significant oscillations in the diurnal ZTD anomaly at the stations over the period January 2010–June 2014	**68**
Figure 3.5b	Spectral plots showing significant oscillations of the diurnal ZTD anomaly at the stations over the period January 2010–June 2014	**69**
Figure 3.6a	Periodograms illustrating significant oscillations of the Intra-seasonal ZTD anomaly at the stations over the period January 2010–June 2014	**70**
Figure 3.6b	Spectral plots illustrating significant oscillations of the Intra-seasonal ZTD anomaly at the stations over the period January 2010–June 2014	**71**
Figure 4.1	Map depicting the location of IGS stations in Africa	**82**
Figure 4.2	Time series plot of the UnB3m, GPT2w, and IGS estimation of ZTD for 2013	**91**
Figure 4.3a	Time series plot of the difference of UnB3m and GPT2w models to IGS estimation of ZTD for 2013	**92**

Figure 4.3b	Plot of the mean absolute difference (errors) for the different stations	**93**
Figure 4.4	Plot of mean ZTD estimates against station elevation	**94**
Figure 4.5	Plot of RMSE versus station elevation	**94**
Figure 4.6	Plot of RMSE versus station absolute latitude	**95**
Figure 4.7	Plot of MEF versus station absolute latitude	**95**
Figure 4.8	Estimated ZTD, ZHD, and ZWD from the Saastamoinen formula, IGS product, GPT2w model, and UNB3m model at HRAO for doy of Year 1-31, 2013. The Saastamoinen formula using meteorological parameters measured with a MET 4A unit for ZHD and ZWD estimation, the ZHD from the IGS product was also retrieved utilizing the measured parameter from the Met 4A unit	**96**
Figure 4.9	Estimated ZTD, ZHD, and ZWD from the Saastamoinen formula, IGS product, GPT2w model, and UNB3m model of HRAO for doy of Year 1-31, 2013. The Saastamoinen formula using standard meteorological parameters for ZHD and ZWD estimation, the ZHD from the IGS product was also retrieved utilizing standard met parameters	**97**
Figure 5.1	Location of AWOS and NIGNET GNSS sites in Nigeria	**108**
Figure 5.2	Performance of the ERAI and NCEP/NCAR for temperature estimation against the AWOS using deterministic metrics	**114**
Figure 5.3	Performance of the ERAI and NCEP/NCAR for mean sea level pressure estimation against the AWOS using deterministic metrics	**114**
Figure 5.4	Performance of the ERAI and NCEP/NCAR for relative humidity estimation against the AWOS using deterministic metrics	**115**
Figure 5.5	Performance of the ERAI and NCEP/NCAR for temperature estimation against the AWOS using probabilistic metrics	**116**
Figure 5.6	Performance of the ERAI and NCEP/NCAR for mean sea level pressure estimation against the AWOS using probabilistic metrics	**116**
Figure 5.7	Performance of the ERAI and NCEP/NCAR for relative humidity estimation against the AWOS using probabilistic metrics	**117**
Figure 5.8	Scatter plots of correlation between ZHD estimated from AWOS datasets and ERAI, NCEP/NCAR, and GPT2 models at five GNSS stations. Each station is shown at the top of each panel. The equation's relation to the ZHD from AWOS and the meteorological models are in the right corner, and adjusted r-squared and RMSE are in the left corner of each panel	**120**

Figure 5.9 Scatter plots of correlation between T_m estimated from AWOS datasets and ERAI, NCEP/NCAR, and GPT2 models at five GNSS stations. Each station is shown at the top of each panel. The equation's relation to the T_m from AWOS and the meteorological models is in the right corner, and adjusted r-squared and RMSE are in the left corner of each panel **121**

Figure 5.10 (a-e) Time series of PWV estimated from GNSS ZTD and different meteorological models (AWOS, ERAI, NCEP/NCAR, and GPT2) at stations 'abuz', 'clbr', 'futy', 'ulag', and 'unec', respectively **123**

Figure 5.11 (a-e) Difference plot for the different models (ERAI, NCEP/NCAR, and GPT2) using AWOS as reference at stations 'abuz', 'clbr', 'futy', 'ulag', and 'unec', respectively **124**

Figure 5.12 Bar chart of the performance of PWV_{ERAI}, PWV_{NCEP}, and PWV_{GPT2} against PWV_{AWOS} using deterministic metrics **125**

Figure 5.13 Line plot of the performance of PWV_{ERAI}, PWV_{NCEP}, and PWV_{GPT2} against PWV_{AWOS} using probabilistic metrics **126**

Figure 5.14 Scatter plots of correlation between PWV estimated from AWOS datasets and ERAI, NCEP/NCAR, and GPT2 models at five GNSS stations. Each station is shown at the top of each panel. The equation relation of the ZHD from AWOS and the meteorological models is in the right corner, and the adjusted r-squared and RMSE are in the left corner of each panel **127**

Figure 6.1 Map depicting the positions of the radiosonde stations in the West African region **138**

Figure 6.2 Map depicting the NCEP/NCAR reanalysis grid nodes over Nigeria **139**

Figure 6.3 Location of GNSS sites in Nigeria. (a) All of the stations in the new Nigerian GNSS Network(NIGNET) under management of the office of the Surveyor General of Nigeria(OSGOF); (b) the GNSS stations and matching automatic weather observing sites(AWOS) sites at which PWV were estimated for the present study **143**

Figure 6.4a Average tropopause height at the 36 NCEP/NCAR grid nodes over Nigeria for 2010–2012 **145**

Figure 6.4b Average tropopause height at the 24 sounding stations over the West African region for 2009–2013 **145**

Figure 6.5 Regression diagram of weighted mean temperature (T_m) with surface temperature (T_s) from (a) 2010 (b) 2011 (c) 2012 and (d) 2010–2012 in **146**

Nigeria based on NCEP/NCAR reanalysis data

Figure 6.6 Regression diagram of weighted mean temperature (T_m) with surface temperature (T_s) from (a) 2009 (b) 2010 (c) 2011 (d) 2012 (e) 2013 and (f) 2009–2013 based on radiosonde (sounding) data over the West African sub-region **147**

Figure 6.7 Regression diagram of weighted mean temperature (T_m) with surface temperature (T_s) based on the combination of NCEP/NCAR reanalysis and radiosonde (sounding) data **148**

Figure 6.8 Plots of the different models at position of NIGNET GNSS Stations **150**

Figure 6.9 Seasonal and annual variability of T_m at locations of GNSS stations in Nigeria **154**

Figure 6.10 A plot of the Range (maximum minus minimum) values of T_m estimates against latitudes of GNSS stations in Nigeria **155**

Figure 6.11 Time series of the differences in estimated PWV using the integral model and the other models (NWMTE-I, NWMTE-II, NWMTE-III, Bevis, UNB3m, GPT2w, and GWMT-IV) at five GNSS stations (ABUZ, CLBR, FUTY, ULAG, UNEC) located in the Nigerian territory **158**

Figure 6.12 Performance of estimated PWV using T_m model based integration formula against the other models (NWMTE-I, NWMTE-II, NWMTE-III, Bevis, UNB3m, GPT2w, and GWMT-IV) at (a) 'ABUZ' , (b) 'CLBR', (c) 'FUTY', (d), 'ULAG' and (e) 'UNEC' stations **160**

Figure 7.1 Location of GNSS stations under the NIIGNET and weather stations in Nigeria; the GNSS stations highlighted with red triangular symbol were adopted for the current study based on their proximity to the weather stations **169**

Figure 7.2 Images representing the agreement plots (or Bland and Altman plot) between GNSS PWV and (a) AIRS (**A**scending) (b) AIRS (**D**escending) and (c) ERA (**I**nterim) at the respective stations **178**

Figure 7.3 Images representing the histogram of the differences between GNSS PWV and (a) AIRS (Ascending) (b) AIRS (Descending) and (c) ERA (Interim) at the respective stations **179**

Figure 7.4 Chart depicting the reliability of the different PWV measuring techniques as determined by the RI. The average RI value for each pair of techniques across all five stations is shown, together with the percentage **182**

of divergence of each pair; lower percentages are indicative of better agreement between pairs

Figure 7.5 Plots of the monthly averages of PWV estimates at five GNSS station over Nigeria in 2013 and 2014. The GNSS and AIRS-Ascending, GNSS and AIRS-Descending, GNSS and ERAI relations at the respective stations are accordingly arranged in columns 1-3 **183**

Figure 7.6 Plots of statistical bias (mm) across the seasonal for the relation between GNSS and AIRS-Ascending (a-d), GNSS and AIRS-Descending (e-h) and GNSS and ERAI (i-l) **185**

Figure 7.7 Plots of NRMSE (%) statistics across the seasons for the relation between GNSS and AIRS-Ascending (a-d), GNSS and AIRS-Descending (e-h) and GNSS and ERAI (i-l) **185**

Figure 7.8 Plots of CV (%) statistics across the seasons for the relation between GNSS and AIRS-Ascending (a-d), GNSS and AIRS-Descending (e-h) and GNSS and ERAI (i-l) **186**

Figure 7.9 Plots of MEF across the seasons for the relation between GNSS and AIRS-Ascending (a-d), GNSS and AIRS-Descending (e-h) and GNSS and ERAI (i-l) **187**

Figure 8.1 Location of GNSS sites in Nigeria (a) depicts all the stations in the new NIGNET under the management of the OSGOF (b) shows the seven chosen GNSS stations and matching AWOS sites at which PWV was estimated for this study **193**

Figure 8.2 Monthly mean GNSS PWV (mm) for seven stations in different climatic regions of Nigeria from 2103 to 2014 **197**

Figure 8.3 Seasonal mean GNSS PWV (mm) for MAM, JJA, SON, and DJF from 2013 to 2014 **198**

Figure 8.4 A scatter plot of the average PWV values at the different GNSS stations against the corresponding latitude of the GNSS station **199**

Figure 8.5 A scatter plot of the average PWV values at the different GNSS stations against the corresponding height of the GNSS station **200**

Figure 8.6a Monthly distribution of PWV (in blue) and rainfall amount (in green) at four GNSS stations (ABUZ, BKFP, CLBR, and ULAG) in Nigeria **204**

Figure 8.6b Distribution of PWV and rainfall in August 2013 at station ABUZ. The red circles indicate peaks in PWV estimates attributed to rainfall and cyan circles are tagged as depressions; (a) shows the distribution PWV alongside a 12-hourly record of rainfall, (b) is an exaggerated plot of the 14 August (DOY226) rainfall storm and (c) is an exaggerated plot of the 17 August (DOY 229) rainfall storm **204**

Figure 8.7 Monthly distribution of PWV (in blue) and relative humidity (in green) at four GNSS stations (ABUZ, BKFP, CLBR, and ULAG) in Nigeria **205**

Figure 8.8 Monthly distribution of PWV (in blue) and daylight cloud amount (in green) at four GNSS stations (ABUZ, BKFP, CLBR, and ULAG) in Nigeria **205**

Figure 8.9 Monthly distribution of PWV (in blue) and wind speed (in green) at four GNSS stations (ABUZ, BKFP, CLBR, and ULAG) in Nigeria **206**

Figure 8.10 The coefficient of determination (R^2 in %) between GNSS PWV and the other climate variables at four GNSS stations (ABUZ, BKFP, CLBR, and ULAG) in Nigeria **208**

Figure 8.11 Monthly distribution of PWV (in blue) and temperature (in green) at four GNSS stations (ABUZ, BKFP, CLBR, and UNEC) in Nigeria **211**

Figure 8.12 Monthly distribution of PWV (in blue) and SSN (in green) at four GNSS stations (ABUZ, BKFP, CLBR, and UNEC) in Nigeria **211**

Figure 8.13 Daily distribution of PWV (in blue) and total solar radiation intensity (in green) at four GNSS stations (ABUZ, BKFP, CLBR, and UNEC) in Nigeria **212**

Figure 8.14 Monthly distribution of PWV (in blue) and TEC (in green) at four GNSS stations (ABUZ, BKFP, CLBR, and UNEC) in Nigeria **212**

Figure 8.15 Daily average TEC (in blue) and PWV (in green) variations at four GNSS stations (ABUZ, BKFP, CLBR, and UNEC) for 2013 **213**

Figure 8.16 Plot of TEC and PWV at two GNSS stations (CLBR and UNEC) for DOY 307, 308, 309, 310 and 311 corresponding to November 2013 storm **215**

Figure 8.17 Plot of TEC and PWV at two GNSS stations (BKFP and UNEC) for DOY 54, 55, 56, 57 and 58 corresponding to February 2014 storm **215**

Figure 8.18 The coefficient of determination (R^2 in %) between GNSS PWV and the different solar attributes at four GNSS stations (ABUZ, BKFP, CLBR, and UNEC) in Nigeria **217**

List of Tables

Table 1.1	Summary of GPS, GLONASS, Galileo, and Compass navigaton systems	**9**
Table 2.1	GRUAN GNSS product requirements	**22**
Table 2.2	IGS tropospheric product	**23**
Table 2.3	Comparison of ZTD estimation using different orbit products (The ZTD estimates obtained using IGS final orbits were used as reference to compute the other result)	**27**
Table 2.4	GNSS Sites and associated temporal weights	**29**
Table 2.5	Comparison of GNSS RO with other atmospheric sounding techniques	**41**
Table 3.1	Summary of statistics for Ordinary Least Squares (OLS) regression model	**57**
Table 3.2	Summary of statistics for Spatial Error Model (SEM)	**58**
Table 3.3	Summary of statistics for Spatial Lag Model (SLM)	**59**
Table 3.4 (a)	Summary of Results for the Mann-Kendall Trend Test based on 2-hourly ZTD data over Nigeria	**64**
Table 3.4 (b)	Summary of Results for the Mann-Kendall Trend Test based on monthly ZTD data over Nigeria	**65**
Table 3.5 (a)	Results of white-noise tests for 2-hourly ZTD data over Nigeria	**66**
Table 3.5 (b)	Results of white-noise tests for monthly ZTD data over Nigeria	**66**
Table 3.6 (a)	Results of tests for Stationarity for 2-hourly ZTD data over Nigeria (DF Test & KPSS Test)	**73**
Table 3.6 (b)	Results of tests for Stationarity for monthly ZTD data over Nigeria (DF Test & KPSS Test)	**74**
Table 4.1	Overview of blind tropospheric correction models	**80**
Table 4.2	Look-up table of meteorological parameters for the UNB3m model, the parameters are user latitude zone (φ) barometric pressure $(P_\circ)$, temperature $(T_\circ)$, Relative Humidity (RH), temperature lapse rate(β) and water vapour pressure height or decrease factor (λ) (modified after Leandro et al., 2006)	**84**
Table 4.3	Station information for selected IGS stations in Africa	**88**

Table 4.4 Performance of the UNB3m and GPT2w for ZTD estimation against the IGS solutions **89**

Table 4.5 Correlation matrix of the IGS product, UNB3m, GPT2w, and station elevation **93**

Table 5.1 Coordinates and name of all AWOS used in the study **104**

Table 5.2 Formulation for the different verification indices used in validating reanalysis over Nigeria **106**

Table 5.3 Summary of adopted processing parameters used in GAMIT software for ZTD estimation in this study **108**

Table 5.4 GNSS stations in the NIGNET and corresponding nearest AWOS **109**

Table 5.5 Summary of features in the new GPT2 empirical meteorological model **110**

Table 5.6 Theoretical influence of individual SDR from ERAI and NCEP on the final PWV estimates **118**

Table 6.1 Radiosonde stations in and around Nigeria **137**

Table 6.2 Summary of adopted processing parameters used in GAMIT software for ZTD estimation in this study **144**

Table 6.3 Performances of the different models for the estimation of T_m against the integration method **151**

Table 6.4 Pearson's correlation coefficient matrix for the different models **152**

Table 6.5 Mean values of the performance indicators for the different models **153**

Table 6.6 Precision of the PWV estimates for the models **157**

Table 7.1 GNSS stations in the NIGNET and corresponding nearest weather station **170**

Table 7.2 GNSS Stations in the NIGNET and corresponding grid node from AIRS model **173**

Table 7.3 GNSS Stations in the NIGNET and corresponding grid node from ERA-Interim model **174**

Table 7.4 Statistics (diurnal and monthly) of relation between precipitable water from GNSS and three other techniques (CORDEX-RCM, AIRS, and ERAI) at four GNSS stations over Nigeria from 2013 -2014 **180**

Table 7.5 Daily precipitable water statistics of the interrelation between CORDEX-RCM, AIRS(A), AIRS(D) and ERAI models at four GNSS stations over Nigeria from 2013-2014 **181**

Table 8.1 Average GNSS PWV and GNSS ZTD relationships over Nigeria from 2013 to 2014 **200**

Table 8.2 Pearson's correlation coefficient matrix for GNSS - PWV and the different rainfall events (rainfall, relative humidity (RH), wind, and daylight cloud amount) four GNSS locations in Nigeria **207**

Table 8.3 Pearson's correlation coefficient matrix for GNSS - PWV and the different solar events (TEC, radiation, SSN, and temperature) at GNSS locations in Nigeria **216**

List of Acronyms

ACC	Anomaly Correlation Coefficient
AFREF	African Reference Frame
AIRS	Atmospheric Infrared Sounder
AMMA	African Monsoon Multidisciplinary Analysis
AWOS	Automatic Weather Observing Station
CODE	Centre for Orbit Determination in Europe
CORDEX	Coordinated Regional Climate Downscaling Experiment
CORS	Continuously Operating Reference Stations
CV	Coefficient of Variation
DD	Double Difference
DOY	Day of the Year
ECWMF	European Centre for Medium-Range Weather Forecasts
ERAI	ERA-Interim
ERP	Earth Rotation Parameters
ES	Nash-Sutcliffe Score
GNSS	Global Navigation Satellite Systems
GPS	Global Positioning System (US GNSS)
GPT	Global Pressure Temperature model
GPT2w	Global Pressure Temperature 2-wet model
IA	Index of Agreement
IGS	International GNSS Service
IWV	Integrated Water Vapour
MAE	Mean Absolute Error
MEF	Model Efficiency
NCAR	National Centre for Atmospheric Research
NCEP	National Centres for Environmental Prediction
NIGNET	Nigerian GNSS Network
NIMET	Nigerian Meteorological Agency
NRMSE	Normalized Root Mean Square Error
NRT	Near Real Time
NWMTE	Nigerian Weighed Mean Temperature Equation
NWP	Numerical Weather Prediction

OLS	Ordinary Least Squares
OSGOF	Office of the Surveyor General of the Federation(Nigeria)
PWV	Precipitable Water Vapour
R^2	Coefficient of Determination
RCMs	Regional Climate Models
RF	Rainfall
RI	Reliability Index
RMSE	Root Mean Square Error
SDR	Standard Deviation of Residuals
SEM	Spatial Error Model
SLM	Spatial Lag Model
STEC	Slant Total Electron Content
TEC	Total Electron Content
VTEC	Vertical Total Electron Content
WGS84	World Geodetic System 84
WMO	World Meteorological Organization
WMTE	Weighed Mean Temperature Equation
ZHD	Zenith Hydrostatic Delay
ZTD	Zenith Total(Tropospheric) Delay
ZWD	Zenith Wet Delay

Chapter 1

Introduction

"We cannot solve our problems with the same thinking we used when we created them"
---Albert Einstein

In this chapter a short background and outline of the climate system and water vapour distribution is provided. The focus is on the use of a global navigation satellite system (GNSS) for water vapour estimation. The potentials and advantages of the estimation of water vapour from GNSS are highlighted. Finally, the aim, objectives, significance, scope and organisation of the research are described.

1.1 Climate System and Water Vapour

Climate is defined as the combined averaged weather conditions (i.e., "*temperature, air pressure, humidity, precipitation, sunshine, cloudiness, and winds*" etc.) over a place or region for a succession of years (Goosse et al., 2010). The climate system consists of five components: the atmosphere, hydrosphere, cryosphere, land surface and biosphere. The atmosphere is composed of oxygen (20.95%), nitrogen (78.09%), carbon dioxide (0.039%), argon (0.93%), and some other gases (Lutgens and Tarbuck, 2004). Temperature varies in the atmosphere and this has led to the atmosphere being divided into five regions, namely the troposphere, stratosphere, mesosphere, thermosphere and exosphere. The lowest part of the earth's atmosphere is the troposphere. The troposphere starts from the surface of the earth to about 9 km at the poles and 17 km at the equator. The lowest part of the troposphere is known as the planetary boundary layer (PBL) and is directly influenced by the activities on the earth's surface. Above the PBL is the free atmosphere where only some internal air turbulence occurs. The top boundary of the troposphere is known as the tropopause and its height is an indicator of tropospheric warming. Within the troposphere, the temperature decreases with height and the value at the tropopause is usually the lowest in the troposphere (Mason et al., 2001; Li, 2013). The region from the tropopause upwards to about 50 km is the stratosphere. In the stratosphere, the temperature increases with height. Although the climate change in the stratosphere does not directly affect the biology of the earth, it may affect the height of the tropopause and thus affect the warming or the cooling of the troposphere. The

mesosphere starts from the top of the stratosphere to about 85 km upwards. In the mesosphere, the temperature decreases with altitude. The top of the mesosphere is known as the mesopause and is the coldest layer of the earth's atmosphere. From the mesopause to about 700 km above the earth is the thermosphere. In the thermosphere, the temperature rises with altitude. Above the thermosphere is the exosphere, which is the outermost layer of the earth's atmosphere. Since this layer is close to the sun and due to low pressure, the temperature is rather high. Gases in this layer are hardly affected by the earth's gravity anymore, thus their atoms and molecules can move into outer space. A unique region of interest in the earth's atmosphere is the ionosphere. The ionosphere ranges from about 60 km to about 1500 km, and it includes the thermosphere and parts of the mesosphere and exosphere (Odijk, 2002). The ionosphere contains ions (charged particles) due to effects from the sun (solar radiation). The ionosphere has a significant effect on electromagnetic waves travelling through it. Figure 1.1 depicts a schematic illustration of the vertical structure of the atmosphere.

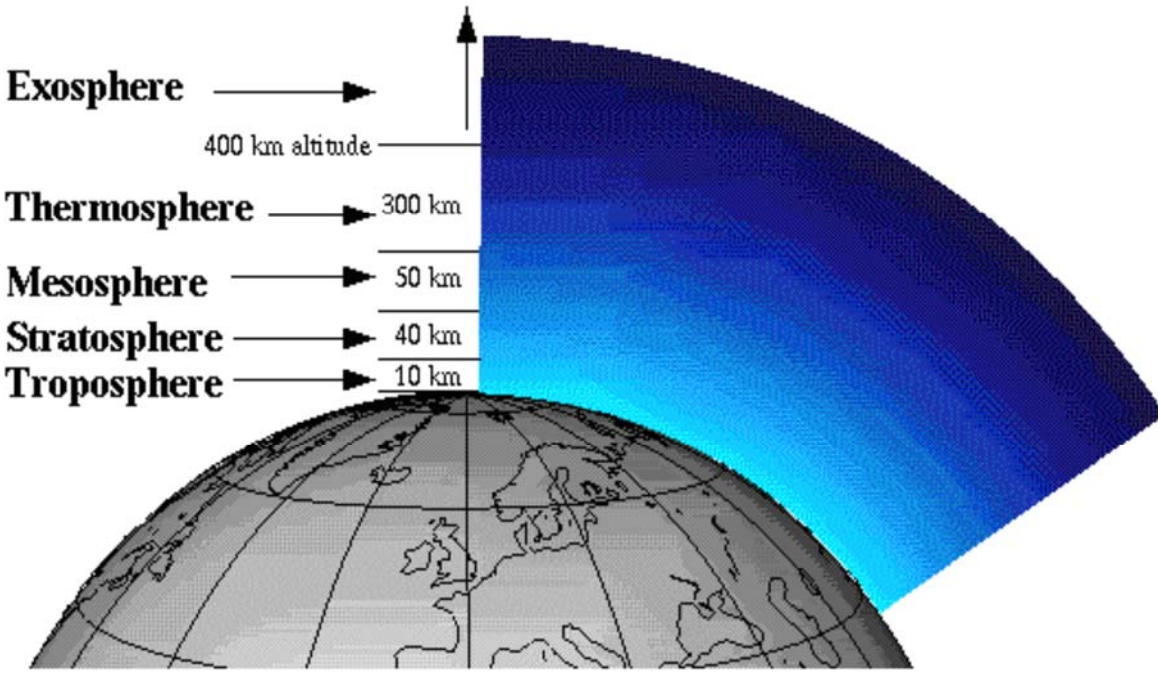

Figure1. 1: Vertical structure of the atmosphere (Source: Tao, 2008)

The hydrosphere is a closed system in which water exists and includes all water resources of the earth, such as lakes, rivers, seas and oceans. About two-thirds of the earth's surface is enclosed by these water resources, especially oceans, which contain about 97% of the earth's water supply. The atmosphere as it exists in its current form is largely due to the imperative influence of the hydrosphere. Oceans are essential in this respect; the oceans play

an important task in the climate system as they store most of the sun's energy that reaches the earth. Due to the large number of plants in the ocean, the oceans are also important sources for releasing oxygen. In addition, the oceans play a key role in the weather system, since many weather events are linked with the air conduction and convection between the oceans and continents (Kennish, 2001).)The global hydrological cycle is shown in Figure (1.2).

The cryosphere encompasses those segments of the earth's surface where water exists in frozen form (i.e. sea ice, lake ice, river ice, snow covers, glaciers, ice sheets and frozen ground, which includes permafrost, etc) (Shrestha and Singh, 2014). The cryosphere is vital in balancing the earth's energy cycle and global climate system. It prevents the earth from becoming too warm by reflecting a high percentage of the sunlight (Li, 2013).

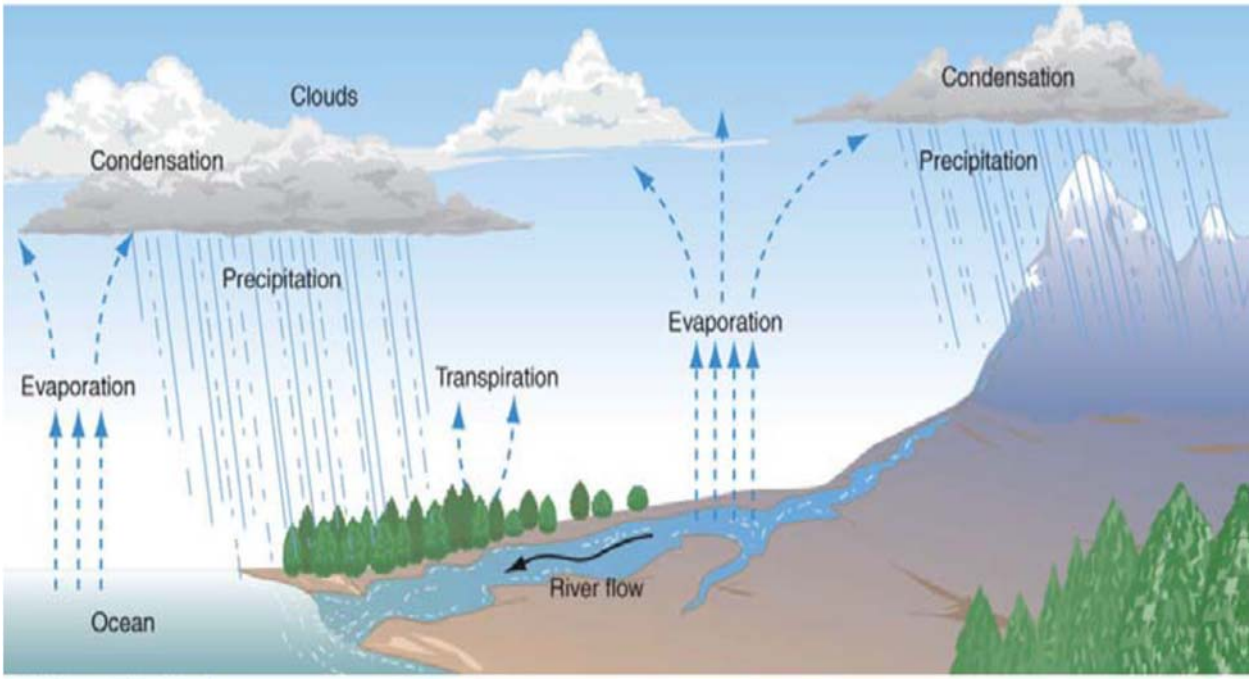

Figure 1.2: The climatic hydrological cycle at global scale (source: Goosse et al., 2010)

The land surface includes all the continents on the earth's surface. It absorbs solar energy and transfers the energy to the atmosphere by latent heat, sensible heat and long wave radiation etc. The land surface is important for energy exchange in the climate system.

The biosphere is the global sum of all ecosystems (Shrestha and Singh, 2014). The biosphere includes all life on earth, including human beings, as well as closed and self-regulating ecosystems. Compared to other components of the climate, the biosphere affects the earth's climate most, e.g. the combustion of fossil fuels by human beings breaks the balance of the carbon cycle in the climate system and increases the quantity of carbon dioxide in the atmosphere.

The earth's climate is transforming, and the transformations are expected to have a massive effect on the inhabitants of our planet, ecosystems, cities and energy use. At the start of the 20th century the global air temperature was about 1.5 degrees Fahrenheit lower than it is today; the rise in the last 30 years has been about 1 degree (IPCC, 2001a). The global temperature is again likely to go up by another 2 to 8.6 degrees Fahrenheit by 2100, as reported by the Intergovernmental Panel on Climate Change (IPCC).

The substantial boost in the earth's average near surface temperature in the lower atmosphere is due to heat preservation caused by the build-up of greenhouse gases (i.e., water vapour, carbon dioxide, methane, nitrous oxides, sulphur hexafluoride, hydro-fluorocarbons, perfluorocarbons and chlorofluorocarbons). These gases form a coverlet around the earth that lets the inward-bound rays of the sun (short-wave radiation) pass through but obstructs the reflected heat rays (long-wave radiation) from being released into space (see, e.g., www.kmaheshwari.com; www.climate.thinkaboutit.eu). This atmospheric heating phenomenon is often referred to as the "greenhouse effect". Although the aforementioned climate change could be caused by natural reasons, such as eruption of volcanoes, the main contributions to the change are made by anthropological factors. Among these anthropological factors, the most important one is the combustion of fossil fuels, which results in an increase in the amount of greenhouse gases in the atmosphere.

Water vapour is a major natural greenhouse gas, which is the source of about 36-70% of the greenhouse effect on Earth excluding clouds; other gases such as carbon dioxide contribute about 9-26%, methane contributes about 4-9%, and ozone contributes 3-7% (IPCC 2001b). It is not feasible to declare that a particular gas causes a definite fraction of the greenhouse effect, for the reason that the influences of the diverse gases are not additives.

Water vapour is one of the more important components of the atmosphere, given that it is the means by which humidity and energy (as latent heat) are transported through the troposphere and lower stratosphere to influence weather. Furthermore, apart from the function of water vapour in balancing the atmospheric heat budget, water vapour plays an essential task in the global hydrological cycle and global climate system (Boutiouta and Lahcene, 2013); it is obviously the source of precipitation, rain, snow, clouds, fog etc. In any vertical column of air, the amount of water vapour gives meteorologists a value of the maximum potential precipitation that could be retrieved from that air column under the right conditions. Also, as water vapour is highly variable both temporally and spatially, it is a

source of inaccuracy to the geodetic community, as the variability affects the models utilized for calculating atmospheric delay adversely.

Regardless of the air mass proportion of water vapour, which is around 1%, the effect it has on meteorology is very significant. It has the ability to cause small as well as large-scale temperature anomalies and is the main mechanism for atmospheric latent heat exchange. Furthermore, when looking at water vapour's role in the climate system, recent studies have estimated that about 70% of the heating of the atmosphere is attributed to water vapour acting as a greenhouse gas. Notwithstanding its significance in atmospheric processes over a broad scope of spatial and secular scales, it is one of the least understood and most inadequately depicted mechanisms of the earth's atmosphere in current climate prediction models. Atmospheric water vapour allows the short wavelength radiation of the sun to pass through the atmosphere, but absorbs long wavelength radiation emitted by the earth's surface. This trapped radiation causes the temperature to increase (Jones, 2010).

Traditionally, the quantity of water vapour in the air is defined by the water vapour mixing ratio, specific humidity, absolute humidity, relative humidity, dew point temperature and wet-bulb temperature (de Haan, 2008) for a given volume of air (V), mass of water (M_w), mass of dry air (M_a), mass of water vapour (M_v), and vapour pressure (P_v). The water vapour mixing ratio is the ratio between M_v and M_a expressed as g/kg. Specific humidity is the ratio of M_v to the sum of M_v and M_a also expressed as g/kg. Absolute humidity is the ratio between M_v and V expressed as g/m^3. A more frequently used and acknowledged parameter for defining water vapour is relative humidity. Less water vapour is often present in cold air than in warm air, so relative humidity is reliant on the combined definite moisture content and air temperature. Also, an increase in air temperature implies the possible existence of more water vapour in the air, and the ratio of the quantity of water vapour in the air corresponding to saturation dwindles. Thus, relative humidity (often in percentages) at all temperatures and pressures is the ratio of P_v to the saturation water vapour pressure. The P_v, is dependent on the temperature and the density of water vapour molecules. The saturation vapour pressure represents the maximum water vapour that can be present in a given volume of air or the pressure at which all water vapour condensates; it is greatly influenced by temperature. The air is saturated with water vapour when the amount of relative humidity in the air is 100%.

Meteorologists and space geodesists have also come up with a number of other terms to describe the quantity of atmospheric water vapour. Most important is the expression of the water vapour content of an air parcel by combining all the water vapour in the vertical column of air. The most commonly used terms are integrated water vapour (IWV) and precipitable water vapour (PWV). Both terms represent the absolute total amount of water in a vertical column of unit cross-sectional area ranging between any two individual levels. The PWV is the IWV scaled by the density of water and is often represented in millimetres. The term PWV will be used in this thesis.

1.2 Water Vapour Observing Systems

Atmospheric water vapour observations may be measured directly by in situ instruments such as radiosondes or humidity sensors on board aircraft (downward-looking radiometry) or, alternatively, from remote sensing estimates from instruments such as microwave radiometers (upward-looking radiometry) or Global Navigation Satellite Systems (GNSS) satellites. For the reason that the measurement system varies, the accuracy of the observed water vapour varies as well.

A radiosonde is a conventional measurement instrument for upper air observations in meteorology. The instrument is designed to be launched via weather balloon for in situ retrieval of vertical profiles of meteorological parameters (namely pressure, temperature, relative humidity, and wind information) (Li et al., 2003; Durre et al., 2006). The radiosonde transmits the measured vertical profiles of all parameters back to a ground station for processing and quality control and subsequently the data can be used for operational meteorology as well as for climate applications. Nevertheless, the use of radiosondes is limited by their low temporal resolution, high cost of operation, decline in their performance in cold, dry weather, and their sparse distribution over oceans. By and large PWV estimates from radiosondes have uncertainty of a few millimetres, which is often within acceptable accuracy limits for meteorologists (Niell et al., 2001). However, they are expensive and inconvenient because only limited measurements are available (two to four launches per day). Due to the cost, radiosonde launch sites are sparsely located across Nigeria, as in many other developing nations of the world.

Radiosondes play a vital role in operational meteorology, as many numerical weather prediction (NWP) schemes are largely trained on radiosonde ascent data, and they have for some time been one of the few sources of high accuracy upper air measurement data. However, with the advent of modern satellites there are more options related to upper air

measurement. Furthermore, it is imperative to bear in mind that radiosonde data have systemic errors (instrumental bias) associated with them (see Haase et al., 2000; Wang and Zhang, 2007).

Water vapour imagery is an important tool for climate investigation and prediction, since it embodies the flow pattern of the upper troposphere. Water vapour is transparent to radiation at visible and 10-12 micron wavelengths. However, water vapour is an exceptional and proficient absorber and emitter of radiation, at wavelengths between 6.5 and 6.9 microns; satellite radiometers measuring the quantity of radiation released by the atmosphere at these wavelengths are therefore capable of sensing water vapour in the atmosphere (see, Grody, 1993; Grody et al., 2001). Water vapour imagery shows the water vapour concentration in the atmospheric layer between 600 and 300 hPa (in the region of 4 to 9 kilometres above the earth's surface), representing the middle and upper part of the troposphere.

The main limitation of satellite water vapour is the strong water vapour absorptions at approximately 300 hPa and 500 hPa; little water vapour information is ever retrieved from below these pressure levels. Satellite water vapour can consequently be regarded primarily as an upper to mid-troposphere tool, as it effectively 'sees' the top of the atmosphere and cannot penetrate further down into the atmosphere than the point at which the absorption takes place. Thermal emission is often affected by the temperature of the atmosphere and the presence of clouds. However, satellite-based observation is the only efficient approach to measure water vapour levels on a large scale.

Ground-based microwave radiometers (water vapour radiometers (WVR)) and water vapour lIDARs (Light Detection and Ranging) can also measure atmospheric water vapour, though these remote sensing techniques are not operational yet. Both systems have their drawbacks. A WVR has technical hitches during rainfall and lIDARs during daylight (de Haan, 2008). Another ground-based water vapour measuring system is the sun photometer with sun and sky scanning radiometer that measures the direct solar irradiance and sky radiance at a number of fixed wavelengths within the visible and near-infrared spectrum. The the sun photometer is disabled under cloudy conditions.

Each of the above techniques, in situ measurement, ground-based or satellite-based remote sensing has various limitations and often does not adequately provide important information on quantity, such as atmospheric water vapour, required by the climatic research (Bevis et al., 1992). A report produced by the US Weather Research Program in May 1995 identified a national call for a dependable, low-cost system for determining atmospheric

water vapour (see Michelsen, 1998). Subsequently, Bevis et al. (1992, 1994) presented a discussion on the GNSS method for measuring water vapour. This discussion revealed the technical challenges in using GNSS to measure atmospheric water vapour, which focuced majorly on the uncertainty of modelling mean atmospheric temperature and other meteorological parameters at GNSS sites. Many researchers have conducted various experiments using a GNSS network of stations for atmospheric sensing and have more recently adopted the GNSS Radio Occultation approach. The new technology of GNSS atmospheric remote sensing has several advantages over the conventional water vapour observing system, including low cost, global coverage, reliable and stable results, high measurement accuracy and all-weather operability, as well as radio frequencies that can penetrate clouds and dust (Awange et al., 2010). This novel technology plays a major role in complementing the existing systems, e.g. radiosonde and WVR. The validation and set-up of an operational framework for this new technology remains the thrust of this research. In the succeeding section of this chapter an overview of the GNSS method and highlights of its application is provided.

1.3 GNSS and its Scientific Applications

The GNSS is an assemblage of satellites that broadcast signals to supply correct position, velocity and time information that is available to any person with a receiver. "The International Civil Aviation Organization (ICAO) defines a GNSS to include all basics of satellite navigation and their augmentations, such as space-based and ground-based augmentations" (ICAO, 1996). Thus, a GNSS must be equipped to give users real-time navigation information at accuracies that are safe for navigation, in addition to independent integrity-checking systems (Zheng, 2006).

As defined previously, GNSS is the generic name for the class of systems of which the American Global Positioning System (GPS) and its Russian counterpart, Global'naya Navigatsionnaya Sputnikovaya Sistema (GLONASS), today are the sole working (indeed, thriving) examples. ICAO defines first-generation GNSS (GNSS-1) to include the active GPS and GLONASS constellations and any civil augmentation systems using space (satellite), aircraft, ground and mobile-based techniques; these are essential to facilitate the essential navigation performance for diverse applications (see Hoffmann-Wellenhof et al., 2008).

Second-generation GNSS (GNSS-2) are a natural advancement of GNSS-1, intended to integrate the diverse satellite navigation systems to render improved service. This

technology also involves the launching of additional new satellites into space to improve and upgrade the existing GPS and GLONASS systems. Europe's input to the GNSS-2, called the GALILEO system, is under development to meet the requirement standards of GNSS-2 for rapid and reliable accurate positioning, with the lastest launch of additional Galileo navigation satellite in May 2016, Galileo system is a step closer to full operational use (see, Pauly et al., 2015 for details on the project status of the Galileo). The Chinese Beidou navigation system, Compass, has a constellation of 23 satellites for regional positioning capabilities as at June 2016. By 2020 it is expected to be ready for global service (see, http://en.beidou.gov.cn/ for details). Summary of the present status, plans, relationships, and dissimilarities among the GPS, GLONASS, Galileo, and compass navigation systems is contained in Table 1.1. All four are global systems available to users worldwide. Principally, the GPS, GLONASS, Galileo and Compass systems use middle Earth orbiting satellites with constellations (existing or intended) of between 24 and 30 space vechcles each. The different GNSS systems have comparable atomic time and geodetic coordinate frames and all broadcast one or more radio frequency bands.

Table 1.1: Summary of GPS, GLONASS, Galileo, and Compass navigaton systems

	GPS	**GLONASS**	**Galileo**	**Compass**
First launch	February 1978	October 1982	December 2005	April 2007
Full Operational Capability	February 1995	January 1996-December 2011	2012-2013	Up to 2020
Nominal Number of satellites	24	24	27	27
Orbital planes	6	3	3	3
Orbital inclination	55^0	64.8^0	56^0	55^0
Orbital period	11h 57.96min	11h 15.73min	14h 4.75min	12h 35min
Geodetic reference system	World Geodetic System (WGS 84)	ParametryZemli 1990 (PZ90) or PE-90 (Parameters of the Earth)	Galileo Terrestrial Reference Frame(GTRF)	China Geodetic System(CGS 2000)
Time system	GPS time, UTC(USNO)	GLONASS time, UTC(SU)	Galileo system time(GST)	Bei Dou system time (BDT)
Signal separation	Code –division multiple access	Frequency –division multiple access	Code –division multiple access	Code –division multiple access
Number of frequencies	3-L1, L2, L5		3(4)-E1, E6, E5a, E5b	3-B1, B2, B3
Frequency(MHz)	L1: 1575.420 L2: 1227.600 L3: 1176.450	G1:1602.000 G2: 1246.000 G3: 1204.704	E1: 1575.420 E6: 1278.750 E5: 1191.795	B1:1575.420 B2: 1191.795 B3: 1268.520

Other regional GNSS systems under development are the Indian Regional Navigation Satellite System (IRNSS) and the Quasi-Zenith Satellite System from Japan. In March 2016, the Indian Space Research Organization annouched the successful launch of the sixth satellite in the IRNSS. Details of the current status, signal structure and future plan of all available GNSS system can be found at https://directory.eoportal.org/web/eoportal/satellite-missions/ .

Traditionally, GNSS evolved as a positioning tool. It allows for true 3-D positioning. Conventional methods of surveying, geodesy and navigation, which involves tedious field measurements for obtaining positional and directional information, have consequently been replaced (partially and only where appropriate) by satellite-based methods, which are less monotonous and cost-effective. The introduction of satellite-based surveying represents progress comparable to that between the abacus and the computer for space geodesists and surveyors. GNSS has made it possible to unify global geodetic networks and consequently to define a global reference frame, thus the positional coordinates of points/stations on the different continents can be expressed in the same reference system (Altamimi et al., 2002; Blewitt, 2015). The precise positioning capability of GNSS aids the military in navigation, target acquisition and weapon guidance systems. Location-based services (LBS) is another application of the navigation capabilities of GNSS (see e.g. Barkhuus and Dey, 2003; Gruteser and Grunwald, 2003; Schiller and Voisand, 2004; Küpper, 2005). Study of relativistic effect for precise velocity determination and precise time measurement and transfer are achievable through GNSS (see, e.g., Levine, 1999; Lombardi, 2001; Zhang et al., 2006, Combrinck, 2013).

Advanced geodetic and geophysical applications, utilizing continuous GNSS observation data, have made it possible to study earth processes on a large scale. Such studies were almost impossible with the classic techniques. Global change in sea level can be monitored using GNSS, by observing the vertical motion of the solid earth at tide gauges (Larson et al., 2012&2013; Löfgren et al., 2010, 2011a&b; Santamaría-Gómez et al., 2012). Determination of mass redistribution within the earth's fluid surround is possible through continuous GNSS measurement based on the measured time variation in the earth's shape, velocity of the solid earth, Earth's gravity field, and Earth's rotation in space (Steigenberger et al., 2006; Blewitt, 2015). From GNSS observations, crustal motion as indicated by the time series/velocity fields of GNSS coordinates at a station above or around an aquifer can be used to study the hydrology of the aquifer (Beutler et al., 1994; Blewitt, 2015). In areas of postglacial rebound (glacial isostatic adjustment) measurements of velocities of stations from

continuous GNSS observations provide information on the manner in which matter flows (i.e. ice-sheet history) and variations in shape in Earth's mantle (Plag et al., 1996). In addition, GNSS continuous observation aids in the study of magmatic processes from observed time variation around stations found in regions of magmatic activity (Steigenberger et al., 2006; Blewitt, 2015). Using a high-rate GNSS system, it is possible to examine the background, early process and explosion of earthquakes, and to combine other data to determine relevant parameters for seismic hazard assessment and post-seismic processes (see Kouba, 2003; Larson et al., 2003; Hammond, 2005; Larson, 2009; Shi et al., 2010; Allen and Ziv, 2011; Geng et al., 2015).

Other scientific applications of GNSS technologies are also found in many fields: archaeology, atmospheric science, environmental science and space sciences, etc. This research will focus attention on the science application of GNSS in meteorology or atmospheric science, which is basically referred to as "ground-based GNSS meteorology".

A network of ground-based GNSS stations is primarily used for surveying, geodesy and navigation purposes. Due to the robustness that the ground-based GNSS technique has shown in studying the distribution of water vapour, many networks of continuously operating reference stations (CORS) are being constructed around the world nowadays for multi-disciplinary applications, which include meteorology (Ware et al., 2000; Wolfe and Gutman, 2000; Combrink et al., 2004; Van der Marel, 2004; Bock et al., 2006; Adams et al., 2011). With a network of GNSS CORS and the tomography technique, slant-path water vapour information can be mapped into a three-dimensional moisture field over the network (Nilsson et al., 2007; Troller et al., 2006; Bender et al., 2009). Assimilation of the slant-path water vapour from GPS into an NWP model has been done in near real-time (Flores et al., 2000; Gendt et al., 2001; de Haan et al., 2009; Bennitt and Jupp, 2012). Also, PWV retrieved from a continuous GNSS station is used in weather forecasting (i.e. severe storm prediction) (see e.g. Liou and Huang, 2000; Reigber, 2002; Nakamura et al., 2004; Nash et al., 2006; Sobolev et al., 2007; Karabatic et al., 2010; Adams et al., 2011; Liang et al., 2015).

The number of GNSS CORS is much larger than the number of radiosonde stations in the world. For example, in Nigeria, there are about 30 ground-based GNSS CORS, owned and managed by different institutions and organisations under various initiatives, while there are only three radiosonde stations in the same area that are in the WMO list of upper stations. The large number of ground-based CORS enables scientists to study water vapour distribution on a larger geographical scale with a dense horizontal resolution. When

compared to other observational techniques, the GNSS water vapour monitoring method yields better results in terms of spatial coverage. It has high temporal resolution and is a continuous monitoring system capable of measuring multiple lines between the station and the GNSS satellites in view at all weather conditions.

All the foregoing discussions demonstrate that GNSS atmospheric remote sensing technology is a key method to improve the sparse spatial and temporal sampling of water vapour observation in Nigeria. GNSS meteorology has transitioned from research into a global operational network. However, there is still no operational GNSS network for GNSS meteorology in Nigeria. Thus, as a practical issue, it is important to build up a network of GNSS stations across Nigeria which can routinely retrieve PWV for weather prediction, atmospheric research and climate monitoring and prediction. This problem is the main motivation of this thesis. In view of the different requirements of GNSS meteorology as identified by Isioye (2011), and the available GNSS CORS network in Nigeria, there is room for looking into this promising technology and creating a working model to accommodate the existing facilities and the general requirement for operational meteorology. These challenges are addressed in this thesis.

1.4 Research Objectives

The primary goal of this research is to develop and assess the accuracy of a water vapour retrieval technique from a network of ground-based GNSS stations with a view to gain understanding of the features of weather and climate associated with the variability of atmospheric moisture over Nigeria. In recognition of the potential of GNSS and the expectations of the geodetic/meteorological community in Nigeria, the objectives of this research are outlined as follows;

1) Building a solid technical basis for ground-based GNSS meteorology in Nigeria to prove the technical ability of GNSS PWV estimation from GNSS data.

2) Developing methods that can use the existing and expected GNSS CORS in Nigeria for estimating PWV in order to address all issues related to the practical application of GNSS meteorology in Nigeria.

3) Analysis of short-term variation and long-term trends in atmospheric parameters estimated from continuous ground-based GNSS station data in Nigeria.

4) Developing techniques that consider the sparse distribution of GNSS in Nigeria for PWV estimation and allow estimation of PWV from surface meteorological observations collected around GNSS sites or from numeric models.

5) Modelling of an ideal weighed mean temperature equation (WMTE) for the country, for use in the current studies and for later use in GNSS meteorological studies in Nigeria.

6) Validation of PWV estimates from GNSS using global NWP, radiosonde, and space-borne techniques (specifically, an atmospheric infrared sounder (AIRS)). This is to allow for the future introduction of GNSS PWV samples as independent quantities into existing or future NWP models.

7) Relating PWV estimates from GNSS with weather events (i.e. solar and rainfall events) in Nigeria. Time series of PWV will be correlated to the weather events that influence the region to further justify the applicability of PWV in weather monitoring and climate studies.

The objectives of the research as outlined above are to answer the following questions:

1. Can zenith total delay (ZTD) be accurately modelled in water vapour estimation without measured meteorological parameters?

2. What is the true accuracy of water vapour estimates derived from networks of ground-based GNSS receivers when compared against other in-situ measurements, remote sensing instruments and NWP models?

3. Are estimates of tropospheric parameters derived from GNSS networks suitable for weather and climatic applications?

4. Are the trends in water vapour estimates in agreement with other constituents of the atmosphere?

5. How well do GNSS water vapour estimates represent real, short and long-term atmospheric fluctuations and are networks of ground-based GNSS receivers useful for climate studies?

1.5 Research Methodology

The methodology applied to this study is briefly described through the flow chart presented in Figure (1.3). In order to answer the fundamental questions of this research as enumerated herein for the development and analysis of a water vapour system for Nigeria, this research was undertaken in five steps as depicted in Figure 1.3.

Firstly, meteorological data were collected from three different categories of datasets, namely: (i) Data from synoptic weather stations (automatic weather-observing stations) across Nigeria to represent surface measurements, (ii) Data from NWP models (ERA-Interim Reanalysis and NCEP/NCAR Reanalysis 2), (iii) Data from global standard atmospheres (global empirical models). Global empirical models circumvent the use of surface meteorological data and assume that the atmosphere behaves in a definite way, depending on the behaviour of the temperature, pressure, and humidity, such as the UNB3M model (Leonardo et al., 2006) and the GPT model (Boehm et al., 2007;Lagler et al., 2013), which are considered in this study. The various meteorological data were interpolated to GNSS receiver stations. It is also assessed whether the technique of using meteorological data from the nearest synoptic weather station is adequate or whether spatial interpolation provides more accurate estimated surface observations at the GNSS antenna site. According to the distribution of the weather stations and GNSS sites in Nigeria, a weighted linear interpolation scheme was adopted (see Bosy et al., 2012; Bai and Feng, 2003; Hadas et al., 2013; Jade and Vijayan, 2008). It uses the surface meteorological data from the four nearest weather stations to each GNSS station to predict values for the GNSS stations. In addition, the gridded data from NWP models (ERA-Interim reanalysis and NCEP/NCAR reanalysis 2) were interpolated to the GNSS stations using the same approach.

Secondly, GNSS data, which included RINEX observation files, precise orbit files, ocean loading files and site log information, were collected at GNSS stations in Nigeria. Data were processed using the GAMIT/GLOBK software, version 10.3 (See, http://www-gpsg.mit.edu/~simon/gtgk/GAMIT_Ref.pdf) to obtain two-hourly and daily ZTD estimates at the station for the period under investigation (2010-2014). Zenith wet delay (ZWD) estimates were obtained from the ZTD estimates by using meteorological parameters estimated from step 1 above.

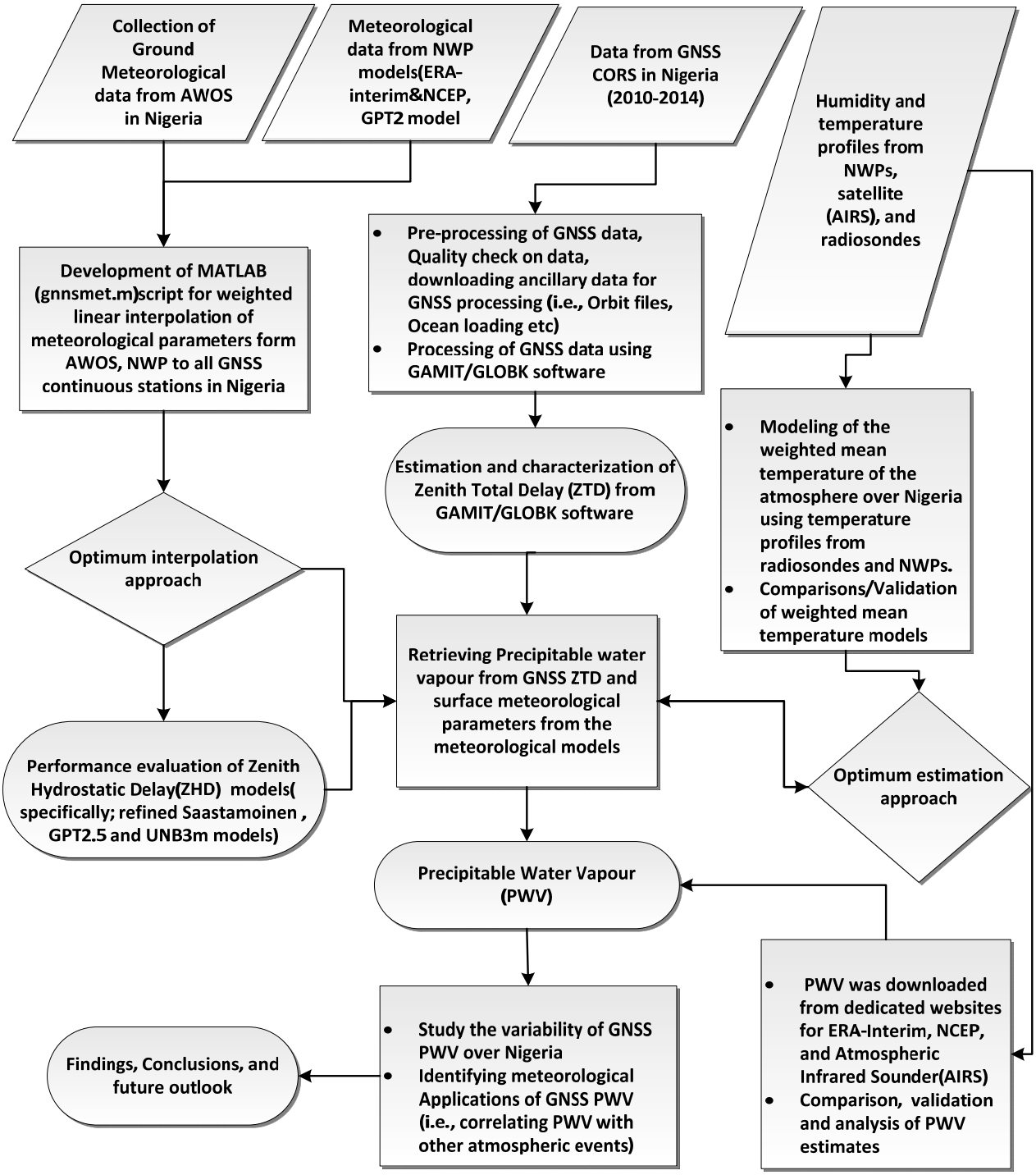

Figure 1.3: Flow chart of the Research Framework

Thirdly, temperature profiles collected from radiosondes and NWP models were used to estimate the mean temperature of the atmosphere and were used together with the ZWD estimate and other constants(specifically; the refractive constants, specific gas constant for water vapour, and water density) to obtain PWV estimates.

Fourthly, the PWV from ERA-Interim and AIRS were obtained the respective data holders. Finally, the estimates from the different sources were validated with the GNSS estimates. PWV from GNSS were correlated to atmospheric weather and solar events over Nigeria. The different steps enumerated above are treated individually in detail in successive chapters of this thesis to attain the goal of the research.

1.6 Scope and Limitation of Study

The purpose of the research is to address all the initial GNSS meteorology issues occurring in Nigeria, using a network of GNSS receivers that currently make up the Nigerian GNSS network (NIGNET). This includes improving and validating the accuracy of GNSS PWV estimates for future weather and climate applications, which are seriously limited by the sparse existing GNSS facilities and co-located meteorological sensors in Nigeria. The focus of many agencies across the globe has been on ZTD assimilation into NWP models for meteorological applications. As such, when evaluating the quality of GNSS water vapour data, much time and thought are given to assessing the quality of the output of the GNSS processing, i.e. ZTD. Often, little consideration is then given to the data with which ZTD estimates are converted into PWV. At present there are no standards for the source of meteorological data used for ZTD to PWV conversion. The source and resolution of the meteorological data are not fixed and are a focus of analysis in this thesis.

The research is greatly dependent on the existing GNSS infrastructure in the country and thus research effort is limited to the demonstration and evaluation of GNSS water vapour estimates, not the assimilation of water vapour to NWP models. However, future research efforts outside this study may be made to involve meteorological scientists so that the PWV estimates can be integrated into NWP models for climatic studies in Nigeria. For the purpose of this thesis, slant path delays are ignored and the focus is only on zenith path delays.

1.7 Organization of Thesis

The reviews, analyses and results of this research are presented in eight chapters. Chapters 2-8 (in journal paper format) comprise submitted and published peer-reviewed journal papers. Where applicable in the thesis, the text remains the same as that published, but has been reformatted for consistency of style and remaining typographical errors were corrected. Also, for unity and to avoid repetition the references are incorporated at the end of the thesis. An outline of the essential structure of this thesis is discussed as follows:

Chapter 2 contains a comprehensive theoretical background on GNSS meteorology and provides an outline of current developments of this new technology. In the chapter, the status of GNSS networks in Africa and the standards and requirements for GNSS meteorology are critically reviewed in view of the African GNSS network. This chapter is drawn from the literature and provides a theoretical basis for GNSS water vapour estimation.

Chapter 3 describes in detail the spatial and temporal distribution of ZTD over Nigeria as estimated by the GAMIT/GLOBK software within NIGNET for the period 2010-2014. The third objective of this research is addresssed in this chapter.

Chapter 4 contains a comparative analysis to understand the accuracy and application of blind tropospheric models in the estimation of ZTD over Africa as whole. The fourth objective of this research work is partly addressed in Chapter 4.

In Chapter 5 the validation of meteorological parameters from reanalysis models (ERA-Interim and NCEP/NCAR 2) against observation from synoptic stations and their application in retrieving PWV from GNSS ZTD over Nigeria are reported. This partly addresses the fourth objective of this research work.

Chapter 6 contains the details of modelling a WMTE for Nigeria and surrounding areas. The accuracy of various mean temperature equations is tested and their influence on PWV estimation is reported. The accuracy of the GNSS-derived PWV is evaluated in the next chapter. This chapter addresses the fifth objective of this research work.

The comparison of the results of GNSS PWV estimates in the previous chapter with PWV estimates from other data sources (specifically AIRS and ERA-Interim) at daily, monthly and seasonal scales over Nigeria are reported in Chapter 7. This chapter addresses the sixth objective of this research work.

Chapter 8 contains a summary of the application of the variability of GNSS PWV estimates for studying and analysing weather events over Nigeria. This chapter addresses the last objective of this thesis.

Lastly, the main findings and conclusion of the research and recommendations for future investigation, improvement and applications are given in Chapter 9.

Chapter 2

The Potential for Observing African Weather with GNSS Remote Sensing**

"Science is based on experiment; on a willingness to challenge old dogma; on an openness to see the universe as it really is. Accordingly, science sometimes require courage-at the very least the courage to question the conventional wisdom"

…..Carl Sagan

Précis

When compared to the wide range of atmospheric sensing techniques, global navigation satellite systems (GNSS) offers the advantage of operating under all weather conditions, is continuous, with high temporal and spatial resolution and high accuracy, and has long-term stability. The utilisation of GNSS ground networks of continuous stations for operational weather and climate services is already in place in many nations in Europe, Asia, and America under different initiatives and organisations. In Africa, the situation appears to be different. The focus of this paper is to assess the conditions of the existing and anticipated GNSS reference network in the African region for meteorological applications. The technical issues related to the implementation of near-real-time (NRT) GNSS meteorology are also discussed, including the data and network requirements for meteorological and climate applications. We conclude from this study that the African GNSS network is sparse in the north and central regions of the continent, with a dense network in the south and fairly dense network in the west and east regions of the continent. Most stations lack collocated meteorological sensors and other geodetic observing systems as called for by the GCOS Reference Upper Air Network (GRUAN) GNSS Precipitable Water Task Team and the World Meteorological Organization (WMO). Preliminary results of calculated zenith tropospheric delay (ZTD) from the African GNSS receiver network indicate spatial variability and diurnal dependence of ZTD. To improve the density and geometry of the existing network, countries are urged to contribute more stations to the African Geodetic Reference Frame (AFREF) programme and a collaborative scheme between different organisations maintaining different GNSS stations on the continent is recommended. The benefit of using spaced based GNSS radio occultation (RO) data for atmospheric sounding is highlighted and filling of geographical gaps from the station-based observation network with GNSS RO is also proposed.

*****This chapter consists of formatted text for one peer reviewed journal paper as follows:***

Isioye, O.A., Combrinck, L., Botai, J.O., & Munghemezulu, C. 2015. The Potential of Observing African Weather with GNSS Remote Sensing, *Advances in Meteorology*, Volume 2015, Article ID 723071, http://dx.doi.org/10.1155/2015/723071.

2.1 Introduction and Background

Satellite-based remote sensing technologies are an integral part of the work of the United Nations Framework Convention on Climate Change (UNFCCC) through the Global Climate Observing System (GCOS). The mandate of GCOS is to determine what data are needed for the monitoring of climate impacts. To this end, GCOS has identified 44 so-called Essential Climate Variables (ECVs) (Mason, 2010*)*. According to GCOS, progress in producing the forty-four ECVs has been lethargic to date. Nonetheless, the increasing importance of adaptation in terms of both costs and needs has heightened the interest in space-based operations (Alessi and Egenhofer, 2011).

Atmospheric water vapour is identified as one of the forty-four ECVs. Atmospheric water vapour is one of the most important components of the atmosphere, since it is the means by which moisture and latent heat are transported to influence weather; furthermore it is a greenhouse gas that plays an essential role in the global hydrological cycle and global climate system (Boutiouta and Lahcene, 2013). Most meteorological processes (convection, cloud formation, precipitation) are influenced by the local as well as large-scale variability in atmospheric water vapour. Traditional methods of collecting data on atmospheric water vapour do not offer the spatial and temporal resolution necessary for in-depth studies of weather and climate (Ware et al., 2000). A better understanding of climate and weather patterns requires datasets that are more comprehensive.

Global Navigation Satellite Systems (GNSS) through a concept referred to as *'GNSS meteorology*', is a contender for providing the water vapour knowledge that atmospheric scientists have been seeking. GNSS receivers/antennas do not require continual calibration as some sensors do for measurement drifts or biases although pressure sensors collocated at GNSS sites occasionally require calibration for instrument drift. Also, large numbers of GNSS measurements can be made temporally and spatially in all weather conditions. Due to the coverage and potential for near real-time data transmission that GNSS water vapour estimates offer, GNSS could be used to determine the distribution of water vapour over a region of interest and thus help in the identification of potential severe weather activity (Jin et al., 2011; Karabatic et al., 2011; Boutiouta and Lahcene, 2013).

The term GNSS meteorology relates to the utilization of the GNSS radio signals to deliver information about the state of the troposphere. This can be achieved from a satellite platform (GNSS radio occultation meteorology) (Anthes et al., 2008; Wickert et al., 2009) and ground permanent stations (Ground based GNSS meteorology) (Bevis et al., 1992, 1994). Continuous observations from GNSS receivers provide an excellent tool for studying the

Earth's atmosphere. GNSS meteorology has transitioned from research into national and regional networks. The collaboration between the geodetic and meteorological communities has contributed to the meteorological community's understanding of the GNSS representation of Water vapour. These and other efforts have resulted in projects and collaboration between GCOS and the International GNSS Service ((IGS) Kouba, 1998; Weber et al., 2002; Dow et al., 2009) focussed on the operational use of GNSS water vapour estimations (Wickert et al., 2012).

The new technology of GNSS atmospheric remote sensing has several advantages over the conventional water vapour observing system, including having global coverage, reliable and stable results, high measurement accuracy, all weather operability and having radio frequencies that can penetrate clouds and dusts (Awange and Grafarend, 2005). In addition, the majority of national geodetic institutions and scientific organisations install GNSS receivers in different regions of the world with dense networks in order to do positioning, mapping, monitor tectonics, etc. Through collaboration with those, data for Zenith Total Delay (ZTD) estimation for meteorology can be obtained at a low or no cost. GNSS meteorology enable Precipitable Water Vapour (PWV) to be inferred with the same accuracy as conventional meteorological measurements, such as radiosondes, Water Vapour Radiometer (WVR), and Microwave Profiler (MWP) measurements, to about 1-2mm PWV accuracy (Bosy et al., 2010). Comparative and validation results of GNSS ZTD/PWV with existing Numeric Weather Prediction (NWP) models such as the European Centre for Medium Weather Forecast (ECMWF) and National Centre for Environmental Prediction (NCEP) are promising as seen from the works of e.g., Chen et al. (2011); Kishore (2011); and Koulali et al. (2012). Also, Teke et al., (2011); Van Malderen, (2014); and Bock et al., (2010), have all reported the performance of GNSS against other geodetic techniques (namely; Very Long Baseline Interferometry (VLBI) and Doppler Oribitography, Radio positioning Integrated by Satellite (DORIS), and Sun photometers from the AErosol RObotic Network (AERONET)) in the estimation of troposphere parameters with results showing strong correlation between them.

There have been several projects from various organizations located on the different continents of the world to derive tropospheric zenith delay measurements from ground-based GNSS, for operational meteorological applications. Examples of such projects in Europe include the COST Action 716 (European Cooperation in the field of Scientific, technical-exploitation of ground-based GPS for numerical weather prediction application, 1998-2004)

(van der Marel, 2004), TOUGH (Targeting Optimal Use of GPS Humidity Data in Meteorology, 2003-2006) (Vedel and Huang, 2004), E-GVAP (The EUMETNET GPS Water Vapour Programme, 2004) (Bennitt and Jupp, 2012). The E-GVAP network consists of more than 1500 GNSS sites mainly in Europe, recently processing and distribution of global GNSS data have started, since many E-GVAP members run global NWP models. In Africa, the AMMA (African Monsoon Multidisciplinary Analysis project, 1999-2005) (Bock and Nuret, 2009; Walpersdorf et al., 2007) worked on PWV estimation and analysis in the African Monsoon region. In North America, the SuomiNet (named to honour meteorological satellite pioneer Verner Suomi) network of receivers which provides real-time estimates of water vapour for a global network of receivers from zenith water vapour measurements are mostly concentrated in the United States (see Ware et al., 2000). Additionally, UCAR's (University Corporation for Atmospheric Research) COSMIC (Constellation Observing System for Meteorology, Ionosphere and Climate) program process GPS data of the PBO (Plate Boundary Observation) GPS network, CocoNet (Caribbean Network), SuomiNet + NOAA (National Oceanic and Atmospheric Administration), USCG/USACE (United State Coast Guard/US Army Corps of Engineers), DOT (Department of Transportation) and other sites to produce near real time (NRT) PWV estimates across North America (Ware et al., 2003). The Japanese GEONET (GPS Earth Observation Network) has the largest array of over 1200 GPS stations in the world. It was established for earthquake hazard research and mitigation; scientific applications of the network have been expanded to include meteorology, and ionospheric research. Currently, the GEONET contributes to the assimilation of GPS precipitable water vapour data into the JMA (Japan Meteorological Agency) Mesoscale Numerical Prediction Model (Nakamura et al., 2004). Furthermore, two European institutes; Météo France and the UK Met office, currently use NRT ZTDs in their numerical weather predictions operations, both report a positive impact from the use of ground based GNSS delay data (de Haan, 2013). Utilizing its capability of water vapour estimation, GNSS has the potential to detect and track extreme changes in weather such as thunderstorms (Nakamuna et al., 2004). In addition, NRT GNSS water vapour monitoring for numerical weather prediction services are active in Germany and Austria (Bosy et al., 2012).

All the foregoing discussions demonstrate that GNSS atmospheric remote sensing technology is a key method to improve spatial and temporal sampling of water vapour observation and that GNSS PWV should be a useful source of humidity information for NWP applications. However, there is still no operational GNSS network for GNSS meteorology in Africa, although the application has been investigated at the Hartebeesthoek Radio

Astronomy Observatory in terms of South Africa only (Combrink et al., 2004). Thus, as a practical issue, it is important to build up a network of GNSS stations across Africa, which can routinely retrieve PWV for weather prediction, atmospheric research, and climate monitoring and prediction. This problem is the main motivation of this review. In view of the different requirements of GNSS meteorology as identified in Isioye (2011), and the available GNSS CORS (Continuously Operating Reference Station) network in Africa, there is the need to look into this promising technology and create a working model to accommodate the existing facilities and the general requirement for operational meteorology. These challenges are addressed in this paper.

2.2 Operational Requirements and Standards for GNSS Meteorology

The IGS troposphere working group (Byun and Bar-Sever, 2009) is currently collaborating with the Global Climate Observing System (GCOS) Reference Upper Air Network (GRUAN). The GRUAN is an international reference-observing network, designed to meet climate requirements and to fill a major void in the current global observing system (Wickert et al., 2012; Wang, 2013). The GRUAN GNSS precipitable water (GNSS PW) task team was established in 2010 as one of six GRUAN task teams. Ground based GNSS PW was identified as the utmost priority measurements for GRUAN, and the GNSS PW task team's goal is to develop explicit guidance on hardware, software and data management practices to obtain GNSS PW measurements of consistent quality at all GRUAN sites. Both GRUAN and IGS have developed a requirement for GNSS products. A summary of GRUAN GNSS product requirements is presented in Table (2.1).

Table 2.1: GRUAN GNSS Product Requirements (modified after, Wickert et al., 2012)

Variable	ZTD	ZWD	PWV	P_S	T_m
Measurement Range	1000-3000 mm	0 – 500 mm	0 – 8 mm	500 – 1100 hPa	20 – 300 K
Accuracy	4 – 6 mm	6 mm	0.1 mm	0.01 hPa	0.2 K
Precision	4- 6 mm	6 mm	0.1 mm	0.5 hPa	0.1 K
Long Term Stability	0.1 – 0.4 mm/dec	0.1 – 0.4 mm/dec	0.01 – 0.06 mm/dec	0.1 hPa/dec	0.05 K/dec
Temporal Resolution	1 h	1 h	1 h	1 h	1 h
Data Latency	1 month	1 month	1 month	1 month	1 month

As part of the collaboration, expectations are that: (a) GRUAN stations should become IGS stations; (b) IGS helps to push GNSS based climate applications according to climatological requirements and process IGS data for climatological applications; (c) Further, collaboration to establish central processing and analysis facilities of which IGS is already playing a leading role has been advocated. The IGS currently estimates ZTD and other atmospheric products through its global network. See Table (2.2) for a summary of IGS atmospheric products

Table 2.2: IGS Tropospheric Products
(http://igscb.jpl.nasa.gov/components/prods.html, assessed 20/02/14)

Product	Accuracy	Latency	Updates	Sample interval
Final tropospheric zenith path delay	4 mm	< 4 weeks	Weekly	2 hours
Ultra-rapid tropospheric zenith path delay	6 mm	2-3 hours	Every 3 hours	1 hours

In addition, the IGS and EUREF (Ihde, 2008; Altiner et al., 2010) have also developed useful guidelines for operational procedure for GNSS Meteorology networks (within the COST716 action user requirements for the use of GNSS in meteorology) (de Haan, 2006). These procedures are summarized under four major component headings as shown in Figure (2.1). The guidelines from IGS in partnership with GRUAN and EUREF represent the standard for GNSS meteorology at the moment and are in agreement with those specified by the WMO.

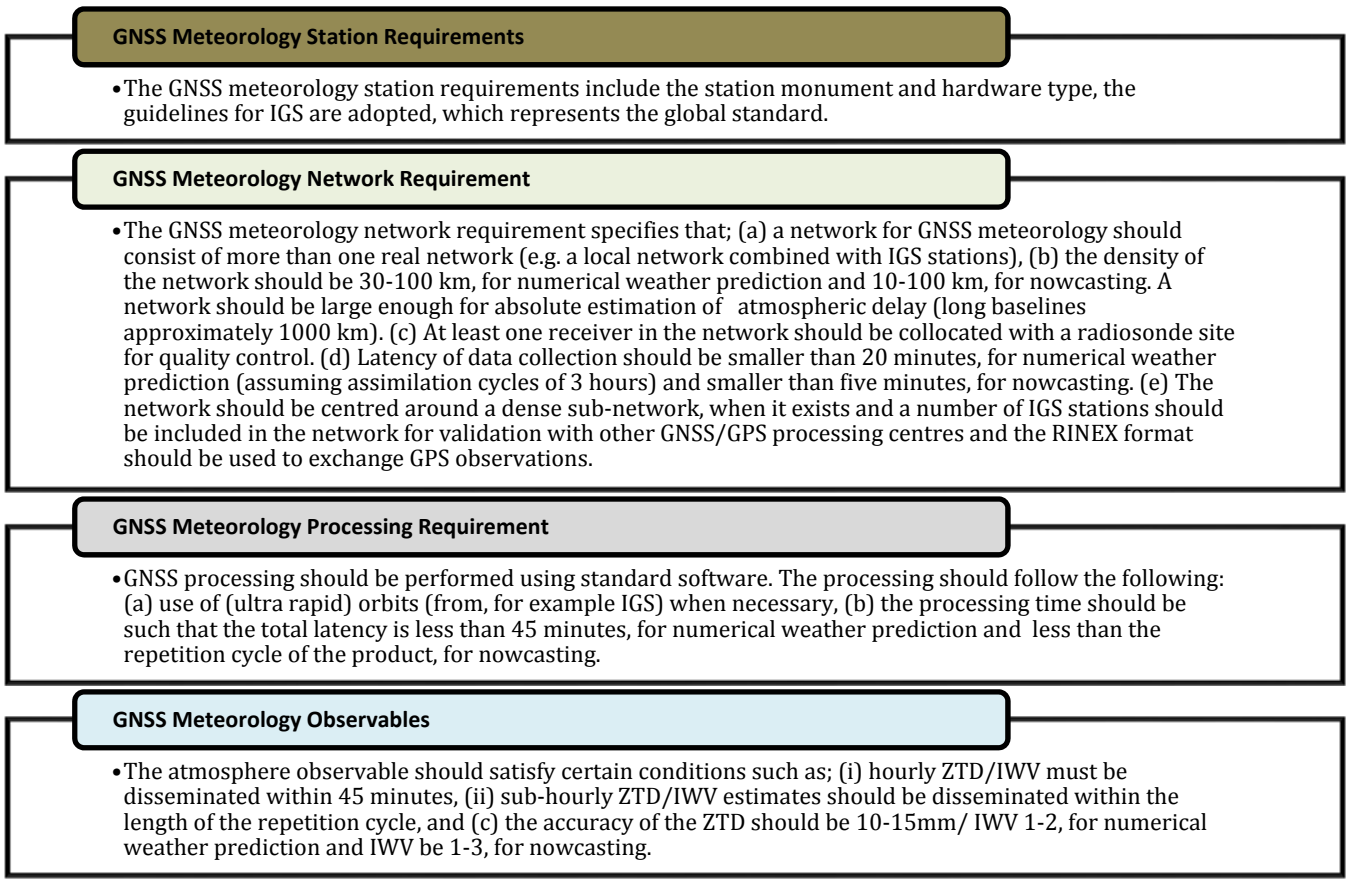

Figure 2.1: Summary of Requirements for GNSS Meteorology from IGS, GRUAN and EUREF

2.3 Status of the African GNSS Network

Networks of GNSS CORS exist in Africa, which contribute to the IGS and are established and managed by African entities and partners. Densification of IGS networks with its products in Africa is the first step towards the realization of the African Geodetic Reference Frame (AFREF) (Neilan and Wonnacott, 2002; Wonnacott, 2005). Some station requirements and regional issues were discussed in detail by Combrinck and Chin (2001). The densification requires that at least one GNSS CORS be established in every African country. Such networks of CORS are to form the basis of and act as focal points for the establishment of national GNSS networks; and where possible, more than one of such stations can be in a country. It is expected that once AFREF has been fully established, every African country will have a GNSS CORS network with capabilities to fully serve varied national needs and provide other useful products to users, e.g., broadcasting differential corrections and to refine the transformation parameters necessary to relate the national systems to the ITRF (International Terrestrial Reference Frame). It is important to

note that all IGS stations in Africa are AFREF stations, but that not all AFREF stations are IGS stations. Furthermore, all AFREF stations are contributing to realize the various national reference frames but not all national GNSS stations are AFREF stations, as is the case already in South Africa, which currently has sixty-six GNSS stations in it national frame but only sixteen stations are AFREF & IGS stations. Figure 2.2 depicts the distribution of AFREF and IGS stations in African. The network is very sparse in the north and central African regions. Currently, there are about thirty-nine IGS stations operating on the African continent, most of the stations are concentrated in the southern part of the continent.

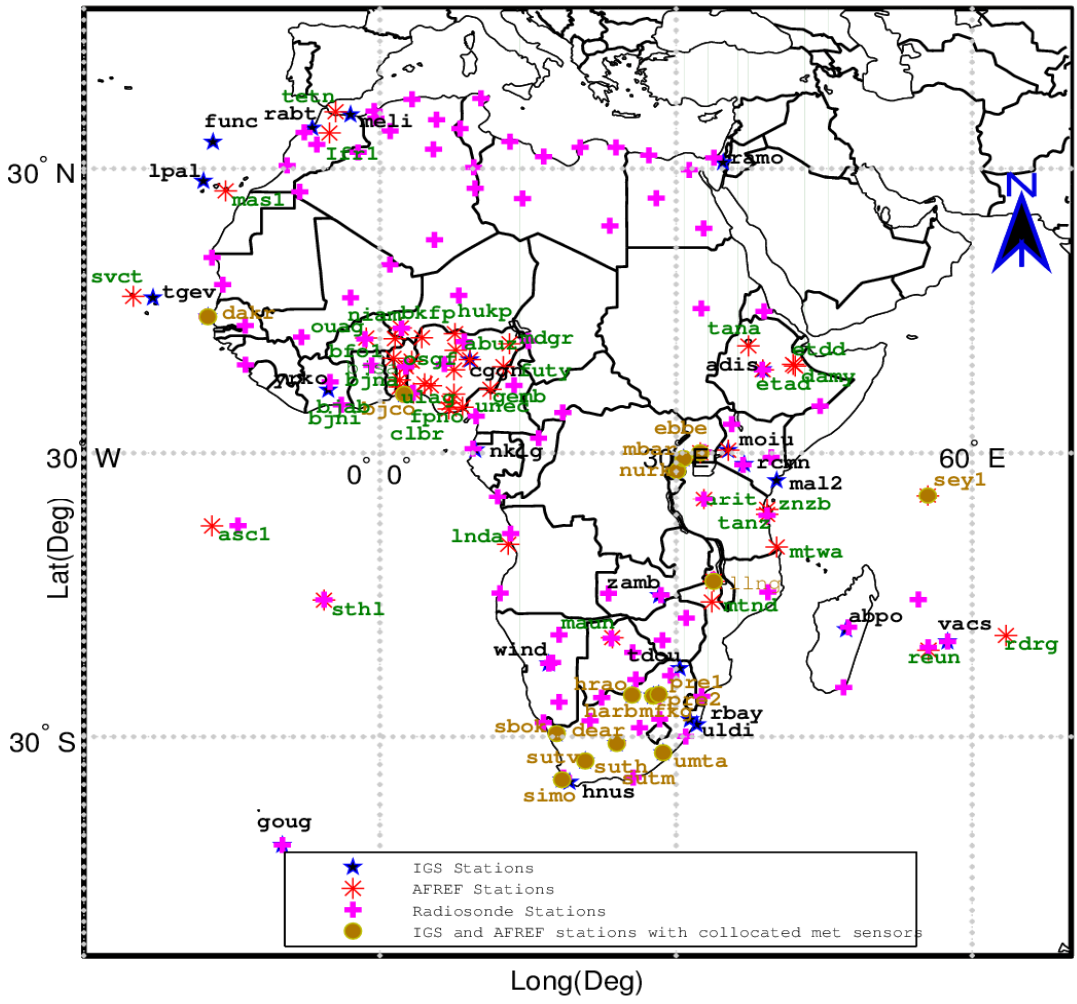

Figure 2.2: Map depicting the position of IGS and AFREF stations in Africa

A quick check on the station availability of AFREF stations from the AFREF data web page (wwww.afrefdata.org) indicates that 81 stations are currently on the scheduled list for daily data logging from individual contributors (countries) in Africa. However, only 25 countries on the continent are currently contributing to the IGS and AFREF. The maximum

daily data archive for AFREF in the last three years (2011, 2012, and 2013) to date (23/02/2014) stands at 54 stations per day. The reason for inconsistent data streaming from the various stations can obviously be due to communication problems, which has to do with internet connectivity, equipment failure, or in some cases electrical power problems, which is less often.

The site log files and type of data archived by both the IGS and AFREF stations in Africa were inspected for the purpose of this study to ascertain if stations are collocated with meteorological sensors, as it is a requirement by the IGS for a GNSS meteorology network. It was, however, observed that only a few stations in Africa have met packs collocated with them (see Figure 2.2). Additionally, not all the GNSS stations collocated with weather sensors that stream meteorological RINEX files to the IGS, as confirmed from the SOPAC web data page (http://sopac.ucsd.edu/cgi-bin/dbDataBysite.cgi). Furthermore, only a few GNSS stations in Africa are collocated with radiosondes as required by the GRUAN PW Task team and the IGS. However, there are a few GNSS stations that are within an appreciable distance to the radiosonde sites, this may as well be the situation for weather sensors. Figure (2.2) further illustrates the distribution of radiosonde stations in Africa as obtained from the Integrated Global Radiosonde Archive (IGRA). Collation of meteorological parameters from the different weather station for interpolation to the GNSS site as reported in Hadas et al., (2013) would be unmanageable in the African context going by instrument variations, political and administrative challenges, cost, and ready access to data.

From the foregoing, the African GNSS network can be seen to have three particularities: (i) the network is sparse considering the requirements for Meteorology, (ii) absence of weather sensors and Radiosondes at GNSS sites, (iii) inconsistency in data streaming from operators due to lack of internet connectivity for data transmission, thereby creating data gaps. The sparseness of the African network implies long inter-station distances; this could also lead to constraints on the orbit solution established by the IGS. Hence, the orbit errors could be more important over Africa than in places with a denser IGS network. These orbit errors would then limit baseline precisions on the long baselines typically found in the African GNSS network. Therefore, the application of GNSS for weather studies will be more limited in Africa; this slight limitation is however not critical as the global orbit adjustments and solutions basically avoids the problem. Thus, the present conditions fall slightly short of international requirements as discussed in the preceding

section of this review. The addition of corner cube reflectors on future and current GNSS satellites will ensure Satellite Laser Ranging (SLR) calibration of the satellite orbits; expansion of the SLR network from the southern part of Africa is required to fully exploit benefits that can be had.

For operational weather service, GNSS PWV estimates are required to be in NRT. The NRT data processing involves acquiring and processing of GNSS and ancillary observations to yield signal delay or PWV estimates within a single NWP assimilation cycle. In operational weather prediction, meteorological observations are typically assimilated every 6 hours. With the new generation of meteorological satellite observations provided at intervals of 1 hour 40 minutes, the assimilation delay currently required by the World Meteorological Observation is approximately 2 hours 15 minutes or 3 hours 20 minutes at most. In the case of the Rapid Update Cycle, running operationally for Environmental Prediction, the assimilation delay is approximately 75 minutes (Dick et al., 2001). In order to ensure that one cycle of observations is processed before the next satellite orbit is completed; GNSS PWV must be calculated in NRT with a minimum loss of accuracy if they are to be a useable data source in NWP models. To fulfil this objective, the issue of the use of real-time orbits is necessary, and must be addressed in the context of the African network. Preliminary investigation into the issue as reported by Isioye (2011) in an experiment that utilised GNSS data for three days (GPS week 1578, day 1-3; which corresponds to day of year 95-97, 2010) collected from ten IGS station of the African GNSS network and which were processed with the IGS final, rapid and ultra-rapid orbits and JPL 15 min orbits. Table 2.3 was adapted from Isioye (2011) and summarize results of a comparison of the different orbit solutions.

Table 2.3: Comparison of ZTD estimation using different orbit products (The ZTD estimates obtained using IGS final orbits were used as reference to compute the other result) (After Isioye, 2011)

Orbit Type	RMS (mm)	Standard deviation (mm)	Mean difference (mm)	Maximum difference (mm)	Minimum difference (mm)
IGS rapid	0.185	0.180	-0.079	0.870	-1.860
IGS ultra Rapid	1.876	1.832	-0.185	29.435	-19.560
JPL 15 min	1.549	1.511	-0.197	9.435	-11.560

The results obtained using the IGS final orbits were taken as reference and all other results were compared to these. These results clearly demonstrate the potential of GNSS for

NRT ZTD estimation and consequently NRT PWV. Further, this confirms that the IGS ultra rapid orbits and the JPL 15 min orbits could be used for NRT GNSS water vapour estimation, since the RMS of the ZTD estimations is 1.9 mm and 1.5 mm, respectively. It is expected that estimated PWV will be less than 1 mm, which is quite acceptable for meteorological applications.

2.4 Preliminary Results on Monitoring of GNSS ZTD Variability using the African GNSS Network

2.4.1 GNSS Data Processing and Tropospheric Product Descriptions

Twelve of the forty four GNSS stations earlier indicated as IGS stations on the African continent were selected for processing and discussion. Data from the period of 2010-2014 were analysed. The selection of the stations for this discussion was based on the availability and continuity of data at a particular station in relation to other stations in the network. Hence, the temporal connectivity weights (T_i) of the stations in the network were computed. Each station was assigned a temporal connectivity weight equal to;

$$T_i = \sum_{k=1}^{N} \frac{1}{n_k} \cdot \delta(k) \ , \qquad (2.1)$$

where N is the total number of days of interest , n_k is the number of data for the kth day , and $\delta(k)=1$ if station has data for the kth day and 0 otherwise. Table 2.4 highlights all IGS stations adopted in the network with associated temporal connectivity weights for the years under review (2010-2014). In Table 2.4, higher T_i denotes higher temporal connectivity.

The GNSS data analysis has been performed with MIT's (Masachussests Institute of Technology) GAMIT/GLOBK software package (GAMIT version 10.3, Herring et al., 2006). The software has the capability to determine positional information alongside tropospheric parameters, which comprises of the ZTD and atmospheric gradient components.

Firstly, to process ZTD from GAMIT, we used final (precise) orbit solution for the satellites from the IGS, adjusting the orbital parameters to avoid day boundary problems. Antenna phase correction is applied following the IGS recommendations (Gendt and Schmid, 2005). The coordinates of the GNSS stations were heavily constrained to their ITRF 2008 (Altamimi et al., 2011) values. Instead of using a single parameter form for the tropospheric parameters, we used a piecewise linear function of ZTD over the session with the number of zenith delay parameters set at thirteen, thus establishing two hours intervals. The constraint

used for zenith delay was 0.2 metres as it is recommended to set it loose enough to encompass any error in wet delay (Herring et al., 2006). The variation is defined as parameters of a first order Gauss Markov process and the zenith variation between points were given as 0.10 m with 100 hrs of correlation time. The a priori tropospheric delay was calculated according to Saastamoinen (1972) based on a standard atmosphere value from the Global Temperature Pressure model (GPT 50). We used the Vienna Mapping function (Boehm et al., 2006) and the GNSS data are used down to a cut-off elevation angle of 10°.

Table 2.4: GNSS sites and associated temporal weights

Station ID	Country	Latitude (Deg)	Longitude (Deg)	Height (m)	Temporal Connectivity Weight (2010-2014)
ADIS	Ethiopia	9.0351	38.7663	2439.1540	212.4104
BJCO	Republic of Benin	6.3847	2.4500	30.6000	203.1985
CGGN	Nigeria	10.1231	9.1183	916.6953	67.0596
DAKR	Senegal	14.7212	342.5605	51.0000	27.3604
HRAO	South Africa	-25.8901	27.6870	1414.3000	232.6287
MBAR	Uganda	-0.6016	30.7379	1337.6533	130.7619
NKLG	Gabon	0.3539	9.6721	31.4800	214.2571
NURK	Rwanda	-1.9446	30.0899	1485.0000	181.8869
RABT	Morocco	33.9981	353.1457	90.1000	215.7409
SUTH	South Africa	-32.3802	20.8105	1799.7660	227.5124
YKRO	Cote d'Ivorie	6.8706	354.7599	270.0000	79.9242
ZAMB	Zambia	-15.4255	28.3110	1324.914	98.2366

The calculated *ZTD* comprises the hydrostatic (*ZHD)* and wet (ZWD*)* component of the delay (Bosy et al., 2012) as shown in Equation (2.2):

$$ZTD = ZHD + ZWD \ . \qquad (2.2)$$

The wet component of the ZTD is the foundation for estimation of water vapour content in the atmosphere. The relation between ZWD and the water vapour content in atmosphere is expressed by IWV (Integrated Water Vapour) and PWV (Precipitable Water Vapour) reported in, e.g., Bevis et al. (1994) and Kleijer (2004) and is expressed as in Equation (2.3):

$$PWV = \frac{IWV}{\rho_w} = \frac{\left[ZTD_{GNSS} - ZHD\right]}{10^{-6} R_w \rho_w \left[k_2' + \frac{k_3}{T_m}\right]} = \Pi\left[ZTD_{GNSS} - ZHD\right] = \Pi \cdot ZWD \ . \quad (2.3)$$

In Equation (2.3), ρ_w is the water density, $R_w = 461.525 \pm 0.003\left[Jkg^{-1}K^{-1}\right]$ is the specific gas constant for water vapour, k_2' and k_3 are refraction constants and T_m is the weighted mean water vapour temperature of the atmosphere measured in Kelvin. It is operationally required to process GNSS data alongside meteorological parameters (temperature, pressure, and humidity) obtained from weather sensors collocated at the GNSS site in the modelling of ZHD and estimation of water vapour. Therefore, with only T_m and local surface pressure, it is possible to reduce ZTD estimates from GNSS processing to PWV as shown in Equation (2.3).

The weighted mean water vapour temperature of the atmosphere T_m of the vertical column of air above the GNSS receiver is thus given as (Davis et al., 1985):

$$T_m = \frac{\int_h^\infty \frac{e}{T} \cdot Z_w^{-1} dh}{\int_h^\infty \frac{e}{T^2} \cdot Z_w^{-1} dh} = \frac{\int_h^\infty \rho_w dh}{\int_h^\infty \left(\rho_w / T\right) dh} \ . \quad (2.4)$$

In Equation (2.4), e is the water vapour pressure, T is the temperature, Z_d^{-1} *and* Z_w^{-1} are the inverse compressibility factors of dry air and water vapour respectively. Thus, T_m can be obtained by integrating the vertical profiles of e and T, the integration is done between the GNSS receiver altitude h and infinity utilising radiosonde profiles or outputs fields of NWP models. This method is limited by the tempo-spatial resolution of these data products, which is a barrier for GNSS meteorology and is rarely used in real time PWV estimation. Bevis et al., (1994) proposed a linear regression model for estimating T_m based on the relationship between surface temperature and T_m and this is widely adopted in many studies, though it accuracy varies across the globe and thus there are many regional/local variants of the model (Sapucci, 2014). A more recent product with NRT capability for estimating T_m is from ECWMF operational analyses provided by the Technical University of Vienna (information online at http://ggosatm.hg.tuwien.ac.at/DELAY/ETC/TMEAN/).

Importantly, meteorological units installed at or near GNSS sites need to be calibrated occasionally for instrument drift and biases, and also surface pressure observations should be

reduced to GNSS antenna height (Vey et al., 2009). Reduction of surface pressure to GNSS antenna height is possible with the hypsometric equation as follows (Vey et al., 2009):

$$P_{GNSS} = P.e^{\frac{-g.\Delta H}{R_d T}} . \qquad (2.5)$$

In Equation (2.5), p_{GNSS} is the pressure at GNSS antenna height (hpa), $R_d = 287,053\left[Jkg^{-1}K^{-1}\right]$ is the gas constant for dry air, p is the pressure at the height of the pressure sensor (hPa) , $\Delta H = H_{GNSS} - H_S$ height difference in metres and T is the actual mean temperature of the layer between the GNSS antenna and the meteorological sensor in Kelvin.

The ZHD can be calculated using empirical models such as the Saastamoinen, Hopfield, Berman, Davis, Ifadis, Askne models etc. as described in Tuka and El-Mowafy (2013). The Saastamoinen model is the most used in geodetic applications and its accuracy has been widely reported (Dodo and Idowu, 2010). The Saastamoinen model for Zenith hydrostatic delay (ZHD), in metres, is expressed as in Equation (2.6):

$$ZHD = 0.002277 \cdot \frac{p}{1 - 0.00266\cos(\phi) - 0.28 \cdot 10^{-6} h} , \qquad (2.6)$$

where P is the surface pressure in hPa, ϕ is latitude in radians and, h is the height of the surface above the ellipsoid (in metres).

The accuracy of PWV is strongly dependent on the accuracy of ZTD values. That is, nearly all of the errors in PWV is introduced during the ZTD estimation (Bevis et al., 1994). The major sources of error in ZTD are GNSS antenna phase centre offsets (PCOs) and phase centre variations (PCVs), and uncertainties in mapping functions. The PCVs and PCOs can together yield systematic effects from 0.3 – 1 mm and seasonal effects < 0.1 mm (maximum amplitude). Similarly, the mapping functions can have systematic effects of 0.1 - 0.5 mm and seasonal effects of 0.1 - 0.5 mm. However, most of these errors are rigorously handled within precise GNSS analysis software.

The accuracy of ZHD is greatly influence by errors in surface pressure and can be approximated by Equation (2.7) (Bai, 2004):

$$\sigma_{ZHD} \approx 0.002277 \cdot \sigma_p . \qquad (2.7)$$

Thus an error, σ_p, in surface pressure of $1\ hpa$ results in a ZHD error, σ_{ZHD}, of 2.6 mm. Similarly, the errors in converting ZWD to PWV are primarily the errors in mean atmospheric temperature (T_m) and are approximated by Equation (2.8) (Wang et al., 2005);

$$\sigma_{\Pi} \approx \frac{1}{1768.72} \cdot \sigma_{Tm} \quad . \tag{2.8}$$

Finally, the accuracy of PWV estimates, according to the law of propagation of errors can be expressed as in Equation (2.9) (Bevis et al., 1992):

$$\sigma_{PWV} = \sqrt{\left(ZWD \cdot \sigma_{\Pi}\right)^2 + \left(\Pi \cdot \sigma_{ZHD}\right)^2 + \left(\Pi \cdot \sigma_{ZTD}\right)^2} \quad . \tag{2.9}$$

Thus for σ_{ZTD} of 4-10 mm, σ_p of $2\ hPa$, and $\sigma_{T_M} < 2\ K$, the accuracy of PWV estimate ranges from about 1.1-1.9 mm. This clearly indicates the level of accuracy required in estimating ZTD, mean temperature and pressure in GNSS meteorology.

The second tropospheric parameter estimated alongside the ZTD from GAMIT geodetic software is the atmospheric gradient. The estimation of the atmospheric gradients which are the effect of azimuthal asymmetry in the atmospheric delay is given as (Herring at al., 2006):

$$AG = Grad_{(N-S)} \cdot M_f \cdot \cos(AZ) + Grad_{(E-W)} \cdot M_f \cdot \sin(AZ). \tag{2.10}$$

Where $\cos(AZ)$, $\sin(AZ)$ are cosine and sine functions of the Azimuth (AZ), and is the mapping function M_f for the gradients. The gradient parameters, $Grad_{(N-S)}$ and $Grad_{(E-W)}$ are given to represent the difference in the North-South and East-West delay at 10° elevation. When using low elevation angle observations, the azimuth asymmetry of the local troposphere gets more important and must be accounted for. Estimating horizontal tropospheric gradients is a common way to cope with these asymmetries and the station coordinate repeatability may be considerably improved by this measure as shown in Miyazaki et al. (2003). The convention of the GAMIT software is to resolve GNSS gradient components at 10° of elevation in centimetres, but using mapping functions measurement of gradients can be converted into the zenith direction in millimetres. Usually, values of GAMIT gradients components do not exceed 15 cm.

In our processing, the a priori constraint for the gradients was set at 0.01 m in the solution gradient and was thus tightly constrained. The variations for the gradients were

defined again as parameters of a first order Gauss Markov process and the gradient variations between points were given as 0.01 m with 100 hours of correlation time.

2.4.2 GNSS ZTD Variability on the African GNSS Network

For the long term trend analysis in climatic changes, a continuous record for at least thirty years is usually necessary (Intergovernmental Panel on Climate Change (IPCC), 2007). Climate requires a long time series of observations. The GNSS data from the African Network cannot yet provide such a long time series. Nevertheless, the four and half years, twelve times per day database of ZTD over twelve stations in the African GNSS network available for this review provides a unique resource for providing insights into the stability and pattern of distribution of ZTD short term temporal variations(diurnal variation) of the ZTD distribution above Africa.

In Figure 2.3, the variation in the daily calculated ZTD is shown at the different sites for days 1-365 in the year 2013. Evident from Figure 2.3 is the consistency in the ZTDs from season to season. Whilst the general trend in the plot within each monthly seasonality period is similar, there is the need to adequately model the trend taking into consideration conditions at each site and the spatial correlation characteristics of the ZTD values.

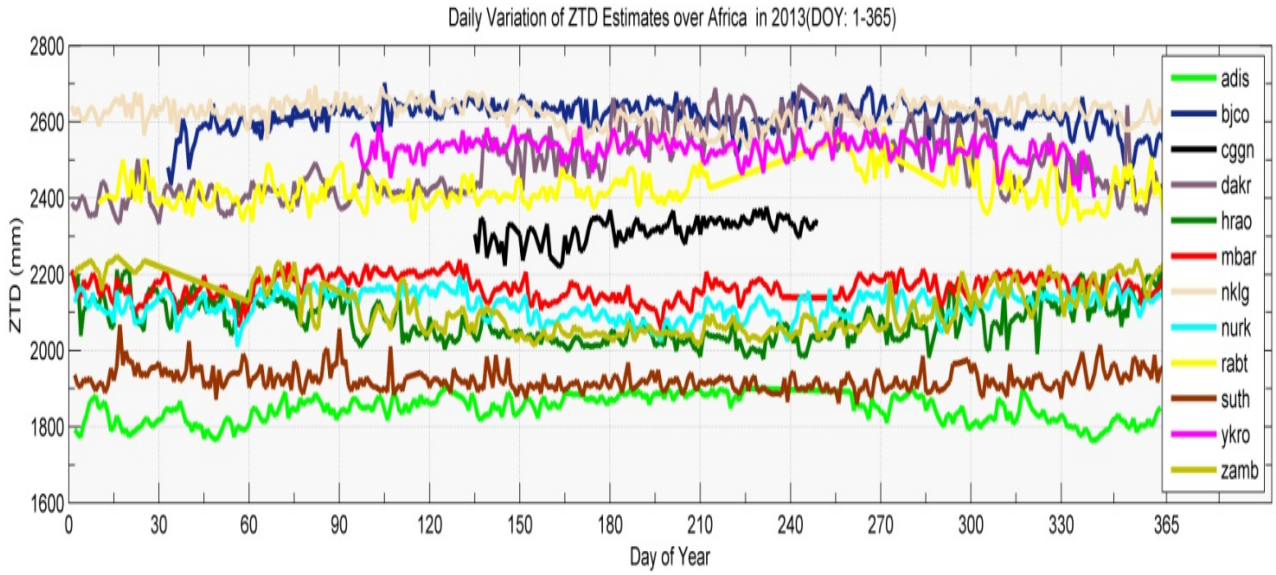

Figure 2.3: Daily variation of ZTD estimates over Africa in 2013 (DOY 1-365)

From our archived GNSS ZTD data we examine the elevation dependence by first taking the mean of all the measurements at a particular site, and then plotting the distribution of mean values versus site elevation as shown in Figure 2.4. Evidently, it appears that there is strong dependence on elevation, though, it is reasonable that ZTD should depend on

elevation; after all, it is the water vapour integrated from the observation site to the top of the atmosphere, and if the observation site is higher there will be less atmosphere, and hence less water vapour, above it. Most sources of water vapour are at Earth's surface. The dependence on elevation is found to be different than that of the major constituents of the dry atmosphere, and it falls off more quickly with elevation than would be expected from total pressure.

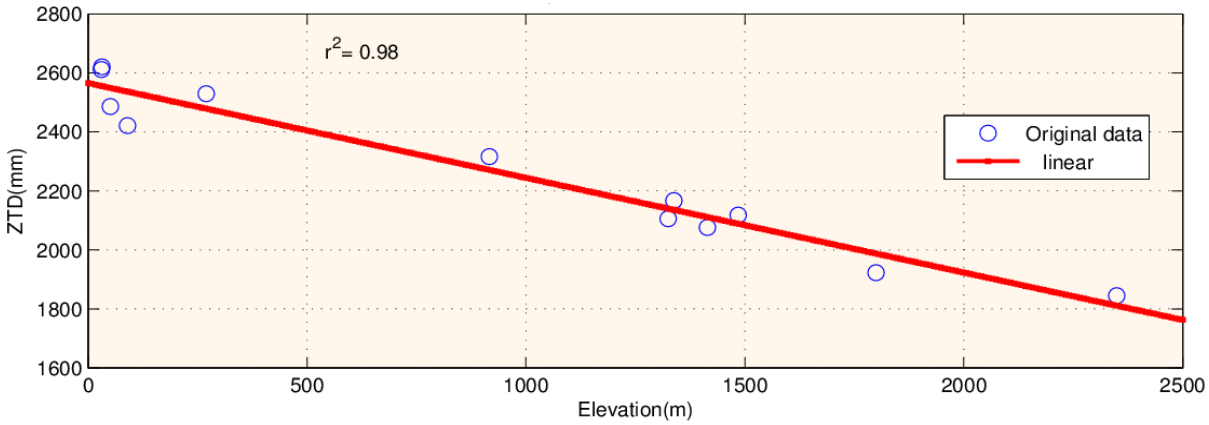

Figure 2.4: Plot of GNSS ZTD against station elevation

To gain insight into the diurnal characteristics of the sites we identified the dominant periods (or frequencies) of the time series at each site using periodograms. A periodogramme for each station based on two hourly data from 2010-2014 is shown in Figure 2. 5 and also, the average two hourly data plot over the same period is presented in Figure 2.6. The periodogrammes illustrate the relative importance of possible frequency values that might explain the oscillation pattern of the calculated ZTDs. An examination of the plots as presented in Figure 2.5 reveals that all sites show a diurnal dependence of ZTD when averaged over a long time period. It is also possible that a site may show a diurnal dependence at one time of the year and not during another as a result of seasonal changes.

From the foregoing spatial and temporal variability in GNSS ZTD across Africa are identified, as the different stations tend to exhibit distinct trends in GNSS ZTD variability. Though, further processing, analysis and modelling of ZTD time series for the purpose of identifying seasonal/annual trends, testing for stationarity (stochastic properties) and homogeneity of ZTD data are needed. The potential of GNSS as tool for meteorology cannot be over emphasized as the variability identified at the different stations can be correlated with other atmospheric parameters which can serve as indicators for the monitoring and predicting of the weather at such places. Furthermore, GNSS meteorology offers the advantage of ZTD

time series being used in NWP models and also ZTD/PWV maps used for nowcasting applications.

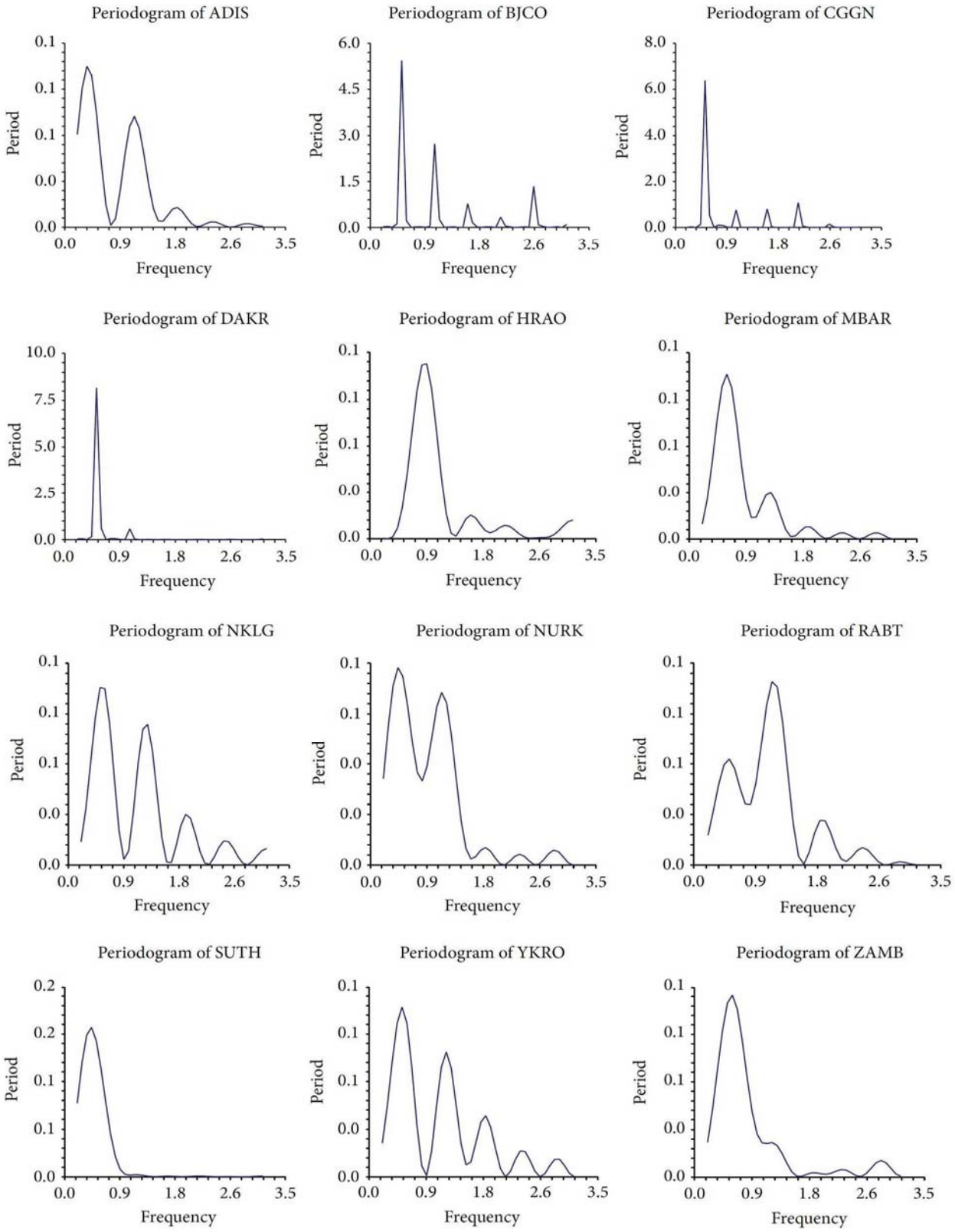

Figure2.5: Periodogramme of ZTD time series

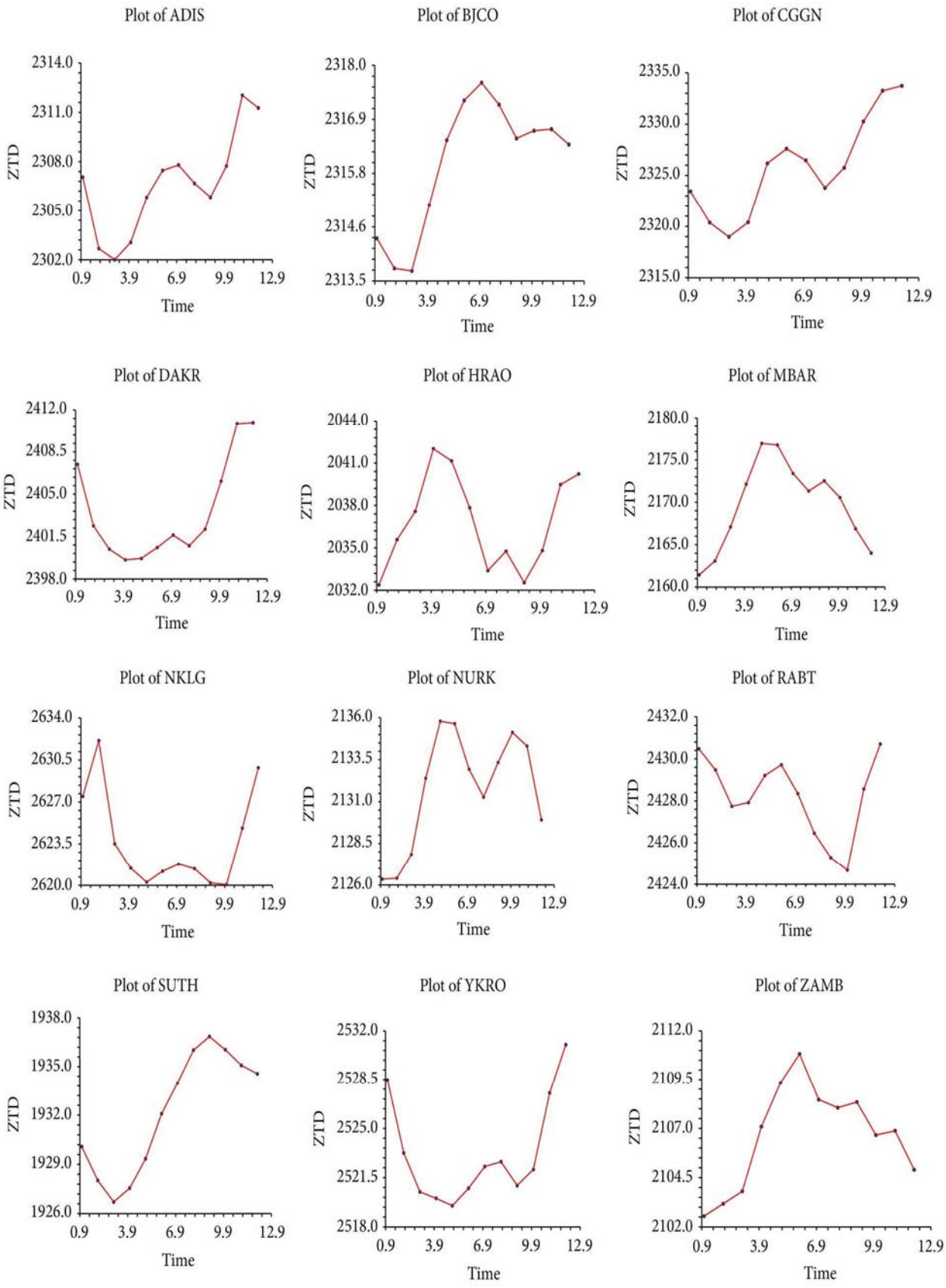

Figure 2.6: Average two Hourly ZTD plots for 2010-2014

2.5 Steps to Improve GNSS Meteorology within the African GNSS Network

The following solutions are offered in view of the peculiarities of the African GNSS network as identified in the preceding section.

2.5.1 Densification of GNSS Networks through collaborative Initiatives

There are other initiatives in Africa that utilizes GNSS data, apart from AFREF, to realize their objectives. This includes the International Space Weather Initiative (ISWI) and the Scintillation receiver Network (SCINDA) (www.fas.org/spp/military/program/nssrm/~initiatives/scinda.html), which both have a strong interest in populating their observing capability in the equatorial regions of Africa. The AMMA GPS project is primarily a meteorological project aimed at West Africa using GPS as a supporting observing technique (Bock and Nuret, 2009; Walpersdorf et al., 2007). The Africa Array, currently focusing on seismology, uses GPS as a positioning tool for seismic deployment and exploration surveys (www.africaarray.psu.edu). Some of the Africa Array GNSS stations are contributing to AFREF. Furthermore, African meridian B-field Education and Research (AMBER) (www.igpp.ucla.edu/public/ekassie/AMBER.html); African GPS Receivers for Equatorial Electrodynamics Studies (AGREES) (www.igpp.ucla.edu/public/ekassie/AGREES.html), all use GNSS data to accomplish their objectives which are specific scientific studies.

Many national agencies in Africa still do not make GNSS data available to the public or to AFREF. In Ethiopia and Malawi there is a dense GNSS network for tectonics monitoring. South Africa has a national network (TRIGNET) of 66 stations. Ghana, Algeria, Egypt, Morocco, and Eritrea have national networks of GNSS stations, but information and data are not yet publicly available to AFREF. In addition, UNAVCO archive data for an ample number of permanent GNSS stations in Africa for different agencies and private organizations. Figure (2.7) illustrates the position different stations in the networks discussed under this section.

Collaboration in terms of data sharing and access between the different initiatives and AFREF operational data centres will go a long way towards improving the density of the current network to enhance meteorological applications.

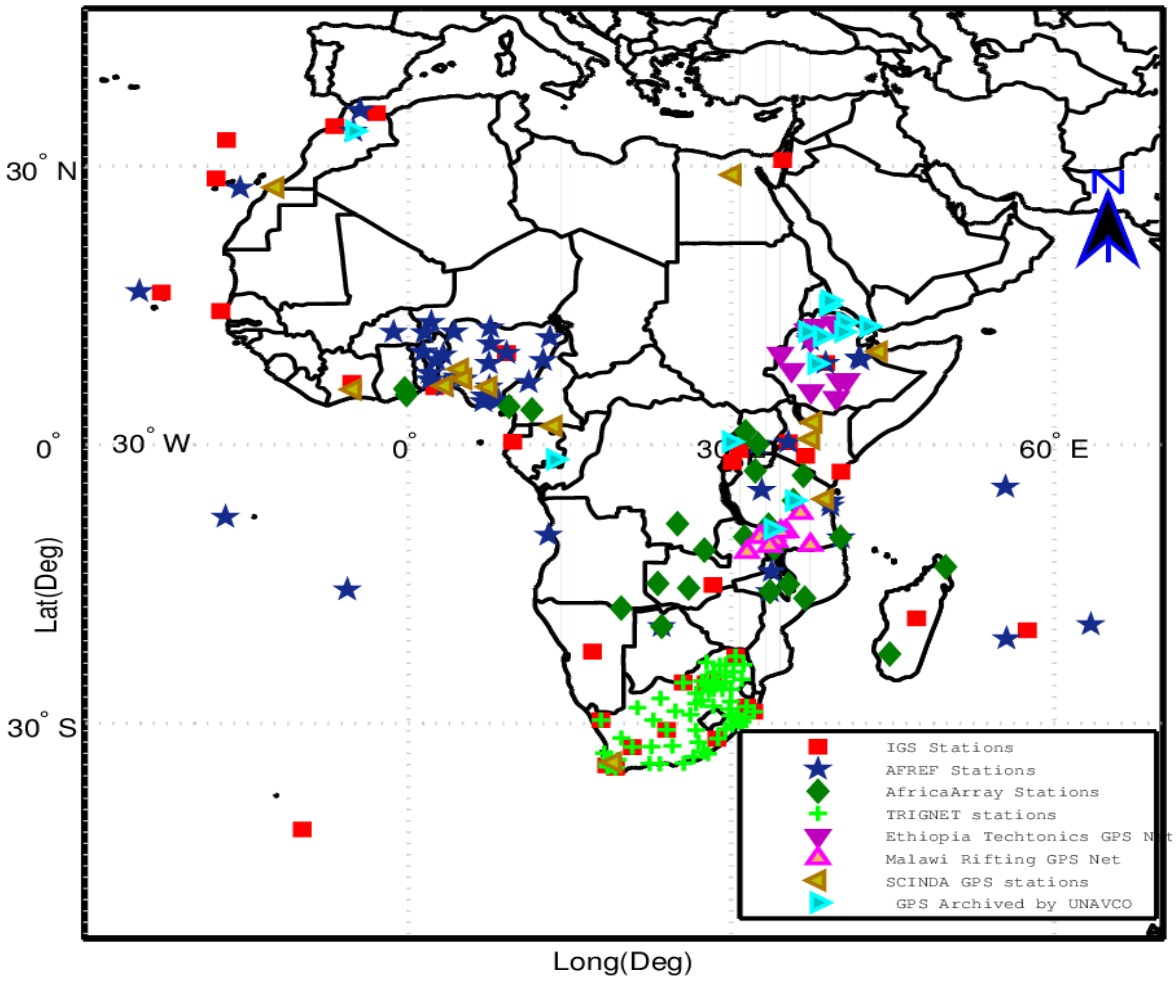

Figure 2.7: Distribution of IGS, AFREF stations and other GNSS stations/networks in Africa

2.5.2 Meteorological parameter modelling from Global/Regional Weather Models

A few continuous GNSS stations are equipped with meteorological sensors on the African network as shown in Figure (2.2). Meteorological sensors provide the unique advantage of obtaining on-site meteorological data directly at the continuous GNSS station. The primary disadvantage of GNSS meteorology packs is the lack of vertical temperature profiles necessary for computing the mean atmospheric temperature (T_m) and they often become noisy when left un-calibrated. Radiosondes offer the advantage of providing surface and vertical profiles of temperature, but only a few radiosondes exist close to stations within the existing African GNSS network. Radiosondes are expensive to launch and performance is hindered under bad weather condition. However, there are varieties of reanalysis models from which to obtain such data, which includes the following:

- The European Centre for Medium-Range Weather Forecasts (ECMWF) 40-year reanalysis (ERA-40) from 1957 - 2002 is based on the ECMWF three-dimensional

variational assimilation system and makes use of both conventional and satellite observations (Uppsala et al., 2005). The ERA-40 is a grid data set with a spectral resolution of $1.125^{\circ} \times 1.125^{\circ}$, at 60 hybrid vertical levels, at 0000, 0600, 1200, and 1800 UTC daily.

- The National Centres for Environmental Prediction/National Centre for Atmospheric Research (NCEP/NCAR) global reanalysis products (NNR-40) are available from 1948 to present. The NNR-40 is again a grid data set having grid size $1.875^{\circ} \times 1.875^{\circ}$, at 28 hybrid vertical levels, available at 0000, 0600, 1200, and 1800 UTC daily (Kalnay et al., 1996).
- The ECMWF Interim reanalysis from 1979 - present, only just recently released in 2011, based on the ECMWF4Dvariational assimilation systems in preparation for the reanalysis to replace ERA-40 (Dee et al., 2011). The ERA Interim is a grid data set with a spectral resolution of $0.75^{\circ} \times 0.75^{\circ}$, having 37 vertical pressure levels. The gridded data products include a large variety of 3-hourly surface parameters, describing weather as well as ocean-wave and land-surface conditions, and 6-hourly upper-air parameters covering the troposphere such as temperature and relative humidity. Vertical integrals of atmospheric fluxes, monthly averages for many of the parameters, and other derived fields have also been produced.

The recent release of ERA-Interim provides a clear advantage over ERA- 40 (Dee et al., 2011). Furthermore, ERA-Interim does not suffer the temporal limitations of ERA-40 thus making it currently the best source for surface pressure and vertical troposphere profiles of temperature and relative humidity necessary for GNSS meteorological calculation. There is a need to assess the applicability of these products in relation to Africa or to develop a regional model for GNSS applications.

2.5.3 Filling the Gaps with GNSS Radio Occultation (RO)

GNSS Radio Occultation (RO) is a kind of novel method for indirect measurement of temperature, pressure, and water vapour in the stratosphere and the troposphere. The technique is based on using the radio signals continuously broadcasted by the GNSS satellites orbiting the globe at an altitude of approximately 20000 kilometres above the surface from a high precision GNSS receiver mounted on a Low Earth Orbiting (LEO) satellite (Kishore et al., 2011). A GNSS radio occultation event (ROE) occurs when a GNSS satellite is setting or rising behind the Earth's limb as seen by a GNSS receiver aboard a LEO satellite. During an

ROE the transmitted signals from the GNSS satellite travelling to the LEO satellite are delayed because of the impacts of the atmosphere and ionosphere (Liou et al., 2007; Li, 2013). This delay can be precisely measured and converted to a vertical profile of bending angles and consequently processed to derive a refractivity profile by applying a series of transformation steps (Kursinski et al., 1995). The refractivity is a part of the electron density in the ionosphere and the temperature, pressure, and water vapour in the troposphere. Hence, the GNSS RO technique can offer useful information about the structure and dynamics of the ionosphere, stratosphere and troposphere.

The RO technique exhibits several beneficial features: First, RO measurements can be obtained under all-weather conditions and are available globally. Furthermore, the retrieved atmospheric profiles have high agreements with atmospheric profiles provided by other methods in the upper troposphere and lower stratosphere (UTLS) region, and the data also have high vertical resolution in the same atmospheric regions (Zhang et al., 2011). Secondly, its measurements are self-calibrated and have long-term stability, which makes RO data highly consistent and can be combined together without the need for inter-calibration (Foelsche et al., 2011).

Due to these features, the GPS RO technique has become a useful instrument for climate monitoring and has been widely applied in the subject area of the Earth's climate and weather. For instance, studies have shown the potential of GNSS RO profiles for characterizing troposphere structures and changes (e.g., Anthes, 2011) and the obtained results are found to be uniform with other observation data records. The RO data have also been employed for the study of the tropopause (e.g., Xu et al., 2011); atmospheric boundary layer (e.g., Sokolovskiy et al., 2006); diurnal tides (e.g., Pirscher et al., 2010); the global gravity wave signatures in the upper troposphere and stratosphere can be obtained from GNSS RO profiles (e.g., Torre et al., 2009). The RO data is also useful for severe weather prediction (e.g., Kuo et al., 2012). The RO data have also shown their usefulness in NWP systems. Research indicates that, after the RO data are ingested in the NWP systems, the quality of the weather forecast products is improved (e.g., Cucurull and Derber, 2008). In summation to the uses in neutral atmosphere, RO data have been successfully applied to the subject of the ionosphere and also space weather (e.g., Carter et al., 2013).

Many research works have shown that the GNSS RO Earth atmospheric observational technique can overcome the restrictions of current observing techniques, such as poor

sampling distribution, the low resolution of radiosondes (from land stations, ships and airplanes) and a low vertical resolution of down-looking satellites (Torre et al., 2009). Table (2.5) contains a comparison of the GNSS RO technique with Ground based GNSS receivers, radiosondes and remote sensing methods with regard to atmospheric observations. The outstanding technique for each category is highlighted in italics. The GNSS RO demonstrates significant advantages over the other three techniques.

Table 2.5: Comparison of GNSS RO with other atmospheric sounding techniques

	Ground-based GNSS	GNSS RO	Radiosonde	Satellite Remote sensing	VLBI	DORIS
Coverage	Ground based and limited by spatial accessibility	*Spaced based and global coverage*	Ground based and limited by spatial accessibility	*Spaced based and global coverage*	Ground based and limited by spatial accessibility	Ground based and limited by spatial accessibility
Vertical Resolution	Very low	*Very high*	High	Low	Very low	Very low
Horizontal resolution	Inhomogeneous	*Homogeneous, dependent on LEO orbit design*	Inhomogeneous	Uniform	Inhomogeneous	Inhomogeneous
Temporal Resolution	*Continuous, higher than other techniques*	Depending on LEO orbit design, normally higher than radiosonde	2-4 times per day	Depending on orbit design, normally higher than radiosonde	Not Continuous	Continuous
Water Condition	*All weather capability*	*All weather capability*	Unavailable in extreme weather conditions	Significantly affected by cloud and particles in the atmosphere	All weather capability	All weather capability
Cost	*Relatively cheap*	Low in a long term	High operation and maintenance cost	Low in a long term	Very Expensive	Low in a long term
Calibration	*Not required*	Not needed, mission independent	Necessary and important	Calibration needed for different instruments	Necessary and important	Necessary and important
Layers of Atmosphere	Not applicable	*All layers*	From the surface up to 30 km	Depending on instrument design	Not applicable	Not applicable
Accuracy	High	*High*	High	Low	*Very High*	High
Stability	*Very high*	*Very high*	Low	High	Very High	High

From the foregoing, the GNSS RO technique is seen as quite promising and stands to fill the existing gaps in atmospheric observation in Africa. It has brought a new impetus for scientists interested in Africa, where traditionally there have been very limited weather observations available. Many countries, such as the USA, Germany, Austria, the Russian Federation, Finland, Italy, Denmark, Argentina, and Brazil have established experimental GNSS RO meteorology projects and launched a number of LEO experimental satellites with GNSS RO receivers (Fu, 2011). New developments of the GNSS RO technique, such as the design of GNSS receivers and the LEO-LEO technique, will offer unprecedented opportunities to obtain a large amount of high-quality and high-resolution observations of the Earth's atmosphere (Kursinski et al., 2009). In the near future, with more GNSS RO satellites becoming available, both the weather and climate studies in previously data-sparse areas will be significantly improved. The GNSS RO missions will provide uniform global coverage observations and fill the geographical gaps from the station-based observation networks. Furthermore, the technique is "mission calibration free" and continuous quality data can be expected over a long-term from GNSS RO missions. This is an important improvement for climate studies such as trend analyses.

With the era of GPS modernization and significant expansion of other GNSS, new satellites with new signals have been developed. Within the next decade, about one hundred new GNSS satellites will be launched and thus new signals will be transmitted from them. These satellites will incorporate modernized GPS, GLONASS systems, and the newly designed Galileo. There are also some regional GNSS such as QZSS from Japan, BeiDou from China and the Indian IRNSS. The next generation RO missions (e.g. FORMOSAT-7/COSMIC-2) will be equipped with new GNSS RO receivers, which are designed to receive signals from these new satellites (Fu, 2011). The horizontal and temporal resolution of RO profiles will be significantly improved due to the increased number of satellites and the improved signal strength and signal spectrum. The quality of the RO technique will also be improved due to the increased number of radio frequencies available for the retrieval process. These new GNSS will utilize different radio frequencies and hence future GNSS RO missions will take advantage of the different signals to improve the retrieval process for better data quality. The continuous and accurate measurements of the atmospheric profiles with good spatial and temporal resolutions from GNSS RO will be available and new opportunities for better understanding of the Earth's atmosphere and ionosphere will follow (Anthes et al., 2000). Many meteorological and climate related applications, such as

numerical weather prediction analysis, climate studies, ionosphere and space weather conditions, will be passed on with the development of new generation GNSS and LEO satellite programs. Therefore, Africa stands to profit immensely from these future GNSS advancements, as they do not require African funding as in the case of ground based GNSS receivers, yet coverage will be the same over Africa as everywhere else with minor variations in latitude.

2.6 Concluding Remarks

The theory and practice of ground-based GNSS water vapour estimation has been systematically discussed and demonstrated in this paper. This is an attempt to analytically investigate ground-based GNSS meteorology issues in Africa. Ground-based GNSS meteorology is a very promising application, which could significantly improve numerical weather and storm predictions. Furthermore, it is of great benefit in climate applications. The application of GNSS meteorology has the benefit of being a more economical and efficient approach. It can be unattended for a long period of time with high reliability, and with low telemetry data transmission cost. The approach also has a high temporal and spatial resolution when compared with conventional weather balloons. Notwithstanding the scientific and societal applications of GNSS meteorology, most GNSS sites and networks on the African continent as identified in this study do not meet the standards required by the IGS, GRUAN and the WMO. South Africa is performing pretty well as a number of GNSS stations in the country have meteorological sensors collocated with them; the compactness of the GNSS network in South Africa appears to be well enough for GNSS meteorology, though more effort is still required. In particular, the Hartebeesthoek Radio Astronomy Observatory (HartRAO) in South Africa appears to be the only super-site that collocates other earth observation systems (seismometer, accelerometer and gravimeter) with GNSS stations (HRAO) and other space geodetic techniques i.e., VLBI, DORIS, WVR and Satellite Laser Ranging (SLR). However, hope is not lost for other African countries going by the different challenges that are unique for the individual countries, as solution were proffered in this review. Opportunities such as the African VLBI Network (AVN) (Gaylard et al. 2011) can be exploited for synergistic collocations where GNSS and other geodetic as well as geophysical equipment can be collocated. It is suggested that regional /global meteorological model (i.e., NCEP/NCAR and ERA Reanalysis) can be investigated for their accuracy on the continent and suitable interpolation algorithm needs to be developed to enable interpolation from such meteorological models to GNSS observation stations owing to the fact that there are no

meteorological sensors installed at most GNSS sites in Africa. Finally, as a step towards attaining an operational GNSS service on the African GNSS network, there is a need for clear policies on data sharing and collaboration among the different organisation that operates GNSS stations on the continent, the idea of collaboration is to add significant extra value to these existing infrastructures. Other potential applications and other techniques of GNSS measurements to meteorology should be explored i.e., GNSS-RO.

Acknowledgement

This study was supported by the University of Pretoria PhD research support grant to the first author. The authors are grateful to the numerous reviewers for the constructive comments that helped to improve the article.

Chapter 3

Evaluation of Spatial and Temporal Characteristics of GNSS-Derived ZTD Estimates in Nigeria**

"GNSS is an enabling technology that can make major contributions to economic growth and societal betterment. It is a key to scientific exploration"

…..P. Doherty 2010

Précis

This study presents an in-depth analysis to comprehend the spatial and temporal variability of zenith tropospheric delay (ZTD) over Nigeria during the period 2010–2014, using estimates from Global Navigation Satellite Systems (GNSS) data. GNSS data address the drawbacks in traditional techniques (e.g. radiosondes) by means of observing periodicities in ZTD. The ZTD estimates show weak spatial dependence among the stations, though this can be attributed to the density of stations in the network. Tidal oscillations are noticed at the GNSS stations. These oscillations have diurnal and semi-diurnal components. The diurnal components as seen from the ZTD are the principal source of the oscillations. This upshot may perhaps be ascribed to temporal variations in atmospheric water vapour on a diurnal scale. In addition, the diurnal ZTD cycles exhibited noteworthy seasonal dependence, with larger amplitudes in the rainy (wet) season and smaller ones in the harmattan (dry) season. Notably, the stations in the northern part of the country reach very high amplitudes in the months of June, July and August at the peak of the wet season, characterised by very high rainfall. This pinpoints the fact that in view of the small amount of atmospheric water vapour in the atmosphere, usually around 10%, its variations greatly influence the corresponding diurnal and seasonal discrepancies of ZTD. This study further affirms the prospective relevance of ground-based GNSS data to atmospheric studies. GNSS data analysis is therefore recommended as a tool for future exploration of Nigerian weather and climate.

*****This chapter consists of formatted text for one peer reviewed journal paper as follows:***

Isioye, O. A., Combrinck, L. & Botai, J.O. 2017. Evaluation of Spatial and Temporal Characteristics of GNSS-Derived ZTD Estimates in Nigeria, *Theoretical and Applied Climatology* (**Revised**)

3.1 Introduction and background

Radio signals broadcast from Global Navigation Satellite Systems (GNSS) satellites encounter a delay as they are transmitted via the atmosphere. By convention, delays along the line of sight to each satellite are mapped to one single parameter, often termed the zenith tropospheric delay (ZTD) (Stoew and Elgered, 2004). The ZTD is the summation of the 'hydrostatic or dry delay (ZHD)' and 'non-hydrostatic or wet delay (ZWD)' components. The ZHD represents about 90% of the ZTD; its value is roughly 2.3 m in the zenith direction and changes with local meteorological parameters (i.e. temperature and atmospheric pressure) at the GNSS site. The ZWD is generally smaller, from a few millimetres to about 40 cm (Andrei and Chen, 2009). Furthermore, under most weather conditions the ZWD experiences much more rapid variation than the ZHD and it is less probable, regardless of surface measurements (Andrei and Chen, 2009). ZWD can be converted into a measurement of precipitable water vapour (PWV) using appropriate formulations (Isioye et al., 2015). PWV is an essential element in energy transfer in the lower atmosphere and in the formation of clouds via latent heat, in the way it strongly influences the variables of numerical weather prediction (NWP) models either directly or indirectly (Jin et al., 2009).

ZTD is an essential parameter of the atmosphere, describing in part the various temporal and spatial characteristics of climatic weather and processes (Jin et al., 2007; 2009). Since the ZTD estimated from GNSS measurements is a function of both the pressure and water vapour in the atmosphere, it oscillates at tidal frequencies (Humphreys et al., 2005; Raju et al., 2009). The periods of tidal oscillations are a segment of a solar or lunar day. The solar diurnal (S1) and semi-diurnal (S2) tides have 24-hour and 12-hour periods, respectively, while the lunar diurnal period (M1) and semi-diurnal period (M2) are approximately 24.8 hours and 12.4 hours long, respectively *(*Jin et al., 2007; Raju et al., 2009*)*. The solar atmospheric tides can be energized in a number of ways, namely from the assimilation of solar radiation, the gravitational drag of the sun and the large-scale latent-heat discharge connected with deep convective clouds in the troposphere, while the lunar atmospheric tides result from the moon's gravity (Hagan et al., 2003). The diurnal cycle of ZTD is one of the most noticeable climate signals associated with most physical processes (such as atmospheric tides) that occur on a short-time scale (Jin et al., 2009).

GNSS-derived ZTD has high temporal resolution compared to classical techniques such as those using radiosondes (Jin et al., 2007; Emardson et al., 1998) and has several additional benefits, such as long-term stability and accessibility under all weather conditions

(Ware et al. 2000). In addition, GNSS-estimated ZTDs are extremely accurate and are known to be consistent with other observational systems, including very long baseline interferometry and radiosondes (Teke et al., 2011). Therefore, GNSS-derived ZTDs have been highly useful in the field of meteorology and climatology on diverse time scales (Jin et al., 2007; 2009). Studies of periodicities and intra-seasonal oscillations have used data from global GNSS to analyse the diurnal and semi-diurnal components of ZTD through harmonic functions, reporting the presence of seasonal ZTD cycles (Jin et al., 2007; 2009).

The Office of the Surveyor General of the Federation (OSGOF) initiated the Nigerian GNSS Reference Network (NIGNET) project in 2008, which has established 14 continuously operating reference stations (CORS) in several sites around the country (Jatau et al., 2010). These stations, illustrated on the map in Figure 3.1, are coordinated by nine international GNSS service (IGS) stations. The NIGNET stations alongside stations from the global IGS network are to contribute towards realisation of the unified African reference frame and also the International Terrestrial Reference Frame (Nwilo et al., 2013; Naibbi and Ibrahim, 2014).

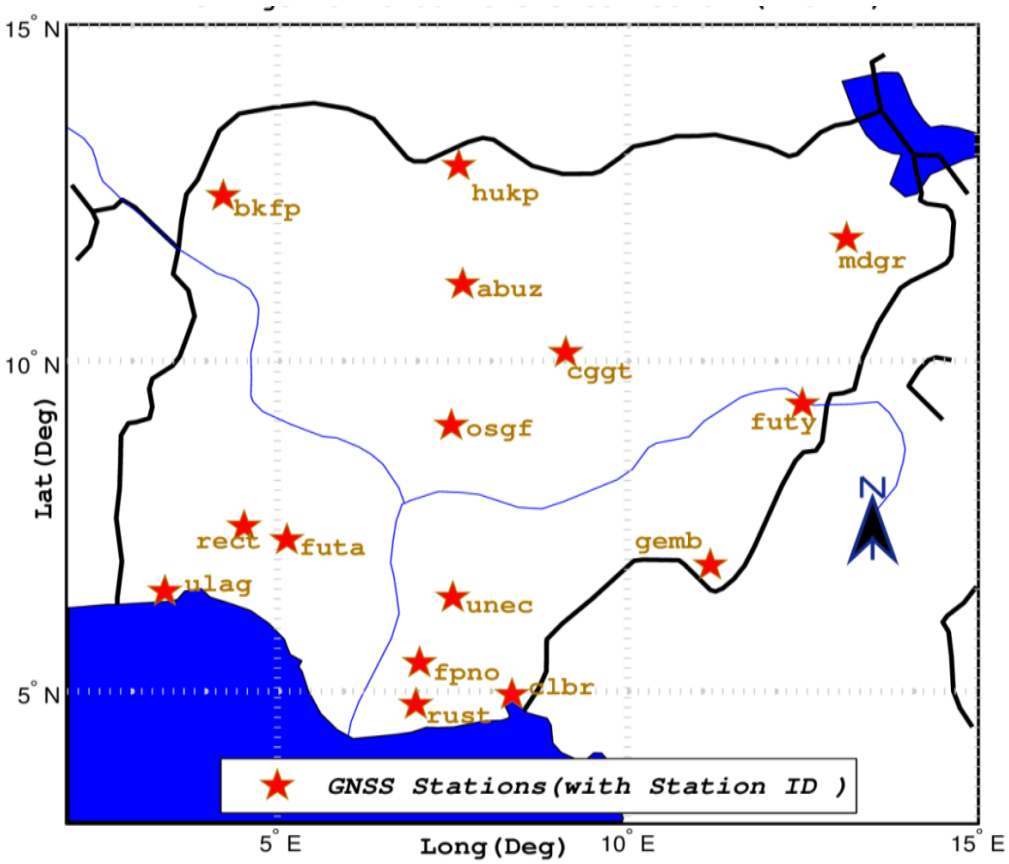

Figure 3.1: Map depicting the location of NIGNET GNSS CORS in Nigeria

The primary goal of this present study is to investigate the spatial and temporal variation of ZTD estimates over Nigeria. In order to understand its general characteristics, an analysis of the spatial and temporal variation of ZTD across the country was performed. This investigation focussed on spatial, diurnal and seasonal variation in a series of two-hourly ZTD estimates based on the 14 GNSS stations over the period 2010–2014. This analysis enables the characterisation of the nature and structure of the troposphere over Nigeria in both the local and the regional sense. In the subsequent section, the technique of 4.5-year (2010–2014) ZTD retrieval from the network of GNSS stations in Nigeria is briefly described. Overviews of the different time series tests (spatial regression models, white-noise test/spectral analysis, and test for stationarity) are discussed in the same section. Results of ZTD variability as observed from the NIGNET are given in the third section, and the final section concludes the document.

3.2 Material and Methods

GNSS data were collected from 14 GNSS CORS of NIGNET. The stations are shown in Figure 3.1. The data with a sampling rate of 30 seconds are publicly available via ftp//www.nignet.net or www.afrefdata.org in Receiver Independent Exchange (RINEX) format. GNSS data analysis was performed with the Massachusetts Institute of Technology (MIT) GAMIT/GLOBK software package, version 10.3 (Herring et al., 2006). The GAMIT/GLOBK software has the capacity to determine 3D positional information alongside tropospheric parameters, which encompasses the ZTD and atmospheric gradient components (Isioye et al., 2015a). The estimated two-hourly ZTDs over a period of 4.5 years were subjected to a spatial and temporal trend test in order to characterise the nature and structure of the troposphere over Nigeria. In the sub-sections that follow, we give an overview of the GNSS data processing and the statistical methods used in the study. All statistical analyses were performed using XLSTAT 2004 (www.xlstat.com) and GeoDA (Anselin, 2003; 2005; http://www.geoda.uiuc.edu). MATLAB software was used to create some of the plots that were presented.

3.2.1 GNSS Data Processing

So as to obtain high-grade ZTD estimates, the GNSS data-processing parameters and models were cautiously set up in the GAMIT/GLOBK software. The IGS final orbits and IGS final earth rotation products were used. Satellite elevation cut-off was set to 10° during the data processing. Station coordinates were heavily constrained to their International

Terrestrial Reference Frame (ITRF) 2008 values (Altamimi et al., 2011). Solid earth tide based on the IERS03 and FES2004 models was used for solid earth tide and ocean tide loading corrections. The constraint used for zenith delay was 0.2 m, as it is recommended to set it loosely enough to encompass any error in wet delay (Herring et al., 2006). Satellite antenna phase centre offset and phase centre variations are based on AZEL for IGS absolute ANTEX files (Gendt and Schmid, 2005). The a priori tropospheric model used is the Saastamoinen model (1972) based on meteorological sources from the global pressure and temperature (GPT) model. The Vienna Mapping Function (Boehm et al., 2006) was used to calculate the zenith delay. The ZTD at each GNSS station was estimated every two hours within a 24-hour window session. These estimations are adequate to characterise the diurnal and intra-seasonal patterns of ZTD in Nigeria and also to lessen the computational load resulting from a long observation period. Details of the strategy adopted for processing the GNSS data from the NIGNET stations has already been reported (Isioye et al., 2015a; 2016).

3.2.2 Spatial Auto-Correlation Analysis

The spatial structure of ZTD between the various stations was examined using spatial data analysis. Spatial data analysis requires the organisation of data in neighbouring clusters; these neighbours are homogeneous within and heterogeneous between certain variables. In spatial regression analysis, the assumptions of ordinary least-squares regression are violated; notably, the assumptions of homogeneity and of independence of error terms do not hold, since spatial dependence and spatial autocorrelation exist in the data.

A variable has spatial autocorrelation if observations that are closer to each other in space have related values. Spatial autocorrelation tests are essentially measures of the similarity between association in values (covariance, correlation or difference) and association in space (contiguity) (Anselin, 1992; Higazi et al., 2013).

There are different measures or indicators of spatial autocorrelation. The global indicators Moran's I (Moran, 1950) and Geary's C statistics (Geary, 1954) are often adopted because their statistical coefficient provides information about the degree and type of spatial autocorrelation available in a data set. Moran's I is a more acceptable measurement and is adopted in many applications and studies (Cliff and Ord, 1975), though Moran's I and Geary's C give comparable results. The Moran's I coefficient is defined as follows:

$$I = \left(\frac{n}{S_0}\right)\frac{\sum_{i=1}^{n}\sum_{j=1}^{n} w_{ij}\left(y_i - \bar{y}\right)\left(y_j - \bar{y}\right)}{\sum_{i=1}^{n}\left(y_i - \bar{y}\right)^2} \qquad (3.1)$$

In equation (3.1), n is the number of observation points, y is the observed point of data, and its corresponding mean is denoted by $\bar{y}$. The estimation of (I) depends on the weight matrix w_{ij} (with j as the nearest neighbour of i), and a wide range of criteria may be used to define neighbours, including a common boundary or distance bands. The weight matrix takes values of zeros and ones (i.e., $w_{ij} = 1$ if j is the nearest neighbour of i, and $w_{ij} = 0$ otherwise). Also, S_0 is the sum of the elements of the weight matrix, that is, $S_0 = \sum_{i=1}^{n}\sum_{j=1}^{n} w_{ij}$. Moran's I is comparable but not the same as a linear correlation coefficient, though it takes values from -1 to +1 (Teng et al., 2014). In the absence of autocorrelation, and irrespective of the specified weight matrix, the Moran's I statistic is of the form $-1/(n-1)$, and as the sample size increases it tends towards zero. The pattern of a distribution is considered random when no statistically significant spatial autocorrelation is observed.. When significant spatial autocorrelation (spatial dependence) exists, spatial heterogeneity also exists, with accordingly non-constant errors.

The introduction of spatial autoregressive models offers one promising support to report for the residual spatial autocorrelation. Several diagnostic tests could be used to test the significance of spatial effects. These notably include the Breusch Pagan test (Breusch and Pagan, 1979) for testing the homogeneity assumption, and Haining (2003) has introduced two spatial regression models, the spatial lag model (SLM) and the spatial error model (SEM). The SLM works best with phenomena where nearby values influence each observation through a migratory process. The SEM accounts better for spatial mismatch, when the process occurs on a scale different from the unit of observation, and in situations with missing variables. The maximum likelihood estimation procedure is used to estimate the parameters of both the SEM and SLM (Higazi et al., 2013).

Both the SLM and SEM were adopted in this study and evaluated using the GeoDa software package (Anselin, 2003; 2005). Using the likelihood ratio, the two models tested the following parameters, $H_0 : \rho = 0$ against $H_1 : \rho \neq 0$ and $H_0 : \lambda = 0$ against $H_1 : \lambda \neq 0$ for SLM and SEM, respectively. This study adopted the ordinary least squares (OLS) regression as the reference to which the SEM and SLM were compared.

3.2.3 Temporal Characteristics (Diurnal and Intra-Seasonal Trends)

3.2.3.1 The Mann Kendall Test

The Mann-Kendall statistical test is endorsed by the World Meteorological Organization (WMO) for the assessment of trends in meteorological data (Mithell et al., 1966). The Mann-Kendall statistical test does not necessitate that data be normally distributed, since it is non-parametric in nature and responds to unexpected breaks that often come with inhomogeneous time series with little sensitivity (Karmeshu, 2012). The test's null hypothesis H_0 assumes that there is no trend in the analysed records. This is tested against the alternative hypothesis H_1, which assumes that there is a trend. For a time series $X_t = \{x_1, x_2, ..., x_n\}$, the Mann-Kendall test statistic S is computed as follows:

$$S = \sum_{i=1}^{n-1} \sum_{j=i+1}^{n} sign\left(x_j - x_i\right) \tag{3.2}$$

$$sign\left(x_j - x_i\right) = \begin{cases} 1 & if\ x_j - x_i > 0 \\ 0 & if\ x_j - x_i = 0 \\ -1 & if\ x_j - x_i < 0, \end{cases}$$

When S is high and positive, it implies that the trend is increasing, while a decreasing trend is indicated by very low negative values (Adamowski and Prokoph, 2013). However, to quantify the significance of the trend statistically, it is essential to compute the probability linked with S and the sample size n. Since we typically assume that data are independent and randomly distributed, thus, the mean of S is zero and the variance is defined by:

$$Var\left(S\right) = \frac{n\left(n-1\right)\left(2n+5\right) - \sum_{i=1}^{m} t_i \left(t_i - 1\right)\left(2t_i + 5\right)}{18} \tag{3.3}$$

In equation (3.3), m is the number of groups of tied ranks (equal observations), each having t_i tied observations. The standard test statistic Z_S is then estimated as follows (Karmeshu, 2012):

$$Z_S = \begin{cases} \dfrac{\left(S+1\right)}{\sqrt{Var\left(S\right)}} & S < 0 \\ 0 & S = 0 \\ \dfrac{\left(S+1\right)}{\sqrt{Var\left(S\right)}} & S < 0 \end{cases} \tag{3.4}$$

Positive values of Z_S indicate increasing trends, while negative values represent decreasing trends. When testing increasing or decreasing monotonic trends at a significance level α, the null hypothesis is rejected for an absolute value of Z_S greater than $Z_{1-\alpha/2}$ (Batisani, 2011). This study applied a significance level of $\alpha = 0.05$, so the corresponding value of $Z_{1-\alpha/2}$ is 1.96. XLSTAT 2014 software was used to perform the statistical Mann-Kendall test.

3.2.3.2 Spectral analysis and testing for white noise

Spectral analysis is a statistical approach to detect regular cyclical patterns, or periodicities in a given data set. Spectral analysis involves the application of finite Fourier transforms in the decomposing data into waves of varying amplitudes and wavelengths. Hence, the Fourier transform decomposition of the time-series model (Y_t) is articulated in terms of sine and cosine components, as follows (Paun et al., 2009):

$$Y_t = \sum_{k=1}^{m} \left(A_k \cos(\omega_k t) + B_k \sin(\omega_k t) \right) + e_t \qquad (3.5)$$

In equation (3.5), N is the number of observations in the original time series (Y_t), m is the number of frequencies in the Fourier decomposition. Thus, $m = N/2$ if N is even, or $m = (N-1)/2$ if N is odd. A_k and B_k denote the cosine and sine coefficients indicative of the amplitude, or height, of the cosine and sine components, respectively. ω_k denotes the Fourier frequencies, $2\pi k/N$, where $k = 1, 2, ..., m$ and $0 \le \omega_k \le \pi$. The random error term is represented as e_t.

In this paper the spectral analysis was performed using the XLSTAT software package. This task was performed using the spectral analysis option from the XLSTAT-Time menu. The estimates from the software are reported as either periodograms or as spectral density estimates. Plots of the periodogram and spectral density against the frequency or period are often used to identify periodicity in time series. Thus, plots from negatively correlated series often have low and high frequencies corresponding to low and high ordinates; this is suggestive of short cycles. Conversely, positively correlated series have long sinusoidal cycles and are characterized by high ordinates at low frequencies and vice versa. Also, a horizontal line symbolises the spectrum for a white-noise process (Tian and Fernandez, 1999). XLSTAT software was again employed to test for white noise in the time series. It optionally displays two test statistics (Fisher's kappa and Bartlett's

Kolmogorov-Smirnov statistic) and the corresponding p-values. According to both tests, the null hypothesis H_0 assumes that a time series is white noise. Thus, when the corresponding p-values are lower than the significance level (typically 0.05), H_0 is rejected (see http://www.xlstat.com~ /xlstattime_help.pdf). Fisher's kappa tests the alternative hypothesis that the series contains an added deterministic cyclic or seasonal constituent of unstipulated regularity (frequency) against the null hypothesis that the series is white noise. On the other hand, the Bartlett Kolmogorov-Smirnov test puts side by side the normalized aggregated periodogram with the uniform aggregated distribution function to test the null hypothesis that the series is white noise (Paun et al., 2009).

3.2.3.3 Test for Stationarity

A stationary time series is one whose statistical properties (mean, variance, autocorrelation etc), do not depend on the time at which the series is observed (i.e., is constant over time). The majority of time series methods are from the supposition of time series data being roughly stationary (i.e., "stationarized"). Identifying that a series is not stationary allows later analysis of how the non-stationarity arose. A non-stationary series can still be stationary in difference or stationary in trend and it is often difficult to distinguish between the different states (MacKinnon, 1996). The *unit root test* is often employed to help achieve a more perfect riposte to the problem. Stationarity tests verify whether a series is stationary or not, and they take two different approaches. Some tests consider as the null hypothesis H_0 that the series is stationary (e.g., KPSS test, Leybourne and McCabe test), while other tests consider as the null hypothesis, on the contrary, that the series is not stationary (e.g., Dickey-Fuller (DF) test, augmented DF test, Phillips-Perron test, DF-GLS test). The version of XLSTAT software used in this study includes the KPSS and DF tests.

The DF (Dickey and Fuller, 1979) test allows one to identify a unit root in a time series. Unit root tests are applicable if the time series Y_t is well categorized by an auto-regressive (AR (1)) model with white noise errors. Considering an AR (1) regression model:

$$y_t = \theta_{y_{t-1}} + \varepsilon_t \qquad (3.6)$$

The unit-root null hypothesis against the stationary alternative corresponds to $H_0 : \theta = 1$ against $H_A : \theta < 1$. Alternatively, the model can be formulated as:

$$\Delta y_t = (\theta - 1) y_{t-1} + \varepsilon_t = \pi y_{t-1} + \varepsilon_t \qquad (3.7)$$

where $\pi = \theta - 1 = \theta(1)$. The unit-root hypothesis then translates into $H_0 : \pi = 0$ against $H_A : \pi < 0$. The DF test is simply the t-test for H_0, given by:

$$\hat{\tau} = \frac{\hat{\theta} - 1}{SE(\hat{\theta})} = \frac{\hat{\pi}}{SE(\hat{\pi})} \qquad (3.8)$$

XLSTAT estimates critical values and p-values for the number of observations used to compute the statistics by running Monte Carlo simulations each time the function is run.

The KPSS test was proposed by Kwiatkowski, Phillips, Schmidt and Shin (1992) and allows one to test the null hypothesis that the series is stationary. In the model:

$$y_t = \varepsilon_t + e_t \qquad (3.9)$$

where e_t is the stationary error, and ε_t is the random walk defined by $\varepsilon_t = \varepsilon_{t-1} + \nu_t$, if the variance is zero, $\sigma_\nu^2 = 0$, then $\varepsilon_t = \varepsilon_0$ for all t and y_t is stationary. Using a linear regression of model $y_t = \hat{\mu} + \hat{e}_t$, the stochastic component is estimated under the null hypothesis, since $\hat{e}_t$ is stationary. Thus, that observation is used to design a test of $H_0 : \sigma_\nu^2 = 0$ against $H_A : \sigma_\nu^2 > 0$. The test statistic is given by:

$$KPSS = \frac{1}{T^2} \frac{\sum_{t=1}^{T} S_t^2}{\hat{\sigma}_\infty^2} \qquad (3.10)$$

where $S_t = \sum_{s=1}^{t} \hat{e}_s$ is a partial sum, and $\hat{\sigma}_\infty^2$ is a heteroskedasticity and autocorrelation consistent estimation of the variance of $\hat{e}_t$.

As with the DF test, these statistics are easy to compute, but their exact and asymptotic distributions are complex. Kwiatkowski et al. (1992) computed the asymptotic critical values using Monte Carlo simulations. XLSTAT allows computation of critical values and p-values adapted to the size of a particular sample, using Monte Carlo simulations for each new run.

3.3 Results and Discussions

ZTD varies both spatially and temporally across the world. Since the ZTD estimated from GNSS is a function of pressure, water vapour and other climatic indices in the atmosphere, which all exhibit periodic variation, ZTD is expected to behave in a similar fashion. This section presents a detailed analysis of the spatial and temporal variability of ZTD over Nigeria during the period 2010–2014 using estimates from GNSS. Remarkably, in West Africa, the climate of Nigeria changes more than that of any other country owing to its location and latitudinal extent (about 1100 km). Consequently, nearly all of the climatic zones of West Africa are contained by Nigeria's precincts. The Nigerian climate is characterised by strong latitudinal zones, as is the case in the West African region. Rainfall is the key climatic variable in explaining the Nigerian climate, as is the impact of wind currents, namely "the equatorial easterlies", "the tropical continental air mass" and "the tropical maritime air mass". Generally, it gets drier as one moves north from the southern coast of the country (Oginni and Adebamowo, 2013).

3.3.1 Spatial Characteristics

The spatial pattern of a distribution is defined by the composition of distinct individual units in space and the geographic association among them. The ability to evaluate spatial patterns is a precondition to understanding the complicated spatial processes responsible for the distribution of a phenomenon.

The spatial variability of ZTD over different GNSS stations depends strongly on their latitude, season, and other natural factors of multivariate source. To analyse this spatial variability, a spatial regression method is used. A fundamental concept in the analysis of spatial autocorrelation for real data is the spatial weights matrix. In this study, a spatial weights matrix of the queen-first order was used to formalize the notion of location. The spatial weights are presented in Figure 3.2.

The result of the OLS regression, as shown in Table 3.1, indicates that the R^2 value across the different months is strong; thus, the model proved significant $(p < 0.05)$. Also, the global Moran autocorrelation coefficient value for the entire dataset is 0.1769, reflecting a weak correlation. Diagnostic tests for OLS assumptions showed no problem involving multi- colinearity. The Jarque-Bera test across all the months reveals that errors are normally distributed; that is, $(p < 0.05)$ for all months. The Breusch-Pagan test shows a non-

heterogeneity of error variance across all the months. The average values of three reference criteria across the months, namely the log likelihood, the Akaike information criterion and the Schwarz information criterion, are -86.8733, 181.746, and 184.3028, respectively. According to Anselin (2005), a well-fitted model comes with a high log likelihood value, while for the Akaike and Schwarz information criterion a low measure indicates a better fit.

Since all the assumptions of the OLS model were not satisfied, particularly the test of spatial dependence (Morgan I), which revealed weak correlation, it was important to look at the SEM and SLM. The SEM and SLM have, respectively, average R^2 values of 39 % and 43.82 % across all the months. The SEM lag coefficient $\lambda = 1.4$ is significant $(p < 0.05)$, like the SLM lag coefficient $\rho = 0.7143$ $(p < 0.05)$, as shown in Tables 3.3 and 3.4, respectively.

	ABUZ	BKFP	CGGT	CLBR	FPNO	FUTA	FUTY	GEMB	HUKP	MDGR	OSGF	RUST	ULAG	UNEC
ABUZ		1	1	0	0	0	0	0	1	0	1	0	0	0
BKFP	1		1	0	0	0	0	0	1	0	0	0	0	0
CGGT	1	1		0	0	0	1	1	0	1	1	0	0	0
CLBR	0	0	0		1	0	0	1	0	0	0	1	0	1
FPNO	0	0	0	1		0	0	0	0	0	0	1	0	1
FUTA	0	0	0	0	0		0	0	0	0	0	0	1	1
FUTY	0	0	1	0	0	0		1	0	1	1	0	0	0
GEMB	0	0	1	1	0	0	1		0	1	0	0	0	0
HUKP	1	1	0	0	0	0	0	0		0	0	0	0	0
MDGR	0	0	1	0	0	0	1	1	0		0	0	0	0
OSGF	1	0	1	0	0	0	1	0	0	0		0	0	1
RUST	0	0	0	1	1	0	0	0	0	0	0		0	1
ULAG	0	0	0	0	0	1	0	0	0	0	0	0		0
UNEC	0	0	0	1	1	1	0	0	0	0	1	1	0	

Figure 3.2: Chart showing weights matrix for GNSS stations

Table 3.1: Summary of statistics for OLS regression model

	Jan	Feb	Mar	Apr	May	Jun	Jul	Aug	Sep	Oct	Nov	Dec
	Model coefficient											
R^2	0.4629	0.5171	0.5613	0.3113	0.4359	0.4684	0.4140	0.3711	0.4381	0.5043	0.6428	0.6563
f-statistics	0.0000	0.0000	0.0000	0.0000	0.0000	0.0000	0.0000	0.0000	0.0000	0.0000	0.0000	0.0000
	Diagnostics for Spatial Dependence (Morgan I test)											
I	-0.1769	-0.1769	-0.1769	-0.1769	-0.1769	-0.1769	-0.1769	-0.1769	-0.1769	-0.1769	-0.1769	-0.1769
p-value	--	--	--	--	--	--	--	--	--	--	--	--
	Reference Criterion for OLS											
Log likelihood	-86.819	-86.9118	-86.9837	-87.8348	-87.1633	-87.1856	-87.2518	-87.2403	-87.2774	-86.921	-85.448	-85.4426
AIC	181.63	181.824	181.967	183.67	182.327	182.371	182.504	182.481	182.555	181.842	178.896	178.885
SC	184.194	184.38	184.524	186.226	184.883	184.927	185.06	185.037	185.111	184.398	181.452	181.441
	Diagnostics for Heteroskedasticity (Breusch-Pagan Test)											
Breusch-Pagan Test value	7.5048	8.2799	7.8924	7.8924	10.6199	10.4088	10.7157	10.0501	10.1115	11.1059	10.2009	9.1555
p-value	0.05744	0.04057	0.04829	0.04829	0.01397	0.01539	0.01337	0.01815	0.01764	0.01117	0.01693	0.02729
	Test for normality											
Jarque-Bera Test value	10.6265	12.6078	11.4499	13.0517	10.7201	8.0108	7.8551	6.6011	6.4233	8.4201	11.0445	8.0784
p-value	0.00493	0.00183	0.00326	0.00147	0.00470	0.01822	0.01969	0.03686	0.04029	0.01485	0.00400	0.01761

Table 3.2: Summary of statistics for SEM

	Jan	Feb	Mar	Apr	May	Jun	Jul	Aug	Sep	Oct	Nov	Dec
	Model coefficient											
R^2	0.3410	0.4075	0.4617	0.4617	0.3079	0.3478	0.2810	0.2283	0.3106	0.3918	0.5618	0.5783
Lambda (λ)	1.4	1.4	1.4	1.4	1.4	1.4	1.4	1.4	1.4	1.4	1.4	1.4
p-value	0.0000	0.0000	0.0000	0.0000	0.0000	0.0000	0.0000	0.0000	0.0000	0.0000	0.0000	0.0000
	Information Criterion for SEM											
Log likelihood	-86.0458	-86.1386	-86.2105	-86.2105	-86.3901	-86.4124	-86.4787	-86.4671	-86.5042	-86.1478	-84.6748	-84.6694
AIC	180.092	180.277	180.421	180.421	180.78	180.825	180.957	180.934	181.008	180.296	177.35	177.339
SC	182.648	182.833	182.977	182.977	183.337	183.381	183.514	183.49	183.565	182.852	179.906	179.895
	Diagnostics for Heteroskedasticity (Breusch-Pagan Test)											
Breusch-Pagan Test value	7.5048	8.2799	7.8924	7.8924	10.6199	10.4088	10.7157	10.0501	10.1115	11.1059	10.2009	9.1555
p-value	0.05744	0.04057	0.04829	0.04829	0.01397	0.01539	0.01337	0.01815	0.01764	0.01117	0.01693	0.02729
	Diagnostics for Spatial Dependence (Likelihood Ratio test)											
Likelihood Ratio value	1.5464	1.5464	1.5464	1.5464	1.5464	1.5464	1.5464	1.5464	1.5464	1.5464	1.5464	1.5464
p-value	0.21367	0.21367	0.21367	0.21367	0.21367	0.21367	0.21367	0.21367	0.21367	0.21367	0.21367	0.21367

Table 3.3: Summary of statistics for SLM

	Jan	Feb	Mar	Apr	May	Jun	Jul	Aug	Sep	Oct	Nov	Dec
	Model coefficient											
R^2	0.4023	0.4625	0.5118	0.4104	0.3722	0.4084	0.3478	0.3001	0.3747	0.4483	0.6025	0.6175
Rho (ρ)	0.7143	0.7143	0.7143	0.7143	0.7143	0.71423	0.7143	0.7143	0.7143	0.7143	0.7143	0.7143
p-value	0.00051	0.00051	0.00051	0.00051	0.00051	0.00051	0.00051	0.00051	0.00051	0.00051	0.00051	0.00051
	Information Criterion for SLM											
Log likelihood	-86.0458	-86.1386	-86.2105	-87.0616	-86.3901	-86.4124	-86.4786	-86.4671	-86.5042	-86.1478	-84.6748	-84.6694
AIC	182.092	182.277	182.421	184.123	182.78	182.825	182.957	182.934	183.008	182.296	179.35	179.339
SC	185.287	185.472	185.616	187.318	185.976	186.02	186.153	186.129	186.204	185.491	182.545	182.534
	Diagnostics for Heteroskedasticity (Breusch-Pagan Test)											
Breusch-Pagan Test value	7.5048	8.2799	7.8924	7.8924	10.6199	10.4088	10.7157	10.0501	10.1115	11.1059	10.2009	9.1555
p-value	0.05744	0.04057	0.04829	0.04829	0.01397	0.01539	0.01337	0.01815	0.01764	0.01117	0.01693	0.02729
	Diagnostics for Spatial Dependence (Likelihood Ratio test)											
Likelihood Ratio value	1.5464	1.5464	1.5464	1.5464	1.5464	1.5464	1.5464	1.5464	1.5464	1.5464	1.5464	1.5464
p-value	0.21367	0.21367	0.21367	0.21367	0.21367	0.21367	0.21367	0.21367	0.21367	0.21367	0.21367	0.21367

From Tables 3.2 and 3.3, it is evident that the reference criteria (log likelihood, Akaike information criterion, and Schwarz criterion) from SEM and SLM differ neither from each other nor from those of the OLS. A very close inspection of the reference information criterion does reveal that SLM is slightly better than the others.

Again from Tables 3.2 and 3.3, in order to account for spatial errors in the models, the Breusch-Pagan test for heteroskedasticity shows non-heterogeneity of error variance across all the months. Interestingly, once more the values are the same in all three models.

A final diagnostic test is the asymptotic significance test on the spatial autoregressive coefficient; the likelihood ratio test is one of the three classical approaches that are used to compare the OLS to the alternative spatial models (SEM and SLM). The results of the likelihood ratio test are, as seen in Tables 3.2 and 3.3, the same for both models, with a non-significant value of 1.5464 confirming the weak significance of the spatial autoregressive coefficient in SEM and SLM. Thus, based on the foregoing, since some assumptions of autocorrelation were satisfied in the OLS, SEM and SLM, it can be concluded that weak spatial autocorrelation exists among the stations.

Importantly, the density of the stations in the network may have greatly influenced the results of the spatial models. Previous studies and reports have shown the strong dependence of ZTD on station elevation, and latitude in a small or local network (Isioye et al. 2014; 2015). Thus, differences in elevation between different stations could have affected their spatial dependence.

3.3.2 Temporal Characteristics (Diurnal and Intra-Seasonal Trends)

Figures 3.3 and 3.4 illustrate the two-hour, average daily (diurnal) and month-to-month (intra-seasonal) area charts of ZTD estimates for 2010–2014. Figure 3.3 indicates that there is no definite trend in the pattern of the daily ZTD estimates at the different stations. However, Figure 3.4 clearly illustrates fluctuations in the datasets across the different months and stations, fluctuations that are fitted with a third-order polynomial trendline. This type of trendline, with one or two minimums or maximums, accurately describes the two distinct seasons in Nigeria: the rainy season and the dry season. Basically, the seasons in Nigeria are governed by the north-east wind typically blowing from late November to mid-March and the tropical continental air mass (south-west wind). The latter originates from the South Atlantic Ocean and comes with the rain, while the earlier is a dust-laden air mass from the Sahara desert often referred to as the harmattan. These two major wind systems are known as the trade winds. In the coastal and south-eastern regions

of Nigeria, the rainy season usually begins in February or March and travels north, reaching most areas by early summer, with rain lasting through September. While the northern part of the country typically has its highest rainfall during August, the coastal areas experience most precipitation in May, June and October. Farther north, it is usually June or July before the rains really commence. Northern Nigeria has a dry season lasting from October to April, with high temperatures and low humidity. The southern coastal regions see a shorter dry season from December to February, as they are closer to the damp ocean winds.

The plots in Figure 3.4 show good agreement with the rainfall/precipitation pattern in Nigeria, and they also demonstrate the latitudinal dependence of ZTD estimates. The stations ABUZ, BKFP, CGGT, FUTY, GEMB, HURK, MDGR, and OSGF, which are all in the northern part of Nigeria, have very low values of ZTD in the months of November, December, January, February, March and April; their highest values occur in the other months, corresponding to the rainy season. The higher values of ZTD can then be attributed to water vapour content, which is often higher during the wet season. The stations in the south — CLBR, FPNO, FUTA, RUST, ULAG, and UNEC — have very high ZTD values throughout the year, except in January and December, which comprise the short dry season in these areas. Humidity is often very high in the southern part of Nigeria and comes with prolonged rainfall during the wet season. Figure 3.4 again confirms the strong correlation between precipitation and ZTD, as both reach their peaks in the months of June, July, August and September across Nigeria.

From the foregoing, it is evident that those seasons that result from planetary oscillations strongly correlate with the corresponding seasonal ZTD time series. A better understanding of these prevailing oscillations will help to improve the periodic models used to estimate ZTD.

Figure 3.3: Area chart of mean, 2-hourly ZTD estimates over Nigeria from 2010–2014

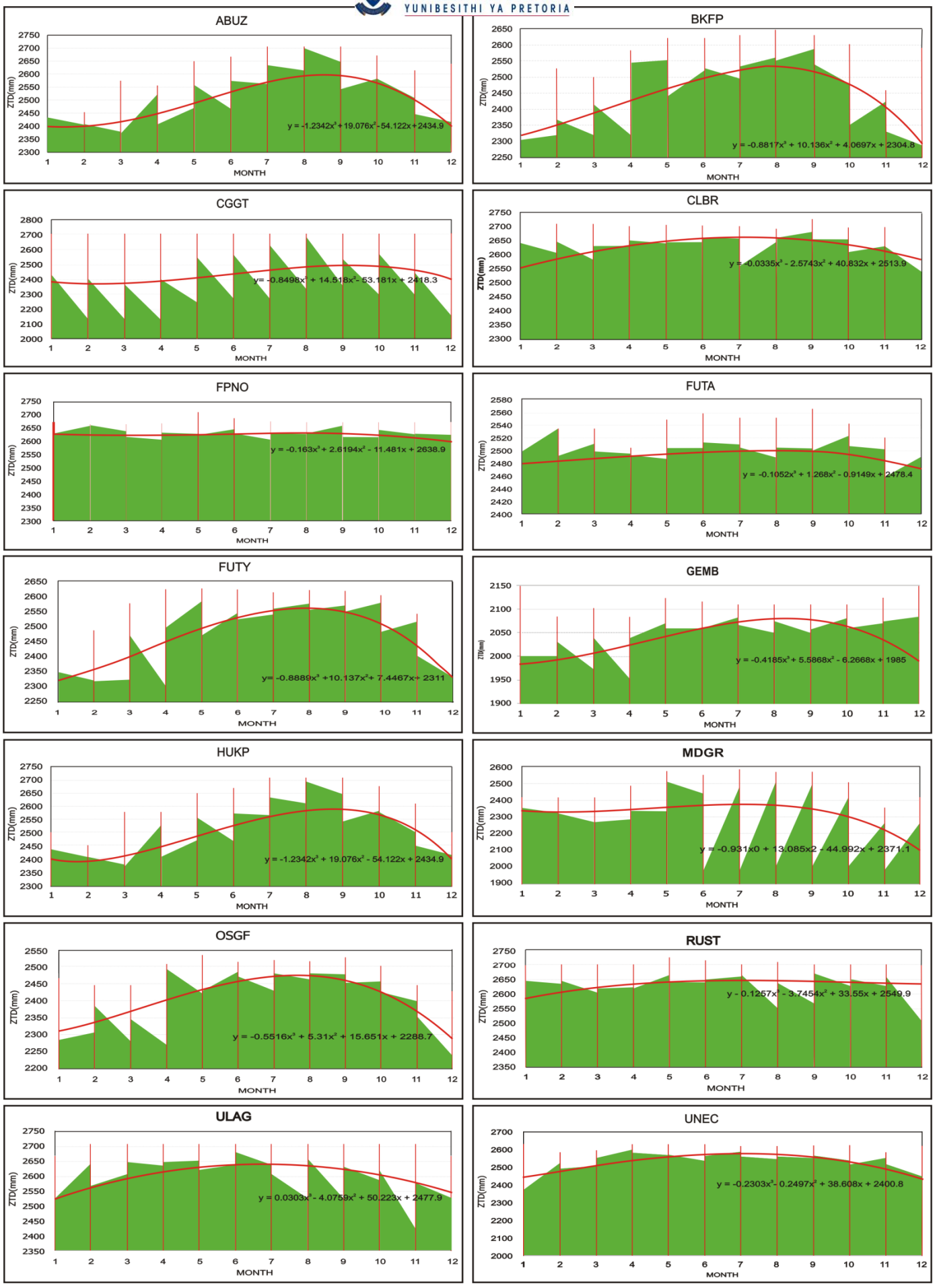

Figure 3.4: Area chart of mean, monthly ZTD estimates over Nigeria from 2010–2014

The result of the Mann-Kendall test on the two-hourly/daily ZTD data is presented in Table 3.4a for the 14 stations. If the significance level α (alpha) = 0.05 is greater than the p value, H_0 is rejected. Rejecting H_0 implies that there is a trend in the time series, while accepting H_0 implies no trend was detected (Karmeshu, 2012; www.xlstat.com). Table 3.4a reveals that the null hypothesis was accepted for only one station, MDGR. Also, the MK test on the month-to-month (intra-seasonal) ZTD data gave similar results, as shown in Table 3.4b; the null hypothesis was again accepted at the same, single station (MDGR). The MK test yields interesting insight into the diurnal and intra-seasonal ZTD data for Nigeria. The intra-seasonal trend has a stronger correlation than the diurnal trend.

Table 3.4a: Summary of results for the Mann-Kendall trend test based on two-hourly ZTD data over Nigeria

Mann-Kendall Trend Test						
Station	**Mann-Kendall Statistics (S')**	**Kendall's tau**	**Var (S)**	**p-value (Two-tailed)**	**alpha**	**Test Interpretation**
ABUZ	366721	0.021	930247282102.333	< 0.0001	0.05	***Reject H_0 (There is trend in time series)***
BKFP	99171	0.006	937688749543.333	< 0.0001	0.05	***Reject H_0***
CGGT	2389054	0.037	6892848566629.000	< 0.0001	0.05	***Reject H_0***
CLBR	127640	0.026	141235146242.333	0.0045	0.05	***Reject H_0***
FPNO	26822	0.016	28281837406.333	0.0206	0.05	***Reject H_0***
FUTA	64982	0.044	23516866705.000	0.003	0.05	***Reject H_0***
FUTY	-163229	-0.014	505733161003.667	0.0630	0.05	***Reject H_0***
GEMB	80094	0.041	35987524776.667	0.0022	0.05	***Reject H_0***
HUKP	24591	0.020	17744891268.667	0.00289	0.05	***Reject H_0***
MDGR	-6224	-0.007	10615306133.000	0.0762	0.05	***Accept H_0 (There is no trend in time series)***
OSGF	125178	0.022	180317206491.000	< 0.0001	0.05	***Reject H_0***
RUST	36004	0.012	68924543036.000	0.0357	0.05	***Reject H_0***
ULAG	-52450	-0.012	125616762453.000	< 0.0001	0.05	***Reject H_0***
UNEC	-27729	-0.005	191544197854.333	< 0.0001	0.05	***Reject H_0***

Table 3.4b: Summary of Results for the Mann-Kendall Trend Test based on monthly ZTD data over Nigeria

Mann-Kendall Trend Test						
Station	**Mann-Kendall Statistics (S')**	**Kendall's tau**	**Var (S)**	**p-value (Two-tailed)**	**alpha**	**Test Interpretation**
ABUZ	1069090.000	0.062	930247282034.667	< 0.0001	0.05	***Reject H_0 (There is trend in time series)***
BKFP	2373574.000	0.138	937688749543.333	< 0.0001	0.05	***Reject H_0***
CGGT	7183809.000	0.110	6892848566629.000	< 0.0001	0.05	***Reject H_0***
CLBR	-126149.000	-0.026	141235146242.333	0.043	0.05	***Reject H_0***
FPNO	-121893.000	-0.073	28281837406.333	< 0.0001	0.05	***Reject H_0***
FUTA	65451.000	0.044	23516866705.000	0.002	0.05	***Reject H_0***
FUTY	1943973.000	0.170	505733161003.667	< 0.0001	0.05	***Reject H_0***
GEMB	371304.000	0.190	35987524776.667	< 0.0001	0.05	***Reject H_0***
HUKP	-329771.000	-0.270	17744891268.667	< 0.0001	0.05	***Reject H_0***
MDGR	-13353.000	-0.015	10615306133.000	0.441	0.05	***Accept H_0 (There is no trend in time series)***
OSGF	366839.000	0.064	180317206491.000	< 0.0001	0.05	***Reject H_0***
RUST	488149.000	0.162	68924543036.000	< 0.0001	0.05	***Reject H_0***
ULAG	610629.000	0.135	125616762453.000	< 0.0001	0.05	***Reject H_0***
UNEC	153224.000	0.026	191544197854.333	0.052	0.05	***Reject H_0***

The MK test statistic (S') from Table 3.4a shows that there is a rising ZTD trend for the stations of ABUZ, BKFP, CGGT, CLBR, FPNO, FUTA, GEMB, HUKP, OSGF and RUST. The S' statistic, however, is not very strong for all the stations, suggesting that the trend is not strong. Upon further analysis of the S' statistic, as shown in Table 3.4b, it becomes evident that the trend is stronger there than previously, with only four stations (CLBR, FPNO, HUKP, and MDGR) exhibiting a negative trend. It is pertinent to note that the MK test often requires longer time series to conclusively analyse trend in a given dataset, however, our study was able meet the minimum required time series as GNSS data from the NIGNET were only available over Nigeria from 2010and afterwards.

It is conventional to ascertain if the trends observed in Tables 3.4a and 3.4b display some hidden periodicity, small periodic variations hidden behind irregular fluctuations that are not flat spectrum (or white noise) over the range of frequencies. In Tables 3.5a and 3.5b the results of the Fisher's kappa and Bartlett's Kolmogorov tests are presented for the diurnal

and intra-seasonal ZTD estimates, respectively. These test whether the time series can be considered white noise or not. In both cases, when considering the p-values for the Fisher's kappa and Bartlett's Kolmogorov-Smirnov tests, it is clear that the series is significantly different from white noise at the significance level of 0.05 for all stations.

Table 3.5a: Results of white-noise tests for 2-hourly ZTD data over Nigeria

Station	Fisher's kappa		Bartlett's Kolmogorov-Smirnov		Test Interpretation
	Value	p-value	Value	p-value	
ABU	6552.987	< 0.0001	0.846	< 0.0001	***Reject H_0 (Trend is significantly different from white noise)***
BKFP	7106.165	< 0.0001	0.847	< 0.0001	***Reject H_0***
CGGT	13138.538	< 0.0001	0.935	< 0.0001	***Reject H_0***
CLBR	1343.373	< 0.0001	0.744	< 0.0001	***Reject H_0***
FPNO	162.497	< 0.0001	0.490	< 0.0001	***Reject H_0***
FUTA	364.712	< 0.0001	0.325	< 0.0001	***Reject H_0***
FUTY	6678.663	< 0.0001	0.435	< 0.0001	***Reject H_0***
GEMB	1029.102	< 0.0001	0.703	< 0.0001	***Reject H_0***
HUKP	866.773	< 0.0001	0.681	< 0.0001	***Reject H_0***
MDGR	1582.510	< 0.0001	0.872	< 0.0001	***Reject H_0***
OSGF	3630.615	< 0.0001	0.807	< 0.0001	***Reject H_0***
RUST	359.204	< 0.0001	0.525	< 0.0001	***Reject H_0***
ULAG	1646.170	< 0.0001	0.649	< 0.0001	***Reject H_0***
UNEC	2860.371	< 0.0001	0.743	< 0.0001	***Reject H_0***

Table 3.5b: Results of white-noise tests for monthly ZTD data over Nigeria

Station	Fisher's kappa		Bartlett's Kolmogorov-Smirnov		Test Interpretation
	Value	p-value	Value	p-value	***Reject H_0 (Trend is significantly different from white noise)***
ABU	447.710	< 0.0001	0.715	< 0.0001	***Reject H_0***
BKFP	7731.363	< 0.0001	0.829	< 0.0001	***Reject H_0***
CGGT	1319.317	< 0.0001	0.866	< 0.0001	***Reject H_0***
CLBR	1839.942	< 0.0001	0.713	< 0.0001	***Reject H_0***
FPNO	188.212	< 0.0001	0.506	< 0.0001	***Reject H_0***
FUTA	434.096	< 0.0001	0.294	< 0.0001	***Reject H_0***
FUTY	6514.433	< 0.0001	0.843	< 0.0001	***Reject H_0***
GEMB	1844.768	< 0.0001	0.664	< 0.0001	***Reject H_0***
HUKP	461.159	< 0.0001	0.608	< 0.0001	***Reject H_0***
MDGR	255.151	< 0.0001	0.713	< 0.0001	***Reject H_0***
OSGF	3856.722	< 0.0001	0.784	< 0.0001	***Reject H_0***
RUST	408.269	< 0.0001	0.468	< 0.0001	***Reject H_0***
ULAG	1757.784	< 0.0001	0.621	< 0.0001	***Reject H_0***
UNEC	2949.609	< 0.0001	0.722	< 0.0001	***Reject H_0***

In order to study periodicities in the time series, we introduced periodograms and spectral plots. Figures 3.5a and 3.5b are the periodogram and spectral plots, respectively, of the two-hourly ZTD time series. Similarly, the monthly (intra-seasonal) ZTD time series are represented in Figures 3.6a and 3.6b. Wide varieties of spectrum can be seen when looking at diurnal and intra-seasonal mean ZTD. The different figures are indicative of some periodicity over the range of frequencies. It can be seen from the periodicity examination of ZTD in Figure 3.5a that the fundamental frequency for most stations (ABUZ, BKFP, CGGT, CLBR, FUTA, FUTY, GEMB, HURK, MDGR, and OSGF) is between 0.4 and 0.5 cycles per hour, corresponding to a wavelength of approximately 24 hours. Several other cycles can also be seen in Figure 3.5a; all the stations, except CLBR, have their lowest amplitude in the range of 1.71–2.61 cycles per hour, corresponding to a wavelength of 5-7 hours. Both the S1 and S2 tidal oscillations are very prominent in these figures showing ZTD, as can also be observed in atmospheric pressure. Beyond this, a few other harmonics are also seen in ZTD, which could be attributed to atmospheric water vapour.

Figure 3.6a illustrates the oscillations in ZTD for the intra-seasonal trends over Nigeria. The amplitudes of these variations are large during the period from June to October and low during the harmattan season.

Figures 3.5a and 3.6a reveal that many sites exhibit a diurnal cycle, especially during the rainy season, when oscillations reach an amplitude of a few millimetres, usually peaking in the mid-afternoon. The smallest diurnal variations are seen at locations surrounded by or close to coastal water, while the largest are found in the northern areas, where there is also a very large variance between the daily minimum and maximum ZTD estimates. Proximity to water also seems to be a controlling factor of the time of day when ZTD has its peak value, with stations close to bodies of water peaking earlier, as seen at ULAG and RUST.

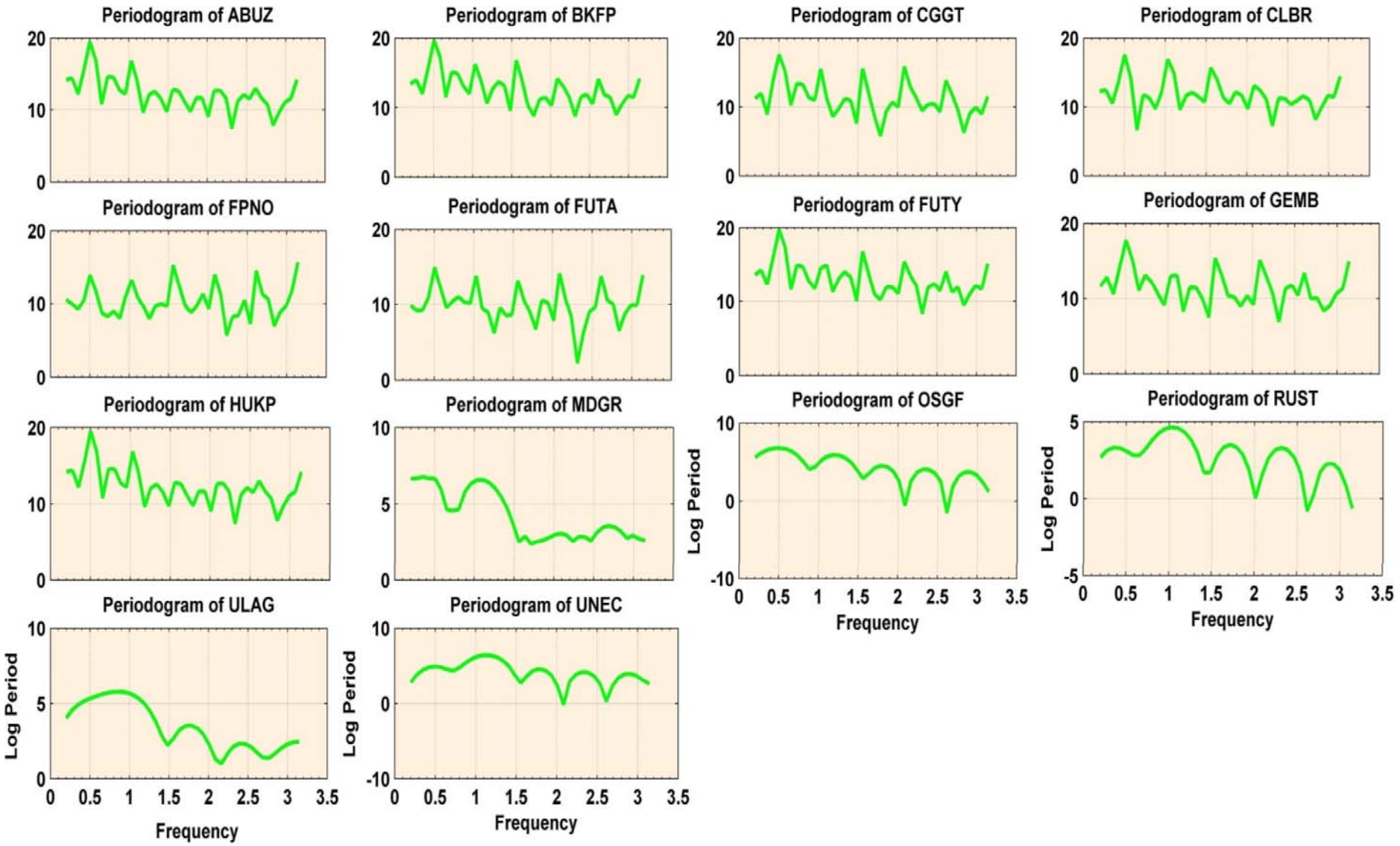

Figure 3.5a: Periodograms illustrating significant oscillations in the diurnal ZTD anomaly at the stations over the period January 2010–June 2014

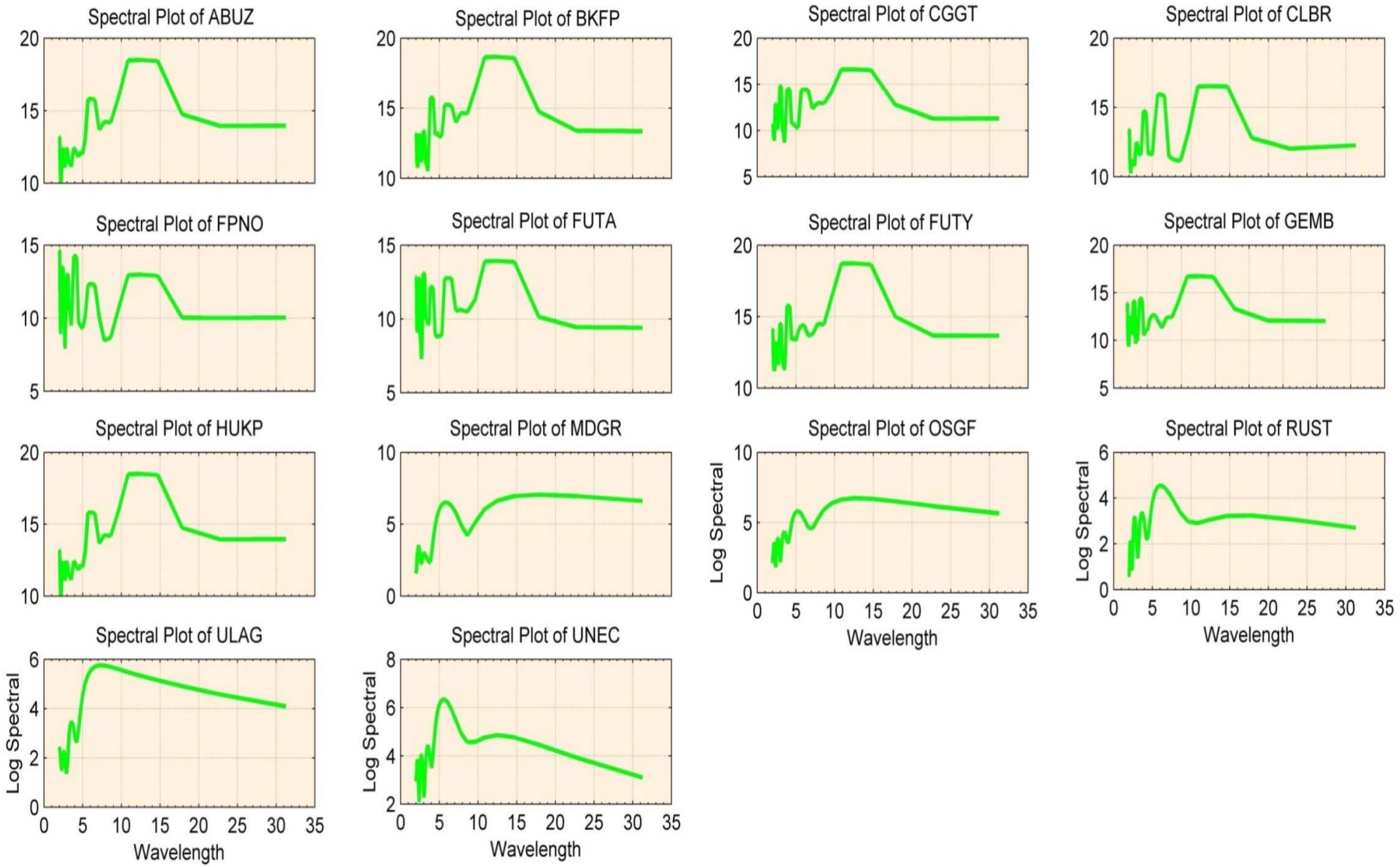

Figure 3.5b: Spectral plots showing significant oscillations of the diurnal ZTD anomaly at the stations over the period of January 2010–June 2014

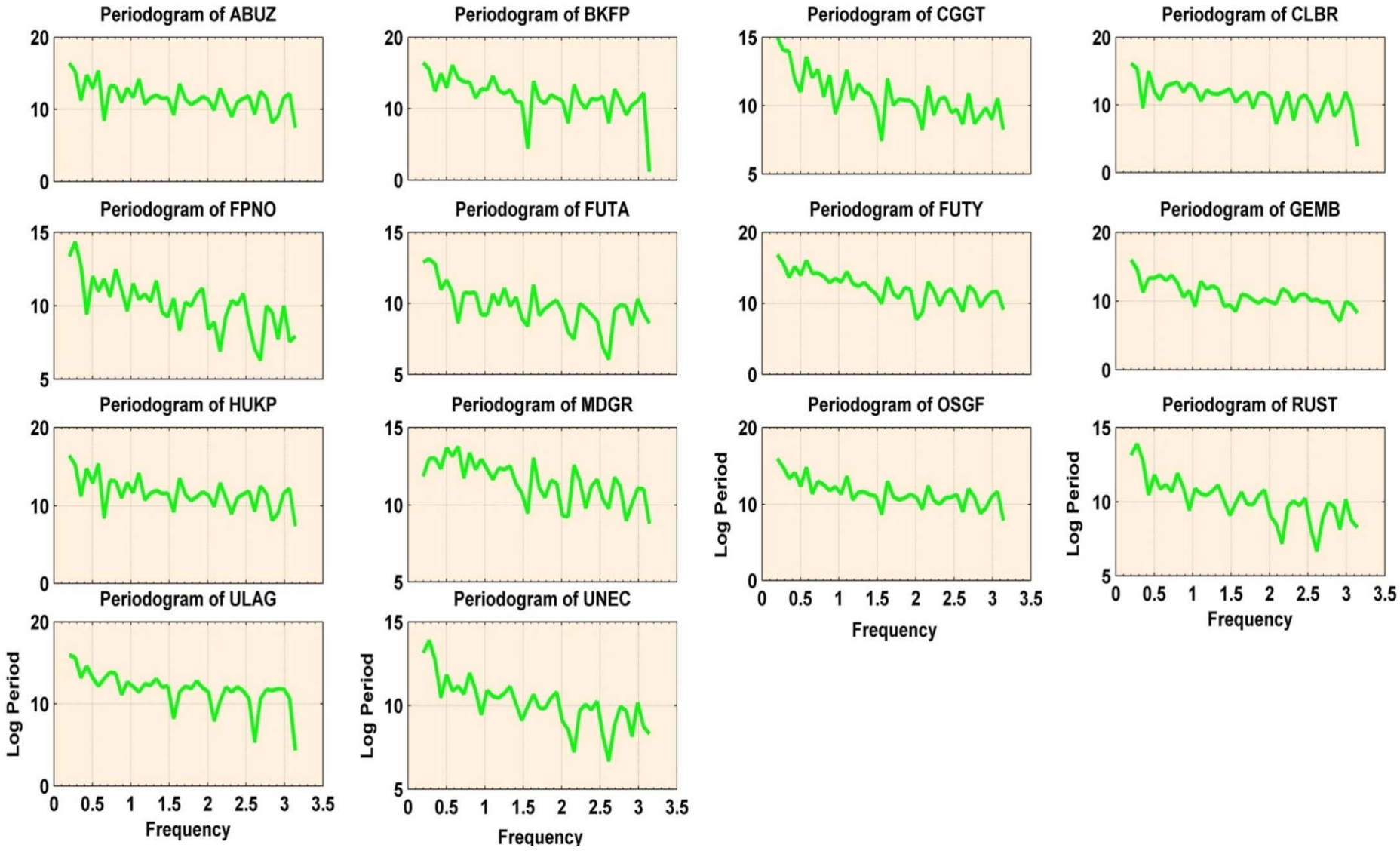

Figure 3.6a: Periodograms illustrating significant oscillations of the Intra-seasonal ZTD anomaly at the stations over the period of January 2010–June 2014

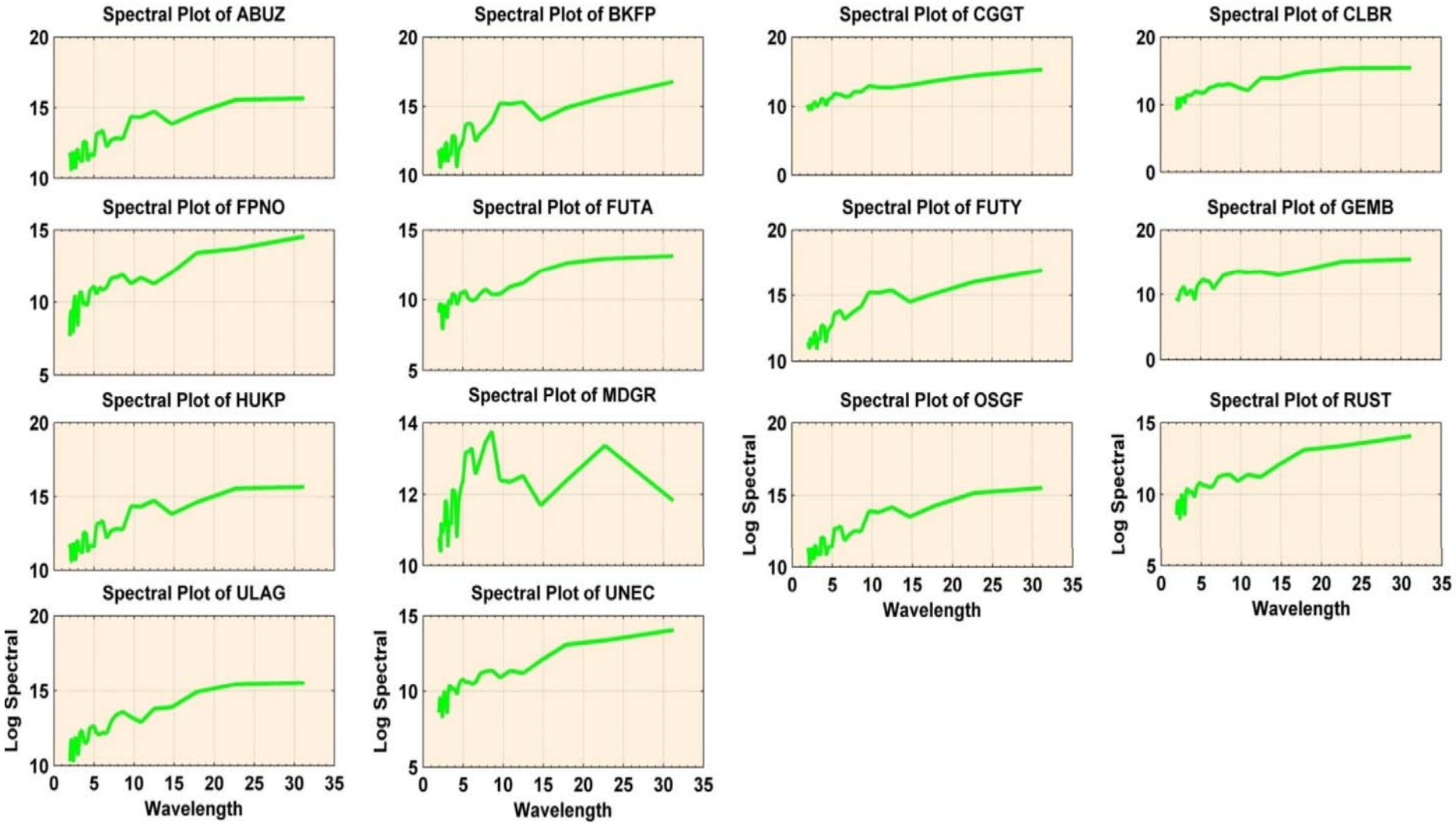

Figure3. 6b: Spectral plots illustrating significant oscillations of the Intra-seasonal ZTD anomaly at the stations over the period of January 2010–June 2014

At most of the stations, ZTD follows a strong intra-seasonal cycle, which is greatest in the wet season and least in the dry season. This seasonality is influenced by the saturation vapour pressure set by local temperatures, but it is also modulated by the seasonal influence of air masses. The intra-seasonal cycle is weakest in the southern area and strongest in the north.

Some stations show diurnal dependence at one time of the year and not during another. This could be due to seasonal changes in synoptic weather, from an active pattern during the dry season that does not exhibit systematic diurnal variation to a more passive pattern in the wet season. The seasonal cycle happens to exhibit the strongest and most significant periodicity at all the GNSS stations.

The spectral plots in Figures 3.5b and 3.6b reflect relatively high variance at small wavelengths, indicative of persistent or positive autocorrelation in the time series. Notable, too, is that the spectral cycles describe all possible oscillation that may have occurred within the time series well, and they also help satisfy the Nyquist sampling theorem.

As a final check on the time series of ZTD estimated on the NIGNET, we consider the DF (unit root) and KPSS tests for stationarity. The results of both tests are presented in Tables 3.6a and 3.6b for the diurnal and intra-seasonal trends, respectively. As shown in Table 3.6a, for all the stations, the DF test rejects the null hypothesis that the series is autocorrelated with (r = 1) and retains the hypothesis that it is stationary, while the KPSS test keeps the null hypothesis at all stations that the series is stationary. However, Table 3.6b presents a contrasting report, as the null hypothesis is rejected by both tests on the intra-seasonal trends. The reason for this is not very clear, but KPSS is more sensitive to prolonged weather events, which usually affect the statistical properties of the ZTD such as mean, variance and autocorrelation, and thus are not constant over the seasons.

Table 3.6a: Results of tests for stationarity for two-hourly ZTD data over Nigeria (DF test and KPSS test)

Station	Dickey-Fuller Test					KPSS Test				
	Tau (Observed value)	Tau (Critical value)	p-value (one-tailed)	alpha	Test Interpretation	Eta (Observed value)	Eta (Critical value)	p-value (one-tailed)	alpha	Test Interpretation
ABU	-10.137	-0.878	< 0.0001	0.05	Reject H_0(There is no unit root for the series and thus the series is stationary)	0.032	0.149	0.715	0.05	Accept H_0 (The series is stationary)
BKFP	-10.801	-0.878	< 0.0001	0.05	Reject H_0	0.008	0.147	1.000	0.05	Accept H_0
CGGT	-6.641	-0.869	< 0.0001	0.05	Reject H_0	0.158	0.154	0.045	0.05	Accept H_0
CLBR	-10.439	-0.855	< 0.0001	0.05	Reject H_0	0.077	0.144	0.301	0.05	Accept H_0
FPNO	-15.586	-0.866	< 0.0001	0.05	Reject H_0	0.041	0.151	0.707	0.05	Accept H_0
FUTA	-14.479	-0.868	< 0.0001	0.05	Reject H_0	0.020	0.151	0.976	0.05	Accept H_0
FUTY	-8.801	-0.860	< 0.0001	0.05	Reject H_0	0.020	0.151	0.973	0.05	Accept H_0
GEMB	-6.829	-0.860	< 0.0001	0.05	Reject H_0	0.053	0.142	0.539	0.05	Accept H_0
HUKP	-6.413	-0.854	< 0.0001	0.05	Reject H_0	0.034	0.151	0.815	0.05	Accept H_0
MDGR	-4.811	-0.845	0.000	0.05	Reject H_0	0.056	0.145	0.503	0.05	Accept H_0
OSGF	-7.779	-0.859	< 0.0001	0.05	Reject H_0	0.036	0.142	0.781	0.05	Accept H_0
RUST	-11.658	-0.842	< 0.0001	0.05	Reject H_0	0.019	0.141	0.980	0.05	Accept H_0
ULAG	-10.353	-0.854	< 0.0001	0.05	Reject H_0	0.031	0.148	0.853	0.05	Accept H_0
UNEC	-9.095	-0.859	< 0.0001	0.05	Reject H_0	0.026	0.150	0.929	0.05	Accept H_0

Table 3.6b: Results of tests for stationarity for monthly ZTD data over Nigeria (DF test and KPSS test)

Station	Dickey Fuller Test					KPSS Test				
	Tau (Observed value)	Tau (Critical value)	p-value (one-tailed)	alpha	Test Interpretation	Eta (Observed value)	Eta (Critical value)	p-value (one-tailed)	alpha	Test Interpretation
ABU	-16.662	-0.878	<0.0001	0.05	Reject H_0 (There is no unit root for the series and thus the series is stationary)	8.264	0.150	<0.0001	0.05	Reject H_0 (The series is not stationary)
BKFP	-4.253	-0.878	0.002	0.05	Reject H_0	13.581	0.147	< 0.0001	0.05	Reject H_0
CGGT	-19.948	-0.869	< 0.0001	0.05	Reject H_0	0.836	0.154	< 0.0001	0.05	Reject H_0
CLBR	-11.337	-0.855	< 0.0001	0.05	Reject H_0	6.533	0.144	< 0.0001	0.05	Reject H_0
FPNO	-11.190	-0.866	< 0.0001	0.05	Reject H_0	1.780	0.151	< 0.0001	0.05	Reject H_0
FUTA	-9.554	-0.868	< 0.0001	0.05	Reject H_0	4.344	0.151	< 0.0001	0.05	Reject H_0
FUTY	-3.892	-0.860	0.012	0.05	Reject H_0	12.169	0.151	< 0.0001	0.05	Reject H_0
GEMB	-6.052	-0.860	< 0.0001	0.05	Reject H_0	6.257	0.142	< 0.0001	0.05	Reject H_0
HUKP	-14.636	-0.854	< 0.0001	0.05	Reject H_0	5.784	0.146	<0.0001	0.05	Reject H_0
MDGR	-18.193	-0.845	< 0.0001	0.05	Reject H_0	1.442	0.145	< 0.0001	0.05	Reject H_0
OSGF	-5.644	-0.859	< 0.0001	0.05	Reject H_0	9.757	0.142	< 0.0001	0.05	Reject H_0
RUST	-16.229	-0.842	< 0.0001	0.05	Reject H_0	3.701	0.141	< 0.0001	0.05	Reject H_0
ULAG	-11.013	-0.854	< 0.0001	0.05	Reject H_0	6.861	0.148	< 0.0001	0.05	Reject H_0
UNEC	-6.940	-0.859	< 0.0001	0.05	Reject H_0	8.479	0.150	< 0.0001	0.05	Reject H_0

3.4 Concluding Remarks

Tropospheric delay was derived from the data collected from the NIGNET using the GAMIT 10.3 software package. GNSS data from the NIGNET are available for the period from 2010 onwards at a sampling rate of 30 sec. The time series of two-hourly GNSS ZTD from 2010–2014 on the NIGNET provides a unique and important dataset to evaluate the spatial dependence of ZTD estimates based on the NIGNET stations. Three spatial statistical models were applied to the ZTD estimates, namely the OLS, SEM and SLM. Diagnostic tests for independence of error terms, homogeneity of variance, normality and spatial dependence were performed for each model. The assumptions of all three models were not completely satisfied. Thus, spatial autocorrelation was not obtained. The weak spatial dependence of ZTD among the stations was attributed to the sparse nature of NIGNET and is also possibly due to the differences in station elevation, as it has previously been shown that ZTD estimates exhibit strong correlation with station elevation and latitude.

The diurnal and intra-seasonal variation of ZTD was also studied with GNSS measurements using the Mann-Kendall Trend test, white noise test/spectral analysis, and tests for stationarity. The Mann-Kendall test is endorsed by the WMO for the assessment of trends in meteorological data, while Fisher's kappa and Bartlett's Kolmogorov-Smirnov statistics were used to test for white noise in the ZTD estimates. A notable trend was identified in the ZTD time series at diurnal and intra-seasonal scales; though a longer period of ZTD measurement is required to report conclusively on the repetitiveness of the trend in ZTD measurements over Nigeria. The corresponding harmonics analysis produced the periodogram and the spectral plots of the time series. The KPSS and DF tests were used to test the stationarity of the ZTD time series. The various periodicities in the GNSS-derived ZTD were studied to account for any variability in ZTD due to atmospheric oscillations, which could improve the existing periodic models for ZTD. The prospect of studying tidal and intra-seasonal oscillations, as well as various planetary waves from ZTDs as determined from GNSS data, is also illustrated by this study. In addition, the diurnal ZTD cycles exhibited significant seasonal dependence, with larger amplitudes in the rainy (wet) season and smaller ones in the harmattan (dry) season. Similarly, the stations in the northern part of the country reached very high amplitudes in June, July and August at the peak of the wet season, characterised by very high rain fall. This pinpoints the fact that with the low amount of atmospheric water vapour in the atmosphere, usually around 10%, its variations greatly influence the corresponding diurnal and seasonal discrepancies of ZTD. The GNSS-estimated

ZTD displayed conspicuous periodicities that characteristically exist in the lower atmosphere where water vapour is dominant, further affirming the prospective relevance of GNSS to atmospheric studies.

Interestingly, results from this study are in good agreement with previous studies around the world (i.e., Jin et al., 2007; 2009; Ahmed et al., 2015). Ahmed et al. (2015) reported linear trends in ZTD using the time series for selected IGS stations in the equatorial, northern polar and southern polar regions. Positive trends of $0.31\,mm\,y^{-1}$, $0.20\,mm\,y^{-1}$, and $0.17\,mm\,y^{-1}$ were found for the equatorial, northern polar and southern polar regions, respectively. Jin et al. (2007) gave a mean ZTD trend of $1.5 \pm 0.001\,mm\,y^{-1}$ for all IGS stations with significant variations in annual ZTD amplitude in the northern and southern hemispheres, with the middle latitudes having larger amplitudes of annual ZTD variation. According Jin et al. (2007), the variation in ZTD on inter-annual and seasonal scales had a maximum value of ZTD in the summer for the northern polar region, in spring for the equatorial region and in the austral summer for the southern polar region. The spring season in the equatorial region of Africa is seen as the wet season and had earlier been reported in our study as a period of high amplitude in ZTD cycles. Diurnal variations in ZTD at a global scale have also been studied and it was found that their magnitude is highest in the equatorial region and lowest in the northern polar region; the diurnal ZTD cycle has significant seasonal dependences with larger amplitudes in summer and smaller ones in winter (i.e., Jin et al., 2009; Ahmed et al., 2015). The relation between diurnal and semi-diurnal cycles of ZTD, as reported by Jin et al. (2009), indicated that amplitudes of ZTD series had a strong and consistent dependence on the latitude with the largest amplitudes of the diurnal and semi-diurnal ZTD cycles found in the low latitude equatorial regions. From the foregoing reported results across the globe it can be seen that ZTD is a significant parameter of the atmosphere, which openly or circuitously reveals the weather and climate processes, variations and atmospheric vertical motions, etc. The high variations and amplitudes in ZTD time series as recorded in the low equatorial region (our region of study) is an indication of the dynamics of the region and this justifies a comprehensive study of ZTD in the region.

The results of our study are preliminary in the sense that more complex statistical tests and a longer time period are required to validate the trend and correlation between the different climate indices and ZTD. Long-term climatology would also benefit from the GNSS-derived ZTD time series if made available. Undoubtedly, this study has demonstrated the viability of the GNSS meteorology technique over Nigeria as a new observational method

with the potential of filling the existing gaps between current observational systems, based on its low cost, continuity, all-weather measuring capability and good spatiotemporal resolution. To explore the Nigerian weather and climate adequately, and to benefit optimally from the GNSS meteorology in Nigeria, further efforts are required. The densification of the NIGNET, which should include the provision of meteorological sensors for PWV retrieval from ZTDs, is suggested. A dense network will contribute valuable water vapour field data for initialisation, setting boundary limits or substantiating local NWPs and high-resolution regional climate models. In addition, such data could improve mid-term weather predictability, which is particularly useful for determining the likelihood of the onset of floods or the converse, severe drought etc. This study has provided the needed background for further study on the subject of climatic application of GNSS atmospheric products in Nigeria. It is pertinent to note that the problem of climate change was indirectly addressed in this research, because the time period of the study (2010-2014) is relatively short compared to the time scale of observable changes due to climate change. Nevertheless, it has laid the foundation for future studies because the amount of water vapour in the atmosphere is of great significance to climate change. Finally, further exploration of the GNSS's capability in weather and climate monitoring is recommended in Nigeria and across the entire West African region.

Acknowledgements

Support and funding for this study was provided by the Tertiary Education Trust Fund (TETFund) of Nigeria, Surveyors Registration Council of Nigeria (SURCON) and University of Pretoria PhD Research Support grant to the first author. The authors would wish to express their profound gratitude to the numerous reviewers for their productive observations that helped to perk up the manuscript. We wish to thank the office of the Surveyor General of the federal republic of the Federation (OSGOF) for the GNSS data.

Chapter 4

Performance Evaluation of Blind Tropospheric Delay Correction Models over Africa **

"The mere formulation of a problem is far more often essential than its solution, which may be merely a matter of mathematical or experimental skill
*.....**Albert Einstein** (1879-1955)*

Précis

Tropospheric delay is a major error source in positioning by Global Navigation Satellite Systems (GNSS). Many techniques are available for tropospheric delay mitigation consisting of surface meteorological models and global empirical models. Surface meteorological models need surface meteorological data to give high accuracy mitigation while the global empirical models need not. However, most GNSS stations in the African region are not equipped with a meteorological sensor for the collection of surface meteorological data during the measurement. Zenith Tropospheric Delay (ZTD) is often calculated by the various high precision GNSS software packages by utilising standard atmosphere values. Lately, researchers in the University of New Brunswick and Vienna University of Technology have both developed global models (University of New Brunswick (UNB3M) and Global Pressure and Temperature 2 wet (GPT2w) models) for tropospheric delay correction, respectively. This report represents an appraisal of the performance of the GPT2w and UNB3M models with accurate International GNSS Service (IGS)-tropospheric estimations for fifteen IGS stations over a period of 1 year on the Africa continent. Both models perform significantly better at low latitudes than higher latitudes. There was better agreement between the GPT2w model and the IGS estimate than the UNB3m at all stations. Thus, the GPT2w model is recommended as a correction model of the tropospheric error for the GNSS positioning and navigation on the African Continent.

***This chapter consists of formatted text for one peer reviewed journal paper as follows:**

***Isioye, O. A.,** Combrinck, L., & Botai, J.O. 2015. Performance Evaluation of Blind Tropospheric Delay Correction Models over Africa, South African Journal of Geomatics, Vol. 4, No. 4, 502-525, November 2015, DOI: http://dx.doi.org/10.4314/sajg.v4i4.8., / www.ajol.info/index.php/sajg/article/view/125795*

4.1 Introduction and background

Tropospheric delay is one of the main error sources in the analysis of space geodetic techniques operating at microwave frequencies, such as Global Navigation Satellite Systems (GNSS), Very Long Baseline Interferometry (VLBI), or Doppler Orbitography and Radio-positioning Integrated by Satellite (DORIS).

The tropospheric delay is usually separated into a hydrostatic delay that is modelled a priori, and a wet delay that is estimated from the space geodetic microwave observations. Modelled hydrostatic delays and the estimated wet delays are usually referred to the zenith direction; corresponding mapping functions are required to convert the slant delays in observation direction to the zenith. In addition, troposphere gradients can be estimated to account for asymmetries of the troposphere.

In GNSS positioning, the tropospheric delay typically ranges between 2.0 m to 2.6 m. The Zenith Hydrostatic Delay (ZHD) constitutes 90% of the Zenith Tropospheric Delay (ZTD), and Zenith Wet Delay (ZWD) is usually less than 10%. The ZHD can be estimated to an accuracy of better than 90% using empirical models that utilizes meteorological data, such as pressure and temperature as well as the position of the user. Some ZHD models include those of Saastamoinen (1972), Hopfield (1969), Berman (1976), Davis et al (1985), Ifadis(1986), Askne and Nordius (1987) etc. A comprehensive review and validations of some of these models can be found in Tuka and El-Mowafy (2013). The Saastamoinen model is the most used model in geodetic applications and its accuracy has been widely reported (Dodo and Idowu, 2010).

In practice, a user often employs a certain troposphere model based on the popularity of the model without giving enough justification as to why it should be used. Limited comparisons between some of the models have been carried out in the past for local or regional applications. However, in this contribution, this issue is addressed more comprehensively considering the peculiarities of the African GNSS network. Most GNSS stations on the African continent are characterised by the lack of collocated meteorological sensors, as it is required for such to be collocated with the GNSS antenna if the GNSS data are to be processed for integrated water vapour content determination (Isioye et al., 2015a). Thus, the inversion of ground meteorological data into the variable vapour content in the atmosphere is very difficult. Even the Saastamoinen model has difficulties in meeting the needs for high accuracy GNSS positioning and meteorological applications, since most

GNSS geodetic software uses the Saastamoinen model with standard atmosphere models for a-poiri estimates.

In view of these shortcomings, it is of practical importance to construct a global model of average tropospheric delay correction with a certain accuracy to be used particularly in the GNSS navigation and positioning in Africa, in which the zenith delay depends only on the latitude, elevation of observing station, and the date of observation. Recently, several of these blind models have been developed such as the University of New Brunswick model; UNB3 (Collins and Langley, 1999), RTCA- Minimum Operational Performance Standards; MOPS (RCTA, 2001); European Geostationary Navigation Overlay Service; EGNOS (Dodson et al., 1999; Penna et al., 2001); UNB3m (where m stands for "modified") (Leandro et al., 2006); European Space Agency; ESA model (ESA Galileo Programme, 2012); Global Pressure Temperature 2; GPT2 (Lagler et al., 2013); and Global Pressure Temperature 2 wet; GPT2w (Boehm et al., 2014). Table 4.1 provides an overview of the different blind models.

Table 4.1: Overview of Blind Tropospheric Correction Models

	RTCA MOPS model	***UNB3m model***	***ESA model***	***GPT2 model***	***GPT2w model***
Temporal Resolution	Annual	Annual	Daily + Annual	Annual + Semi annual	Annual + Semi annual
Spatial Resolution	15°	15°	1.5°	5°	1°
Source of climatological dataset	U.S. standard atmospheric supplements, 1966 (COESA, 1966)	U.S. standard atmospheric supplements, 1966 (*COESA,* 1966)	Numerical Weather Prediction model - ERA 15	Numerical Weather Prediction model - ERA Interim	Numerical Weather Prediction model - ERA Interim
ZHD model	Saastamoinen (1972)	Davis et al,, 1985	Saastamoinen (1972)	Saastamoinen (1972)	Saastamoinen (1972)
ZWD model	Askne and Nordius (1987)	Davis et al,, 1985	Askne and Nordius (1987)	Saastamoinen (1972)	Askne and Nordius (1987)
Mapping function	Black and Eisner Mapping Function (Black and Eisner, 1984)	Niell Mapping Function (Niell, 1996)	Niell Mapping Function (Niell, 1996)	Global Mapping Function (Boehm et al., 2006b)	Vienna Mapping function (Boehm et al., 2006a)

It is evident from Table 4.1 that the models can be classified into two groups, one based on a set of tabulated climatological data and the other from Numerical Weather

Prediction (NWP) models. In the first category, the UNB3m is a refined version of UNB3 model (Leandro et al., 2006) and thus superior to RTCA MOPS, which is the same as the UNB3 model except for the replacement of the Niell mapping function with the Black and Eisner model (Leandro et al., 2006). Considering the other set of models, which are dependent on NWP data, theGPT2w model looks quite outstanding going by the spatial resolution of the model and also for the fact that the Vienna Mapping function is known to model tropospheric delay better that the Niell mapping function adopted by the ESA model (see, Won et al., 2010; Zus et al., 2015).

This paper presents an assessment of the UNB3m and GPT2w tropospheric models. The Zenith tropospheric estimations were compared from both models with the International GNSS Service (IGS) estimates. The study utilized the new IGS ZTD product (available at ftp://cddis.gsfc.nasa.gov/gps/products/trop_new) for the interval January 2013 to December 2013 and for 15 sites distributed on the African continent as indicated by the squares in Figure 4.1. The new IGS ZTD product is based on the precise point positioning (PPP) technique. It has a higher sampling rate and lower formal errors than the legacy IGS ZTD product and can be obtained with typical formal errors of 1.5–5 mm from the IGS (Byun and Bar-Sever, 2009). Gaps are common in the data, but at least 3 month of ZTD estimates are available for each site. The IGS data are down sampled from 5 minute to daily intervals. Detailed method of analysis and inferences are presented in the following sections of this paper.

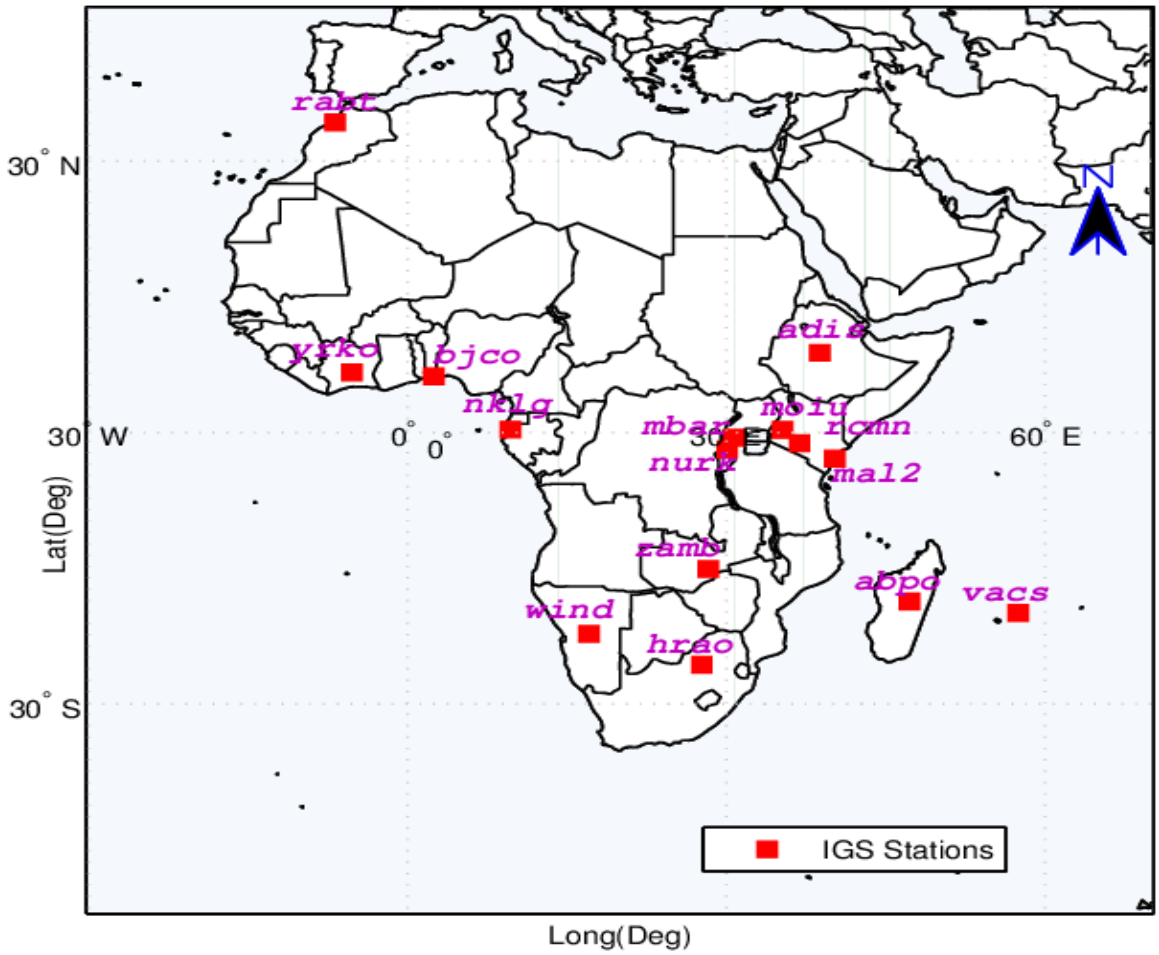

Figure 4.1: Map depicting the location of IGS stations in Africa

4.2 Description of tropospheric correction models adopted in this study

4.2.1 Saastamoinen model

Saastamoinen (1972) applied the gas laws to refractivity by considering the atmosphere as a mixture of dry air and water vapour. The model considers the temperature in the troposphere as decreasing with increasing height at a uniform rate, which varies slightly with latitude and season. However, in the polar region, there is a permanent inversion in the lower troposphere where the actual temperature increases with height. Saastamoinen assumed the neutral atmosphere to consist of two layers: the polytropic troposphere, which extends from the earth's surface to an altitude of approximately 11-12 km and the stratosphere, which is an isothermal layer, extending to approximately 50 km. The atmospheric water vapour is confined in the region of the troposphere only.

The Saastamoinen model for ZHD, in metres, is expressed as:

$$ZHD = 0.002277 \cdot \frac{P}{1 - 0.00266\cos(2\phi) - 0.28 \cdot 10^{-6} h} \quad . \tag{4.1}$$

In Equation (4.1), P is the surface pressure in mbar, ϕ is latitude in radians and, h is the height of the surface above the ellipsoid (in metres).

In the zenith wet delay model, Saastamoinen (1972) assumed that there is a linear decrease of temperature with height, and that the water vapour pressure decreases with height. The variation of the water vapour pressure $e_s\ (mbar)$ is expressed by the following expression:

$$e_s = RH \times 6.11 \times 10^{\frac{7.5T_s}{T_s + 273.15}} \quad . \tag{4.2}$$

In Equation (4.2), RH is the relative humidity to be determined from local observations, and the surface temperature in Kelvin is T_s.

Saastamoinen (1972) gave the expression for the zenith wet delay model using the refractivity constant of Essen and Froome (1951) and for mid-latitudes and average conditions:

$$ZWD = 0.002277\left(\frac{1255}{T_s} + 0.05\right)e_s \quad . \tag{4.3}$$

4.2.2 UNB3m Hydrostatic Delay Model

Leandro et al. (2006) presented a hybrid neutral atmosphere model designed for radiometric space users. This model, called UNB3m, has its algorithm based on the prediction of meteorological parameter values, which are then used to compute hydrostatic and non-hydrostatic zenith delays using the Saastamoinen model.

In order to account for the seasonal variation of the neutral atmosphere behaviour, a look-up table of meteorological parameters is used. The parameters are barometric pressure, temperature, water vapour pressure (WVP), temperature lapse rate (β) and water vapour pressure height factor (λ). This look-up table was derived from the U.S. Standard Atmosphere Supplements, 1966 (COESA, 1966; Orliac, 2002). Table (4.2) lists the look-up table values for UNB3m. The data are divided into two groups, to account for the annual average (mean) and amplitude of a cosine function for each parameter. Both amplitudes and averages vary with respect to latitude, for all parameters. In the development of the UNB3m model, water vapour pressure in an earlier version of UNB3 was replaced with relative

humidity values in Table (4.2). This addressed the problem of overestimation of humidity in the UNB3 model. In UNB3m, all computations for the point of interest are done initially using relative humidity, which is subsequently converted to water vapour pressure for use in the zenith delay computation. The conversion is done in line with the conventions of the International Earth Rotation and Reference Frame Services (IERS) (McCarthy & Petit, 2004; Leandro et al., 2006). Further details about the earlier model's (UNB3) development and performance are contained in Collins and Langley (1997, 1998).

Table 4.2: Look-up table of meteorological parameters for the UNB3m model, the parameters are user latitude zone (φ) barometric pressure $(P_\circ)$, temperature $(T_\circ)$, Relative Humidity (RH), temperature lapse rate (β) and water vapour pressure height or decrease factor (λ) (modified after Leandro et al., 2006)

Average for each parameter					
φ (deg)	$P_o[hPa]$	$T_o[K]$	$RH(\%)$	$\beta_o[K/m]$	$\lambda[-]$
15	1013.25	299.65	75.0	0.00630	2.77
30	1017.25	294.15	80.0	0.00605	3.15
45	1015.75	283.15	76.0	0.00558	2.57
60	1011.75	272.15	77.5	0.00539	1.81
75	1013.00	263.65	82.5	0.00453	1.55
Amplitude of a cosine function for each parameter					
φ (deg)	$P_o[hPa]$	$T_o[K]$	$RH(\%)$	$\beta_o[K/m]$	$\lambda[-]$
15	0.00	0.00	0.00	0.00000	0.00
30	-3.75	7.00	0.0	0.00025	0.33
45	-2.25	11.00	-1.0	0.00032	0.46
60	-1.75	15.00	-2.5	0.00081	0.74
75	-0.50	14.50	2.5	0.00062	0.30

The first step in the UNB3m algorithm is to obtain the meteorological parameter values for a particular latitude and day of year using the look-up table. By definition, the origin of the yearly variation is day of year (doy) 28. This procedure is similar to the one used in the computation of the Niell mapping functions. The interpolation between latitudes is done with a linear function. The annual average of a given parameter can be computed as:

$$Avg_{\phi} = \begin{cases} Avg_{15}, if\ \phi \le 15 \\ Avg_{75}, if\ \phi \ge 75 \\ Avg_i + \dfrac{\left(Avg_{i+1} - Avg_i\right)}{15}\left(\phi - Lat_i\right), if\ \ 15 < \phi < 75 \end{cases} . \qquad (4.4)$$

In Equation (4.4) ϕ stands for the latitude of interest in degrees, Avg_{ϕ} is the computed average, i is the index of the nearest lower tabled latitude and Lat is their latitude (from Table4. 2). The annual amplitude can be computed in a similar manner:

$$Amp_{\phi} = \begin{cases} Amp_{15}, if\ \phi \le 15 \\ Amp_{75}, if\ \phi \ge 75 \\ Amp_i + \dfrac{\left(Amp_{i+1} - Amp_i\right)}{15}\left(\phi - Lat_i\right), if\ \ 15 < \phi < 75 \end{cases} . \qquad (4.5)$$

In Equation (4.5) Amp_{ϕ} is the computed amplitude. After average and amplitude are computed for given latitude, the parameter values can be estimated for the desired day of year according to:

$$X_{\phi,doy} = Avg_{\phi} - Amp_{\phi} \cos\left(\left(doy - 28\right)\frac{2\pi}{365.25}\right), \qquad (4.6)$$

where, $X_{\phi,doy}$ represents the computed parameter value for latitude ϕ and day of year (doy). This procedure is followed for each one of the three needed parameters. Once all parameters are determined for given latitude and day of year, the zenith hydrostatic delay can be computed according to:

$$ZHD = \frac{10^{-6} k_1 R}{g_m} \cdot P_{\circ} \cdot \left(1 - \frac{\beta H}{T_{\circ}}\right)^{\frac{g}{R\beta}} \qquad (4.7)$$

where, $T_{\circ}$, $P_{\circ}$, and β are meteorological parameters computed according to (4.4), (4.5), and (4.6); H is the orthometric height in metres; $k_1 = 77.60 Kmbar^{-1}$; R is the gas constant for dry air $\left(287.054 Jkg^{-1}K^{-1}\right)$; g is the surface acceleration of gravity in ms^{-2} ; g_m is the acceleration of gravity at the atmospheric column centroid in ms^{-2} and can be computed from:

$$g_m = 9.784\left(1 - 2.66 \times 10^{-3} \cos\left(2\phi\right) - 2.8 \times 10^{-7} H\right) \qquad (4.8)$$

Leandro et al. (2006) presented the wet tropospheric refractivity for the station on the Earth's surface as a function of predicted meteorological parameter values. The model is analogous to the hydrostatic component and is expressed as (Farah, 2011):

$$ZWD = \frac{10^{-6}\left(T_m k_2' + k_3\right) R}{g_m \lambda' - \beta R} \frac{e_\circ}{T_\circ} \left(1 - \frac{\beta H}{T_\circ}\right)^{\left(\frac{\lambda' g}{R\beta}\right)-1} . \qquad (4.9)$$

In equation (4.9) $T_\circ$, $e_\circ$ λ, $P_\circ$, and β are meteorological parameters computed according to equations (4.4-4.6); $k_2' = 16.60$ K hpa^{-1}; $\lambda' = \lambda + 1$ (unitless); T_m is the mean temperature of water vapour in Kelvin and can be computed from:

$$T_m = \left(T_\circ - \beta H\right)\left(1 - \frac{\beta R}{g_m \lambda'}\right) . \qquad (4.10)$$

4.2.3 Global Pressure Temperature wet (GPT2w) Model

GPT2w is an extension of GPT and GPT2 (Boehm et al., 2007; Lagler et al., 2013) with improved capability to determine zenith delays in blind mode. The tropospheric model GPT2 itself is an enhancement of the Global Pressure and Temperature model (GPT; Boehm et al. 2007) and the Global Mapping Function (GMF; Boehm et al., 2006b). The development and validation of GPT2 as well as the comparison with GPT/GMF have been described in detail by Lagler et al. (2013). In its current version the ZHD and ZWD are a function of air pressure, temperature, water vapour pressure, latitude, and ellipsoidal height. The internally derived parameters (pressure, temperature, temperature lapse rate, water vapour pressure, hydrostatic and wet mapping function coefficients) are obtained from the statistical analysis of monthly mean ERA-Interim (European Centre for Medium- Range Weather Forecasts Re-Analysis) profiles over the time period 2001 to 2010. The mean values $\left(A_\circ\right)$ as well as annual $\left(A_1, B_1\right)$ and semi-annual amplitudes $\left(A_2, B_2\right)$ for selected parameter *r* are computed as in Equation (4.11) and are stored as average value as well as amplitude of annual and semi-annual variations on a global grid with a resolution of 5° x 5° at mean ETOPO5 (Earth topography) height.

$$r(t) = A_0 + A_1 \cos\left(\frac{doy}{365.25} 2\pi\right) + B_1 \sin\left(\frac{doy}{365.25} 2\pi\right) + A_2 \cos\left(\frac{doy}{365.25} 4\pi\right) + B_2 \cos\left(\frac{doy}{365.25} 4\pi\right) . \qquad (4.11)$$

The parameters of Equation (4.11) are estimated at the four grid points surrounding the target location before extrapolating the parameters vertically to the desired height and interpolating the data from those base points to the observational site in the horizontal direction. The extrapolation of the hydrostatic mapping function follows Niell (1996), whereas the wet mapping function is assumed to be constant in the vicinity of the Earth surface. The extrapolation of the pressure relies on an exponential trend coefficient related to the inverse of the virtual temperature, and the linear extrapolation of the temperature utilizes the GPT2 inherent temperature lapse rate. Surface grids for specific humidity within the GPT2 model have been derived from linear interpolation between pressure levels in the vicinity of Earth's surface. These parameters are used to determine values of zenith wet delays, by using the expressions of Saastamoinen (1972), although this approach is not optimal, it represents the starting point for the improved version of it. Thus, the GPT2w as an extension to GPT2 comes with an improved capability to determine zenith wet delays in blind mode (Boehm et al., 2014; Moller et al., 2013; Schingelegger et al., 2014). The Saastamoinen formula was replaced with Askne and Nordius (1987) in the GPT2w model as reflected in Equation (4.12).

$$ZWD = 10^{-6}\left(k_2' + {k_3}/{T_m}\right)\frac{R_d}{(\lambda+1)g_m}e_s. \qquad (4.12)$$

In Equation (4.12), k_2' and k_3 are refractivity constants, R_d is the specific gas constant for the dry component, g_m is the gravity acceleration at the centre of mass of the vertical atmospheric column and e_s is the water vapour pressure at the site.

Additionally, the GPT2w blind troposphere delay model provides the mean values plus annual and semi - annual amplitudes of pressure, temperature and its lapse rate, water vapour pressure and its decrease factor λ, weighted mean temperature, as well as hydrostatic and wet mapping function coefficients of the VMF1 (Vienna Mapping Function 1). It also benefits from an improved spatial resolution of 1°.

All climatological parameters have been derived consistently from monthly mean pressure level data of ERA-Interim fields with a horizontal resolution of one degree, and the model is suitable to calculate slant hydrostatic and wet delays down to three degrees elevation at sites in the vicinity of the Earth surface using the date and approximate station coordinates as input.

.

4.3 Assessment of the accuracies of the UNB3m and GPT2w Models

The accuracies of the UNB3m and GPT2w models were evaluated using the new IGS ZTD product for the interval January 2013 to December 2013 and for 15 sites distributed on the African continent. A summary of the individual station information is presented in Table 4.3.

Table 4.3: Station Information for selected IGS stations in Africa

Station	Country	Latitude(deg)	Longitude (deg)	Ellipsoidal Height
ABPO	Madagascar	-19.02	47.23	1552.99
ADIS	Ethiopia	9.04	38.77	2439.15
BJCO	Benin Republic	6.38	2.45	30.60
HRAO	South Africa	-25.89	27.69	1414.30
MAL2	Kenya	-3.00	40.19	-20.40
MBAR	Uganda	-0.60	30.74	1337.65
MOIU	Kenya	0.29	35.29	2201.53
NKLG	Gabon	0.35	9.67	31.48
NURK	Rwanda	-1.94	30.09	1485.30
RABT	Morocco	34.00	-6.85	90.10
RCMN	Kenya	-1.22	36.89	1607.54
VACS	Mauritius	-20.30	57.49	420.40
WIND	Namibia	-22.57	17.09	1734.70
YKRO	Cote d'Ivoire	6.87	-5.24	270.00
ZAMB	Zambia	-15.43	28.31	1324.91

The following performance indicators were adopted for the evaluation: Normalised Mean Absolute Error (NMAE) (Shcherbakov et al., 2013), Root Mean Square Error (RMSE), Model Efficiency (MEF) (Murphy, 1988), Reliability Index (RI) (Leggett and Williams, 1981), and Correlation coefficient (r) . These performance indicators are represented as follows;

$$NMAE = \frac{\sum_{i=1}^{N}\left(\left|Bias_i\right|\right)}{N\bar{O}} \quad , \tag{4.13}$$

$$RMSE = \sqrt{\frac{\sum_{i=1}^{N}\left(Bias_i\right)^2}{N}} \quad , \tag{4.14}$$

$$MEF = 1 - \frac{\sum_{i=1}^{N}\left(Bias_i\right)^2}{\sum_{i=1}^{N}\left(\left|\left(P_i - \bar{O}\right)\right| - \left|\left(O_i - \bar{O}\right)\right|\right)^2} \quad , \tag{4.15}$$

$$RI = \exp\sqrt{\frac{1}{N}\sum_{i=1}^{N}\left(\log\frac{O_i}{P_i}\right)^2}\ , \tag{4.16}$$

$$r = \frac{\sum_{i=1}^{N}\left(P_i-\bar{P}\right)\left(O_i-\bar{O}\right)}{\left[\sum_{i=1}^{N}\left(P_i-\bar{P}\right)^2\cdot\sum_{i=1}^{N}\left(O_i-\bar{O}\right)^2\right]^{1/2}}\ . \tag{4.17}$$

In Equations (4.13) – (4.17), N is the number of observations, O_i and P_i are the "i^{th}" observed and model estimated values, $\bar{O}$ and $\bar{P}$ are the mean observed (IGS estimates) and model (UNB3m and GPT2w) estimated values, respectively, and $Bias_i = P_i - O_i$. A summary of the results of the different performance evaluator is presented in Table 4.4.

Table 4.4: Performance of the UNB3m and GPT2w for ZTD estimation against the IGS solutions

	NMAE	***RMSE***	***MEF***	***RI***	***NMAE***	***RMSE***	***MEF***	***RI***	***NMAE***	***RMSE***	***MEF***	***RI***
	ABPO				***ADIS***				***BJCO***			
GPT2w	0.0134	31.0320	0.8350	1.0152	0.0095	22.4626	0.8277	1.0123	0.0085	29.5480	0.7997	1.0115
UNB3M	0.0194	45.1071	0.3519	1.0223	0.0173	36.3694	0.3798	1.0199	0.0150	45.4024	0.4138	1.0176
	HRAO				***MAL2***				***MBAR***			
GPT2w	0.0114	30.9544	0.8617	1.0149	0.0110	34.5622	0.6444	1.0135	0.0092	24.6734	0.5230	1.0115
UNB3M	0.0159	39.0528	0.6419	1.0189	0.0142	43.6633	0.3361	1.0171	0.0161	40.5798	0.4471	1.0190
	MOIU				***NKLG***				***NURK***			
GPT2w	0.0092	26.0287	0.4370	1.0136	0.0069	22.7098	0.3916	1.0087	0.0100	26.4390	0.6495	1.0126
UNB3M	0.0154	34.8988	0.4482	1.0184	0.0193	55.4938	0.4100	1.0215	0.0170	42.3982	0.4510	1.0202
	RABT				***RCMN***				***VACS***			
GPT2w	0.0126	37.8190	0.5758	1.0157	0.0133	33.1069	0.4855	1.0160	0.0143	44.2097	0.7774	1.0185
UNB3M	0.0217	63.9707	0.4605	1.0265	0.0147	38.1572	0.4522	1.0185	0.0211	57.0262	0.5229	1.0242
	WIND				***YKRO***				***ZAMB***			
GPT2w	0.0140	35.3518	0.7838	1.0180	0.0080	26.2248	0.6363	1.0105	0.0132	33.1040	0.9013	1.0158
UNB3M	0.0218	48.4544	0.5628	1.0248	0.0158	44.7696	0.4170	1.0179	0.0302	70.1788	0.4344	1.0338

The NMAE measures the absolute deviation of the simulated values (UNB3m and GPT2w) from the observations (IGS estimates), normalised to the mean; a value of zero indicates perfect agreement and greater than zero an average fraction of the discrepancy normalised to the mean, the NMAE value from all the stations are indicative of the good performance of the GPT2w model. Similarly, RMSE measures the average square error with values near zero indicating a close match, the GPT2w model has a minimum RMSE of

22.4626 mm at ADIS and a maximum of RMSE of 44.2097 mm at VACS while for the UNB3m model, a maximum RMSE occur at ZAMB with a value of 70.1788 mm and minimum RMSE of 34.8988 mm at MOIU, thus, again the GPT2w performs better at all the stations. The MEF, which is a measure of the square of the deviation of the model's values (UNB3m and GPT2w) from the observations (IGS), normalised to the standard deviation of the observed data (IGS values). MEF values range from [0, 1] as agreement between predicted values and observations change from no agreement (MEF = 0) to perfect agreement (MEF = 1). From Table 4.4 it is evident that the GPT2w model performs better at the stations with a range of 0.9013 to 0.3916, except at NKLG where a value of 0.3916 was obtained, the UNB3m model had a range of 0.6419 to 0.3361 which is indicative of a lower variability in the MEF compared to the GPT2w. The RI quantifies the average factor by which the model estimates differ from the IGS solutions. For example, an RI of 2 indicates that a model predicts the observations within a multiplicative factor of two, on average. Ideally, the RI should be close to one. When the RMSE is calculated for log transformed values of the predictions and observations, the RI is the exponentiated RMSE. The RI value for the two models under consideration is indicative of the strength of both models to predict ZTD within an acceptable average factor.

The time series plot of the UNB3m model, the GPT2w model, and the reference model (IGS) is shown in Figure 4.2. The ZTD estimated from GNSS as provided by the IGS show excellent diurnal characteristics, as the daily variations are very noticeable. However, the UNB3m and GPT2w models do not give good account for the daily variation in the ZTD estimates, but does provide a good estimate of the average daily variation across all the stations. The presence of the semi-annual amplitudes in the ZTDs is also evident in the plot of the GPT2w model across all the stations. Very prominent in the IGS, UNB3m and GPT2w time series is the annual cycle of the ZTD. Furthermore, the time series and Absolute Mean Difference (Error) (MAE) of the difference between each model and the IGS solution is presented in Figures 4.3(a) and (b). From both figures, it is clear that the difference in ZTD estimate between the GPT2w and the IGS estimates is smaller than that of the UNB3m and the IGS estimates at all stations.

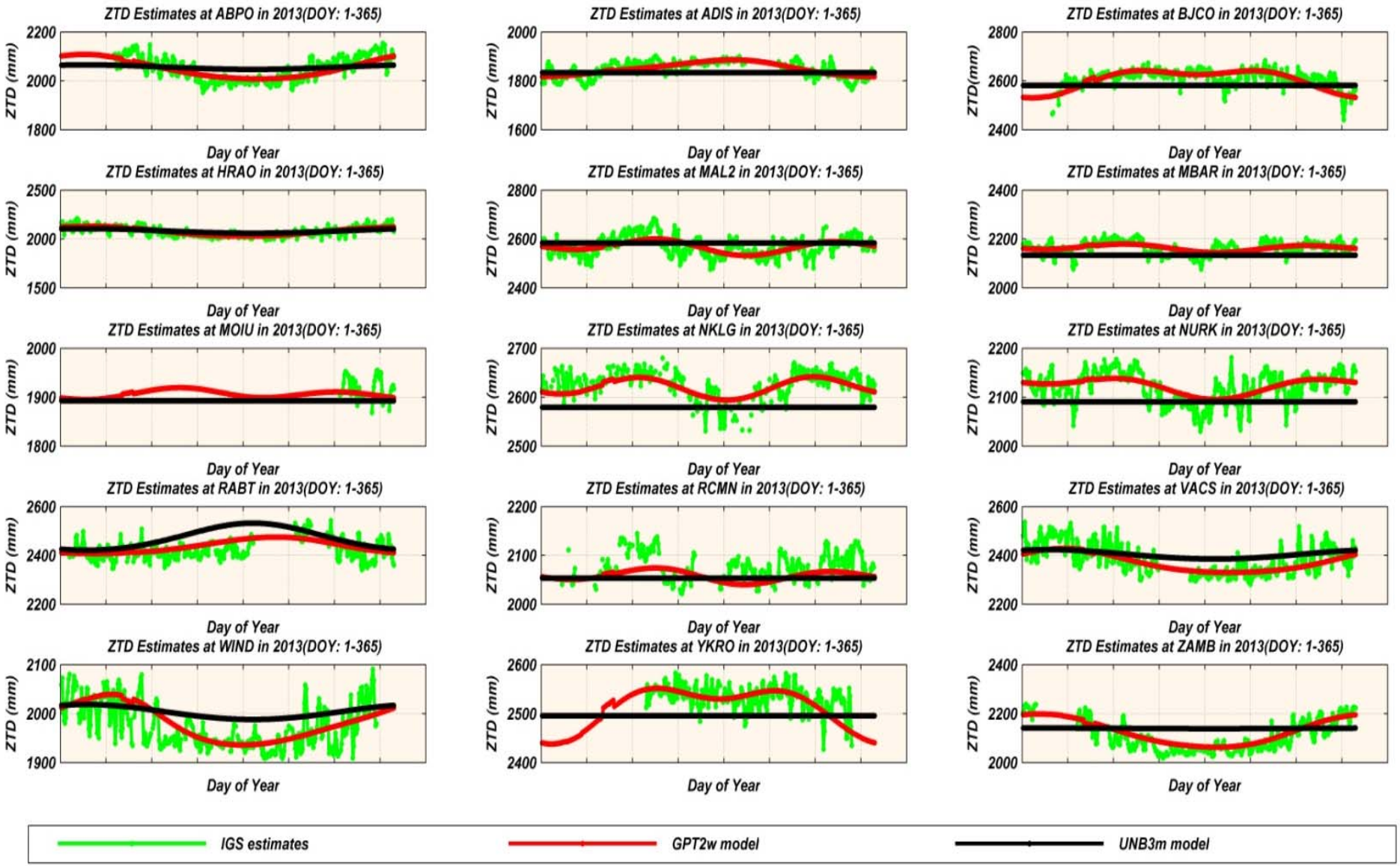

Figure 4.2: Time series plot of the UnB3m, GPT2w, and IGS estimation of ZTD for 2013

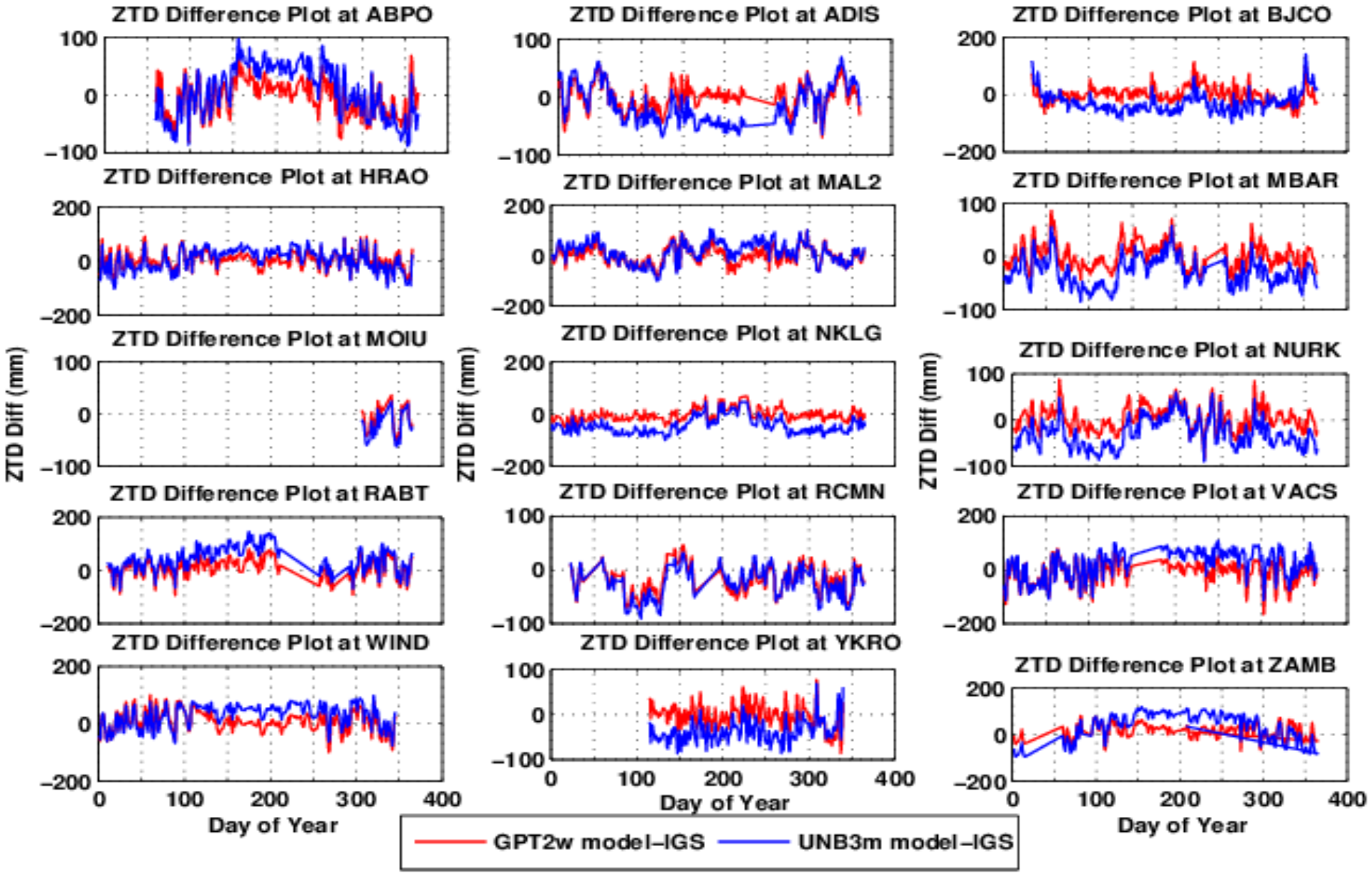

Figure 4.3(a): Time series plot of the difference of UnB3m and GPT2w models to IGS estimation of ZTD for 2013

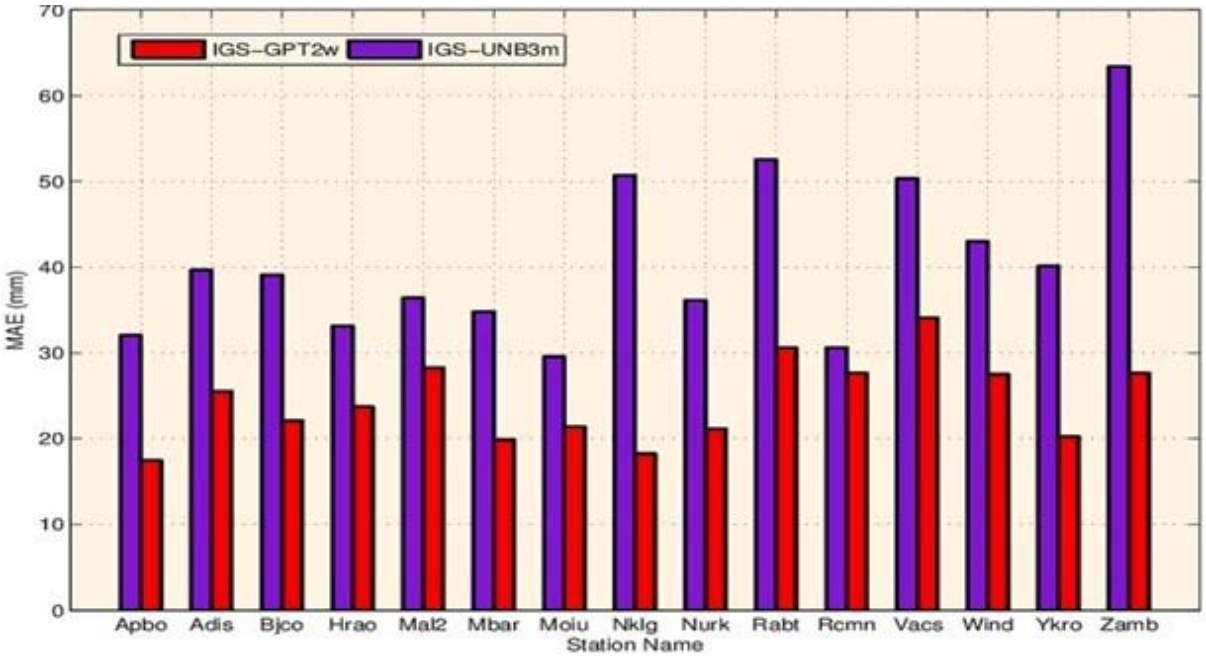

Figure 4.3(b): Plot of the Mean Absolute difference (errors) for the different stations

A fundamental input parameter in the estimation of ZTD from the UNB3m and GPT2w model is the station elevation. It is therefore important to identify the dependence of the ZTD estimates on elevation and also the effect of the individual station elevation and their corresponding RMSE as contained in Table 4.4. The correlation coefficient (r) was employed to ascertain the linear inter-relationship among the IGS product, UNB3m, GPT2w, and station elevation. The resultant correlation matrix is presented in Table 4.5.

Table 4.5: Correlation matrix of the IGS *product, UNB3m, GPT2w, and station elevation*

	Elevation	**IGS**	**GPT2W**	**UNB3m**
Elevation	1	-0.9800	-0.9825	-0.9942
IGS	-0.9800	1	0.9995	0.9939
GPT2w	-0.9825	0.9995	1	0.9953
UNB3m	-0.9942	0.9939	0.9953	1

From Table 4.5 it is clear that the ZTD estimates from the models under investigation exhibit a very strong negative correlation. Thus, an increase in station elevation results in corresponding decrease in the amount of ZTD over the station. This is further confirmed from Figure 4.4, that the best line of fit for the IGS, UNB3m and GPT2w when plotted against the corresponding station elevation has a negative gradient, indicating the inverse proportional relationship by all three models under investigation.

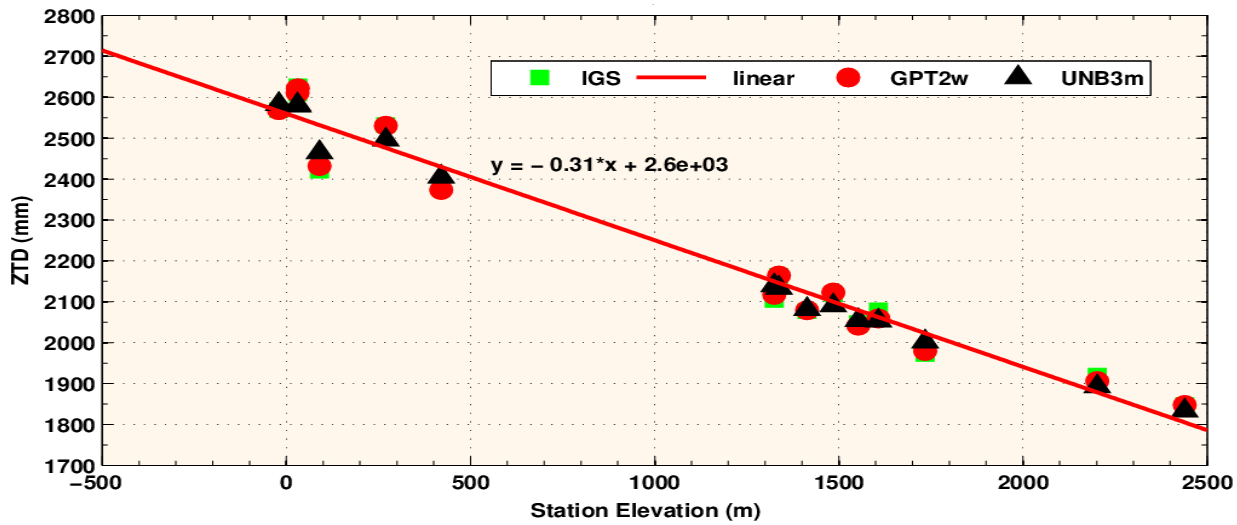

Figure 4.4: Plot of mean ZTD estimates against station elevation

Furthermore, the RMSE of the different stations as presented earlier in Table 4.4 were plotted against the station elevation to ascertain the influence of the latter on the corresponding RMSE. From Figure 4.5 it is evident that no relationship exists between the RMSE and station elevation, which implies that the station elevation does not influence the magnitude of error in ZTD estimates from the UNB3m and GPT2w models. It is again observed in Figure 4.5 that the RMSE for the GPT2w model was smaller at all height values than those of the UNB3m model.

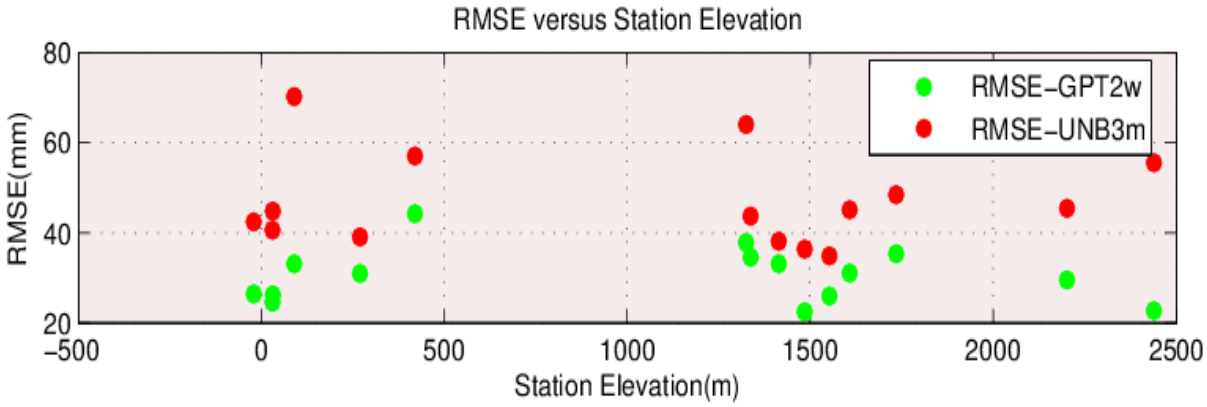

Figure 4.5: Plot of RMSE versus station elevation

The latitudinal dependence of the models was also investigated by comparing the station latitude with the corresponding RMSE and MEF values as shown in Figures 4.6 and 4.7. In Figure 4.6, it is indicative that both the UNB3m and GPT2w models perform better at low latitude ranges, i.e., from $1^{\circ}-10^{\circ}$. Again, the GPT2w performs better at all latitudes.

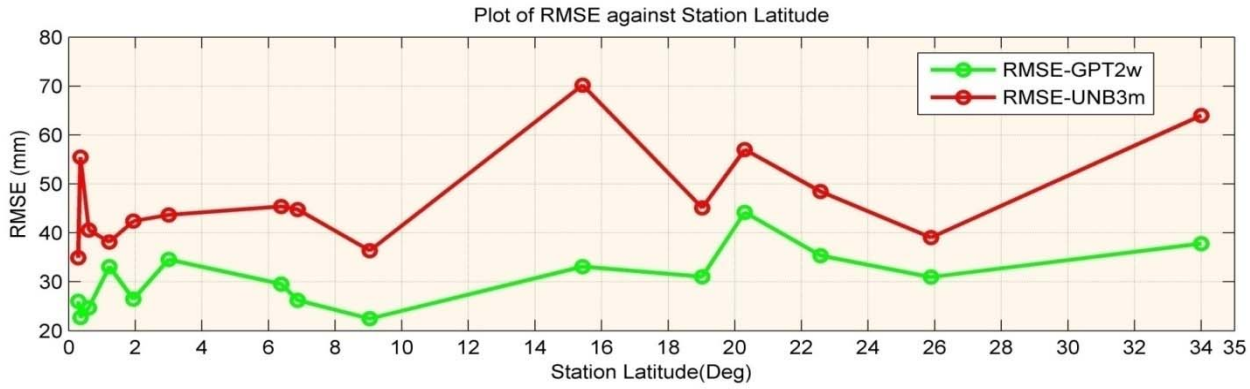

Figure 4.6: Plot of RMSE versus station absolute latitude

As seen in Figure 4.7, the MEF value for the GPT2w appears to be small at low latitudes range of $0^{\circ}-2^{\circ}$, at the same latitude range the UNB3m model is seen to agree with the GPT2w model. Again, the GPT2w have better MEF values for all of the station latitude ranges, except at the stations situated almost at the equator (MBAR, NKLG, and NURK).

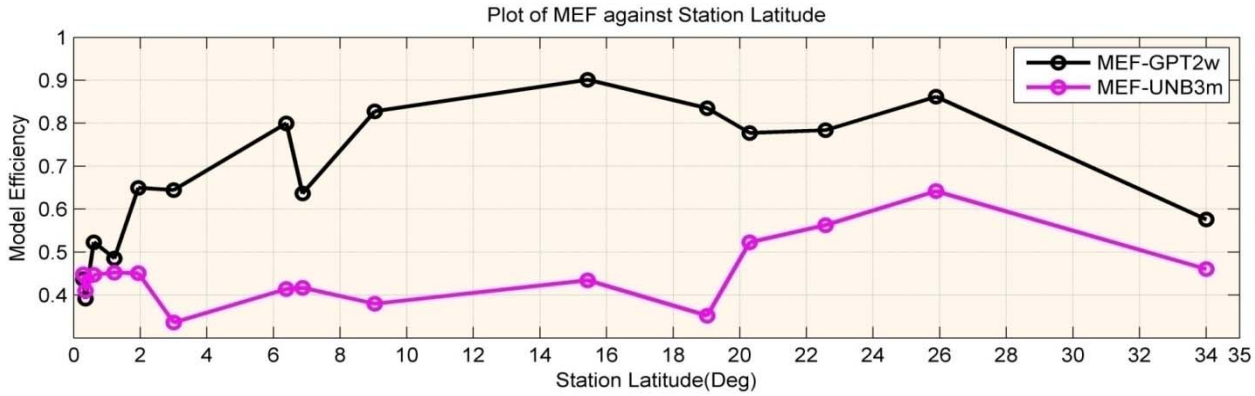

Figure 4.7: Plot of MEF versus station absolute latitude

Figures 4.8 and 4.9 are the ZTD, ZHD and ZWD time series of HRAO for the month of January 2013. HRAO is one the few IGS stations on the continent of Africa that is collocated with meteorological sensors as identified by Isioye et al., 2015a. The station is equipped with a MET 4 meteorological system and data was downloaded at ftp://cddis.gsfc.nasa.gov/pub/gps/data/daily/. This is a high accurate meteorological measurement system for GNSS meteorology and environmental monitoring; it measures pressure with an accuracy of +/- 0.05 hpa from 500 to 1100 hpa, temperature +/- 0.2 deg Celsius, and humidity +/- 2% to 100% at standard temperature.

In Figure 4.8, ZTD was computed with the Saastamoinen formula using measured pressure and temperature at the site and was compared with the IGS product, UNB3m and GPT2w models. The corresponding ZHD and ZWD are according to Equations 4.1 and 4.3.

From Figure 4.8 it is indicative that the ZTD trend from the Saastamoinen model agrees very well with the IGS solution, with the GPT2w showing very little variation from the IGS solution, and the UNB3m appearing almost constant throughout. The ZHD from IGS product was retrieved from the measured pressure values at the station with the Saastamoinen formula. It can be seen that there is strong agreement among the IGS, Saastamoinen and GPT2w models, this can be interpreted as an indication of the effectiveness of the GPT2w models, and the UNB3m model could still not account for the variation in daily ZHD at the station. Looking at the ZWD estimates, there is again very strong agreement between the Saastamoinen and IGS product. The UNB3m and GPT2w models show weakness in accounting for the daily variation in ZWD estimation, though a careful scrutiny of the data reveal insignificant variations in the ZWD values for the GPT2w model.

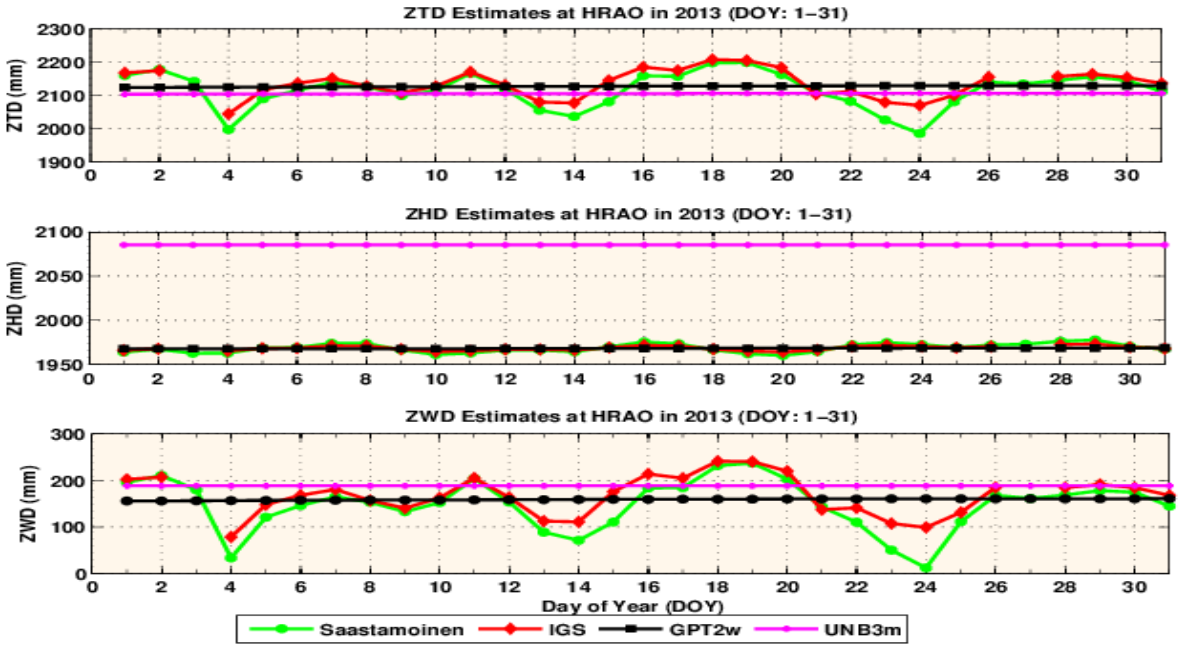

Figure 4.8: Estimated ZTD, ZHD, and ZWD from the Saastamoinen formula, IGS product, GPT2w model, and UNB3m model at HRAO for doy of Year 1-31, 2013. The Saastamoinen formula using meteorological parameters measured with a MET 4A unit for ZHD and ZWD estimation, the ZHD from the IGS product was also retrieved utilizing the measured parameter from the Met 4A unit

Figure 4.9 presents some very contrasting results, ZTD was computed with the Saastamoinen formula using standard pressure and temperature values at the site and was compared with the IGS product, UNB3m and GPT2w models. The corresponding ZHD and ZWD from the Saastamoinen formula are according to Equations 4.1 and 4.3. From Figure 4.9 it is clear that the Saastamoinen formula fails to agree with the other methods, with the

GPT2w and the UNB3m models appear almost constant throughout. The ZHD from IGS product was retrieved from the standard pressure values at the station with the Saastamoinen formula. It can be seen that there is strong agreement between the IGS estimates, and GPT2w model, thus this is another indication of the effectiveness of the GPT2w model, both the UNB3m and Saastamoinen formula could still not account for the variation in daily ZHD at the station and the Saastamoinen formula appears to overestimate the quantity. Looking at the ZWD estimates, there is very strong agreement between the Saastamoinen formula and the GPT2w model. Careful inspection of the data reveals small variations in the ZWD values for the GPT2w model. Again the UNB3m model shows weakness in accounting for the daily variation in ZWD estimation.

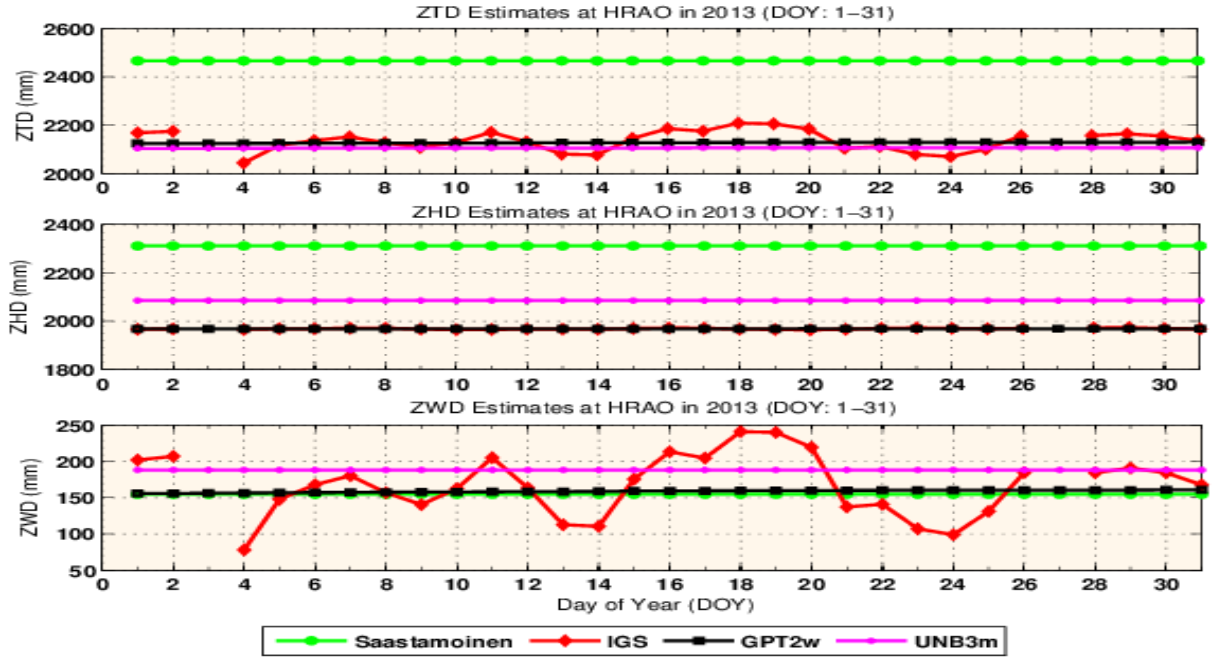

Figure 4.9: Estimated ZTD, ZHD, and ZWD from the Saastamoinen formula, IGS product, GPT2w model, and UNB3m model of HRAO for doy of Year 1-31, 2013. The Saastamoinen formula using standard meteorological parameters for ZHD and ZWD estimation, the ZHD from the IGS product was also retrieved utilizing standard met parameters

4.4 Concluding Remarks

We have estimated the accuracies of the UNB3m and GPT2w tropospheric correction models over Africa by using the ZTD time series from the global IGS GNSS network in Africa, and Saastamoinen formula based on measured meteorological parameters. The UNB3m and GPT2w models are unique representations of the two distinct groups of blind tropospheric models in global use. The UNB3m model utilises a lookup table with annual

mean and amplitude of temperature, pressure, and water vapour pressure varying with regard to latitude and height. These parameters are computed for a particular latitude and day of the year using a cosine function of the annual variation and a linear interpolation for latitude. Similarly, the GPT2w is based on gridded values of water vapour pressure, water vapour decrease factor, and weighted mean temperature. All climatological parameters have been derived consistently from monthly mean pressure level data of ERA-Interim fields with a horizontal resolution of 1°. Thus, based on the comparisons we arrive at the following conclusions:

I. The accuracy of ZTD correction from the GPT2w model is well within the range of 50 mm, and this accuracy can meet the needs of the tropospheric delay correction of the order of meters, in GNSS positioning.

II. Both models perform well at the low equatorial region of Africa and respond to station elevation in the similar fashion.

III. The GPT2w represents an excellent model for ZHD estimation due to its high accurate pressure estimates.

IV. The GPT2w model shows very good signatures of seasonal ZTD trend but weak daily variations, but in both cases better than the UNB3m model.

V. The Saastamoinen model performs poorly with the use of standard atmospheric parameters and thus fails to address the peculiarities of the African GNSS network which is characterized by a lack of sensors for measuring meteorological data. Thus, better estimates of ZTD from GNSS can be obtained with the GPT2w model without actual field measurements.

Finally, there was better agreement between the GPT2w and IGS estimate at all stations. Therefore, the GPT2w model can be used as a correction model of the tropospheric error for the GNSS real-time positioning and navigation on the African Continent.

Acknowledgement

This study was supported by HartRAO and funded by the University of Pretoria PhD Research Support grant to the first author. The authors would like to express their profound gratitude to the numerous reviewers for their constructive comments that helped to improve the manuscript.

Chapter 5

Evaluation of Surface Variables from Global Reanalysis Models and their Application in Precipitable Water Vapour Retrieval from GNSS Observations over Nigeria **

"I do not know what I may appear to the world, but to myself I seem to have been only like a boy playing on the sea-shore, and diverting myself in now and then finding a smoother pebble or a prettier shell than ordinary, whilst the great ocean of truth lay all undiscovered before me."

— Isaac Newton

Précis

This study investigated the accuracy and suitability of using reanalysis datasets in retrieving atmospheric precipitable water vapour (PWV) from ground-based global navigation satellite system (GNSS) observations over Nigeria. To achieve the objective of the study, the research was conducted in two parts. In the first part of the study, three surface variables (temperature, pressure, and humidity) from NCEP/NCAR and ERA-Interim Reanalysis models were compared with observations at 26 automatic weather observing stations in order to ascertain the accuracy of the models. In the second part of the study the feasibility of retrieving PWV from GNSS using reanalysis data was investigated. The GPT2 empirical meteorological model, of which the climatological dataset is on fields of ERA-Interim and which is specifically recommended for GNSS and other geodetic applications, was investigated as well. Standard verification indices as recommended by the World Meteorological Organization were adopted in evaluating the models. The results established perfect agreement between the theoretically simulated precision of PWV estimated from ERA-Interim and NCEP/NCAR and that based on actual or practical formulations and data. Both estimates show that PWV can be retrieved to within a precision of about 1 mm provided GNSS-derived zenith tropospheric delay is of high precision. Finally, based on the results and findings of this study, the use of reanalysis models in the retrieval of PWV from GNSS is recommended for users in Nigeria and also to improve on the precision of PWV retrieval from GNSS. We further recommend that a regional/local model of the atmospheric mean temperature be developed.

This chapter consists of formatted text for one peer reviewed conference paper as follows:

Isioye O. A. 2016. *Evaluation of Surface Variables from Global Reanalysis Models and theirAapplication in Precipitable Water Vapour Retrieval from GNSS Observations over Nigeria.* In the Proceedings of the 29th International Technical Meeting of the satellite division of the Institute of Navigation (ION GNSS + 2016), September 12-16, pp.1617-1641, Portland, Oregon, USA (**STUDENT AWARD PAPER,** *https://www.ion.org/gnss/abstracts.cfm?paperID=4432*

5.1 Introduction and Background

For many meteorological applications, measured or observed station data have restricted spatial coverage, and so reanalysis data are used as a substitute. Reanalysis data are created from consistent reprocessing of archived weather data by means of three- (or four-) dimensional data assimilation schemes based on physical models (Gleisner et al., 2005; Liu et al., 2012; Dee et al., 2014). In recent times, advances in technology have yielded significant progress in the value and quantity of the ensuing reanalysis datasets (Bosilovich et al., 2013; Hartmann et al., 2013; Dee et al., 2014; Kaiser-Weiss et al., 2015). These developments have catalysed swift progression in the acceptance of reanalysis datasets for a varied and emergent variety of purposes. The accuracy requirement from different users varies and suitability for one function does not certify suitability for all functions. It is crucial for different users to comprehend which (if any) of the accessible reanalysis datasets are suitable for their applications (Kaiser-Weiss et al., 2015; Gregow et al., 2015). Evaluating the appropriateness of reanalysis datasets for a particular application involves combining facts regarding the comparative strengths/weaknesses of the obtainable datasets, the degree to which such features influence the reliability of derived results and the distinctive precision and accuracy requirements of the user (Kaiser-Weiss et al., 2015).

One area in which reanalysis datasets have gained prominence is in the emerging discipline of GNSS meteorology. Modelled atmospheric parameters from GNSS space and ground-based systems are often assimilated into numerical weather prediction (NWP) models, and both have been shown to yield significant benefits in operational NWP weather forecasting (Gent et al., 2004; Vedel et al., 2004; Elgered et al., 2005; Poli, 2006; Marc et al., 2007; Bennitt and Jupp, 2012; Cucurull et al., 2012; Dousa and Vaclavovic, 2014). Conversely, surface variables from reanalysis models are employed in the accurate estimation of three-dimensional positions and zenith tropospheric delay (ZTD) from GNSS observations (Vedel et al., 2001; Chen et al., 2011; Pany et al., 2001; Jupp et al., 2003; Hobiger et al., 2010; Fund et al., 2011; Alves et al., 2015; Wilgan et al., 2015), and also in the conversion of ZTD into precipitable water vapour (PWV) (Jade et al., 2005; Jade and Vijayan, 2008; Bosy et al., 2010; Simeonov et al., 2015).

The National Centre for Environmental Prediction and National Centre for Atmospheric Research (NCEP/NCAR) and the European Centre for Medium-Range Weather Forecasts (ECMWF) are providers of reanalysis datasets on a global scale. Both at global

and regional scales the different variables from ECMWF and NCEP reanalysis models have been appraised and reported (Provost and Escoffier, 1998; Hanson et al., 2004; Zhao and Fu, 2009; Yu et al., 2010; Marques et al., 2010; Liu et al., 2012). Although products from the two major providers of reanalysis datasets demonstrate good abilities in capturing the character of some variables, there are many discrepancies in these variables from model to model, and from variable to variable (Zhu 2009; Marques et al., 2009, 2010; Yu et al., 2010; Simmons et al., 2010; Liu et al., 2012; Trambauer et al., 2014). Bozzano et al. (2004) compared surface meteorological data (air temperature, relative humidity, barometric pressure, wind speed and direction) from the Spar buoy located in the Ligurian Sea with ECMWF reanalysis data. The comparison shows that the reanalysis model reproduces significant differences in the result of the variables. Similar studies have also found that reanalysis models act better over land than over oceans (Trenberth et al. 2005; Aquila et al., 2005; Jakobson et al., 2012; Tastula et al., 2013). Studies have also shown that the performance of reanalysis models varies in the different regions of the earth, i.e. drought variability as assessed based on datasets from ECMWF and NCEP reanalysis models on two different continents produced varying results. In the USA there was good agreement between the reanalysis models and observations, while in Europe the two datasets revealed significant variance (Bordi et al., 2006). Also, Grotijahn (2008) reported that ERA-40 data from ECMWF have more moisture in the tropics, while in the subtropics NCEP reported more moisture.

Studies have compared NCEP/NCAR reanalysis datasets against those of ECMWF reanalysis and good agreements were reported (Fan and Wang, 2004; Sun et al., 2008; Yue and Wang, 2008; Zhu, 2009). Conversely, poor agreement between the NCEP and ECMWF dataset is reported, for example in temperature in the southern high latitudes (Connolley and Harangozo, 2001) and monsoon onset in West Africa (Sultan et al., 2007). Several other studies around the world have shown that ECMWF reanalysis datasets perform better than NCEP reanalysis when compared to observational data (Bromwich et al., 1995; Provost and Escoffier, 1998; Cui et al., 2000; Inoue and Matsumoto, 2004; Hanson et al., 2004; Zhao and Fu, 2006; Zhao and Fu, 2009; You et al., 2010; Yu et al., 2010; Marques et al., 2010; Liu et al., 2012). Conversely, Tastula et al. (2012), Gleisner et al. (2005), Béranger et al. (2006), and Aoki and Kutsuwada (2008) have all reported better performance in NCEP data in comparison with ECMWF data.

Previous investigations on the applicability of reanalysis models have assisted those working in different fields to be aware of the strengths and weaknesses of the different global

reanalysis products over the different continents and regions where such studies were carried out. Consequently, reanalysis datasets should be assessed cautiously prior to being applied in associated research. Thus, the major objective of this study is to confirm whether reanalysis datasets do in reality characterize the exact state of the atmosphere over Nigeria and also to ascertain if the accuracy of the reanalysis datasets are sufficient for some scientific application, such as in the aforementioned field of GNSS meteorology. In this paper, we illustrate the inter-comparisons that were undertaken to elucidate the relative properties of the near-surface temperature, pressure, and humidity over Nigeria in two global reanalysis datasets (NCEP/NCAR reanalysis from the NCEP and ERA-Interim (ERAI) from ECWMF) on a time scale of days to three years (2010-2012). Independent observations from Nigerian weather stations were used for the inter-comparisons. Finally, the suitability of estimating PWV from GNSS ZTD using reanalysis data and the global pressure and temperature (GPT) empirical model was also investigated.

This paper is organised in the following manner: In Section 5.2 a detailed description of the dataset used and the methodology employed in this study is given. Results and discussions are contained in Section 5.3, and final concluding remarks are contained in Section 5.4.

5.2 Data and Methods

5.2.1 Reanalysis Datasets

Surface temperature, humidity and pressure data were collected from the two NWP models in Network Common Data Form (NetCDF) format.

The NCEP/NCAR reanalysis project makes use of a state-of-the-art analysis/forecast system to carry out data assimilation by utilising a historic dataset from 1948 to the present (Sarazin et al., 2003). As reported by Kalnay et al. (1996), NCEP/NCAR reanalysis was the foremost of its class for the National Oceanic and Atmospheric Administration (NOAA). The NCEP used the same climate models that were prepared with a wide range of weather observations, which includes observations from ships, planes, RAwinsonde Observations (RAOBs), station data, satellite observations, and several other datasets. The NCEP/NCAR reanalysis is a gridded dataset having a grid size of $2.5^{\circ} \times 2.5^{\circ}$, at 17 hybrid vertical levels, available at 0000, 0600, 1200, and 1800 UTC daily (Kalnay et al., 1996; Kistler et al., 2001). The NCEP/NCAR reanalysis data used in this research were obtained from the

NOAA/OAR/ESRL PSD (Boulder, Colorado, USA), via their website at http://www.esrl~.noaa.gov/psd/.

The ERAI is a global atmospheric reanalysis from 1979 to the present, which is continuously updated in real time. The ERAI was only recently released in 2011, and is based on cycle 31r2 of the ECMWF's Integrated Forecast System (IFS), which was introduced in 2006. The system includes an ECMWF 4D variational assimilation system in preparation for the reanalysis to replace ERA-40 and is well documented in Dee et al. (2009, 2011) and Simmons et al. (2014). The ERAI is a grid dataset with a spectral resolution of approximately 80 km (T255 spectral) on 60 vertical levels from the surface up to $0.1\,hPa$. The gridded ERAI data products consist of a huge range of three-hourly surface parameters, unfolding weather along with ocean-wave and land-surface conditions, six-hourly upper-air parameters covering the troposphere such as temperature and relative humidity, vertical integrals of atmospheric fluxes, monthly averages for many of the parameters, and other derived fields (see Dee et al., 2011). Data used for this study were obtained at http://apps.ecmwf.int/~datasets/data/interim-full-daily/levtype=sfc/ .

Although the two reanalysis models are based on different horizontal resolutions, the data were downloaded at the same grid point: the ERAI data were downloaded by specifying a $2.5^{\circ} \times 2.5^{\circ}$ grid. A total of 36 grid nodes cover the country of Nigeria.

5.2.2 Observational Data

The Nigerian Meteorological Agency operates over 50 automated weather observing stations (AWOS) that have been established in different synoptic stations distributed all over Nigeria in order to measure and determine surface observations in addition to the manual observing stations. The AWOS systems consist of the integrated sensor suite, sensor interface module, console receiver, solar panel, and a computer system (see https://www.wmo.int/~pages/prog/www/IMOP/publications/IOM-94-TECO2006/P3(20)_Aderinto_Nigeria.pdf). Each AWOS observes a wide range of parameters. For the purpose of this study, 26 AWOS were selected across Nigeria, and were primarily chosen based on their accessibility to data and their proximity to the GNSS stations. Daily and sub-daily pressure, temperature and humidity data from the 26 stations were collected for the period 2010 to 2012. Table 5.1 provides the coordinates and descriptions of the AWOS.

Table 5.1: Coordinates and name of all AWOS used in the study

Station name	Latitude (Deg)	Longitude (Deg)	Altitude (m)	Coverage
Abuja	9.2500	7.0000	343	2010-2012
Akure	7.2833	5.3000	375	2010-2012
Bauchi	10.2833	9.8167	609	2010-2012
Calabar	4.9667	8.3500	64	2010-2012
Enugu	6.4667	7.5500	137	2010-2012
Gasau	12.1667	6.7000	463	2010-2012
Ibadan	7.4333	3.9000	227	2010-2012
Ibi	8.1833	9.7500	110	2010-2012
Ikeja	6.5833	3.3333	39	2010-2012
Jos	9.6333	8.8500	1285	2010-2012
Kano	12.0500	8.2000	472	2010-2012
Kastina	13.0167	7.6833	506.1	2010-2012
Lafia	8.4833	8.5000	385	2010-2012
Lagosrf	6.4500	3.4000	19.5	2010-2012
Maiduguri	11.8500	13.0833	353	2010-2012
Makurdi	7.7333	8.5333	112	2010-2012
Obudu	6.6000	9.3167	284	2010-2012
Ondo	7.1000	4.8333	287	2010-2012
Oshodi	6.5000	3.3833	19	2010-2012
Owerri	5.4833	7.0000	19	2010-2012
Port-Harcourt	4.8500	7.0167	24.7	2010-2012
Sokoto	13.0167	5.2500	350	2010-2012
Uyo	5.5000	7.9167	38	2010-2012
Yelwa	10.8833	4.7500	244	2010-2012
Yola	9.2333	12.4667	190.5	2010-2012
Zaria	11.1000	7.6833	655	2010-2012

5.2.3 Validation of Reanalysis Dataset using AWOS over Nigeria

Surface variables from the two reanalysis models were interpolated onto the AWOS locations using a bilinear interpolation approach. A weighted average of four adjoining grid points is used to determine the interpolated value. The concept of bilinear interpolation is described by Bosy et al. (2010, 2012) and Hadas et al. (2013).

In the interpolation scheme for every individual AWOS station within the network, values of meteorological parameters from the four nearest ERAI and NCEP/NCAR reanalyses gridded data are utilized. The value of a particular parameter, ξ , indicating the temperature (T), relative humidity (H), and pressure (P) at an AWOS station, is estimated from the known grid points as a weighted average:

$$\overline{\xi}_{AWOS} = \sum_{i=1}^{n} \xi_i w_i \Big/ \sum_{i=1}^{n} w_i , \tag{5.1}$$

where ξ_i are meteorological parameters T_i, P_i, and H_i from n points, at which observations were made (reanalysis grids), while weights w_i are computed depending on interpolated parameters.

For temperature $\xi = T$, weight w_i is computed on the basis of Equation 5.2:

$$w_i = \left(h_{AWOS} - h_i\right)^{-4} , \tag{5.2}$$

where $h_{AWOS} - h_i$ is the height difference between AWOS and the NWP grid point i, and h_i is the geopotential height in the case of ERA-Interim and NCEP/NCAR reanalysis data. For AWOS, station height is corrected to obtain the geopotential height of the point.

The weight for humidity $\xi = H$ derives from Equation 5.3:

$$\frac{1}{w_i} = \left(x_{AWOS} - x_i\right)^2 + \left(y_{AWOS} - y_i\right)^2 + \left(h_{AWOS} - h_i\right)^2 , \tag{5.3}$$

where x_{AWOS} and y_{AWOS} are planar coordinates of the AWOS station and x_i and y_i are the coordinates of the known weather station or grid node of the NWP model, as the case may be.

For pressure $\xi = P$, weight w_i is computed from Equation 5.4:

$$w_i = \left[\left(x_{AWOS} - x_i\right)^2 + \left(y_{AWOS} - y_i\right)^2\right]^{-2} . \tag{5.4}$$

Rankine and Bamber (*2009*) present a barometric levelling formula for recalculating pressure value to the elevation of the interpolated station. The formula is as shown in Equation 5.5:

$$\log \xi_i = \log P_i + \frac{h_i - h_{AWOS}}{18400\left(1 + \left(T_{AWOS} + T_i\right)/546\right)} . \tag{5.5}$$

In the final stage, the weighted average is obtained from the calculated values using weights from Equation (5.1).

Numerous verification criteria were used to validate the reanalysis datasets over Nigeria. The verification procedures adopted are based on indices recommended by the World Meteorological Organization (WMO) (WMO, 1992; 2002), which were broadly classified into two categories: (1) the deterministic/dimensional metrics (2) non-dimensional/probabilistic metrics.

Firstly, we considered the deterministic/dimensional metrics, four-model performance indicators to verify the results of the reanalysis model were used in this category. This

includes the mean absolute error (MAE) (Shcherbakov et al., 2013), root mean square error (RMSE) (WMO, 1992), standard deviation of residuals (SDR) (WMO, 1992), and anomaly correlation coefficient (ACC) (Jolliffe and Stephenson, 2003). Here, the MAE measures the absolute deviation of the simulated values (NCEP/NCAR and ERAI) from the observations (AWOS). Similarly, RMSE measures the average square error and SDR is a measure of the dynamical correspondence. A value near zero indicates a close match for the MAE, RMSE and SDR. ACC values range from [-1, 1]; a positive value indicates perfect coincidence between observed and forecast anomalies. In turn, a negative value occurs when the pattern is reversed.

Table 5.2: Formulation for the different verification indices used in validating reanalysis over Nigeria

MAE	$1/N \sum_{i=1}^{N} (\lvert Diff_i \rvert)$
RMSE	$\sqrt{\frac{\sum_{i=1}^{N} (Diff_i)^2}{N}}$
SDR	$\sqrt{\left[\frac{\sum_{i=1}^{N} (Diff_i)}{N} - (\bar{O} + \bar{P})\right]^2}$
ACC	$\frac{\sum_{i=1}^{N} (P_i - \bar{P})(O_i - \bar{O})}{\left[\sum_{i=1}^{N} (P_i - \bar{P})^2 \cdot \sum_{i=1}^{N} (O_i - \bar{O})^2\right]^{1/2}}$
MEF	$1 - \frac{\sum_{i=1}^{N} (Diff_i)^2}{\sum_{i=1}^{N} \left(\lvert (P_i - \bar{O}) \rvert - \lvert (O_i - \bar{O}) \rvert\right)^2}$
ES	$1 - \frac{\sum_{i=1}^{N} (Diff_i)^2}{\sum_{i=1}^{N} (O_i - \bar{O})^2}$
IA	$1 - \frac{\sum_{i=1}^{N} \lvert Diff_i \rvert}{\sum_{i=1}^{N} \left(\lvert P_i - \bar{O} \rvert + \lvert O_i - \bar{O} \rvert\right)}$
RI	$\exp \sqrt{\frac{1}{N} \sum_{i=1}^{N} \left(\log \frac{O_i}{P_i}\right)^2}$

Secondly, the non-dimensional/probabilistic metrics were used to verify the reanalysis datasets. The model efficiency (MEF) (Murphy, 1988; Leuning et al., 1998; Yu et al., 2011), Nash-Sutcliffe score (ES) (Nash and Sutcliffe, 1970), index of agreement (IA) (Legates and McCabe Jr, 1999; Willmott et al., 2012), and reliability index (RI) (Leggett and Williams,

1981) were employed. The MEF is a measure of how well the model (NCEP/NCAR and ERAI) forecasts the observed (AWOS) values relative to the average of the observations. Similarly, the IA is a standardised measure of the degree of model prediction error. MEF and IA values vary between 0 and 1, MEF/IA = 0 implies no agreement between forecast values and observations, MEF/IA = 1 implies perfect agreement. The ES is a normalised measure that determines the scale of the residual variance relative to the measured data variance and varies between negative infinity and one. An ES value of one implies perfect agreement between simulated values (NCEP/NCAR and ERAI) and observations (AWOS). The RI quantifies the average factor by which the model (NCEP/NCAR and ERAI) estimates differ from the AWOS observations. A large RI value is indicative of large divergence between the forecast and measured values. The value of RI=1 is the case of perfect forecasting. The mathematical formulation of the different verification indices (performance indicators) is represented in Table 5.2.

In Table 5.2, the difference between "i^{th}" observed(O_i) and model estimated(P_i) values is given as $Diff_i$, the average of the observed and model-estimated values is indicated by $\overline{O}$ and $\overline{P}$, respectively, and the number of observations indicated by N.

5.2.4 Application of Reanalysis Dataset in GNSS Atmospheric Precipitable Water Vapour Estimation

For the purpose of estimating atmospheric PWV from GNSS, we processed GNSS data at five stations on the Nigeria GNSS network (NIGNET) for the year 2013. The choice of selection of the GNSS stations was based on their proximity to AWOS sites (see Figure 5.1).

We processed the GNSS data using GAMIT/GLOBK software. In order to acquire reliably accurate ZTD estimates, the GNSS data-processing parameters and models were cautiously set up in the GAMIT/GLOBK software. A summary of these are presented in Table 5.3. The ZTD at each GNSS station was estimated daily within a 24-hour window session. Details of the strategy adopted for processing the GNSS data from the NIGNET stations have already been already reported (Isioye et al., 2015a).

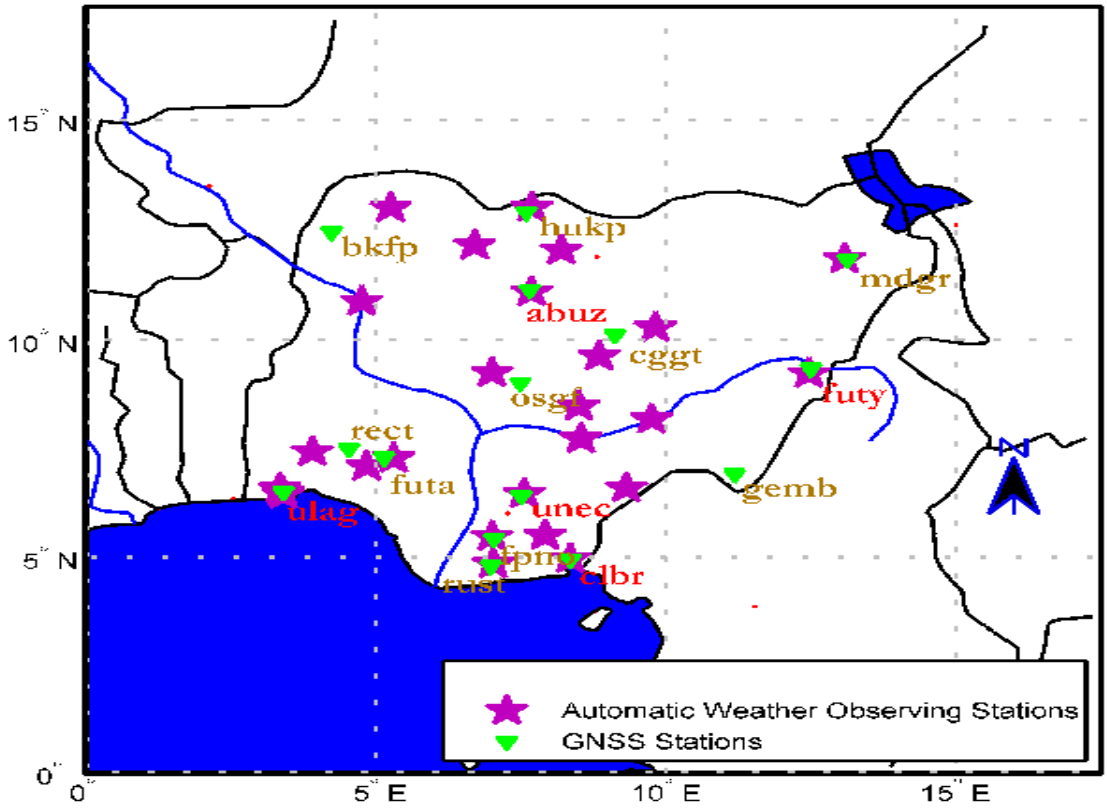

Figure 5.1: Location of AWOS and NIGNET GNSS sites in Nigeria

Table 5.3: Summary of adopted processing parameters used in GAMIT software for ZTD estimation in this study

Item	Strategies & models
Observations	Double difference ionospheric free (IF) combination at 30 s sampling rate
Elevation cut-off	10 degrees
Satellite orbits/earth rotation parameters (EOP)	IGS final orbits (SP3) and IGS final ERP products
Tropospheric delay	Saastamoinen model (1972)+ random-walk process
Ionospheric delay	Double difference IF linear combination
Mapping function	Vienna mapping function (Boehm et al., 2006a)
Station coordinates	Heavily constrained to their ITRF 2008 values (Altamimi et al., 2011)
Meteorological observation source	GPT 50
Station displacement	Solid earth tide based on IERS03, and ocean tide loading correction based on FES2004
ZTD estimates	Daily
Relative Troposphere constraints	The constraint used for zenith delay was 0.2 m, as it is recommended to set it loose enough to encompass any error in wet delay (Herring et al., 2006)
Satellite antenna PCO & PCV	AZEL for IGS absolute ANTEX files (Gendt and Schmid 2005)

The derived ZTD represents a summation of the zenith hydrostatic delay (ZHD) and the zenith wet delay (ZWD) and is expressed as:

$$ZTD = ZHD + ZWD \tag{5.6}$$

The ZHD is often calculated using empirical models (i.e. Saastamoinen or Hopfield models), together with measured station level pressure at the GNSS station. Ideally, meteorological sensors need to be collocated with the GNSS antenna for the purpose of accurate estimation of ZHD. However, all the GNSS sites that currently make up the NIGNET do not have the required meteorological unit collocated with them, and this is also the case with many other GNSS stations on the African continent (Isioye et al., 2015a). Alternatively, surface temperature and pressure data from nearby weather stations were transferred to the GNSS using the approach described in Bai and Feng (2003), and Musa et al. (2010). In the approach, mean sea level temperatures and pressure values were transferred to the GNSS site as follows:

$$\left.\begin{aligned} T_{GNSS} &= T_{MSL} - 0.0065 \cdot H_{GNSS} \\ P_{GNSS} &= P_{MSL}\left(1 - 0.0000226 \cdot H_{GNSS}\right)^{5.225} \end{aligned}\right\}. \tag{5.7}$$

Table 5.4: GNSS stations in the NIGNET and corresponding nearest AWOS

GNSS Station	AWOS Station	Station Height (m)		Horizontal Distance (m)
		GNSS	AWOS	
abuz	Zaria	705.054	655.000	6855.027
clbr	Calabar	916.432	64.000	1822.215
futy	Yola	247.392	190.500	14391.763
ulag	Lagos RF	44.563	19.500	7447.335
unec	Enugu	254.391	137.000	6800.764

In Equation (5.7), T_{GNSS} and P_{GNSS} are reduced temperature and pressure at the GNSS site; T_{MSL} and P_{MSL} are the corresponding mean sea level values of temperature and pressure at the AWOS site, respectively. Equation (5.7) takes into account the sensitivity of the variability of pressure and temperature at the GNSS antenna height $\left(H_{GNSS}\right)$. As noted earlier,

the selection of the GNSS stations under investigation in this study was based on proximity to AWOS. Table 5.4 lists the GNSS stations and the corresponding nearest AWOS.

The ZWD was derived from Equation (5.6) according to the relation $ZWD = ZTD - ZHD$. Also, the reanalysis datasets were interpolated to the GNSS station using the earlier approach explained in Section 5.3. We find it vital at this point to include the GPT2 meteorological model in the PWV estimation. The accuracy of the model in estimating PWV has already been reported by Mengistu Tsidu et al. (2015). The GPT2 is an improvement of the global pressure temperature (GPT) model (Boehm et al., 2007), and is a state-of-the-art empirical model that has been produced from a combination of GPT and global mapping function and addresses all known weaknesses of both (Lagler et al., 2013). The GPT/GPT2 models are highly recommended for GNSS application. The GPT2 empirical model is based on 10 years (2001-2010) of global monthly mean profiles for pressure, temperature, specific humidity and geopotential from ERAI. Thus, the GPT2 can be viewed as a modification of the ERAI, which is already under investigation in this study. GPT2 provides pressure and temperature at any site on the earth's surface. The global accuracy of pressure and temperature estimates from GPT2 is reported in Lagler et al. (2013). Isioye et al. (2015c) further confirm the excellent pressure estimates from GPT2 in the estimation of ZHD using the empirical Saastamoinen formula. Table 5.5 presents a summary of the features of the GPT2 model.

Table 5.5: Summary of features in the new GPT2 empirical meteorological model

	GPT2
NWM data	Monthly mean profiles from ERAI at 37 pressure levels from 2001-2010
Representation	Spherical harmonics up to degree and order of 9 at mean sea level and 5° grid at mean ETOPO5 heights
Temporal variability	Mean, annual, and semi-annual terms
Phase	Estimated
Temperature reduction	Mean, annual semi-annual terms of temperature lapse rate estimated at every grid point
Pressure reduction	Exponential based on virtual temperature at each point

Estimated pressure values from the AWOS, ERAI, NCEP, and GPT2 models alongside estimated ZTD from GNSS data by the GAMIT software were utilized in estimating ZHD. Thus, the corresponding ZHD was estimated from the Saastamoinen

formula. The PWV is related to ZWD using the following (Bevis et al., 1992; 1994; Isioye et al., 2015a):

$$PWV = \frac{IWV}{\rho_w} = \frac{\left[ZTD_{GNSS} - ZHD\right]}{10^{-6} R_w \rho_w \left[k_2' + \frac{k_3}{T_m}\right]} = \Pi\left[ZTD_{GNSS} - ZHD\right] = \Pi \cdot ZWD \ . \quad (5.8)$$

In Equation (5.8), IWV is the integrated water vapour, ρ_w is the water density, $R_w = 461.525 \pm 0.003\left[Jkg^{-1}K^{-1}\right]$ is the specific gas constant for water vapour, $k_2' = 22.1 \pm 2.2 Kmb^{-1}$ and $k_3 = 373900 \pm 0.012 K^2 mb^{-1}$ are refraction constants, and T_m is the mean water vapour temperature of the atmosphere measured in Kelvin. We adopted the formula of Bevis et al. (1992), which suggests the estimation of T_m from surface temperature T_s because of the good correlation between the two variables. Thus, according to Bevis et al. (1992), T_m is represented as shown in Equation (5.9), and T_s from the different meteorological models under investigation is again used to correspond with ZHD estimated from the same sources.

$$T_m = 70.2 + 0.72 T_s \ . \quad (5.9)$$

The total uncertainty of PWV derived from GNSS can be calculated from uncertainties associated with each input variable. Thus, all sources of uncertainty should be summarised to an uncertainty budget, as suggested by Immler et al. (2010). According to Immler et al. (2010), we have:

$$\sigma_{PWV} = \left[\sum_{j=1}^{N}\left(\frac{\partial f\left(v_1,...,v_N\right)}{\partial v_i}\sigma_i\right)^2\right]^{\frac{1}{2}} \ . \quad (5.10)$$

In Equation (5.10), $f\left(v_i,...,v_N\right)$ is the practical relationship connecting the GNSS-derived PWV and the input variables. The uncertainty of the respective variables is denoted by σ_i. Thus Equation (5.8) can be rewritten as:

$$PWV = \frac{10^6}{R_w \rho_w \left(k_2' + k_3/T_m\right)} \cdot \left(ZTD - ZHD\right) \ . \quad (5.11)$$

The ZHD in Equation (5.11) for a given GNSS station can be calculated from the Saastamoinen formula, which is given as follows:

$$ZHD = 0.002277 \cdot \frac{P}{1 - 0.00266\cos(2\phi) - 0.28 \cdot 10^{-6} h} \quad . \tag{5.12}$$

In Equation (5.12), the surface pressure in hPa is indicated by P, the latitude ϕ is in radians, and the height of the surface above the ellipsoid (in metres) is represented by h. Inserting Equation (5.12) into (5.11) yields:

$$PWV = \frac{10^6}{R_w \rho_w \left(k_2' + k_3/T_m\right)} \cdot \left(ZTD - \frac{0.002277 P}{1 - 0.00266\cos(2\phi) - 0.28 \cdot 10^{-6} h} \right) . \tag{5.13}$$

According to Equation (5.10), the precision of the PWV is given as

$$\sigma_{PWV}^2 = \left(\eta_3 \cdot \frac{k_3}{T_m^2} \cdot \sigma_{T_m} \right)^2 + \left(-\frac{\eta_3}{T_m} \cdot \sigma_{k_3} \right)^2 + \left(-\eta_3 \cdot \sigma_{k_2'} \right)^2 + \left(\frac{\eta_1}{\rho_w} \cdot \sigma_{ZTD} \right)^2 + \left(-\frac{\eta_1}{\rho_w} \cdot \eta_2 \cdot \sigma_P \right)^2 , \tag{5.14}$$

where $\eta_j, j = 1...3$ are defined as

$$\eta_1 = \frac{10^6}{R_w \left(k_2' + \frac{k_3}{T_m} \right)^2} \tag{5.15}$$

$$\eta_2 = \frac{0.002277}{1 - 0.00266\cos(2\phi) - 0.28 \cdot 10^{-6} h} \tag{5.16}$$

$$\eta_3 = \frac{\eta_1 \left(ZTD - \eta_2 \cdot P \right)}{\rho_w} \quad . \tag{5.17}$$

5.3 Results and Discussions

5.3.1 Results on the Validation of the ERAI and NCEP/NCAR Reanalysis Models

Firstly, we considered the results of the deterministic/dimensional metrics, which include four model performance indicators to verify the results of the reanalysis model used in this category. The results of the different performance indicators (namely the MAE, RMSE, SDR and ACC) are presented in Figures 5.2, 5.3, and 5.4 for surface temperature, mean sea level pressure and relative humidity values, respectively.

According to Figure 5.2, the MAE values for the ERAI and NCEP/NCAR models are approximately less than 4 Kelvin at all the AWOS. The RMSE values, which are indicative of the accuracy of the models in estimating surface temperature for both models from Figure 5.2, range from 3.029 to 0.083 Kelvin for ERAI and 3.772 to 0.062 Kelvin for NCEP/NCAR at the AWOS. Most of the AWOS have lower RMSE values for ERAI than NCEP/NCAR, except for AWOS at Jos, Kastina and Obudu. The precision of the temperature estimate from both models is described by the SDR values; SDR is less than 3 Kelvin for both models and a higher value at most of the stations for the ERAI model (Abuja, Bauchi, Calabar, Enugu, Ibadan, Ibi, Jos, Kano, Lafia, Lagos/RF, Maiduguri, Owerri, P/Harcourt, Sokoto, Uyo, Yelwa, and Yola) is indicative of low precision of ERAI at the stations. The ACC value is positive for all stations for the NCEP/NCAR model and the ACC is also stronger at all the AWOS for the NCEP model. Moreover, near zero and negative ACC values for ERAI are indicative of poor coincidence between ERAI and AWOS estimates.

The performance indicators for the pressure values as presented in Figure 5.3 indicate that the ACC again favours the NCEP model, with higher positive values recorded across all stations when compared with the ERAI. The MAE ranges from 2.731-0.842 hPa for the NCEP and 2.645-1.014 hPa for ERAI. The accuracy of the two models as presented by the RMSE shows that maximum RMSE values of 2.632 hPa and 2.685 hPa were obtained for the ERAI and NCEP, respectively. Many stations had an RMSE of less than 1 hPa for both the ERAI and NCEP (i.e. Akure, Calabar, Enugu, Gusau, Ibi, Kano, Makurdi, Owerri, P/harcourt, Sokoto, Uyo, and Yelwa). Furthermore, Figure 5.3 indicates that the precision of the models is shown by the SDR. SDR values for the ERAI range from 1.890 to 1.031 hPa, and from 1.777 to 0.697 hPa for NCEP/NCAR, although the values of the SDR were lower for the NCEP/NCAR model, except at AWOS in Ibi, Jos, Maiduguri, Makurdi, Obudu, and Zaria.

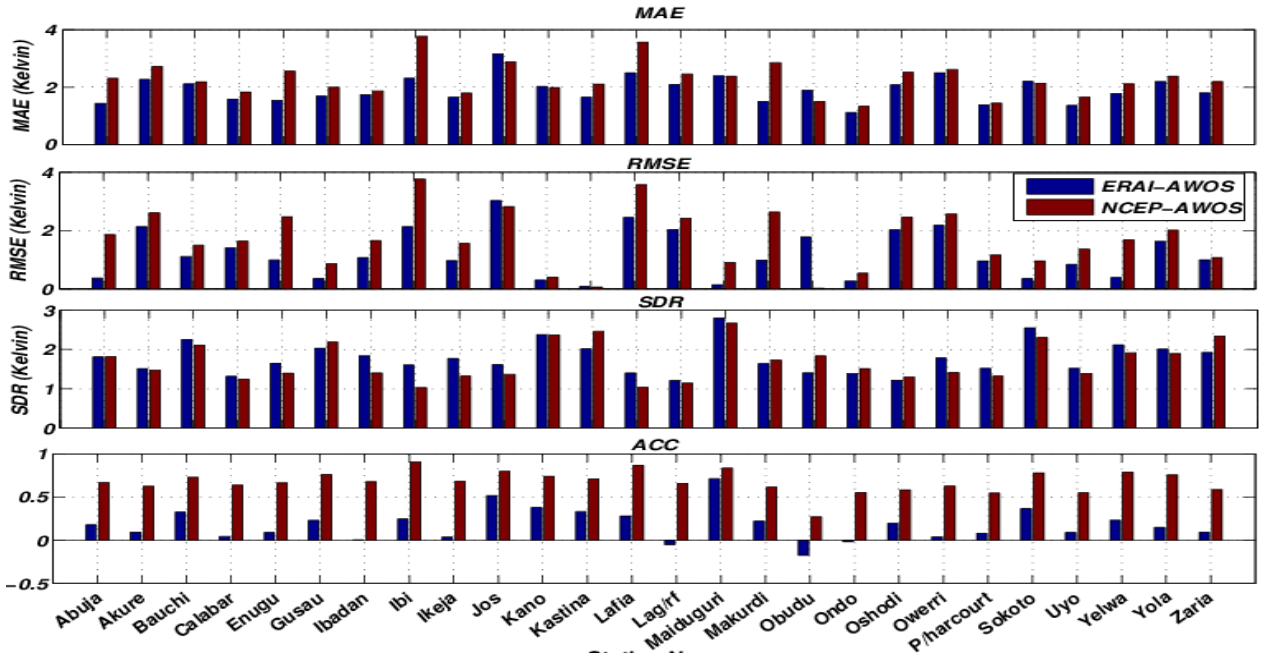

Figure 5.2: Performance of the ERAI and NCEP/NCAR for temperature estimation against the AWOS using deterministic metrics

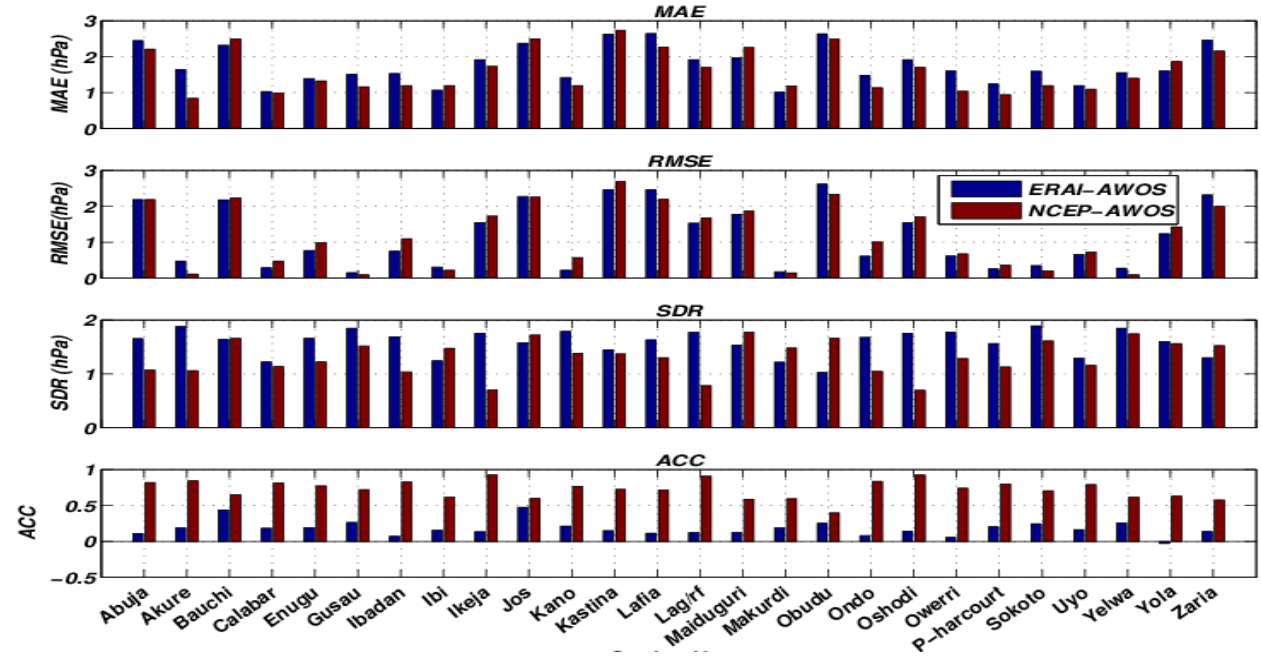

Figure 5.3: Performance of the ERAI and NCEP/NCAR for mean sea level pressure estimation against the AWOS using deterministic metrics

According to Figure 5.4, the MAE values for the ERAI and NCEP/NCAR models range from 15.769 to 6.591% and 19.245 to 7.477%, respectively. The RMSE values, which are indicative of the accuracy of the models in estimating surface relative humidity, range from 17.520 to 8.031% for ERAI and 38.162 to 9.125% for NCEP/NCAR at the AWOS, as

shown in Figure 5.4. Most of the AWOS have lower RMSE values for ERAI than NCEP/NCAR, except for AWOS at Abuja, Jos, Kano, Kastina, and Zaria. The precision of the relative humidity estimates from both models is described by the SDR values, which for the ERAI range from 17.320 to 7.718%, and from 35.992 to 8.018% for NCEP/NCAR. The ACC is again in favour of the NCEP/NCAR model for relative humidity estimation.

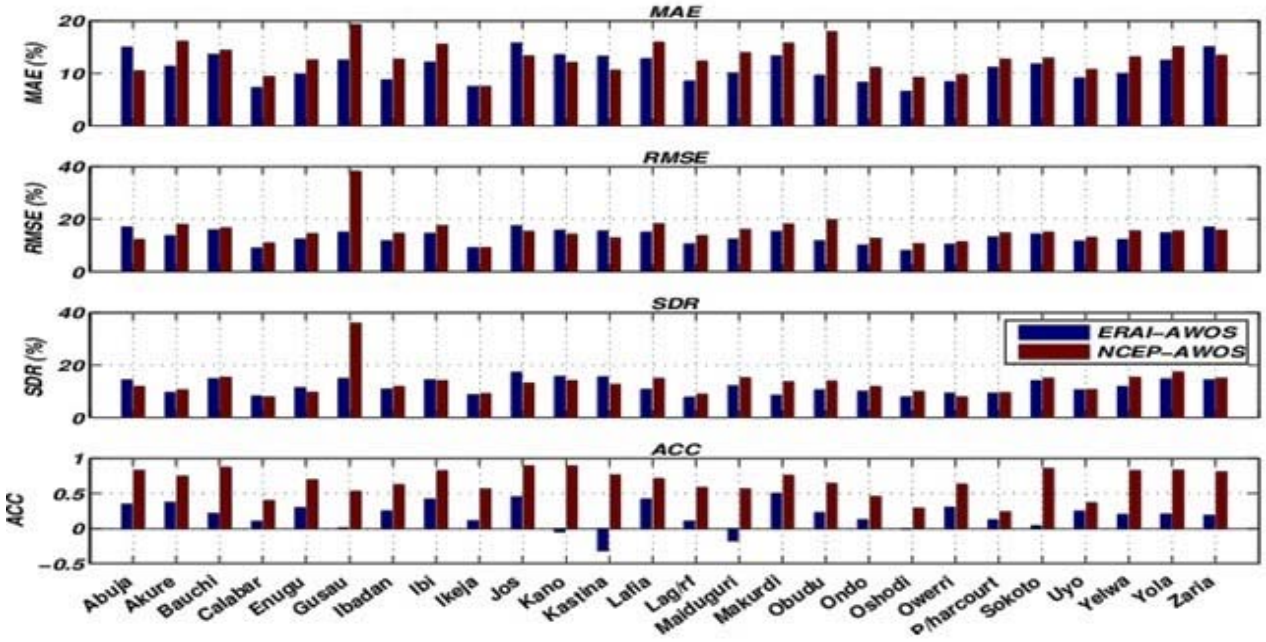

Figure 5.4: Performance of the ERAI and NCEP/NCAR for relative humidity estimation against the AWOS using deterministic metrics

Secondly, we discuss the result of the non-dimensional/probabilistic metrics that were used to verify the reanalysis datasets. The results of the different metrics (namely the MEF, ES, IA, and RI) are presented in Figures 5.5, 5.6, and 5.7 for surface temperature, mean sea level pressure and relative humidity values, respectively.

According to Figure 5.5, the MEF values for the ERAI and NCEP/NCAR models are positive at all the AWOS, although the NCEP model outperformed the ERAI at all the stations. The IA results are quite similar to the MEF; here again the NCEP outperformed the ERAI at the stations. The RI value of approximately one for the two models under deliberation is suggestive of the strength of both to forecast surface temperature within a tolerable average factor. However, the ES is negative at most stations for the models under consideration, which suggests that they are poor at predicting surface temperature.

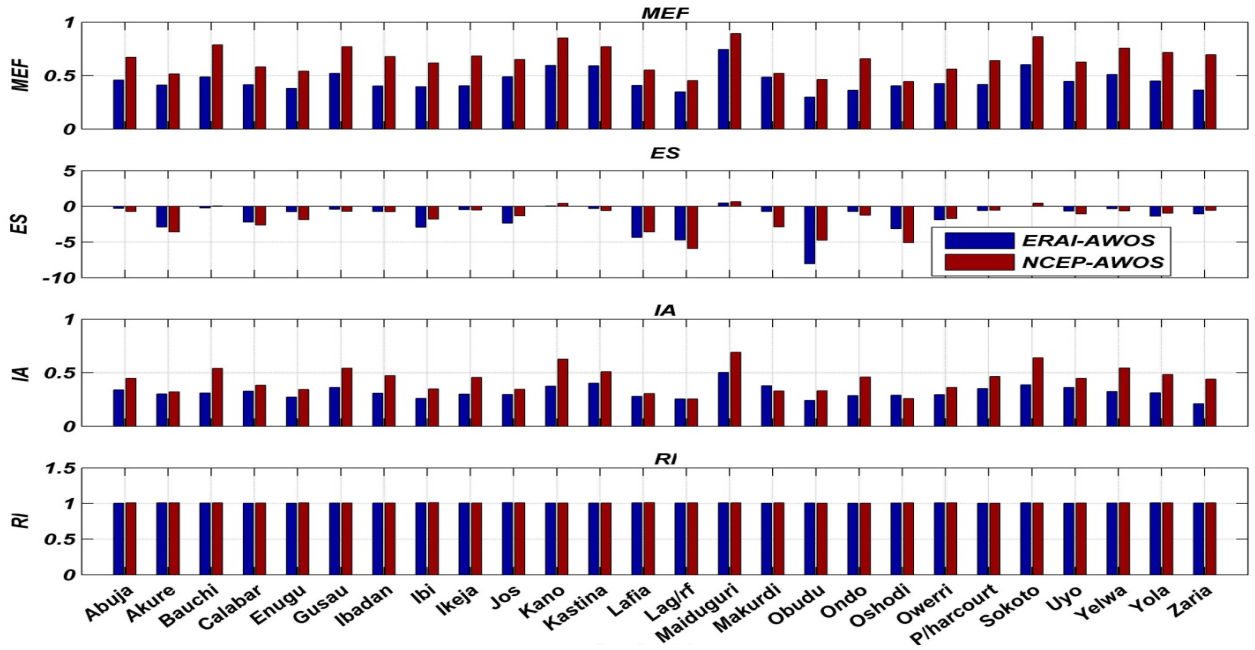

Figure 5.5: Performance of the ERAI and NCEP/NCAR for temperature estimation against the AWOS using probabilistic metrics

The MEF and IA values appear higher at all the stations for the NCEP/NCAR model, as seen in Figure 5.6. The RI value of approximately one for the models under consideration is suggestive of the strength of both models to forecast surface pressure within an acceptable average factor. Again, the ES is negative at most stations for both models under consideration, which suggests that the models are poor at predicting surface pressure.

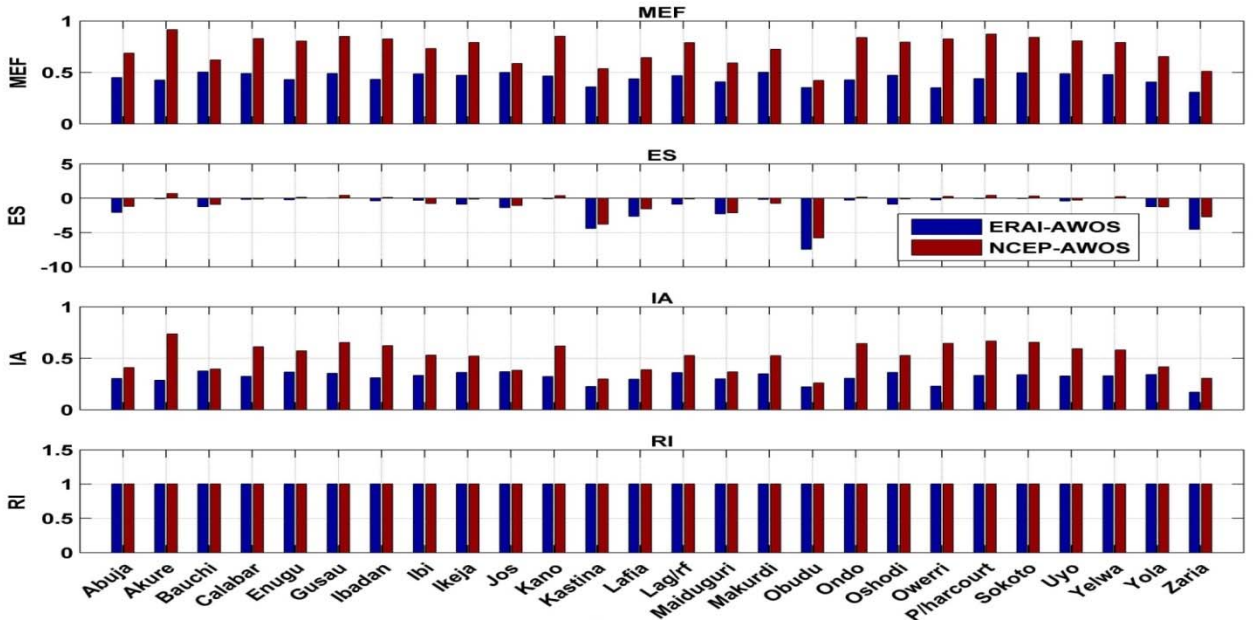

Figure 5.6: Performance of the ERAI and NCEP/NCAR for mean sea level pressure estimation against the AWOS using probabilistic metrics

The MEF values in Figure 5.7 clearly indicate that the NCEP/NCAR performs better at the stations with a range of 0.904 - 0.402, whereas the ERAI model has a range of 0.632 to 0.193, which is suggestive of lower changeability in the MEF in contrast to the NCEP/NCAR. Also, IA values in Figure 5.7 show that NCEP/NCAR performs better at the stations with a range of 0.711 to 0.241, whereas the ERAI model has a range of 0.431 to 0.153, which is suggestive of lower changeability in the MEF compared with the NCEP/NCAR. Again, the ES is negative at most stations for both models under consideration, which indicates that the models are poor at predicting relative humidity. The RI value is slightly greater than one and in most cases can be approximated to two for the models under deliberation, which indicates the weakness of both models to forecast relative humidity within a tolerable average factor.

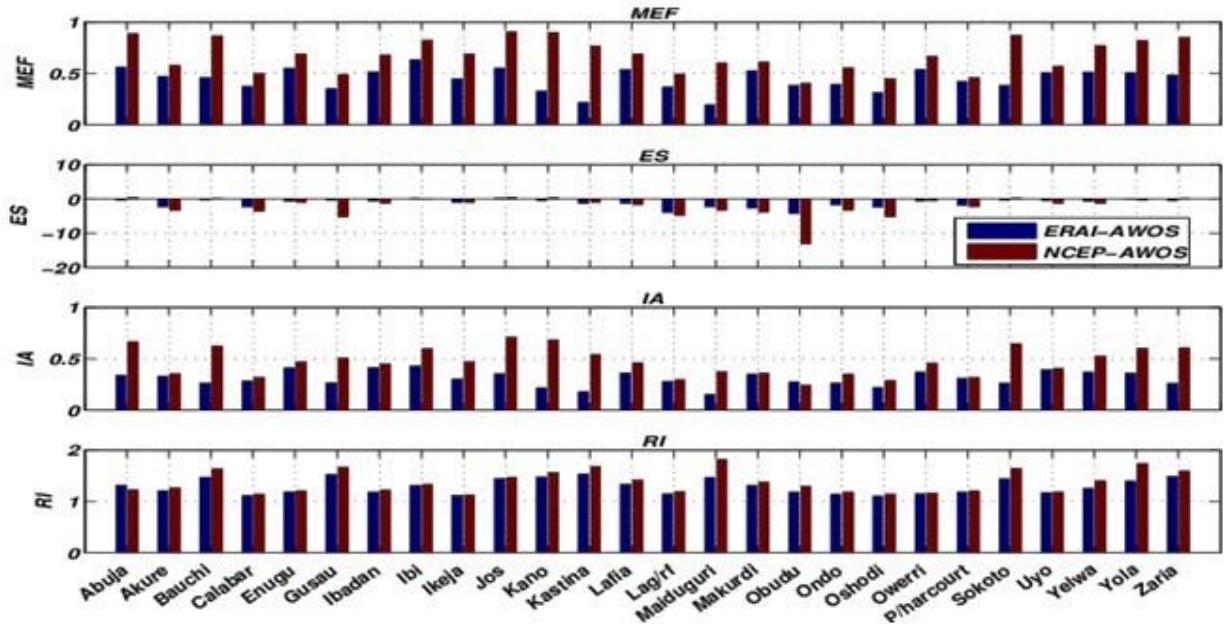

Figure 5.7: Performance of the ERAI and NCEP/NCAR for relative humidity estimation against the AWOS using probabilistic metrics

From the foregoing, it is important to theoretically test the suitability of using parameters from reanalysis models in PWV estimation from GNSS based on the results of the verification indices already discussed. Thus, considering the five GNSS stations adopted for this study, we took the mean value of ZTD at each of them over a period of one year. The precision of estimated ZTD from GNSS processing software is often between 1 and 5 mm and higher values are usually excluded as outliers, thus we chose a value of 5 mm for σ_{ZTD}. Also, the average value of T_m over the same period was as estimated from ERAI and NCEP

datasets in Equation (5.9), which were adopted for the individual stations; σ_{T_m} was chosen as the maximum SDR value for each model from Figure 5.2, although surface temperature is known to differ from T_m, but we assumed that the SDR value would be in the same range. Similarly, using pressure estimates from ERAI and NCEP at the GNSS stations, we again adopted the maximum SDR value for ERAI and NCEP pressure estimates in Figure 5.3 as the corresponding σ_p value for each of the models. The values of $\rho_w = 1025\ kg/m^3$, $R_w = 461.525\ Jkg^{-1}K^{-1}$, $k_2' = 22.1\ Kmb^{-1}$, $k_3 = 373900\ K^2mb^{-1}$, $\sigma_{R_w} = \pm 0.003\ Jkg^{-1}K^{-1}$, $\sigma_{k_2'} = \pm 2.2\ Kmb^{-1}$, and $\sigma_{k_3} = 0.012\ K^2mb^{-1}$ are commonly established constants. Using the different variables as input into Equation (5.14), we are able to estimate theoretically the maximum precision of PWV estimates from reanalysis datasets at five GNSS sites in Nigeria. An outline of the results is obtainable in Table 5.6. In all cases σ_{PWV} was less than unity.

Table 5.6: Theoretical influence of individual SDR from ERAI and NCEP on the final PWV estimates

Station	$ZTD\,(mm)$	$P\,(hPa)$	$T_m\,(K)$	$\sigma_{ZTD}\,(mm)$	$\sigma_P\,(hPa)$	$\sigma_{T_m}\,(K)$	$\sigma_{PWV}\,(mm)$
			ERAI				
abuz	2303.726	925.860	282.652	5.000	1.890	2.804	0.533
clbr	2622.559	1000.700	284.502	5.000	1.890	2.804	0.467
futy	2469.491	977.680	284.721	5.000	1.890	2.804	0.106
ulag	2609.215	1001.500	285.801	5.000	1.890	2.804	0.457
unec	2525.811	977.760	284.575	5.000	1.890	2.804	0.185
			NCEP/NCAR				
abuz	2303.726	927.780	282.231	5.000	1.777	2.674	0.517
clbr	2622.559	1003.000	284.459	5.000	1.777	2.674	0.438
futy	2469.491	979.480	284.422	5.000	1.777	2.674	0.095
ulag	2609.215	1003.700	285.339	5.000	1.777	2.674	0.429
unec	2525.811	979.330	283.646	5.000	1.777	2.674	0.171

From the results presented in Table 5.6, it is evident that both meteorological models, when combined with GNSS ZTD, can retrieve atmospheric PWV to within acceptable or tolerable precision limits. The next section attempts the practical estimations of PWV from reanalysis datasets.

5.3.2 Analysis of PWV Derived from GNSS and ECMWF/NCEP/GPT2 Dataset

This section looks into the practical application of a reanalysis data set in PWV estimation from GNSS observations. Of particular note is the introduction of the GPT2

model, which is an empirical model based on a reanalysis dataset specifically developed to support GNSS applications.

5.3.2.1 Comparison of ZHD from AWOS, ECMWF, NCEP, and GPT2 Dataset

The scatter plots of the comparison of results of the ZHD estimated at five GNSS sites for days 1-365 of the year 2013, using datasets from the AWOS, ERAI, NCEP/NCAR, and GPT2 meteorological models as inputs into the Saastamoinen formula (Equation 5.12), are presented in Figure 5.8. The results of the comparison at the five GNSS stations between $ZHD_{(AWOS)}$ versus $ZHD_{(NCEP/NCAR)}$, and $ZHD_{(AWOS)}$ versus $ZHD_{(GPT2)}$ show an increasing linear fit (i.e., positive slope) at all the stations, while those of $ZHD_{(AWOS)}$ versus $ZHD_{(ERAI)}$ have a decreasing linear fit (i.e., negative slope). Also, the $ZHD_{(GPT2)}$ model shows the strongest relationship with the $ZHD_{(AWOS)}$, taking into account the R-squared value at all the stations. In terms of accuracy as indicated by the RMSE values, $ZHD_{(ERAI)}$ gave values of 0.0739 mm, 0.1209 mm, 0.1148 mm, 0.1591 mm and 0.0594 mm for ABUZ, CLBR, FUTY, ULAG, and UNEC, respectively. These RMSE values from the $ZHD_{(ERAI)}$ were less than their corresponding values from $ZHD_{(NCEP/NCAR)}$ and $ZHD_{(GPT2)}$ at all the stations. These results are practical indications of the role of uncertainty in GNSS PWV attributable to uncertainty in surface pressure estimation.

5.3.2.2 Comparison of T_m estimated from T_s of AWOS, ECMWF, NCEP, and GPT2 Dataset

The influence of the uncertainty from temperature estimates on GNSS PWV is of practical importance as well. The scatter plots of the comparison of results of the T_m estimated at five GNSS sites for days 1-365 of the year 2013, using datasets from the AWOS, ERAI, NCEP/NCAR, and GPT2 meteorological models as inputs into the Bevis formula (Equation 5.9), are presented in Figure 5.9. The results of the comparison at the five GNSS stations between $T_m(AWOS)$ versus $T_m(NCEP/NCAR)$, and $T_m(AWOS)$ versus $T_m(GPT2)$ show an increasing linear fit (i.e., positive slope) at all the stations, while those of $T_m(AWOS)$ versus $T_m(ERAI)$ have a decreasing linear fit (i.e., negative slope) trend, which is quite similar to those of the ZHD estimates in Figure 5.8. Also, the $T_m(GPT2)$ model shows the

strongest relationship with the $T_m(AWOS)$ according to the R-squared value at all the stations.

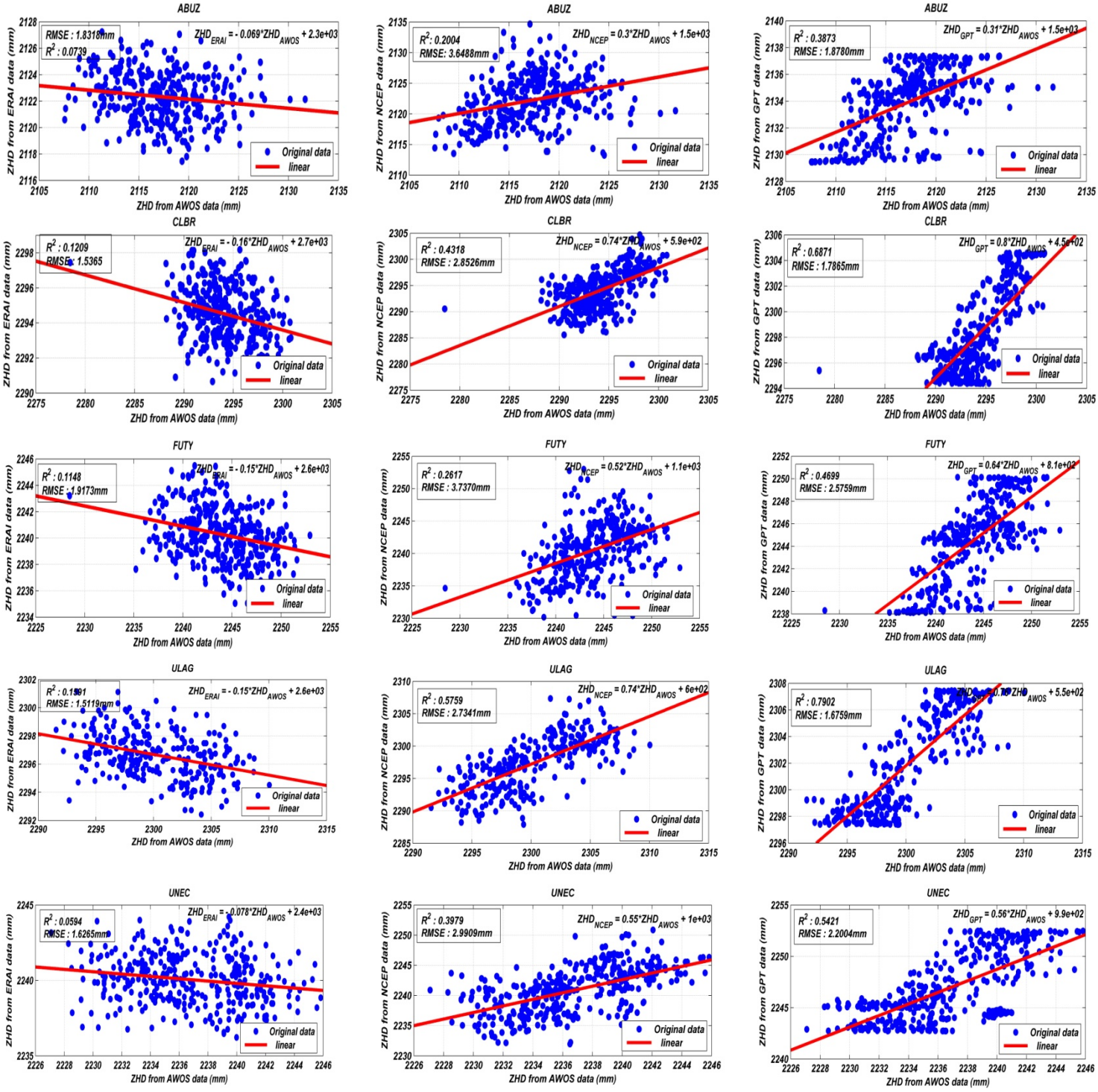

Figure 5.8: Scatter plots of correlation between ZHD estimated from AWOS datasets and ERAI, NCEP/NCAR, and GPT2 models at five GNSS stations. Each station is shown at the top of each panel. The equation's relation to the ZHD from AWOS and the meteorological models are in the right corner, and adjusted r-squared and RMSE are in the left corner of each panel

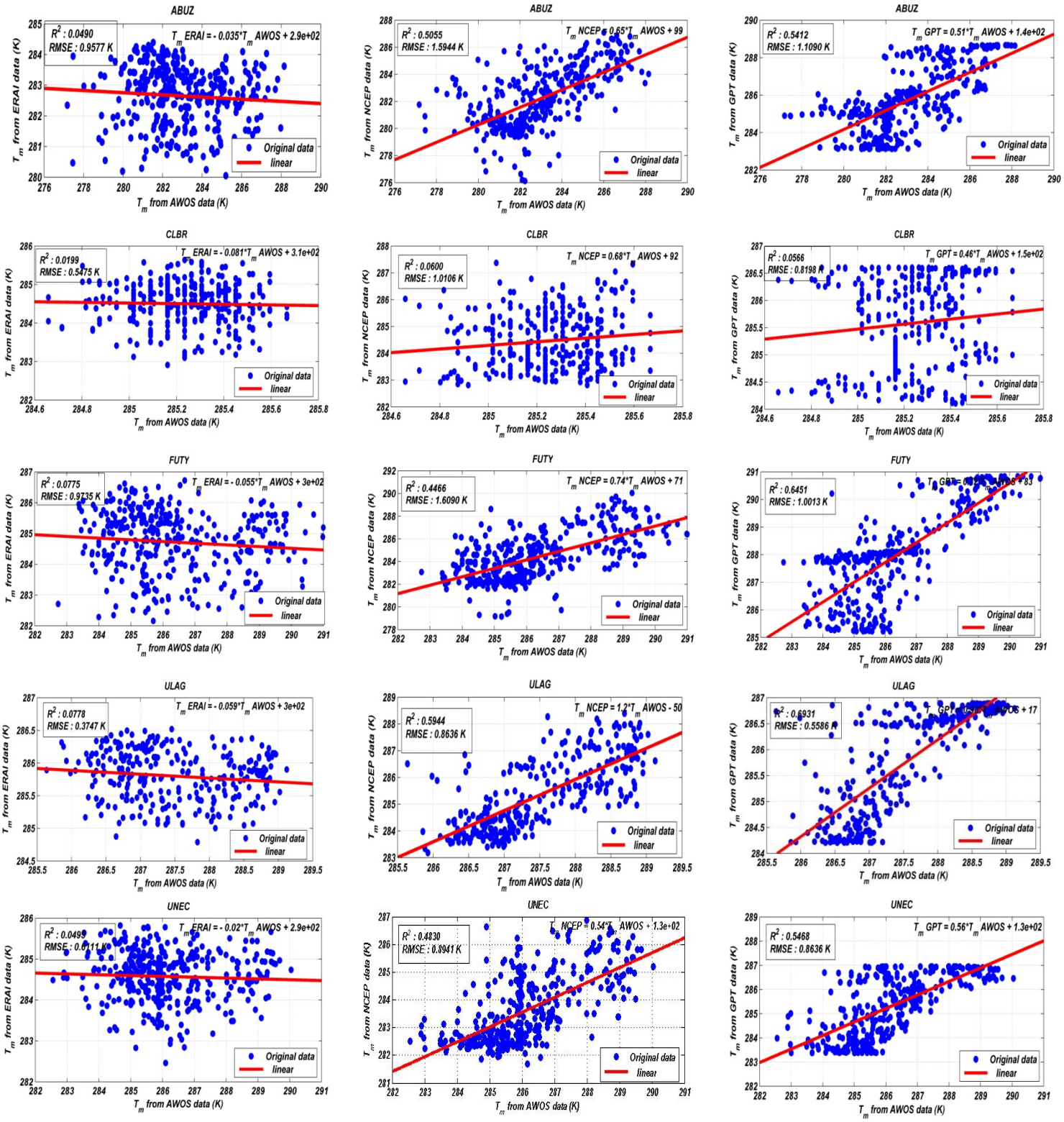

Figure 5.9: Scatter plots of correlation between T_m estimated from AWOS datasets and ERAI, NCEP/NCAR, and GPT2 models at five GNSS stations. Each station is shown at the top of each panel. The equation's relation to the T_m from AWOS and the meteorological models is in the right corner, and adjusted r-squared and RMSE are in the left corner of each panel

In terms of accuracy (as indicated by the RMSE values), $T_m(ERAI)$ gave values of 0.9577 K, 0.5475 K, 0.9735 K, 0.3747 K, and 0.6111 K for ABUZ, CLBR, FUTY, ULAG, and UNEC, respectively. These RMSE values from the $T_m(ERAI)$ were less than their corresponding values from $T_m(NCEP/NCAR)$ (1.5944 K, 1.0106 K, 1.6090 K, 0.8636 K, and 0.8941 K) and $T_m(GPT2)$ (1.1090 K, 0.8198 K, 1.0013 K, 0.5586 K and 0.8636 K) at all the stations. These results are practical indications of the role of uncertainty in GNSS PWV attributable to uncertainty in T_m estimation. However, it is believed that the accuracy of T_m at the stations would have been improved if the parameters of Equation (5.9) had been fine-tuned to the area of study. Modelling or localising T_m is outside the scope of the present study.

5.3.2.3 Comparison of PWVs from AWOS, ECMWF, NCEP, and GPT2 Dataset

So as to evaluate the accuracy of PWV estimated from GNSS ZTD and the different meteorological datasets (AWOS, ERAI, NCEP/NCAR, and GPT2), PWV as calculated from the AWOS (PWV_{AWOS}) dataset was compared with the others. Figures 5.10(a)-(e) and 5.11(a)-(e) show the times series of day-to-day variation of estimated PWV and the differences of estimated PWV from the different meteorological sources at the five GNSS sites (ABUZ, CLBR, FUTY, ULAG, and UNEC) respectively for a period of one year starting from January 2013 and ending in December 2013. The PWV estimates vary across the GNSS stations and also for the days of the year for the different models under consideration. The average estimated values for PWV_{AWOS}, PWV_{ERAI}, PWV_{NCEP}, and PWV_{GPT2} are as follows: 30.0678 mm, 29.2313 mm, 29.1770 mm, and 27.6197 mm, respectively, at ABUZ; 53.3686 mm, 53.1908 mm, 53.2380 mm, and 52.7819 mm, respectively, for CLBR; 36.8813 mm, 37.2046 mm, 37.0694 mm, and 36.7916 mm, respectively, for FUTY; 50.6211 mm, 50.9065 mm, 50.7024 mm, and 50.0212 mm, respectively, at ULAG; and 47.1295 mm, 46.3468 mm, 46.0527 mm, and 45.3258 mm, respectively, for UNEC. The average PWV values from the different models show good agreement. The PWV_{GPT2} value appears to be lowest at all the stations.

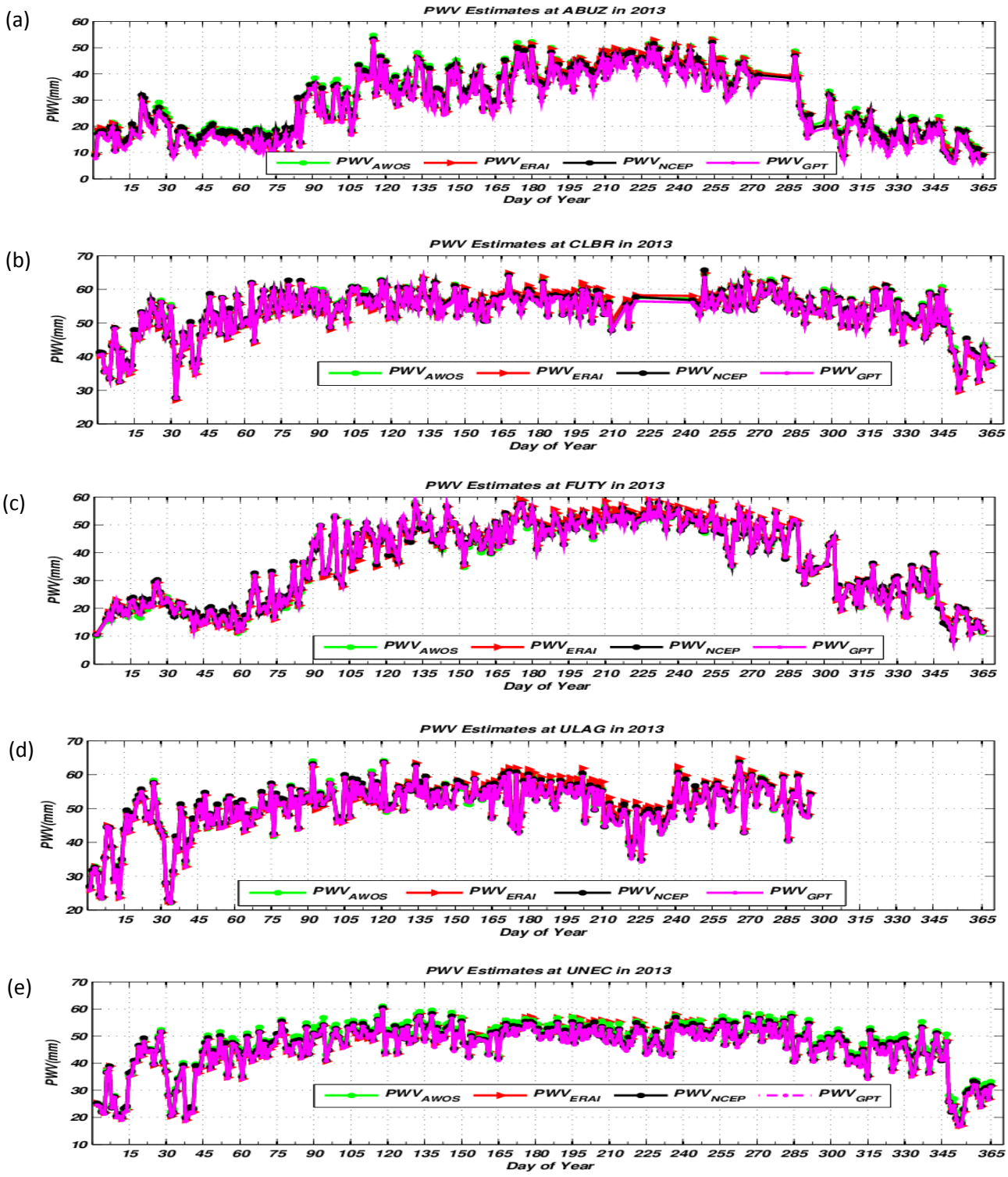

Figure 5.10a-e: Time series of PWV estimated from GNSS ZTD and different meteorological models (AWOS, ERAI, NCEP/NCAR, and GPT2) at stations 'abuz', 'clbr', 'futy', 'ulag', and 'unec', respectively

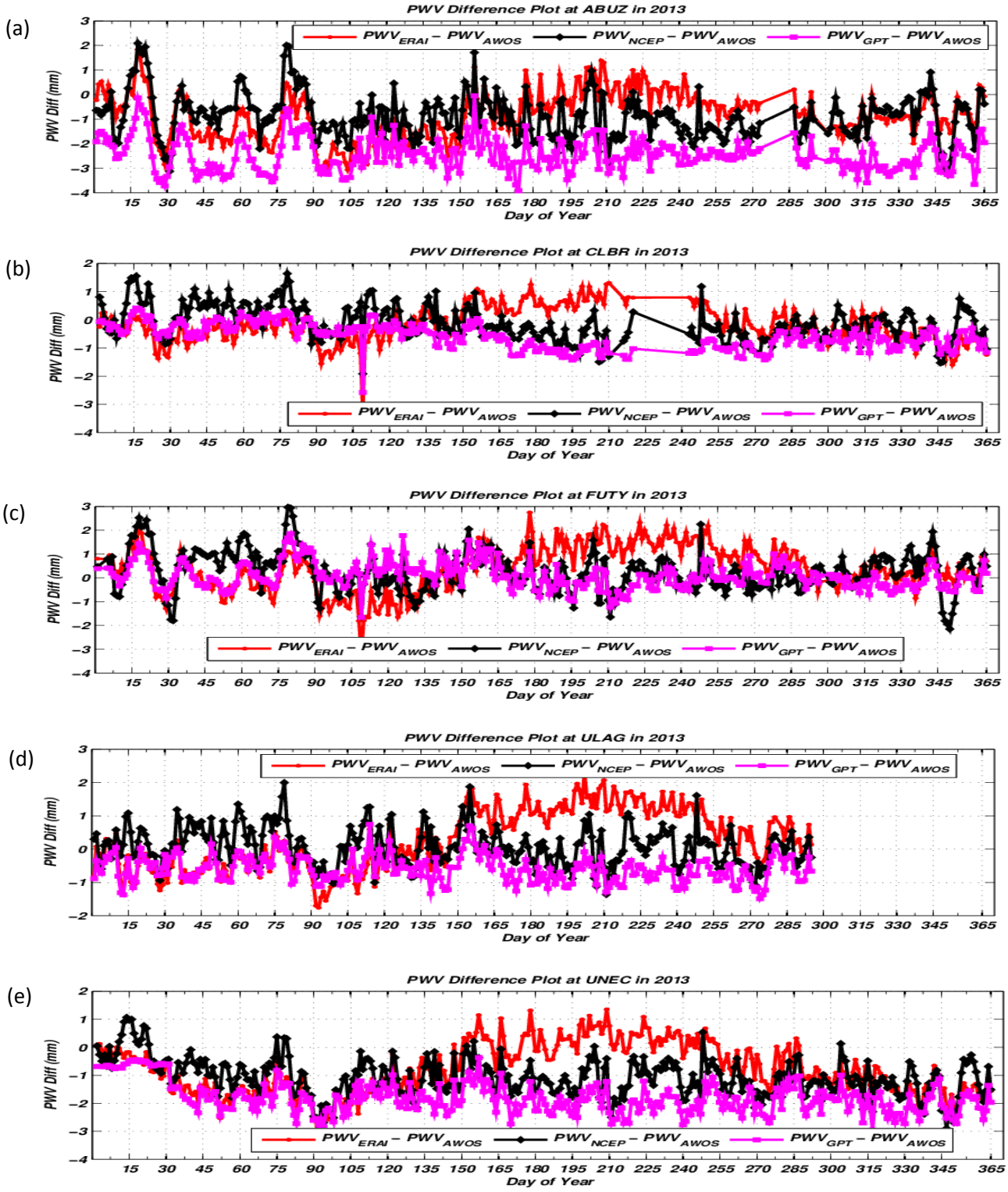

Figure 5.11a-e: Difference plot for the different models (ERAI, NCEP/NCAR, and GPT2) using AWOS as reference at stations 'abuz', 'clbr', 'futy', 'ulag', and 'unec', respectively

To evaluate the PWV estimates and differences as shown in Figures 5.11a-e further, we employ different verification indices, which are the deterministic and probabilistic metrics discussed earlier. Figures 5.12 and 5.13 show the results of the verification indices.

In Figure 5.12, the MAE values for PWV_{ERAI}, PWV_{NCEP}, and PWV_{GPT2} when compared with PWV_{AWOS} range from 1.0440 mm - 0.5197 mm, 1.1285 mm - 0.4654 mm, and 2.4481 mm - 0.4300 mm, respectively. The RMSE values, which are indicative of the accuracy of the meteorological models in estimating PWV for the three models from Figure 5.12, range from 0.9746 mm - 0.6162 mm for PWV_{ERAI}, 0.9025 mm - 0.5758 mm for PWV_{NCEP}, and 0.6586 mm - 0.3939 mm for PWV_{GPT2} at the GNSS stations. PWV_{ERAI} had the highest RMSE values at all the stations, while PWV_{GPT2} had the smallest estimates of RMSE at all the stations. The precision of the PWV estimate from the different models is described by the SDR values, which for the PWV_{ERAI} range from 1.284mm - 0.6413 mm, from 1.2754 mm - 0.5815 mm for PWV_{NCEP}, and from 2.5352 mm - 0.5638 mm for PWV_{GPT2}. Thus, the PWV_{GPT2} has more variability across the stations. The ACC is positive for PWV_{ERAI}, PWV_{NCEP}, and PWV_{GPT2} at all the GNSS stations and is an indication of perfect coincidence between the PWV_{AWOS} estimates and the estimates from each of the other models (PWV_{ERAI}, PWV_{NCEP}, and PWV_{GPT2}).

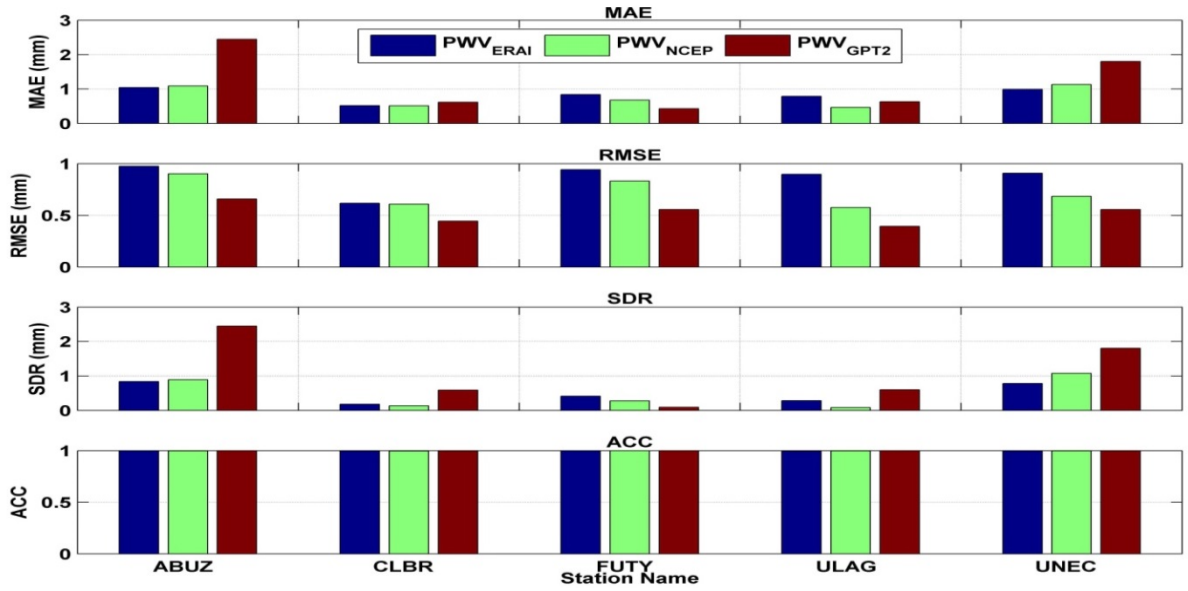

Figure 5.12: Bar chart of the performance of PWV_{ERAI}, PWV_{NCEP}, and PWV_{GPT2} against PWV_{AWOS} using deterministic metrics

From Figure 5.13, the MEF, ES, IA, and RI values for the PWV_{ERAI}, PWV_{NCEP}, and PWV_{GPT2} at all the stations can be approximated to a unity. This is an indication of the

strength of the estimates. Notably, the PWV_{ERAI}, PWV_{NCEP}, and PWV_{GPT2} values were higher at some stations than at others. However, PWV_{GPT2} exhibits some weakness across most of the stations.

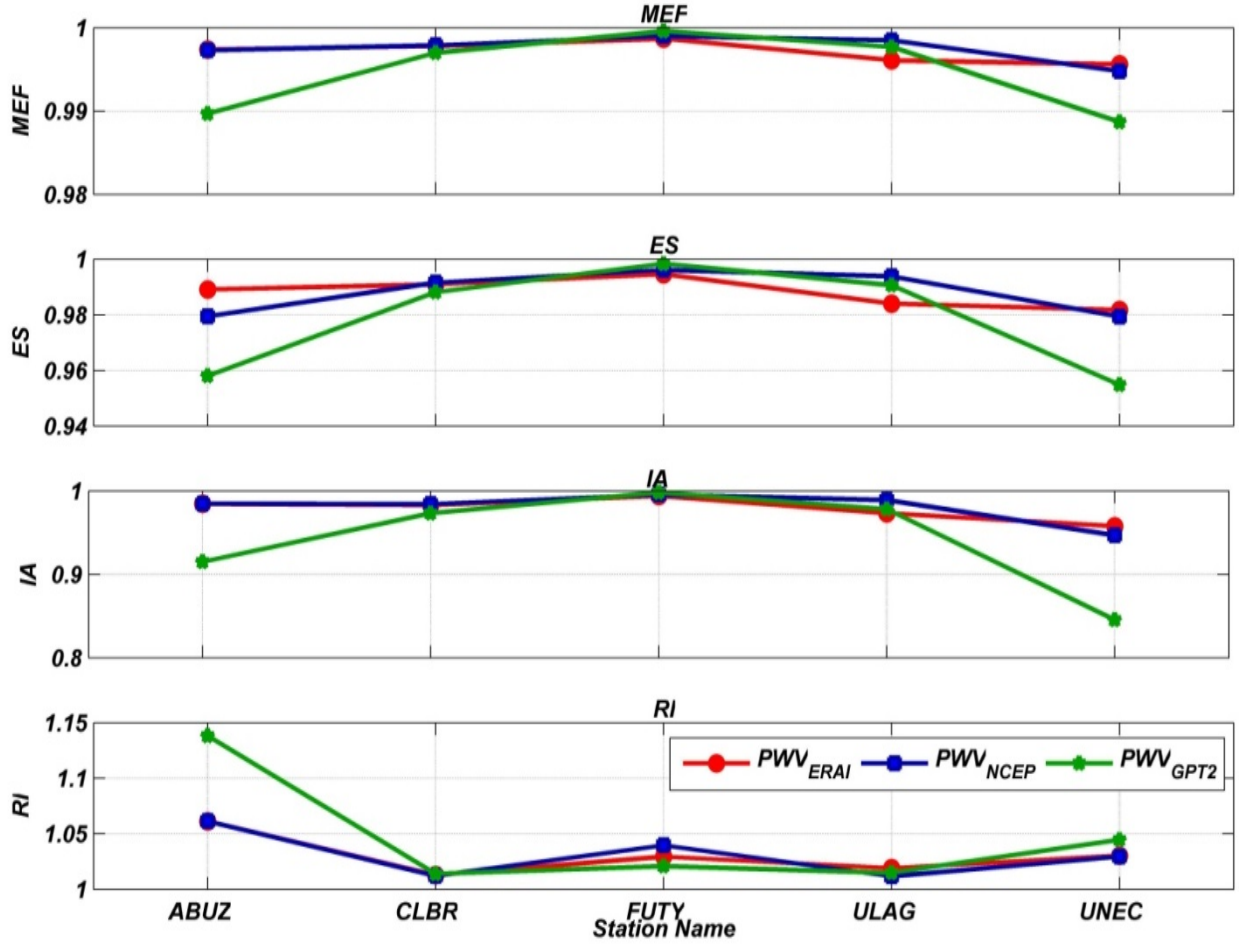

Figure 5.13: Line plot of the performance of PWV_{ERAI}, PWV_{NCEP}, and PWV_{GPT2} against PWV_{AWOS} using probabilistic metrics

As a final check on the PWV estimates from the PWV_{ERAI}, PWV_{NCEP}, and PWV_{GPT2}, we looked at the internal consistency of the estimates by regressing them with PWV_{AWOS} estimates over a period of one year at five GNSS stations, as shown in Figure 5.14. The data points shown in Figure 5.14 are compactly clustered around the regression lines. This indicates that the PWV_{ERAI}, PWV_{NCEP}, and PWV_{GPT2} are excellent models for the retrieval of PWV from GNSS ZTD. In addition, the RMSE from the regression for all the stations is less than unity, and the R-squared value of approximate unity further indicates the strong internal consistency of the PWV_{ERAI}, PWV_{NCEP}, and PWV_{GPT2} against the PWV_{AWOS}.

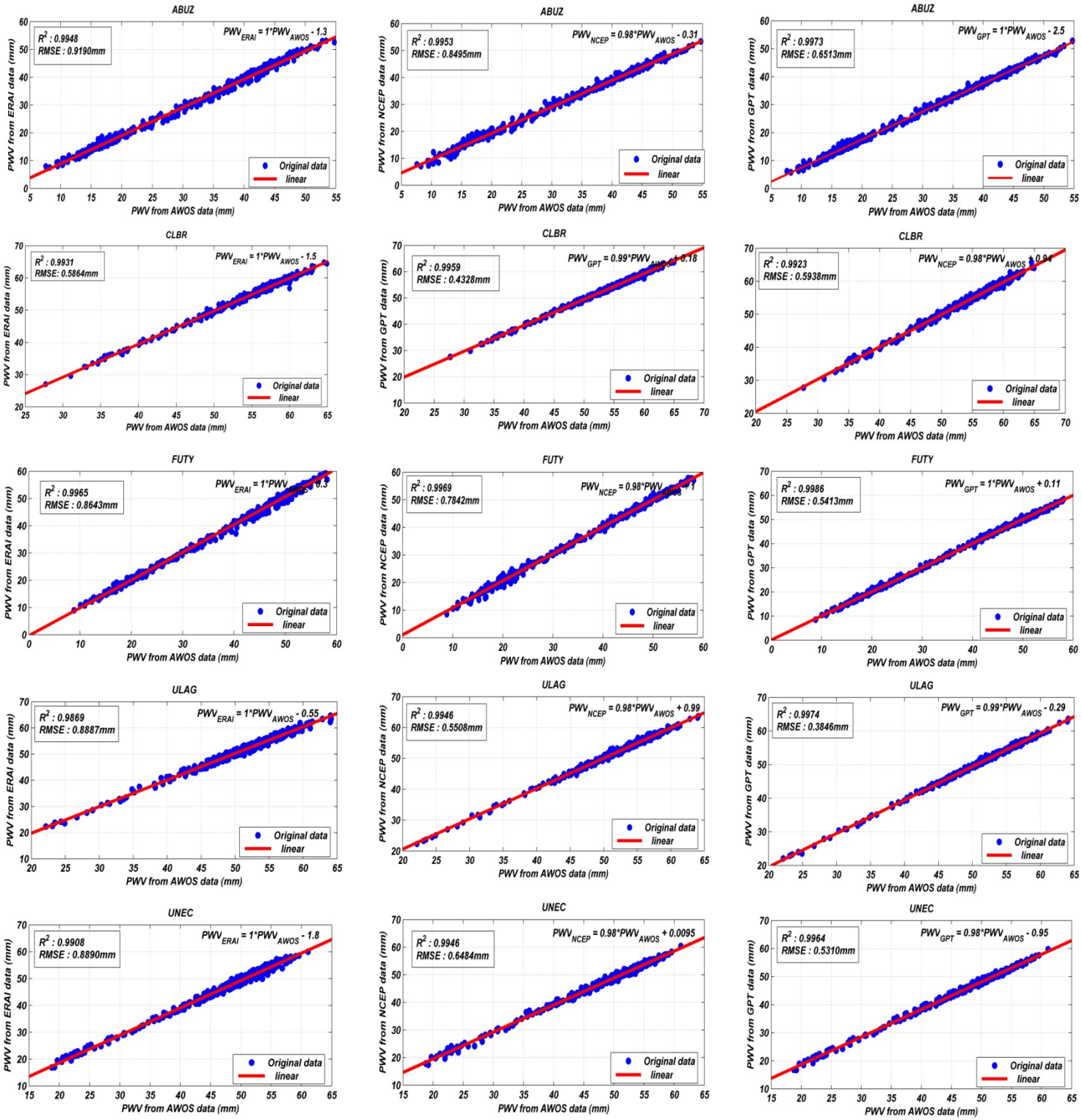

Figure 5.14: Scatter plots of correlation between PWV estimated from AWOS datasets and ERAI, NCEP/NCAR, and GPT2 models at five GNSS stations. Each station is shown at the top of each panel. The equation relation of the ZHD from AWOS and the meteorological models is in the right corner, and the adjusted r-squared and RMSE are in the left corner of each panel

According to the foregoing, theoretical and practical PWV precision are in agreement with each other. Figures (5.8) and (5.9) have larger RMSE values when compared to corresponding values in Figure 5.14. This is an indication that the combined influence of the uncertainty in ZHD and T_m on the precision of PWV is small. However, the uncertainty of T_m is the most influential on the final uncertainty of PWV after the ZTD. Thus, we can rewrite Equation 5.14 as follows and the final precision of PWV remains unaffected:

$$\sigma_{PWV}^2 = \left(\eta_3 \cdot \frac{k_3}{T_m^2} \cdot \sigma_{T_m}\right)^2 + \left(-\frac{\eta_3}{T_m} \cdot \sigma_{k_3}\right)^2 + \left(-\eta_3 \cdot \sigma_{k_2'}\right)^2 . \qquad (5.18)$$

Using Equation (5.18) in place of Equation (5.14), we obtained the same results as those presented in Table 5.6. Equation (5.18) thus signifies the importance of accurate modelling of T_m in the estimation of PWV from GNSS observations.

5.4 Concluding Remarks

In this study, surface variables (temperature, pressure and relative humidity) from two reanalysis models (ERAI and NCEP/NCEP2) were evaluated against AWOS during a three-year period (2010-2012) over Nigeria for the purpose of ascertaining the suitability of reanalysis models in the retrieval of atmospheric PWV from GNSS observation. The study further introduces the GPT2 empirical meteorological model, whose climatological datasets are based on ERAI reanalysis and which has specifically been developed for GNSS and other geodetic applications. Thus, in the second part of the study the practical application of using the ERAI, NCEP/NCAR2, and GPT2 model in retrieving PWV from GNSS ZTD was demonstrated. The results were compared against a reference model from the AWOS dataset. Standard verification indices as suggested by the WMO were employed in a comparison of the results. The adopted verification indices were of two categories, namely deterministic (MAE, RMSE, SDR, ACC) and probabilistic (MEF, ES, IA, RI) metrics. It was necessary to choose from a wide range of statistics because they reveal different things about the models under investigation. Consequently, based on the various investigations and analysis, we reached the following conclusions:

i. Of the two reanalysis datasets studied and for the sample stations chosen, NCEP/NCAR offers the greatest serial correlation with perfect coincidence with AWOS observations and the greatest internal consistency over the time period (2010-

2012) for the three surface variables (temperature, pressure, and relative humidity). This assertion is based on the MEF, IA, and ACC values at all the stations.

ii. In terms of accuracy, precision and systematic error as determined by the RMSE, SDR and MAE metrics, the two reanalysis datasets show varying discrepancies at the different stations for all three variables. Thus, it is difficult to decide conclusively which model is more accurate or precise in estimating the surface variables under investigation.

iii. The RI values calculated from ERAI data for the period under investigation compare well (RI ~ 1) with those of the NCEP/NCAR at all 26 AWOS stations for temperature and pressure estimates. This signifies that both models can estimate temperature and pressure values within an acceptable average factor.

iv. In estimating relative humidity, the reanalysis models appear not to be good predictors. Relative humidity varies widely at the stations, with RMSE ranging from 17.520 to 8.031% for ERAI and 38.162 to 9.125% for NCEP/NCAR. The slight overestimation of observed relative humidity by both the ERAI and NCEP/NCAR as indicated by their RI values (RI ~ 2) further confirms the defects or inability of the reanalysis models to simulate relative humidity values properly in the area under study.

v. In the estimation of ZHD from GNSS ZTD, station pressure value plays a prominent role, as can be seen in the Saastamoinen formula and mean temperature.

vi. The GPT model presented itself as a very promising model for the estimation of PWV, as it had the strongest correlation with the AWOS values in the estimation of ZHD, T_m, and PWV. The most important shortfall of the model is that it can only be used in diurnal or seasonal estimation of PWV; it does not give sub-daily (semi-diurnal) meteorological parameters as obtainable from NCEP and ERAI. It must also be noted that large weather changes at synoptic time scales are not accounted for in all the models and thus abrupt changes in parameters that influence the retrieval of PWV from ZTD may not be adequately accounted for.

vii. The PWV_{ERAI}, PWV_{NCEP}, and PWV_{GPT2} at all the stations show very strong internal consistency and near perfect correlation when regressed against PWV_{AWOS}. Notably,

the PWV_{ERAI}, PWV_{NCEP}, and PWV_{GPT2} were also better at some stations. However, PWV_{GPT2} exhibits some weakness across most of the stations.

viii. There is perfect agreement between the theoretically simulated precision of PWV estimated from ERAI and NCEP and that based on actual or practical formulations and data. Both estimates show that PWV can be retrieved to within a precision of about 1 mm provided that GNSS ZTD is of high precision.

ix. To improve on the precision of PWV retrieval from GNSS ZTD, it is recommended that a regional/local model of the atmospheric mean temperature (T_m) should be developed for Nigeria. A simple approach to this will be to fine-tune the parameters of the Bevis formula adopted in this study, as already suggested by Bevis et al. (1992).

x. Finally, based on the results and findings of this study, the use of reanalysis models in the estimation of PWV from GNSS ZTD is recommended for users in Nigeria.

Acknowledgements

The authors acknowledge the office of the Surveyor General of Nigeria for making GNSS data freely available for this study, Thanks to NOAA and ECMWF for freely making reanalysis datasets accessible. GAMIT/GLOBK GNSS processing software was also made unreservedly accessible by MIT through a licence granted to HartRAO. Meteorological data from automatic weather stations were purchased from the Nigerian Meteorological Agency in Lagos. The primary author would in addition like to acknowledge the financial support from the Tertiary Education Trust Fund of Nigeria, Surveyors Registration Council of Nigeria and University of Pretoria's PhD Research Support Bursary. Finally, the authors would like to thank the various reviewers for their positive remarks that assisted in improving the manuscript.

.

Chapter 6

Modelling Weighted Mean Temperature in the West African Region: Implications for GNSS Meteorology **

""You never change things by fighting the existing reality.
To change something, build a new model that makes the existing model obsolete."
— R. Buckminster Fuller

Précis

Weighted mean temperature (T_m) *is a critical parameter in the estimation of Precipitable Water Vapour (PWV) from ground-based Global Navigation Satellite System (GNSS) receivers. In this study, three models of* T_m *are developed for GNSS meteorological applications in the West African region, Nigeria in particular. The first is a least squares linear regression model based on NCEP/NCAR reanalysis II data for Nigeria from 2010–2012. A regression of 37,330 data pairs of surface temperature and* T_m *calculated from the vertical profiles of temperature above each grid node of the reanalysis model was used to produce the Nigerian Weighted Mean Temperature Equation-I (NWMTE-I) model after outlier data were removed. By using the same approach, NWMTE-II was obtained from 11,433 radiosonde profiles from 24 sounding stations in the West African region for the period 2009–2013. NWMTE-III was produced from a combination of the data used to build NWMTE-I and NWMTE-II. To evaluate the accuracy of these three models, they were compared with four global models based on* T_m *obtained by using the integral method, the reference model for this study. The Normalised Mean Absolute Error, Root Mean Square Error, Model Efficiency, Reliability Index, and Correlation Coefficient were used as the performance indicators. The performances of the developed models were promising compared with the global models, justifying the need to use measured meteorological parameters when estimating* T_m *and fine-tuning* T_m *to specific areas or regions. Finally, NWMTE-III is recommended for Nigerian users and NWMTE-II for users in the West African region.*

*****This chapter consists of formatted text for one peer reviewed journal paper as follows:***

Isioye, O.A., Combrinck, L., &Botai, O.J .2016.Modelling Weighted Mean Temperature in West African Region: Implication for GNSS Meteorology. *Meteorological Applications*, volume 23, issue 4, 614-632, http://dx.doi.org/10.1002/met.1584.

6.1 Introduction and Background

Water vapour is one of the largely important components of the atmosphere given that it is the means by which moisture and energy (as latent heat) are transported through the troposphere and lower stratosphere to influence weather. In addition to its role in balancing the atmospheric heat budget, water vapour plays an essential role in the global hydrological cycle and global climate system (Boutiouta and Lahcene, 2013) as the source of precipitation (rain, snow), clouds and fog.

In any vertical column of air, the amount of water vapour offers meteorologists a value of the maximum potential precipitation that could be retrieved from that air column under the right conditions. Although the air mass fraction of water vapour may approximately be around 1%, its effect on meteorology is very strong. It has the ability to cause small- and large-scale temperature anomalies and influence atmospheric latent heat exchanges. Water vapour plays a major role n the climate system: recent studies have estimated that about 70% of the warming of the atmosphere is attributed to water vapour acting as a greenhouse gas. Despite its significance to atmospheric processes over a broad range of spatial and temporal scales, however, it is one of the least understood and inadequately described components of the Earth's atmosphere in current climate prediction models (Jones, 2010).

Traditionally, atmospheric water vapour observations may be measured directly by in-situ instruments such as from radiosondes or humidity sensors on-board aircraft (downward looking radiometry) or indirectly, based on remote sensing estimates from instruments such as microwave radiometers (upward looking radiometry). Because the measurement techniques differ, the accuracy of the observed water vapour differs as well. Conventional techniques of measuring atmospheric water vapour do not offer the spatial and temporal resolution required for comprehensive investigation of the weather and climate systems (Ware et al., 2000). A better understanding of climate and weather patterns thus requires data sets that are more comprehensive.

The Global Navigation Satellite System (GNSS), through a concept referred to as 'GNSS meteorology', provides water vapour knowledge to atmospheric scientists. A network of ground-based GNSS stations is primarily used for surveying, geodesy, and navigation purposes. Due to the robustness that the ground-based GNSS technique has shown in studying the distribution of water vapour, many networks of Continuously Operating Reference Stations (CORS) are being constructed around the world for multidisciplinary

applications including meteorology (see, e.g., Ware et al., 2003; Nakamura et al., 2004; Walpersdorf et al., 2007; Adams et al., 2011; Braun et al., 2012; de Haan, 2013).

The global number of CORS is much larger than the number of radiosonde stations. For example, in Nigeria, about 30 ground-based GNSS CORS are owned and managed by different institutions and organisations under various initiatives, while only three radiosonde stations in the same area are on the list of upper stations published by the World Meteorological Organisation (WMO). The large number of ground-based CORS enables scientists to study water vapour distribution in a large geographical scale with a dense horizontal resolution. Compared with other observational techniques, the GNSS water vapour monitoring method yields better results in terms of spatial coverage and has high temporal resolution. In addition, as a continuous monitoring system, it is capable of measuring multiple lines between the station and the GNSS satellites under all weather conditions.

The principal error source in the GNSS technology is a delay experienced by the GNSS signal in propagating through the electrically neutral atmosphere, typically referred to as a tropospheric delay. The tropospheric delay can estimated together with the other parameters within GNSS data processing scientific software packages from continuous GNSS observations or campaigns. The zenith tropospheric delay (ZTD) represents the total delay through the atmosphere in the direction of the zenith. The ZTD comprises the hydrostatic (ZHD) and wet (ZWD) components of the delay (Bosy et al., 2012; Isioye et al., 2014, 2015a), as shown in Equation (6.1):

$$ZTD = ZHD + ZWD \ . \qquad (6.1)$$

The wet component of the ZTD is the foundation for the estimation of water vapour content in the atmosphere. Meteorologists and geodesists have defined numerous terms to articulate the quantity of atmospheric water vapour. More important is the expression of the water vapour content of an air parcel by combining all water vapour in the vertical column of air. The most commonly used terms are Integrated Water Vapour (IWV) and Precipitable Water Vapour (PWV). Both terms represent the absolute total amount of water in a vertical column of the unit cross-sectional area ranging between any two individual levels. The term PWV is used in this report. The relation between ZWD and water vapour content in the atmosphere expressed by IWV and PWV is reported by Isioye et al. (2015a) and expressed in Equation (6.2):

$$PWV = \frac{IWV}{\rho_w} = \frac{\left[ZTD_{GNSS} - ZHD\right]}{10^{-6} R_w \rho_w \left[k_2' + \frac{k_3}{T_m}\right]} = \Pi\left[ZTD_{GNSS} - ZHD\right] = \Pi \cdot ZWD \ . \quad (6.2)$$

In Equation (6.2), ρ_w is water density, $R_w = 461.525 \pm 0.003 \left(Jkg^{-1}K^{-1}\right)$ is the specific gas constant for water vapour, k_2' and k_3 are refraction constants, and T_m is the weighted mean water vapour temperature of the atmosphere measured in Kelvin (K) . This is operationally required to process GNSS data alongside the meteorological parameters (temperature, pressure, humidity) obtained from weather sensors collocated at the GNSS site in order to model ZHD and estimate water vapour. Therefore, with only T_m and local surface pressure, it is possible to reduce ZTD estimates from GNSS processing to PWV, as shown in Equation (6.2).

The T_m of the vertical column of air above the GNSS receiver is thus given as (Davis et al., 1985).

$$T_m = \frac{\int_h^\infty \frac{e}{T} \cdot Z_w^{-1} dh}{\int_h^\infty \frac{e}{T^2} \cdot Z_w^{-1} dh} = \frac{\int_h^\infty \rho_w dh}{\int_h^\infty \left(\rho_w / T\right) dh} \ . \quad (6.3)$$

In Equation (6.3), e is water vapour pressure, T is temperature, and Z_d^{-1} *and* Z_w^{-1} are the inverse compressibility factors of dry air and water vapour, respectively. Thus, utilising radiosonde profiles or the outputs fields of Numerical Weather Prediction (NWP) models, T_m can be obtained by integrating the vertical profiles of e and T between the GNSS antenna height (h) and infinity. This approach is restricted by the tempo-spatial resolution of these data products, which is a hurdle for GNSS meteorology and is seldom used in real-time PWV estimation (Isioye et al., 2015a). Bevis et al. (1992) proposed a widely adopted linear regression model for estimating T_m based on the relationship between surface temperature $\left(T_s\right)$ and T_m. According to they authors, T_m is linearly related to T_s, as shown in Equation (6.4):

$$T_m = a + bT_s \ . \quad (6.4)$$

By using 8700 radiosonde profiles collected at 13 stations over the United States for a two-year period, they developed a model of T_m, as given in Equation (6.5):

$$T_m = 70.2 + 0.72T_s \ . \qquad (6.5)$$

Equation (6.5) is widely adopted in many studies (e.g. Raju et al., 2007; Fernandez et al., 2010; Musa et al., 2011; Ning et al., 2013), although its accuracy varies worldwide. To obtain the best results, it is recommended that the constants a and b be fine-tuned to areas of interest for the different seasons (Bevis et al., 1992, 1994; Ross and Rosenfeld, 1997).

Countless users of GNSS meteorology have fine-tuned the constants a and b to optimise Equation (6.4) for their regions, often also by season (in Brazil (Sapucci, 2014); in tropical regions of India (Singh et al., 2013); in the Western Pacific region (Suparta & Iskandar, 2013); in Algeria (Boutiouta and Lahcene, 2013); and in China (Cao et al., 2008; Lilong et al., 2012; Wang et al., 2012; Yanxin et al., 2013).

In addition to developing linear models from radiosonde data sets, atmospheric profiles from NWP models have also been used in global modelling of T_m. Schueler *et al.* (2001) used global fields from numerical models of the National Centres for Environmental Prediction (NCEP) and proposed three global models: the harmonic model, linear surface temperature model, and mixed harmonic-temperature model. The results of the evaluation demonstrated that IWV values with a satisfactory degree of accuracy (range of $0.2-0.3\ kg/m^2$) can be obtained from GNSS data anywhere in the world by using the mixed harmonic-temperature model. Jade et al. (2005) used the mixed model to analyse GNSS IWV data in India and their results were in agreement with those of Schueler et al. (2001). Yao et al. (2012) presented a global weighted mean temperature (GWMT) model based on the Global Pressure Temperature (GPT) model and the Bevis $T_m - T_s$ relationship, showing that the GWMT model also can yield highly precise PWV values. He et al. (2013) described the development and refinement of different GWMT models and later presented the GWMT-IV model as a better real-life alternative. The GWMT-IV model is discussed in detail in section 6.2 of this report.

Furthermore, researchers from the University of New Brunswick and Vienna University of Technology have both developed global models (the UNB3m and Global Pressure and Temperature 2 wet(GPT2w) models, respectively) to estimate T_m, as documented in Leandro et al. (2006, 2008) and Boehm et al. (2014), respectively. The performance of both models in estimating T_m remains widely unknown on the African continent. Nevertheless, a study by Isioye et al., 2015b on the performance of the UNB3m

and GPT2w models reveals the performances of the duo models in estimating ZTD on the African continent.

In this study, a new approach was taken to estimating T_m from a combination of radiosonde data and NCEP/NCAR (National Centre for Atmospheric Research) reanalysis data over Nigeria. Thus, the present study compares the quality of T_m values generated from existing global models (Bevis model, GWMT-IV, UNB3m, and GPT2w) and from three new models (Nigerian Weighted Mean Temperature Equation (NWMTE)-I, -II, and -III) over Nigeria.

This paper is organised in this manner. Section 6.2 gives a detail description of dataset used and presents the methodology employed in the present study. Results and discussions on the validation of the different T_m models are given in section 6.3. Section 6.4 looks into the practical effect of T_m on PWV estimation. Final concluding remarks are given in section 6.5. The results of this study demonstrate the performance of various models which are employed in estimating T_m and their inferences on GNSS meteorology.

6.2 Materials and Methods

6.2.1 Data and Location

6.2.1.1 Radiosonde Data

Integrated Global Radiosonde Archive (IGRA) data were used as input in-situ observations to estimate T_m. The IGRA is a newly released radiosonde data set from the National Oceanic and Atmospheric Administration (NOAA) National Climatic Data Centre. The data set consists of daily quality assured soundings (one to four times per day) from over a 1500 stations scattered globally, from 1938 to the present (see Durre et al., 2006). Observations are available for standard surface, tropopause, and significance levels. Variables include pressure, temperature, geopotential height, dew point depression, wind direction, and wind speed at surface, tropopause, and at mandatory pressure levels (Elliott & Gaffen, 1991). Mandatory pressure levels include those specified by the WMO (WMO, 1996: 1000, 925, 850, 700, 500, 400, 300, 250, 200, 150, 100, 70, 50, 30, 20, and 10 hPa). The data set for this study was obtained from ftp://ftp.ncdc.noaa.gov/pub/data/igra. Table 6.1 contains information on the radiosonde stations selected for this study. Nigeria has only three stations

in the IGRA network: only two (WMO 65046 and 65202) were adopted based on their operational status, whereas the third (WMO 65123) did not seem to be functional.

Table 6.1: Radiosonde stations in and around Nigeria

Station ID	Town	Country	Latitude (Deg)	Longitude (Deg)	Height (m)	Operational status
61024	Agadez	Niger	16.97	7.98	502	1994–2014
61052	Niamey-Aero	Niger	13.48	2.17	227	1950–2014
61202	Tessalit	Mali	20.2	0.98	494	1974–2010
61223	Tombouctou	Mali	16.72	-3	264	1973–2012
61291	Bamako/Senou	Mali	12.53	-7.95	381	1968–2014
61415	Nouadhibou	Mauritania	20.93	-17.03	3	1968–2014
61442	Nouakchott	Mauritania	18.1	-15.95	2	1999–2014
61641	Dakar/*Yoff*	Senegal	14.73	-17.5	27	1963–2014
61687	Tambacounda	Senegal	13.77	-13.68	49	1984–2014
61831	Conakry	Guinea	9.57	-13.62	49	1993–2009
64400	Point *Noire*	Congo	-4.82	11.9	17	1999–2014
64458	Ouesso	Congo	1.62	16.05	352	1999–2014
64500	Libreville	Gabon	0.47	9.42	12	1992–2014
64650	Bangui	CAR	4.4	18.52	366	1952–2012
64700	N'djamena	Chad	12.13	15.03	295	1964–2014
64870	Ngaoundere	Cameroon	7.35	13.57	1114	2001–2014
64910	Douala *Obs*	Cameroon	4	9.73	9	1964–2014
65046	Kano	Nigeria	12.05	8.53	476	1972–2013
65202	Lagos/*Oshodi*	Nigeria	6.55	3.35	14	1953–2014
65330	Parakou	Benin	9.35	2.62	393	2006–2008
65344	Cotonou	Benin	6.35	2.38	6	2005–2013
65418	Tamale	Ghana	9.5	-0.85	173	2006–2008
65503	Ouagadougou	Burkina Faso	12.35	-1.52	316	1975–2014
65578	Abidjan	Cote d'Ivoire	5.25	-3.93	8	1957–2014

The radiosonde stations were identified from the accessible sites in the West African region with a latitude range of $5^{\circ}S - 25^{\circ}N$ and longitude range of $20^{\circ}W - 20^{\circ}E$. A diagrammatic presentation of the stations is shown in Figure 6.1. The data collected and used in this study cover the period 2009–2013.

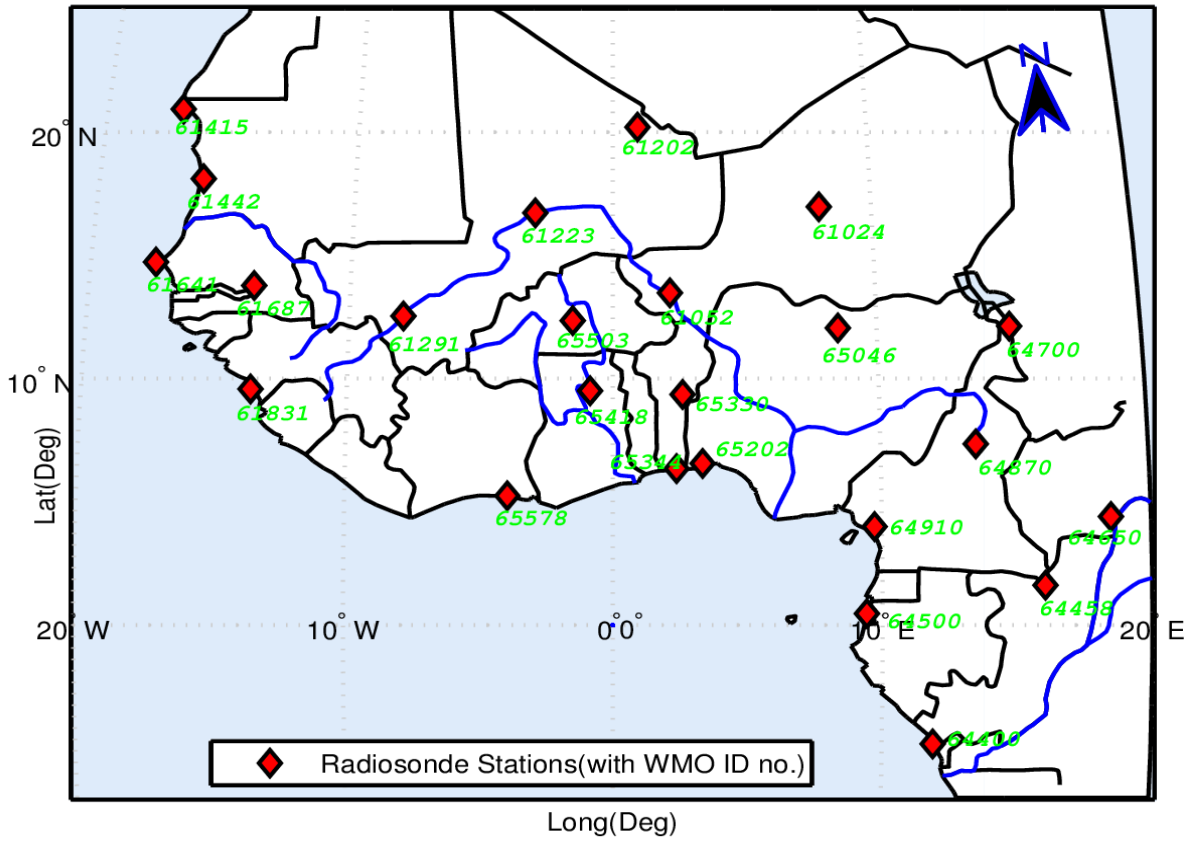

Figure 6.1: Map depicting the positions of the radiosonde stations in the West African region

6.2.1.2 NWP Data

NWP model data provide the unique advantage of multi-level observation (i.e. from surface to stratosphere). Thus, the surface and vertical profiles of temperature, humidity, and geopotential height data were collected from the NCEP/NCAR reanalysis model. Data from the model were obtained in the NetCDF (network Common Data Form) format.

The NCEP/NCAR Reanalysis 1 project uses a state-of-the-art analysis/forecast system to perform data assimilation using data from 1948 to the present. A large subset of this data is available from PSD in its original four times daily format and as daily averages (see, www.esrl.noaa.gov). The NCEP/NCAR Reanalysis 1 is a gridded data set having a grid size of $2.5^{\circ} \times 2.5^{\circ}$, at 17 hybrid vertical levels (1000, 925, 850, 700, 600, 500, 400, 300, 250, 200, 150, 100, 70, 50, 30, 20, 10), available 0000, 0600, 1200, and 1800 UTC daily (Kalnay et al., 1996). The NCEP/NCAR reanalysis data used in this research were provided by the NOAA/OAR/ESRL PSD, Boulder, Colorado, USA, from its website at http://www.esrl.noaa.gov/psd/. On a $2.5^{\circ} \times 2.5^{\circ}$ grid, 36 grid points cover Nigeria, as shown in

Figure 6.2. Daily surface and pressure-level temperature, relative humidity, and geopotential height data were collected over the period 2010–2012 for this study.

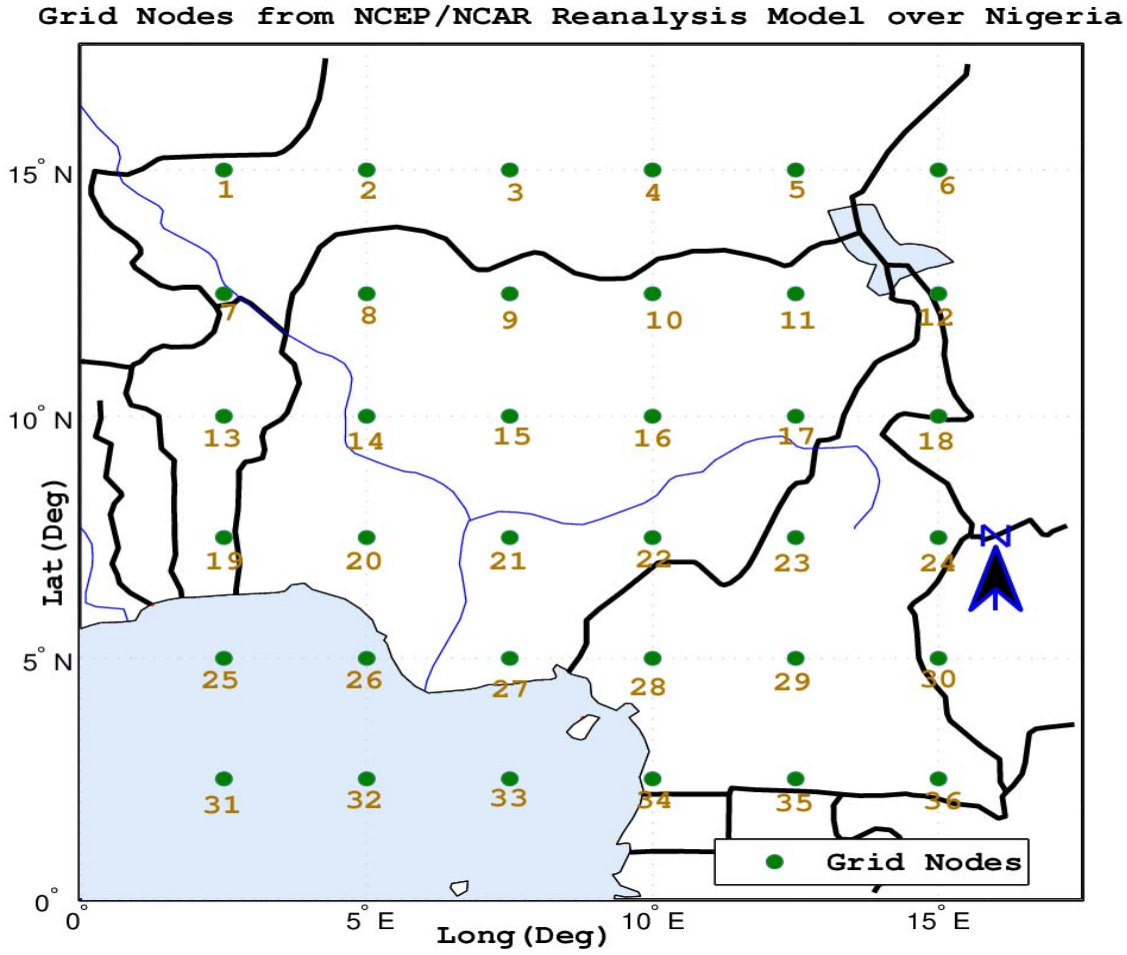

Figure 6.2: Map depicting the NCEP/NCAR reanalysis grid nodes over Nigeria

6.2.2 Estimation of Tropopause Height from the NCEP/NCAR Reanalysis Model and Sounding Data

The present study adopts a different approach to express the height range of data used to determine T_m as opposed to authors who adopt onlya height range without paying attention to the variation in tropopause height, because the integration in Equation (6.3) is from the surface to the top of the troposphere. Tropopause height was calculated for each grid node of the reanalysis model and at each station for the radiosonde.

Tropopause height was determined by using the thermal definition of the tropopause. For the thermally defined tropopause height, the WMO tropopause height definition was used (WMO, 1957). The temperature gradient or thermal criterion defines the tropopause

height at the point where $dT/dH > -2K/km$ (where T and H denote temperature and altitude, respectively), provided that the average lapse rate between this level and all higher levels within $2\ km$ does not fall below $-2K/km$. The lapse rate is calculated by using Equation (6.6):

$$\delta T_i = (T_{i+1} - T_i)/(H_{i+1} - H_i). \qquad (6.6)$$

In order to avoid very high or very low tropopause height, the search range for the tropopause was chosen to be 7 – 18 km. Starting from lower to higher altitude levels, the first point where $dT/dH > -2K/km$ and the average lapse rate between this level and higher levels within $2\ km$ does not fall below $-2K/km$ is the tropopause height.

6.2.3 Determination of T_m from the NCEP/NCAR Reanalysis Model and Sounding Data (Integral Method)

The weighted mean temperature T_m was estimated by using Equation (6.3). By using the radiosonde profiles or the output fields of NWP models, the integral in Equation (6.3) was discretized into sums of contributions from successive layers:

$$T_m = \frac{\sum_1^n \overline{\left(\frac{e_i}{T_i}\right)} \Delta S_i}{\sum_1^n \overline{\left(\frac{e_i}{T_i^2}\right)} \Delta S_i}. \qquad (6.7)$$

In Equation (6.7) $\overline{\left(\frac{e_i}{T_i}\right)} = \left(\frac{\frac{e_i}{T_i} + \frac{e_{i-1}}{T_{i-1}}}{2}\right)$, $\overline{\left(\frac{e_i}{T_i^2}\right)} = \left(\frac{\frac{e_i}{T_i^2} + \frac{e_{i-1}}{T_{i-1}^2}}{2}\right)$, ΔS_i is the depth of the atmosphere at the $i\ th$ layer, n is the number of layers. More layers result in higher accuracy. The number of layers at each station or grid node is a factor in the average tropopause height over the period 2010–2012 as determined from Equation (6.6). Data from radiosonde stations and NCEP grid nodes that failed to meet the conditions in Equation (6.6) were removed from the computation in Equation (6.7), the water vapour pressure and temperature at the top of the atmosphere at the $i\ th$ layer, are given as e_i and T_i respectively. e_{i-1}, and T_{i-1} are water vapour pressure and temperature at the bottom of the atmosphere at the $i\ th$ layer, respectively.

6.2.3.1 Harmonic Model from Global NCEP/NCAR Reanalysis Data

A simple approach for computing T_m is to employ its statistical average value and account for seasonal variations by applying a first-order harmonic function. There are several variants of the harmonic model (Emardson et al., 1998; Schueler et al., 2001; Yao et al., 2012; Wang et al., 2005; Chen et al., 2014). Of particular interest is the variant presented by He et al. (2013), hereinafter referred to as Global Weighted Mean Temperature-IV (GMWT-IV). This was further developed to improve the accuracy of preceding models, which is based on five-year (January 2005 to December 2009) global NCEP2 reanalysis data. T_m was estimated from the different pressure level over the period 2005–2009 by using Equation (6.3).

The GWMT-IV model is valid to heights between 0 and 7 km. Further, the mean lapse rate was localised and made a variable compared with early models, which considered it to be a global constant. Thus, T_m at any particular grid point decreases linearly with height as shown in Equation (6.8):

$$T_m(\varphi,\lambda,h) = \beta_m(\varphi,\lambda)\cdot h + T_m^{\circ}(\varphi,\lambda) \quad . \tag{6.8}$$

In Equation (6.8) $\beta_m(\varphi,\lambda)$ is the lapse rate of T_m at the latitude of φ and longitude of λ. $T_m^{\circ}(\varphi,\lambda)$ and $T_m(\varphi,\lambda,h)$ are T_m at the mean sea level and orthometric height, respectively. The time series of $T_m^{\circ}(\varphi,\lambda)$ and $\beta_m(\varphi,\lambda)$ were treated in a similar fashion. Thus, we have

$$T_m^0(\varphi,\lambda) = mean + amp_1\cdot\cos\left(2\pi\frac{doy-D_1}{365.25}\right) + amp_2\cdot\cos\left(4\pi\frac{doy-D_2}{365.25}\right), \tag{6.9}$$

where, $mean$, amp_1, and amp_2 are the annual mean value, annual, and semi-annual variations of T_m at the mean sea level. D_1 *and* D_2 are the phases of annual and semi-annual variation of T_m at the mean sea level. $mean$, amp_1, and amp_2 were expanded into spherical harmonics up a degree and order $N_{\max}$, i.e., $mean$ was computed as follows:

$$mean = \sum_{n=0}^{N_{\max}}\sum_{m=0}^{n}\overline{P}_{nm}(\sin\varphi)\cdot\left[\overline{A}_{nm}\cos(m\lambda) + \overline{B}_{nm}\sin(m\lambda)\right] . \tag{6.10}$$

In Equation (6.10), $\overline{P}_{nm}$ is the fully normalised associated Legendre polynomial, which was used to compute the corresponding coefficients $\left(\overline{A}_{nm},\overline{B}_{nm}\right)$ up to a degree and order of 30 using the least squares method.

6.2.3.2 UNB3m Model

This neural atmospheric model was produced by altering the algorithms and the parameter values in the UNB3 look-up table (see, Leandro et al., 2008). It calculates the mean temperature of water vapour alongside the other meteorological parameters for a given latitude, height, and day of year (DOY). A look-up table is used to calculate mean sea level values for the pressure, temperature, relative humidity, and lapse rate parameters for a given latitude and DOY. Thus, T_m is given as

$$T_{m(UNB3m)} = T\left(1 - \frac{\beta R}{g_m \lambda'}\right) \quad . \tag{6.11}$$

In Equation (6.11), T is temperature in Kelvin, R is the gas constant for dry air $\left(287.054\, JKg^{-1}K^{-1}\right)$, g_m at the atmospheric column centroid is the acceleration of gravity in m/s^2, β is the temperature lapse rate, $\lambda' = \lambda + 1(unitless)$, and λ is the water vapour pressure height factor.

6.2.3.3 GPT2w model

GPT2w is an extension of GPT and GPT2 (Boehm et al., 2007; Lagler et al., 2013) with enhanced potential to resolve zenith delays, slant delays and T_m in blind mode at locations in the surrounding area of the Earth's surface using the date and estimated station coordinates as inputs. GPT2w is based on gridded meteorological parameters and provides the mean, annual , semi-annual values and amplitudes of pressure, temperature and its lapse rate, water vapour pressure and its decrease factor, weighted mean temperature, and the hydrostatic and wet mapping function coefficients of the Vienna mapping function 1 (Boehm et al., 2014). The gridded T_m was originally obtained from Equation (6.3) and, like other climatological parameters of GPT2w, derived consistently from monthly mean pressure-level data of ERA-Interim fields with a horizontal resolution of 1°. The ERA Interim reanalysis from 1979 to present, recently released in 2011, is based on the European Centre for Medium Range Weather Forecasts(ECMWF) 4D-variational assimilation systems (see Dee et al., 2011). The ERA Interim is a gridded data set with a spectral resolution of $0.75^\circ \times 0.75^\circ$, having 37 vertical pressure levels. The gridded data products comprise a multiplicity of 3hr surface and upper-air parameters, unfolding weather in addition to ocean-wave, and land-surface conditions.

6.2.4 Estimating Precipitable Water Vapour from GNSS Observations

For the purpose of evaluating the effects of the different T_m models on estimated atmospheric PWV from GNSS, GNSS data at five (ABUZ, CLBR, FUTY, ULAG, UNEC) out of the 15 stations on the Nigeria GNSS Network (NIGNET) for the year 2013 were processed. The choice of selection of the GNSS stations was based on data availability and their proximity to automatic weather observing sites (AWOS) (see Figure 6.3).

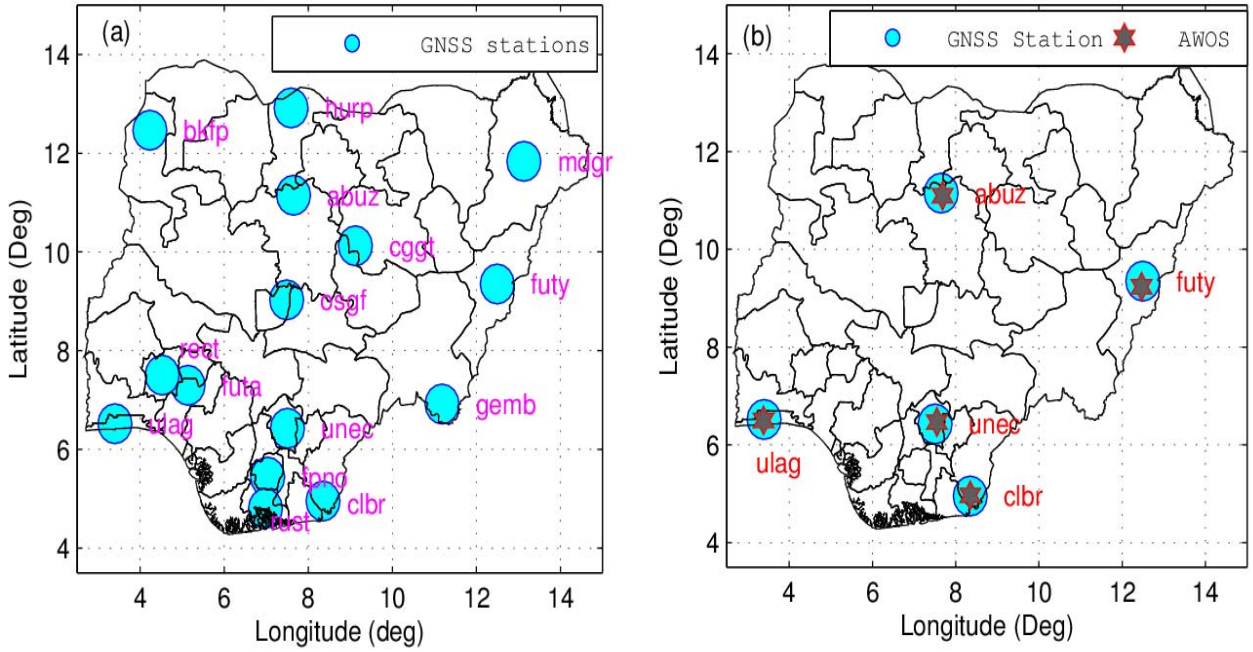

Figure6. 3: Location of GNSS sites in Nigeria. (a) All of the stations in the new Nigerian GNSS Network(NIGNET) under management of the office of the Surveyor General of Nigeria(OSGOF); (b) the GNSS stations and matching automatic weather observing sites(AWOS) sites at which PWV were estimated for the present study

GNSS observation data files in Receiver Independent Exchange Format (RINEX) were processed using GAMIT/GLOBK software. In order to acquire reliably accurate ZTD estimates, the GNSS data-processing parameters and models were cautiously set up in the GAMIT/GLOBK software. A summary of these is presented in Table 6.2. The ZTD at each GNSS station was estimated daily within a 24-hour window session. Details of the adopted strategy for processing the GNSS data from the NIGNET stations has already been already reported (Isioye et al., 2015a). PWV was estimated from the ZTD values and other constants defined in Equation (6.2) alongside the different T_m models.

Table 6.2: Summary of adopted processing parameters used in GAMIT software for ZTD estimation in this study

Parameter	**Description/Value**
Observations	Double difference Ionospheric free (IF) combination at 30s sampling rate
Elevation cut-off	10 degrees
Satellite Orbits/Earth Rotation Parameters (EOP)	IGS final orbits (SP3) and IGS final ERP products
Tropospheric delay	*Saastamoinen model (1972)*+ random-walk process
Ionospheric delay	Double difference Ionospheric free (IF) linear combination
Mapping function	Vienna Mapping Function (Boehm et al. 2006)
Station coordinates	Heavily constrained to their ITRF 2008 values (Altamimi et al. 2011)
Meteorological Observation Source	GPT 50
Station Displacement	Solid Earth tide based on IERS03, and Ocean tide loading correction based on FES2004
ZTD estimates	Daily
Relative Troposphere constraints	The constraint used for zenith delay was 0.2 m as it is recommended to set it loose enough to encompass any error in wet delay (Herring et al. 2006)
Satellite antenna PCO & PCV	AZEL for IGS absolute ANTEX files (Gendt and Schmid 2005)

Surface pressure and temperature at nearby AWOS were interpolated to GNSS stations for the retrieval of PWV from estimated ZTD values, because no GNSS site used in this study had a collocated meteorological sensor. Interpolated pressure values were reduced to actual station level pressure using the approach of Isioye et al. (2015a).

6.3 Results, Model Validation and Discussions

6.3.1 Results of the Models

The calculated tropopause height at each radiosonde station and NCEP/NCAR reanalysis grid point were used to determine the range of integration of Equation (6.3). Figures 6.4a and 6.4b show the average tropopause height at each NCEP/NCAR reanalysis grid node and sounding station, respectively.

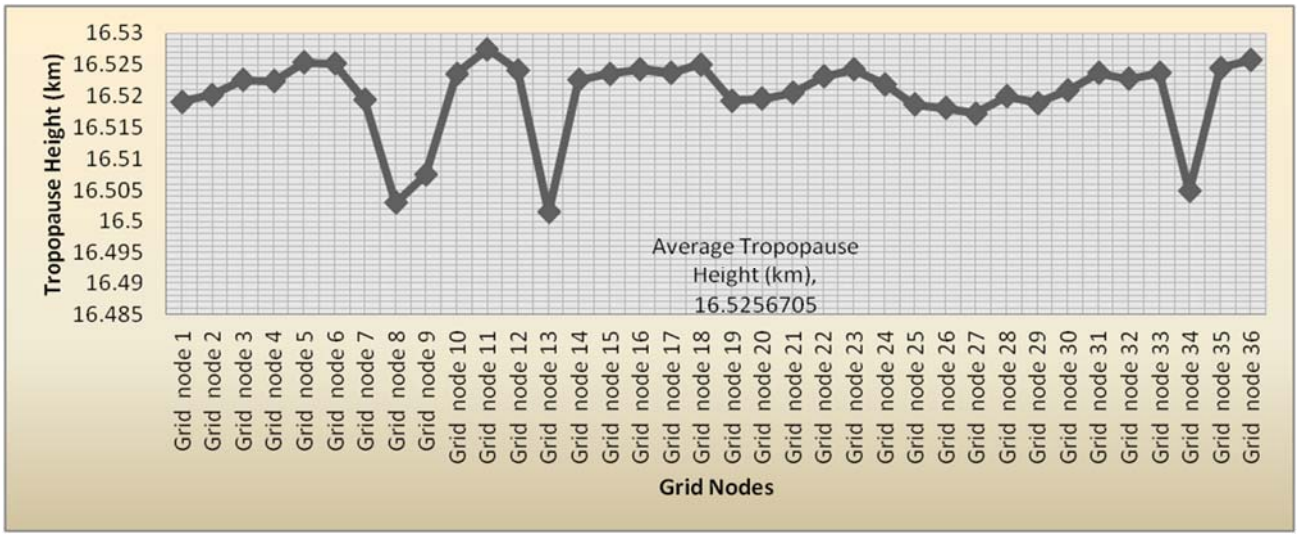

Figure 6.4a: Average tropopause height at the 36 NCEP/NCAR grid nodes over Nigeria for 2010–2012

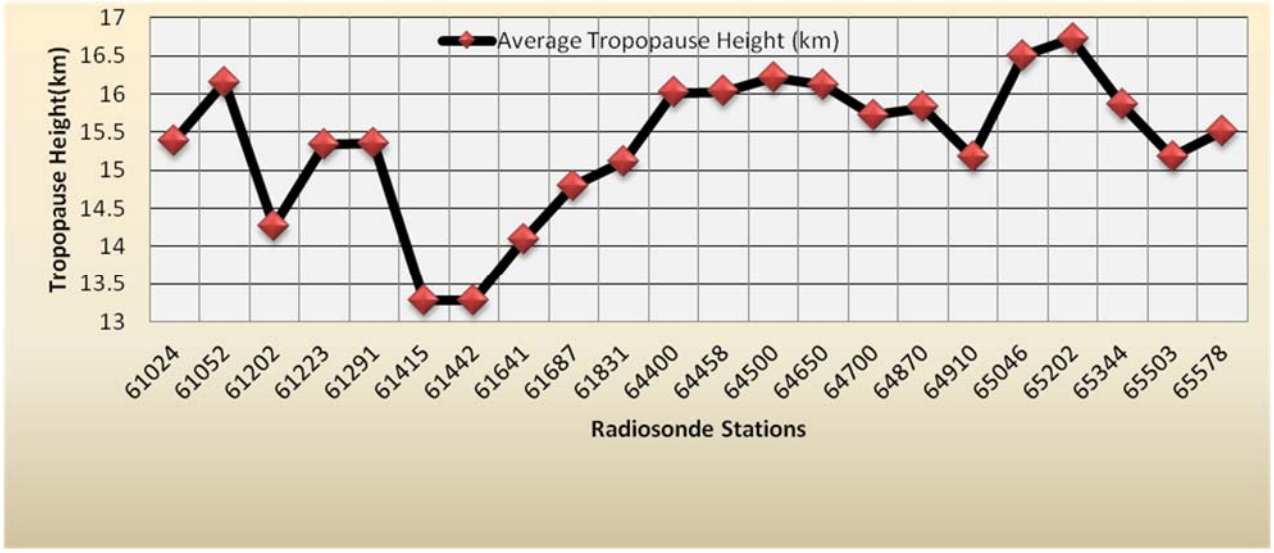

Figure 6.4b: Average tropopause height at the 24 sounding stations over the West African region for 2009–2013

By using 3 years of data taken from the NCEP/NCAR reanalysis (2010–2012) over Nigeria, T_m was calculated at each grid node that covers the Nigerian territory by using Excel software. The integral in Equation (6.3) was discretised into sums of contributions from successive layers as indicated in Equation (6.6), the T_m obtained was linearly regressed with T_s. The relationship differed slightly each year from 2010 to 2012 ($T_m = 0.512T_s + 136$, $T_m = 0.483T_s + 144.59$ and for 2010, 2011, and 2012, respectively). The result from the

combination of data over the three-year period yields a linear regression relationship as indicated in Equation (6.12). Equation (6.12) is hereinafter referred to as NWMTE-I. Figure 6.5 is its regression diagram showing the statistics of the model.

$$T_m = 0.4883T_s + 143.75 \qquad (6.12)$$

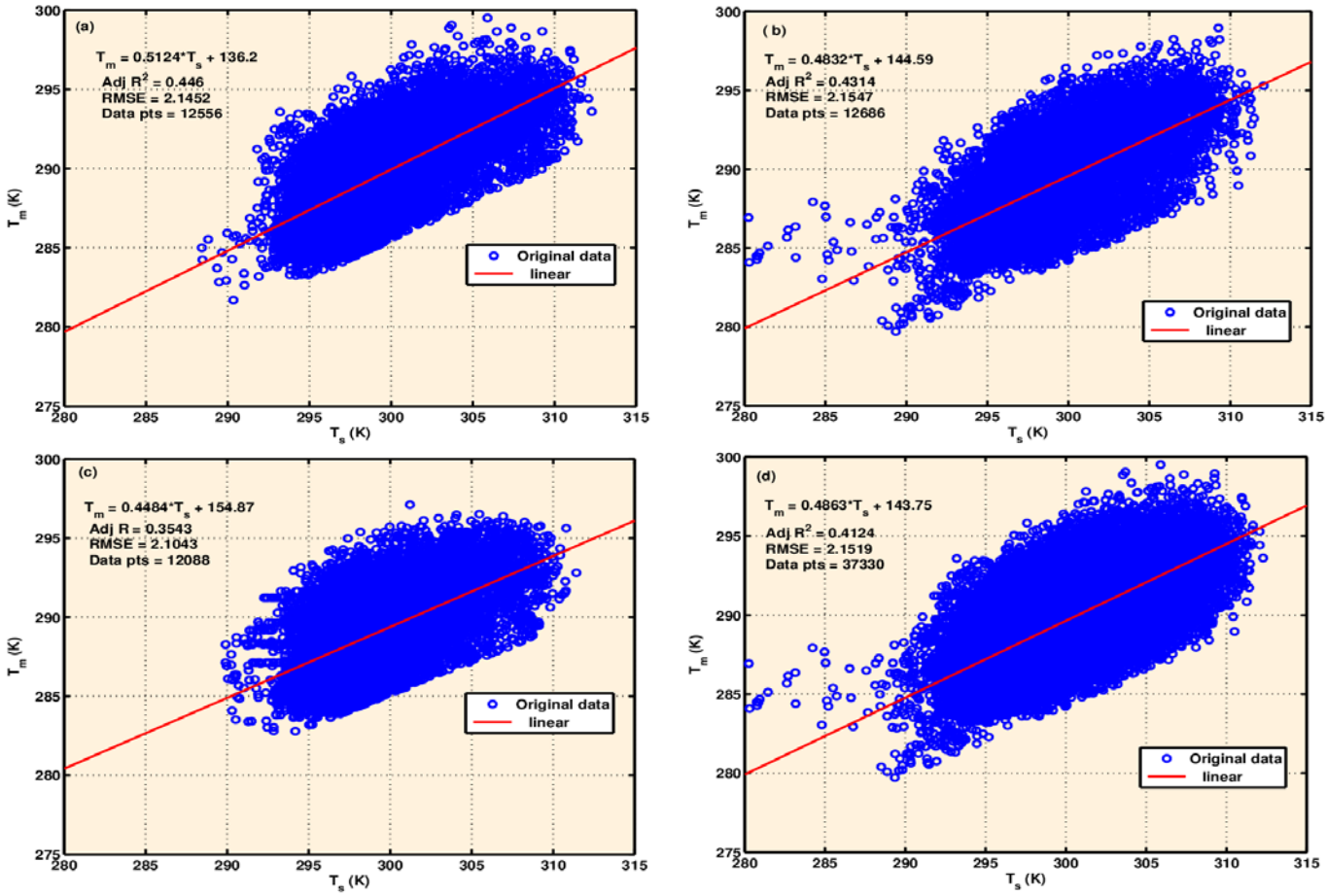

Figure 6.5: Regression diagram of weighted mean temperature (T_m) with surface temperature (T_s) from (a) 2010 (b) 2011 (c) 2012 and (d) 2010–2012 in Nigeria based on NCEP/NCAR reanalysis data

Similarly, by employing the radiosonde sounding data over West Africa, T_m vaules were linearly regressed with T_s. From the data combination at all stations, the $T_m - T_s$ relationship from the sounding data from 2009–2013 yielded Equation (6.13), hereinafter referred to as NWMTE-II. Figure 6.6 is its regression diagram showing the statistics of the model.

$$T_m = 0.5743T_s + 116.60 \qquad (6.13)$$

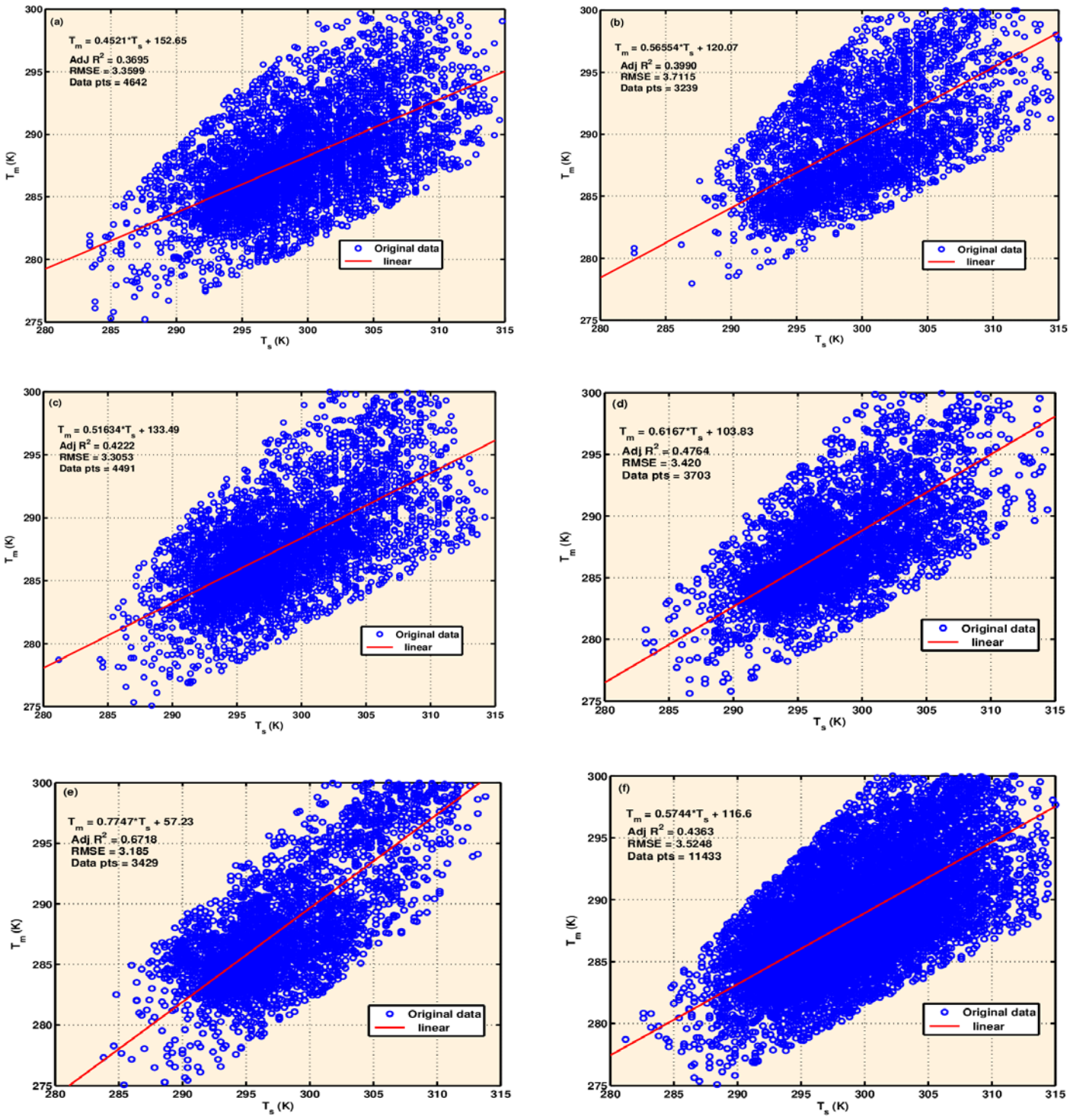

Figure 6.6: Regression diagram of weighted mean temperature (T_m) with surface temperature (T_s) from (a) 2009 (b) 2010 (c) 2011 (d) 2012 (e) 2013 and (f) 2009–2013 based on radiosonde (sounding) data over the West African sub-region

Finally, a regression model was obtained based on the combination of data sources from the $NWMTE-I$ and $NWMTE-II$ models. Thus, NWMTE-III was obtained, as shown in Equation (6.14). Figure 6.7 is its regression diagram showing the statistics of the model.

$$T_m = 0.5245T_s + 132.12 \qquad (6.14)$$

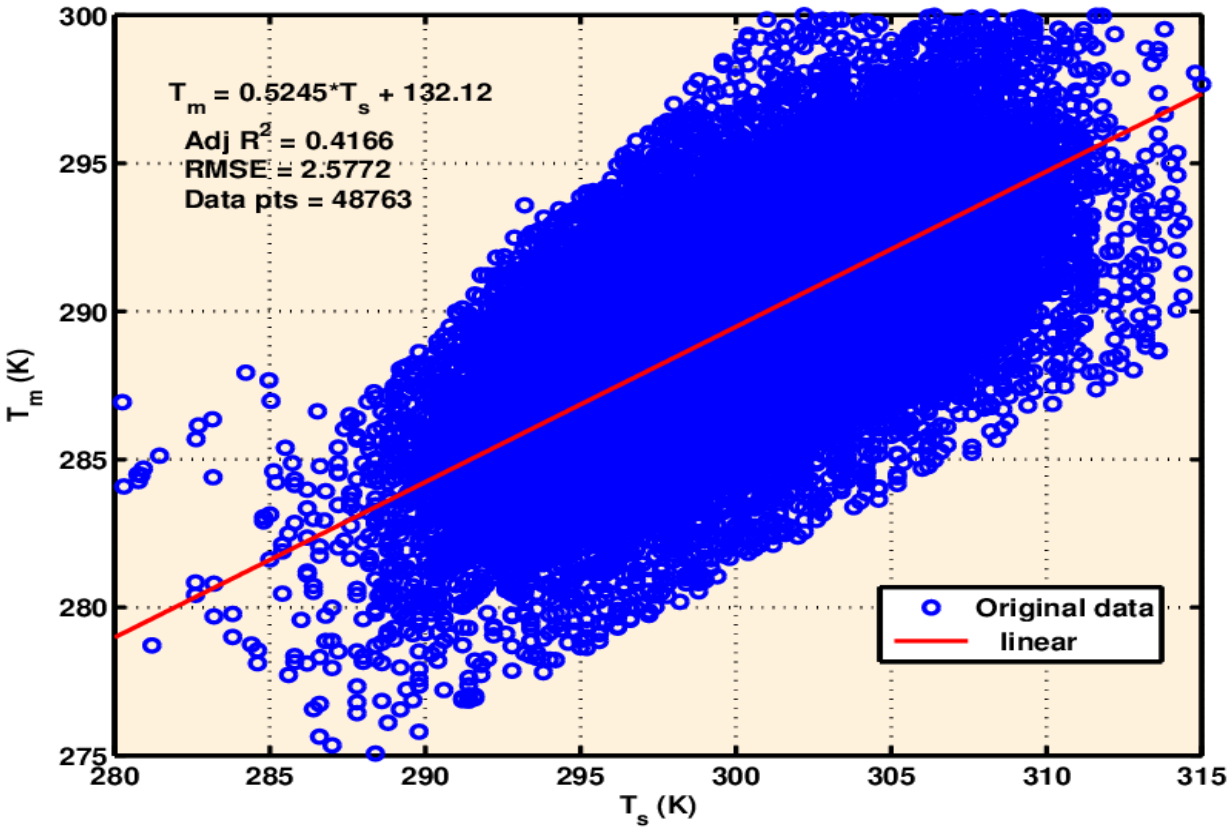

Figure 6.7: Regression diagram of weighted mean temperature (T_m) with surface temperature (T_s) based on the combination of NCEP/NCAR reanalysis and radiosonde (sounding) data

6.3.2 Validation of Models

In order to evaluate the accuracy of the three models developed in this study, they were compared with four global models (Bevis, UNB3m, GPT2w, GWMT-IV models) based on T_m obtained by using the integral method (Equation (6.3)), which is regarded as the standard or actual estimation method of T_m. Five model performance indicators were employed: the normalised mean absolute error (NMAE) (Shcherbakov et al., 2013), root - mean-square error (RMSE), model efficiency (MEF) (Murphy, 1988), reliability index (RI) (Leggett and Williams, 1981), and correlation coefficient (r). Isioye et al. (2015b) have

demonstrated the efficacy of the model performance indicators and their mathematical formulations are contained in therein.

The NMAE measures the absolute difference between the forecasted values (from NWMTE-I, NWMTE-II, NWMTE-III, Bevis, UNB3m, GPT2w, and GWMT-IV models) and the reference (Integral method), normalised to the mean. A NMAE value of zero indicates a perfect agreement. Similarly, RMSE measures the average square error; a value near zero indicates a close match for the RMSE. The MEF is a measure of how well the models (NWMTE-I, NWMTE-II, NWMTE-III, Bevis, UNB3m, GPT2w, and GWMT-IV models) forecast the observed (Integral method) values relative to the average of the observations. MEF values vary between 0 and 1, MEF = 0 implies no agreement between forecasted values and observations, MEF = 1 implies a perfect agreement. The RI quantifies the average factor by which the models (NWMTE-I, NWMTE-II, NWMTE-III, Bevis, UNB3m, GPT2w, and GWMT-IV models) estimates differ from the reference observations. A large RI value is indicative of large divergence between the forecasted and measured values. The value of RI=1 is the case of perfect forecasting. The r coefficient provides an indication of the linear relationship between the observed and estimated data, values range from [-1, 1], a positive value indicates a perfect coincident between observed and forecast anomalies. In turn, a negative value occurs when pattern is reversed.

In order to ascertain the accuracy of the eight models for estimating T_m, they were compared at the location of 15 GNSS stations over the Nigerian territory against the integral model of Equation (6.3). Figure 6.8 depicts the performance of the various models at locations of GNSS stations in Nigeria for 2014. Figure 6.8 shows that T_m from the UNB3m model is constant at each station throughout the year and thus not sensitive to daily or seasonal variations in the weather. The GPT2w and GWMT-IV models do follow a cyclical pattern and can thus be seen to be sensitive to seasonal variations in T_m. The integration method and the NWMTE-I, NWMTE-II, NWMTE-III, and Bevis models reflect the daily variation in T_m from Figure 6.8. This could be attributed to their direct dependence on temperature.

The performance of the various models at the location of the GNSS stations, as indicated by the NMAE, RMSE, MEF, and RI performance indicators, is presented in Table 6.3. The Pearson's correlation coefficient matrix is presented in Table 6.4.

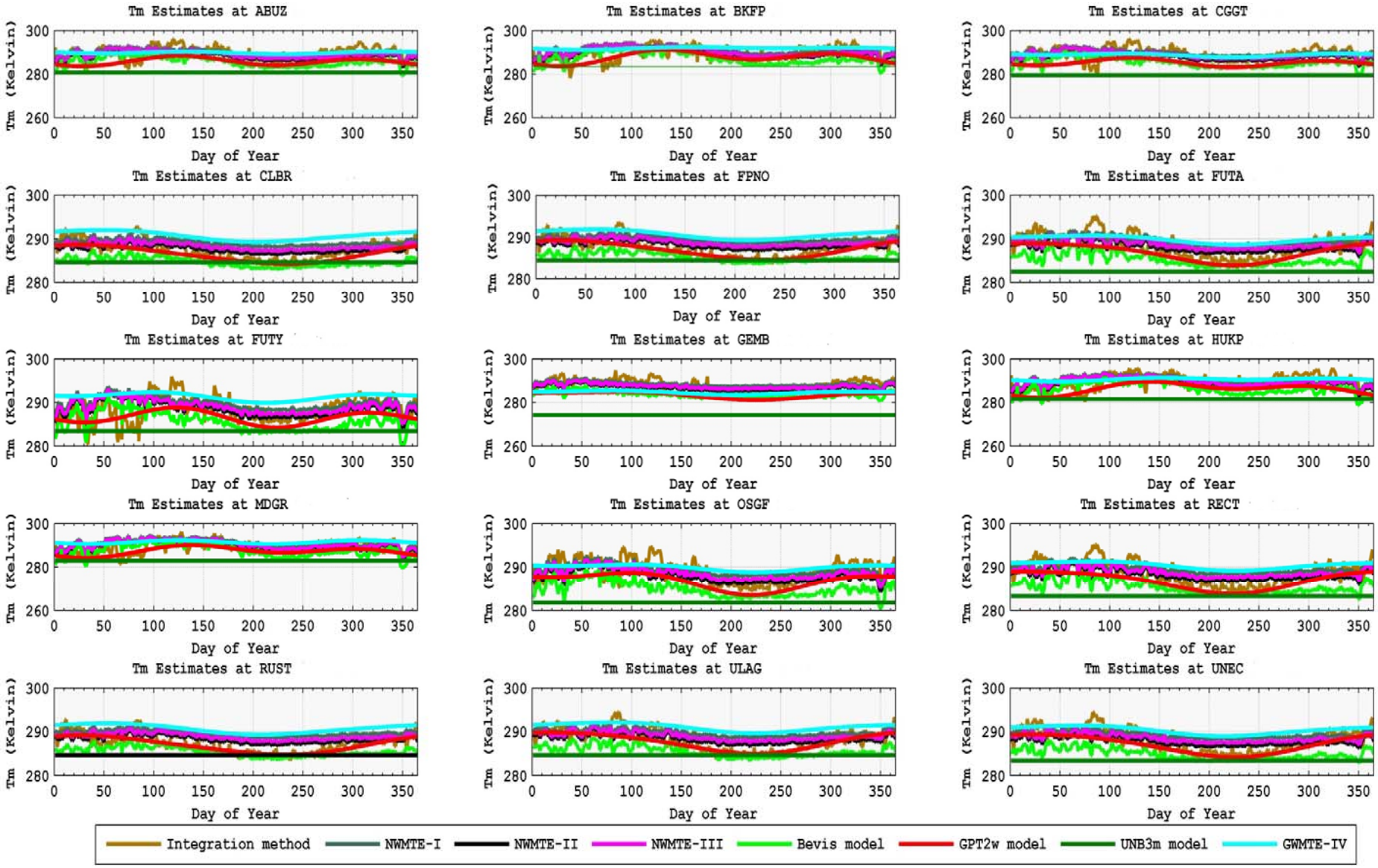

Figure 6.8: Plots of the different models at position of NIGNET GNSS Stations

Table 6.3: Performances of the different models for the estimation of T_m against the integration method

	NMAE	RMSE	MEF	RI	NMAE	RMSE	MEF	RI	NMAE	RMSE	MEF	RI
	ABUZ				BKFP				CGGT			
NWMTE-I	0.0077	2.8051	0.5647	1.0098	0.0088	3.3905	0.5501	1.0118	0.0077	2.9682	0.5238	1.0103
NWMTE-II	0.008	2.9603	0.5871	1.0103	0.0086	3.2356	0.5935	1.0113	0.0079	3.0408	0.5454	1.0106
NWMTE-III	0.0076	2.7944	0.5801	1.0097	0.0085	3.2253	0.5732	1.0112	0.0075	0.9091	0.5347	1.0101
Bevis	0.0145	4.7787	0.509	1.0167	0.0125	4.2638	0.5534	1.0149	0.0148	4.7929	0.4892	1.0168
GPT2w	0.013	4.2959	0.5467	1.015	0.0094	3.2284	0.6715	1.0112	0.0138	4.5048	0.5237	1.0158
UNB3M	0.0296	9.0606	0.3431	1.0322	0.0215	6.9318	0.4081	1.0244	0.0326	9.8929	0.3275	1.0353
GWMT-IV	0.008	2.7822	0.3324	1.0097	0.0102	3.7851	0.4751	1.0132	0.0078	2.789	0.3229	1.0097
	CLBR				FPNO				FUTA			
NWMTE-I	0.0073	2.4473	0.5759	1.0086	0.0081	2.7304	0.5706	1.0095	0.0073	2.448	0.5766	1.0085
NWMTE-II	0.0052	1.763	0.63	1.0061	0.0057	1.9205	0.614	1.0067	0.0062	2.1955	0.6528	1.0076
NWMTE-III	0.0059	1.9573	0.5818	1.0068	0.0065	2.2007	0.5853	1.0077	0.0064	2.1969	0.6142	1.0076
Bevis	0.0101	3.363	0.5557	1.0118	0.0085	3.0067	0.5927	1.0105	0.0116	3.9254	0.5673	1.0137
GPT2w	0.0045	1.681	0.5117	1.0058	0.0038	1.5162	0.5828	1.0093	0.0063	2.2951	0.5698	1.008
UNB3M	0.0104	3.6642	0.4502	1.0128	0.0114	3.9932	0.4461	1.014	0.0209	6.5996	0.3894	1.0233
GWMT-IV	0.0113	3.5504	0.5462	1.0124	0.0109	3.4529	0.5605	1.0121	0.0074	2.5133	0.5982	1.0088
	FUTY				GEMB				HUKP			
NWMTE-I	0.0082	3.1888	0.4889	1.0111	0.0054	1.9226	0.6042	1.0067	0.009	3.3991	0.5536	1.0118
NWMTE-II	0.0076	2.9656	0.4915	1.0103	0.0067	2.4977	0.6146	1.0087	0.0093	3.3815	0.5816	1.0118
NWMTE-III	0.0075	2.9682	0.4873	1.0103	0.0057	2.0933	0.6287	1.0073	0.0089	3.3072	0.5704	1.0115
Bevis	0.0131	4.2652	0.4538	1.0149	0.0168	5.2071	0.4533	1.0183	0.0139	4.713	0.5234	1.0165
GPT2w	0.0087	2.964	0.5897	1.0103	0.017	5.1219	0.4801	1.018	0.0116	3.9502	0.5393	1.0138
UNB3M	0.0177	5.7397	0.4085	1.0202	0.0493	14.4009	0.2077	1.0525	0.0271	8.527	0.3749	1.0302
GWMT-IV	0.0111	3.918	0.5048	1.0137	0.0129	4.1445	0.4924	1.0145	0.0093	3.3023	0.4508	1.0115
	MDGR				OSGF				RECT			
NWMTE-I	0.0088	3.4876	0.5633	1.0121	0.0066	2.2825	0.6109	1.0079	0.0071	2.4095	0.5827	1.0084
NWMTE-II	0.0078	3.0968	0.6052	1.0108	0.0069	2.5008	0.6489	1.0087	0.0061	2.175	0.6632	1.0075
NWMTE-III	0.0079	3.1856	0.5884	1.0111	0.0065	2.2856	0.6418	1.0079	0.0063	2.1676	0.6264	1.0075
Bevis	0.0108	3.7012	0.5514	1.0129	0.0143	4.6651	0.5281	1.0163	0.0116	3.9236	0.5707	1.0137
GPT2w	0.008	2.7679	0.5806	1.0096	0.0087	2.9217	0.5754	1.0102	0.0065	2.3529	0.5622	1.0082
UNB3M	0.0215	6.8264	0.3818	1.0241	0.025	7.6925	0.3588	1.0272	0.0184	5.9564	0.4071	1.021
GWMT-IV	0.0098	3.5417	0.5256	1.0124	0.0072	2.4683	0.518	1.0086	0.0082	2.7861	0.595	1.0097
	RUST				ULAG				UNEC			
NWMTE-I	0.0089	2.9325	0.5468	1.0102	0.0077	2.6123	0.5898	1.0091	0.0072	2.4029	0.582	1.0084
NWMTE-II	0.0058	1.9403	0.6058	1.0068	0.0057	1.964	0.6527	1.0068	0.0059	2.0533	0.643	1.0071
NWMTE-III	0.0069	2.3225	0.5837	1.0081	0.0064	2.1637	0.6048	1.0075	0.0062	2.0907	0.5995	1.0073
Bevis	0.0071	2.5767	0.6123	1.009	0.0091	3.2008	0.6067	1.0112	0.0114	3.8232	0.562	1.0134
GPT2w	0.0035	1.3686	0.5558	1.0048	0.0038	1.5584	0.6064	1.0054	0.0047	1.7958	0.5363	1.0062
UNB3M	0.0097	3.461	0.4507	1.0121	0.0122	4.2634	0.4471	1.0149	0.0164	5.3666	0.4196	1.0189
GWMT-IV	0.0117	3.6481	0.5297	1.0127	0.0106	3.4414	0.5697	1.012	0.0086	2.8745	0.6107	1.01

Table 6.4: Pearson's correlation coefficient matrix for the different models

Variables	IM	NWMTE-I	NWMTE-II	NWMTE-III	Bevis	GPT2w	GWMT-IV	IM	NWMTE-I	NWMTE-II	NWMTE-III	Bevis	GPT2w	GWMT-IV	IM	NWMTE-I	NWMTE-II	NWMTE-III	Bevis	GPT2w	GWMT-IV
				ABUZ							BKFP							CGGT			
IM	1	0.3725	0.3725	0.3725	0.3725	0.2983	0.3409	1	0.3323	0.3323	0.3323	0.3323	0.4117	0.2950	1	0.3166	0.3166	0.3166	0.3166	0.5577	0.4831
NWMTE-I		1	1.0000	1.0000	1.0000	0.2622	0.2428		1	1.0000	1.0000	1.0000	0.2450	-0.0015		1	1.0000	1.0000	1.0000	0.4664	0.5245
NWMTE-II			1	1.0000	1.0000	0.2622	0.2428			1	1.0000	1.0000	0.2450	-0.0015			1	1.0000	1.0000	0.4664	0.5245
NWMTE-III				1	1.0000	0.2622	0.2428				1	1.0000	0.2450	-0.0015				1	1.0000	0.4664	0.5245
Bevis					1	0.2622	0.2428					1	0.2450	-0.0015					1	0.4664	0.5245
GPT2w						1	0.7170						1	0.7585						1	0.8124
GWMT-IV							1							1							1
				CLBR							FPNO							FUTA			
IM	1	0.6648	0.6648	0.6648	0.6648	0.6269	0.6198	1	0.6777	0.6777	0.6777	0.6777	0.6267	0.6358	1	0.6372	0.6372	0.6372	0.6372	0.6321	0.6561
NWMTE-I		1	1.0000	1.0000	1.0000	0.5743	0.5741		1	1.0000	1.0000	1.0000	0.5578	0.6253		1	1.0000	1.0000	1.0000	0.4880	0.5626
NWMTE-II			1	1.0000	1.0000	0.5743	0.5741			1	1.0000	1.0000	0.5578	0.6253			1	1.0000	1.0000	0.4880	0.5626
NWMTE-III				1	1.0000	0.5743	0.5741				1	1.0000	0.5578	0.6253				1	1.0000	0.4880	0.5626
Bevis					1	0.5743	0.5741					1	0.5578	0.6253					1	0.4880	0.5626
GPT2w						1	0.9556						1	0.9623						1	0.9575
GWMT-IV							1							1							1
				FUTY							GEMB							HUKP			
IM	1	0.2073	0.2073	0.2073	0.2073	0.4113	0.1875	1	0.5370	0.5370	0.5370	0.5370	0.5896	0.5557	1	0.3236	0.3236	0.3236	0.3236	0.4677	0.4597
NWMTE-I		1	1.0000	1.0000	1.0000	0.2579	0.4304		1	1.0000	1.0000	1.0000	0.5052	0.4972		1	1.0000	1.0000	1.0000	0.2661	0.2014
NWMTE-II			1	1.0000	1.0000	0.2579	0.4304			1	1.0000	1.0000	0.5052	0.4972			1	1.0000	1.0000	0.2661	0.2014
NWMTE-III				1	1.0000	0.2579	0.4304				1	1.0000	0.5052	0.4972				1	1.0000	0.2661	0.2014
Bevis					1	0.2579	0.4304					1	0.5052	0.4972					1	0.2661	0.2014
GPT2w						1	0.8068						1	0.9140						1	0.8657
GWMT-IV							1							1							1
				MDGR							OSGF							RECT			
IM	1	0.3154	0.3154	0.3154	0.3154	0.4901	0.3756	1	0.5468	0.5468	0.5468	0.5468	0.5281	0.5249	1	0.6431	0.6431	0.6431	0.6431	0.6240	0.6541
NWMTE-I		1	1.0000	1.0000	1.0000	0.2834	0.2114		1	1.0000	1.0000	1.0000	0.4761	0.4521		1	1.0000	1.0000	1.0000	0.4916	0.5728
NWMTE-II			1	1.0000	1.0000	0.2834	0.2114			1	1.0000	1.0000	0.4761	0.4521			1	1.0000	1.0000	0.4916	0.5728
NWMTE-III				1	1.0000	0.2834	0.2114				1	1.0000	0.4761	0.4521				1	1.0000	0.4916	0.5728
Bevis					1	0.2834	0.2114					1	0.4761	0.4521					1	0.4916	0.5728
GPT2w						1	0.7577						1	0.9960						1	0.9524
GWMT-IV							1							1							1
				RUST							ULAG							UNEC			
IM	1	0.6684	0.6684	0.6684	0.6684	0.6079	0.6100	1	0.7007	0.7007	0.7007	0.7007	0.6231	0.6599	1	0.6716	0.6716	0.6716	0.6716	0.6485	0.6609
NWMTE-I		1	1.0000	1.0000	1.0000	0.5533	0.5963		1	1.0000	1.0000	1.0000	0.5643	0.6510		1	1.0000	1.0000	1.0000	0.5565	0.6091
NWMTE-II			1	1.0000	1.0000	0.5533	0.5963			1	1.0000	1.0000	0.5643	0.6510			1	1.0000	1.0000	0.5565	0.6091
NWMTE-III				1	1.0000	0.5533	0.5963				1	1.0000	0.5643	0.6510				1	1.0000	0.5565	0.6091
Bevis					1	0.5533	0.5963					1	0.5643	0.6510					1	0.5565	0.6091
GPT2w						1	0.9644						1	0.9313						1	0.9680
GWMT-IV							1							1							1

The mean values for the different performance indicators for all models are presented in Table 6.5. The mean NMAE, RMSE, MEF, and RI results clearly demonstrate the strength of the three local models (NWMTE-I, NWMTE-II, NWMTE-III) compared with the others. It is evident that the UNB3m model is not appropriate for use within the study area since it scores very low in all evaluation tests. Although the Bevis model is an acceptable choice for many regional studies, the results in this study clearly show that local empirical models are better tailored to the geographical and climate characteristics of the studied region.

Table 6.5: Mean values of the performance indicators for the different models

MODEL/PERFORMANCE INDICATOR	NMAE	RMSE	MEF	RI
NWMTE-I	0.0077	2.7618	0.5656	1.0096
NWMTE-II	0.0069	2.5127	0.6086	1.0087
NWMTE-III	0.0070	2.3912	0.5867	1.0088
Bevis	0.0120	4.0138	0.5419	1.0140
GPT2w	0.0082	2.8215	0.5621	1.0101
UNB3m	0.0216	6.8251	0.3880	1.0242
GWMT-IV	0.0097	3.2665	0.5088	1.0114

From Table 6.4, the result of the Pearson's correlation coefficient test presents a slightly different view of the models. The GPT2w model exhibits the strongest correlation with the reference model (integral method) at six stations in the northern part of the country. Interestingly, the NWMTE-I, NWMTE-II, NWMTE-III, and Bevis models also exhibit positive correlation among themselves because of their direct dependence on surface temperature measurements at the individual stations. In addition, they exhibit stronger correlation at the remaining nine stations, thus outnumbering the other models. The GPT2w model presents itself as a promising model. However, it lacks the ability of response to adverse atmospheric conditions because of its dependence on DOY, station height, and latitude. This is in contrast to the NWMTE-I, NWMTE-II, NWMTE-III, and Bevis models, which are directly dependant on measured temperature at the respective stations.

6.3.3 Spatiotemporal Variation of T_m Models

The result of the variation of T_m from the different models at locations of GNSS sites in Nigeria at seasonal and annual scales is presented in Figure 6.9. This is a plot of the T_m values from the different models against the latitude of the corresponding GNSS site.

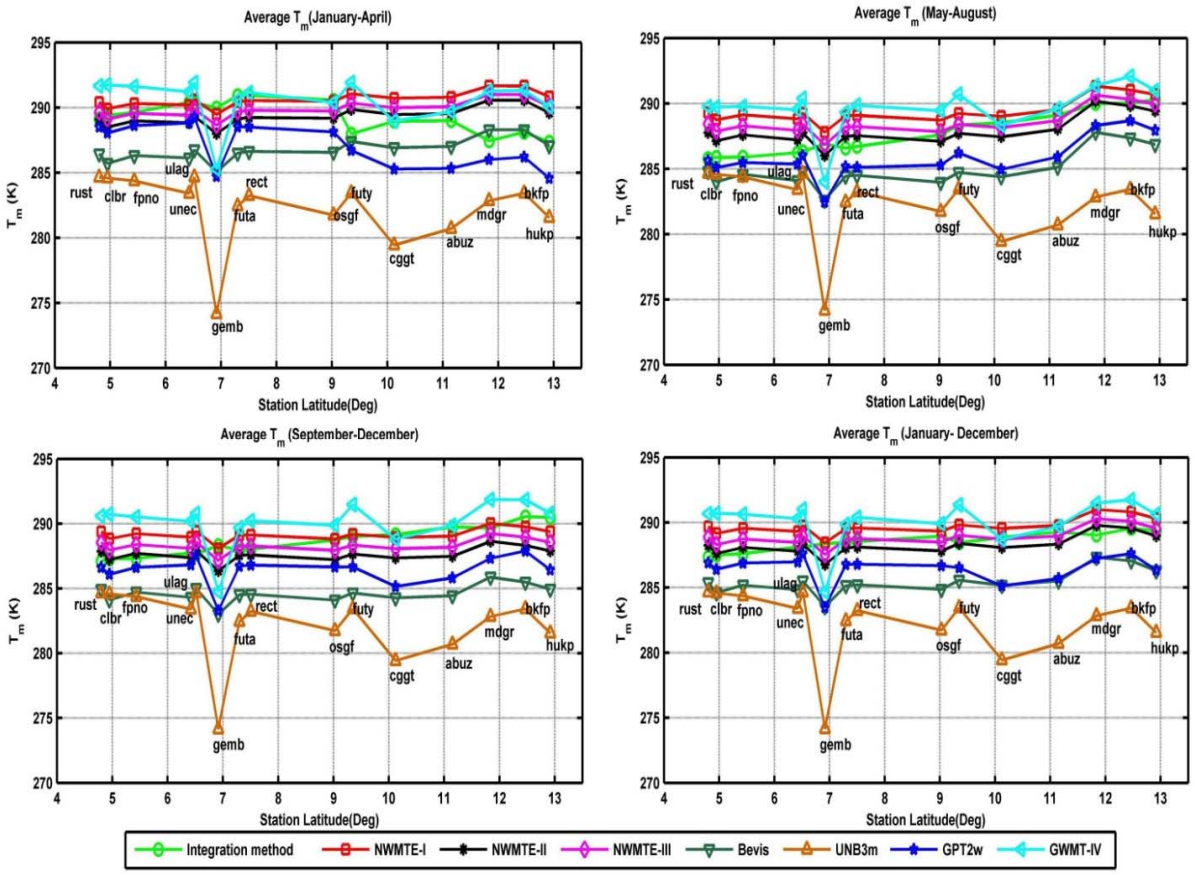

Figure 6.9: Seasonal and annual variability of T_m at locations of GNSS stations in Nigeria

The three seasonal periods shown in Figure 6.9 are January to April, which is the dry season in both the northern and southern part of the country, May to August, which is the peak of the rainy seasons, and September to December, which includes months of dry weather (Harmattan) in the north and low rain in the south. The T_m values are lower for all the models in the rainy season (May to August) than in other periods. Also, very high values of T_m can be seen in dry season (January to April) for all of the models, except for the UNB3m model whose values remains unchanging throughout the year. It is very conspicuous in the Figure 6.9 that the latitudinal effect on the absolute values of T_m from the models is very weak. This is contrary to the general expectation of an increasing or decreasing trend. Thus, the spatial variability of T_m over different GNSS stations in Nigeria not only depends on the station latitude and season, but also on other natural factors (e.g. station elevation). This assertion is further verified from the Figure 6.9, the five stations with altitude higher than 500m above mean sea level (amsl) have lower T_m values for all the

models (i.e., OSGF (532.64 m amsl), HUKP (563.31 m amsl), ABUZ (705.05 m amsl), CGGT (916.43 m amsl), and GEMB (1795.61m amsl)) and stations with lower altitude had higher T_m values. When T_m estimates from the reference model were compared against other models for the different seasons, it is evident that the UNB3m, GPT2w and Bevis models under estimates T_m, whereas overestimated values were seen in the GWMT-IV model and very good agreement was seen in the NWMTE-I, II, and III models.

In order to further analyse the latitudinal dependence of T_m, the range (differences between the maximum and minimum value) of T_m for the different models at the GNSS locations were estimated. The range values were compared to see how each model oscillates around its maximum and minimum values and if this depends on the latitude of the station (See Figure 6.10).

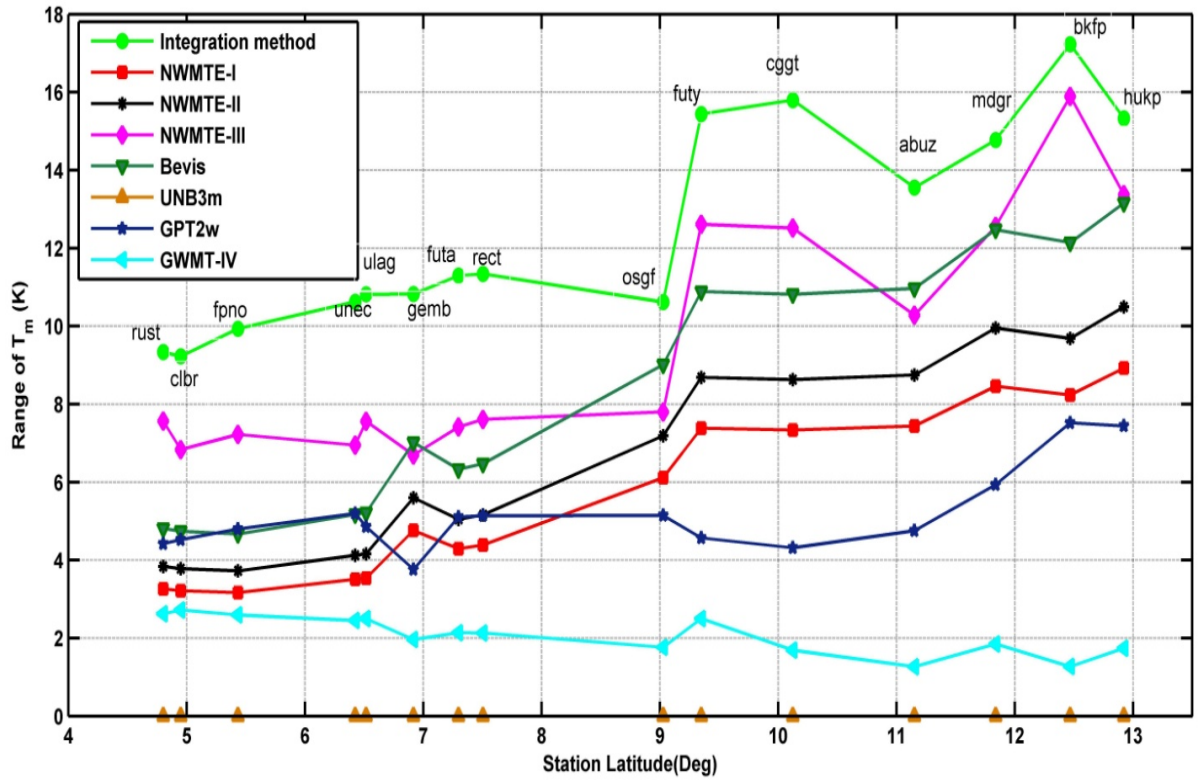

Figure 6.10: A plot of the Range (maximum minus minimum) values of T_m estimates against latitudes of GNSS stations in Nigeria

From Figure 6.10, it is apparent that the range in T_m at most of the stations increases with latitude (i.e., movement from south to north). A sharp increase in the range values is seen at the location of GNSS stations (OSGF, FUTY, CGGT, ABUZ, MDGR, BKFP, and

HUKP) in the northern part of Nigeria. This is expected because of the extreme cold and hot weathers during the dry season in this region, which often results in high variations in surface temperature. Also, it can be seen that the range of T_m for the integral method (reference model) is greater when compared to the other models; it is closely followed by the NWMTE-III model. The UNB3m and GWMT-IV models did not follow same trend; the UNB3m model is constant all the through the year and had zero range value. This result gives good insight into the relations between T_m and climatic zones in Nigeria. Remarkably, the climate of Nigeria changes more than any other country in West Africa due to its location and latitudinal extent (about 1100 km). Consequently, nearly all of the climatic zones of West Africa are contained within Nigeria.

6.4 Implications of T_m Modelling for GNSS Meteorology

6.4.1 Precision of PWV from T_m Models

From the foregoing, it is pertinent to note that the errors in converting ZWD into PWV are primarily those in T_m, because its accuracy has a great influence on the conversion of ZWD into PWV. According to Equation (6.2), the constants ρ_w, R_w, k_2', and k_3 are known with sufficient accuracy. Thus, the major error contributor is the uncertainty of T_m. If the law of error propagation is applied to Equation (6.2), the following approximate formula is obtained:

$$\sigma_{PWV} = \sqrt{\left(ZWD \cdot \sigma_{\Pi}\right)^2 + \left(\Pi \cdot \sigma_{ZHD}\right)^2 + \left(\Pi \cdot \sigma_{ZTD}\right)^2} \quad . \tag{6.15}$$

In Equation (6.15), the variables σ_{pwv}, σ_{ZHD}, σ_{ZTD}, and σ_{Π} are the errors in PWV, ZHD, ZTD, and Π, respectively. The error in Π is expressed in terms of T_m and its associated error $\left(\sigma_{T_m}\right)$ as follows:

$$\sigma_{\Pi} \approx \frac{\Pi \sigma_{T_m}}{T_m} \approx \frac{1}{1768.72} \cdot \sigma_{Tm} \quad . \tag{6.16}$$

The ZTD can be obtained with typical formal errors of 1.5–5 mm from the IGS (Byun & Bar-Server, 2009). Further, it can be modelled with an accuracy of a few mm if pressure measurement is obtained on site at a GNSS station. Thus, if we assume a maximum error of 5 mm in the ZTD and ZHD estimates, a typical value of 108 mm for ZWD, an average mean

temperature of 285 K, and the corresponding RMSE of the different models as presented in Table 6.5, then the precision of PWV can be found (see Table 6.6). Although theoretically, all the models show an almost mm level of accuracy in predicting PWV, the NWMTE-III still found to be more suitable for users in the West African region. The next sub-section takes a look at the actual effects of the different models on GNSS PWV estimates.

Table 6.6: Precision of the PWV estimates for the models

	ZWD (mm)	T_m **(K)**	Π	σ_{T_m} **(K)**	σ_{Π}	σ_{ZTD} **(mm)**	σ_{ZHD} **(mm)**	σ_{PWV} **(mm)**
NWMTE-I	108	285	0.1624	2.7618	0.0016	5	5	1.16
NWMTE-II	108	285	0.1624	2.5127	0.0014	5	5	1.16
NWMTE-III	108	285	0.1624	2.3912	0.0014	5	5	1.16
Bevis	108	285	0.1624	4.0138	0.0023	5	5	1.17
GPT2w	108	285	0.1624	2.8215	0.0016	5	5	1.16
UNB3m	108	285	0.1624	6.8251	0.0039	5	5	1.22
GWMT-IV	108	285	0.1624	3.2665	0.0019	5	5	1.17

6.4.2 Analysis of Derived PWV from GNSS and the various T_m models

This Section looks into the practical application of the various models introduced in the preceding sections. PWV was estimated using the different models at five GNSS stations spread across Nigerian territory. Again, the PWV estimate from the integral method is considered as the reference. The time series of the differences in PWV estimate between the reference and other models is shown in Figure 6.11.

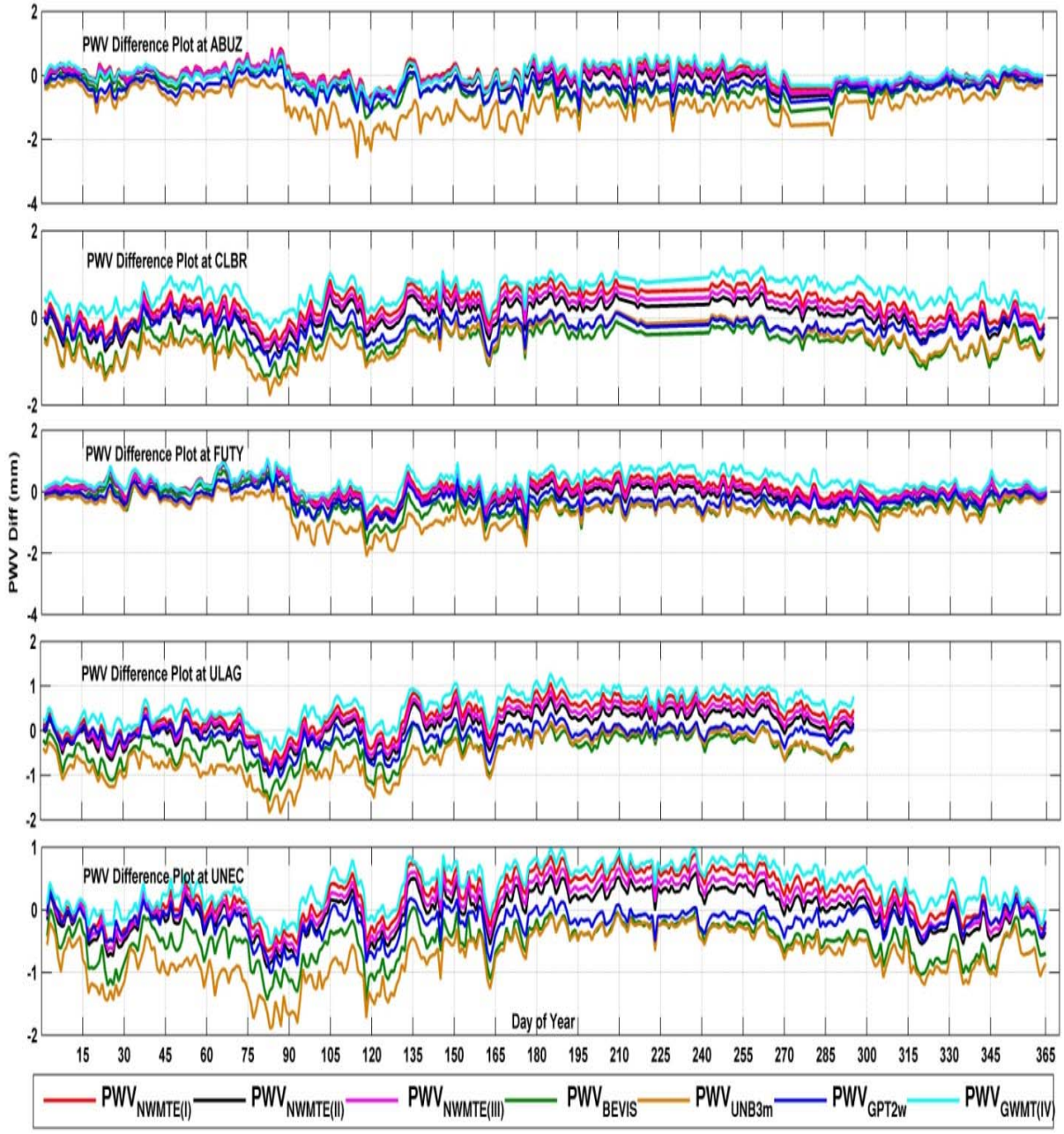

Figure 6.11: Time series of the differences in estimated PWV using the integral model and the other models (NWMTE-I, NWMTE-II, NWMTE-III, Bevis, UNB3m, GPT2w, and GWMT-IV) at five GNSS stations (ABUZ, CLBR, FUTY, ULAG, UNEC) located in the Nigerian territory

The variation in the models as shown in Figure 6.11 is suggestive of the respective strength of the models at the individual stations. The UNB3m and GWMT-IV exhibit noticeable discrepancies from other models but mere visual inspection may be inadequate to ascertain the effect of the accuracies of the models on PWV estimation. Thus, seven different model performance indicators (namely, NMAE, MAE, RMSE, SDR, MEF, RI, and r) were considered. MAE (Mean Absolute Error) measures the absolute deviation of the models

values (NWMTE-I, NWMTE-II, NWMTE-III, Bevis model, UNB3m model, GPT2w model, and GWMT-IV) from the reference (Integration model). Similarly, SDR (Standard Deviation of Residuals) is a measure of the dynamical correspondence (or precision). A value near zero indicates a close match for the MAE and SDR. Other indicators have already been described in the preceding section of this report. Results of the various comparisons at the individual GNSS stations are presented in Figures 6.12(a) - (e).

(a)

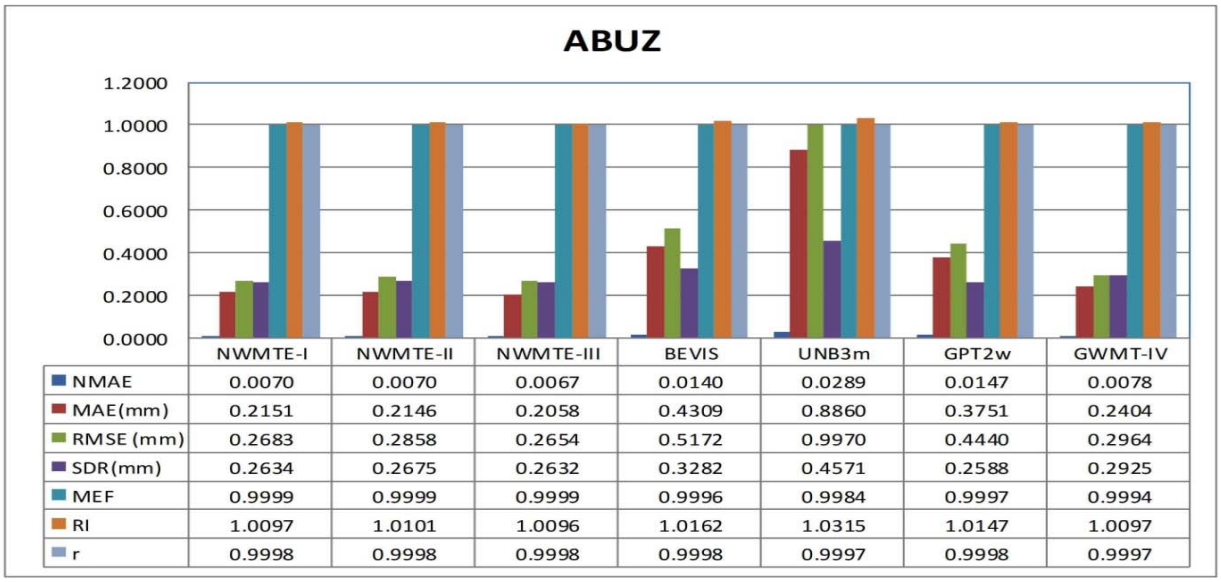

	NWMTE-I	NWMTE-II	NWMTE-III	BEVIS	UNB3m	GPT2w	GWMT-IV
NMAE	0.0070	0.0070	0.0067	0.0140	0.0289	0.0147	0.0078
MAE(mm)	0.2151	0.2146	0.2058	0.4309	0.8860	0.3751	0.2404
RMSE (mm)	0.2683	0.2858	0.2654	0.5172	0.9970	0.4440	0.2964
SDR(mm)	0.2634	0.2675	0.2632	0.3282	0.4571	0.2588	0.2925
MEF	0.9999	0.9999	0.9999	0.9996	0.9984	0.9997	0.9994
RI	1.0097	1.0101	1.0096	1.0162	1.0315	1.0147	1.0097
r	0.9998	0.9998	0.9998	0.9998	0.9997	0.9998	0.9997

(b)

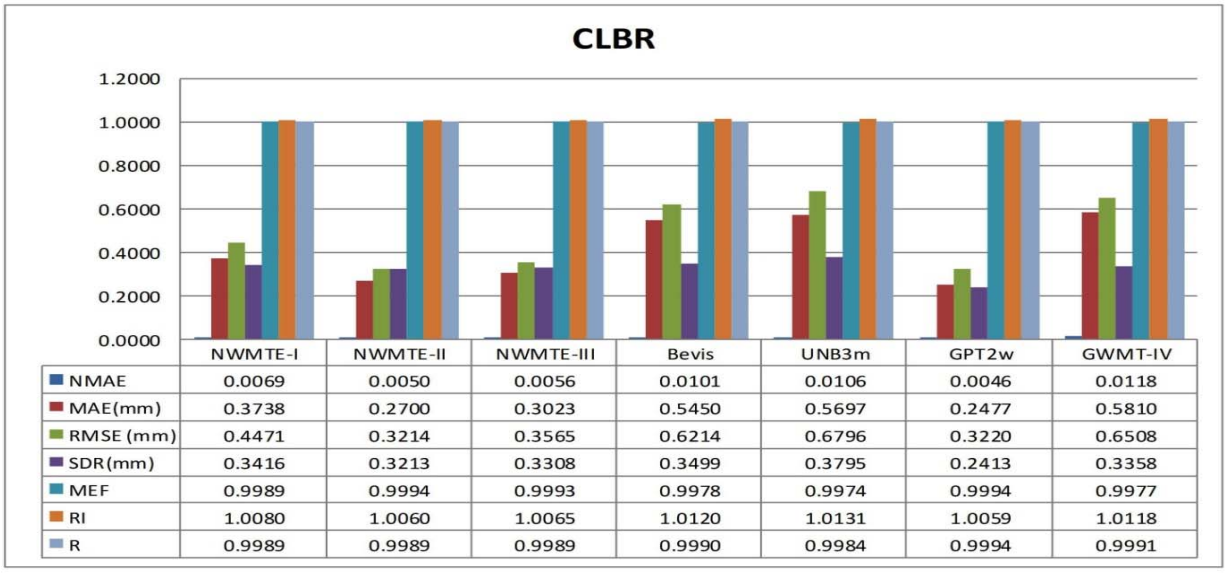

	NWMTE-I	NWMTE-II	NWMTE-III	Bevis	UNB3m	GPT2w	GWMT-IV
NMAE	0.0069	0.0050	0.0056	0.0101	0.0106	0.0046	0.0118
MAE(mm)	0.3738	0.2700	0.3023	0.5450	0.5697	0.2477	0.5810
RMSE (mm)	0.4471	0.3214	0.3565	0.6214	0.6796	0.3220	0.6508
SDR(mm)	0.3416	0.3213	0.3308	0.3499	0.3795	0.2413	0.3358
MEF	0.9989	0.9994	0.9993	0.9978	0.9974	0.9994	0.9977
RI	1.0080	1.0060	1.0065	1.0120	1.0131	1.0059	1.0118
R	0.9989	0.9989	0.9989	0.9990	0.9984	0.9994	0.9991

(c)

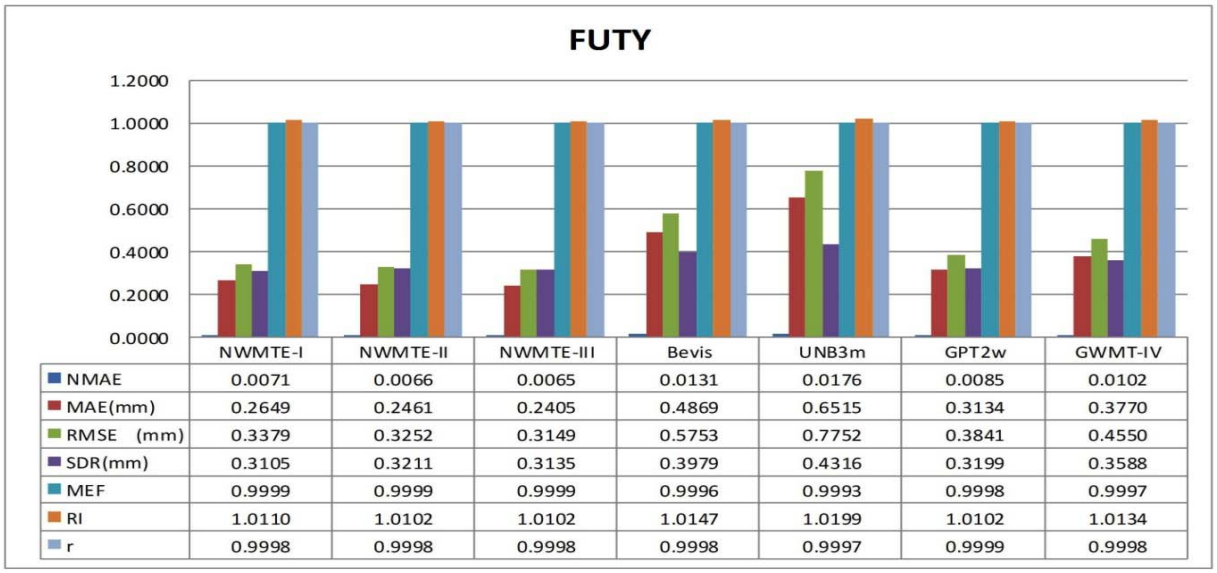

	NWMTE-I	NWMTE-II	NWMTE-III	Bevis	UNB3m	GPT2w	GWMT-IV
NMAE	0.0071	0.0066	0.0065	0.0131	0.0176	0.0085	0.0102
MAE(mm)	0.2649	0.2461	0.2405	0.4869	0.6515	0.3134	0.3770
RMSE (mm)	0.3379	0.3252	0.3149	0.5753	0.7752	0.3841	0.4550
SDR(mm)	0.3105	0.3211	0.3135	0.3979	0.4316	0.3199	0.3588
MEF	0.9999	0.9999	0.9999	0.9996	0.9993	0.9998	0.9997
RI	1.0110	1.0102	1.0102	1.0147	1.0199	1.0102	1.0134
r	0.9998	0.9998	0.9998	0.9998	0.9997	0.9999	0.9998

(d)

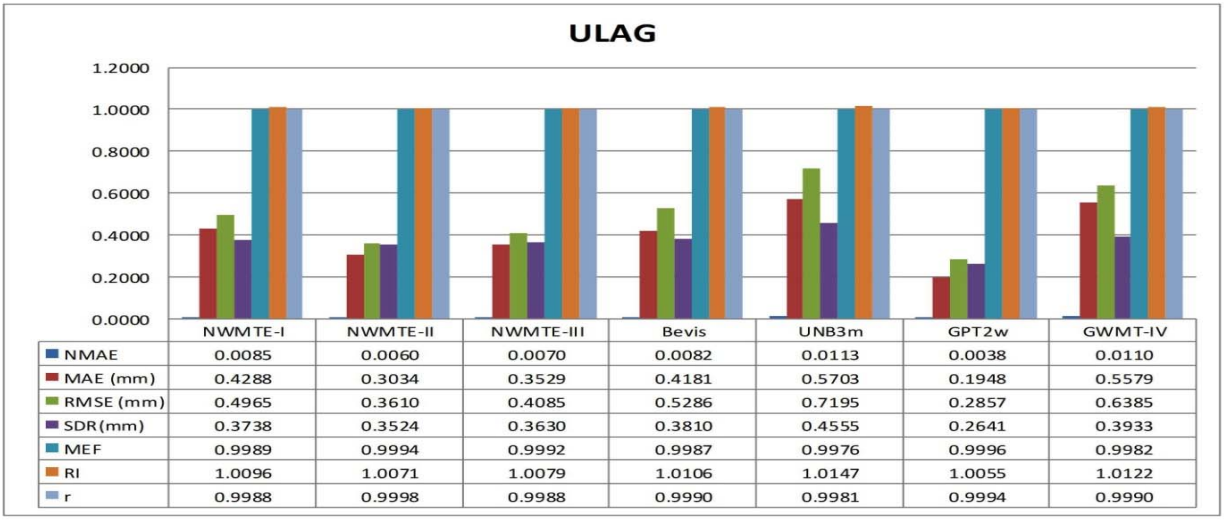

	NWMTE-I	NWMTE-II	NWMTE-III	Bevis	UNB3m	GPT2w	GWMT-IV
NMAE	0.0085	0.0060	0.0070	0.0082	0.0113	0.0038	0.0110
MAE (mm)	0.4288	0.3034	0.3529	0.4181	0.5703	0.1948	0.5579
RMSE (mm)	0.4965	0.3610	0.4085	0.5286	0.7195	0.2857	0.6385
SDR(mm)	0.3738	0.3524	0.3630	0.3810	0.4555	0.2641	0.3933
MEF	0.9989	0.9994	0.9992	0.9987	0.9976	0.9996	0.9982
RI	1.0096	1.0071	1.0079	1.0106	1.0147	1.0055	1.0122
r	0.9988	0.9998	0.9988	0.9990	0.9981	0.9994	0.9990

(e)

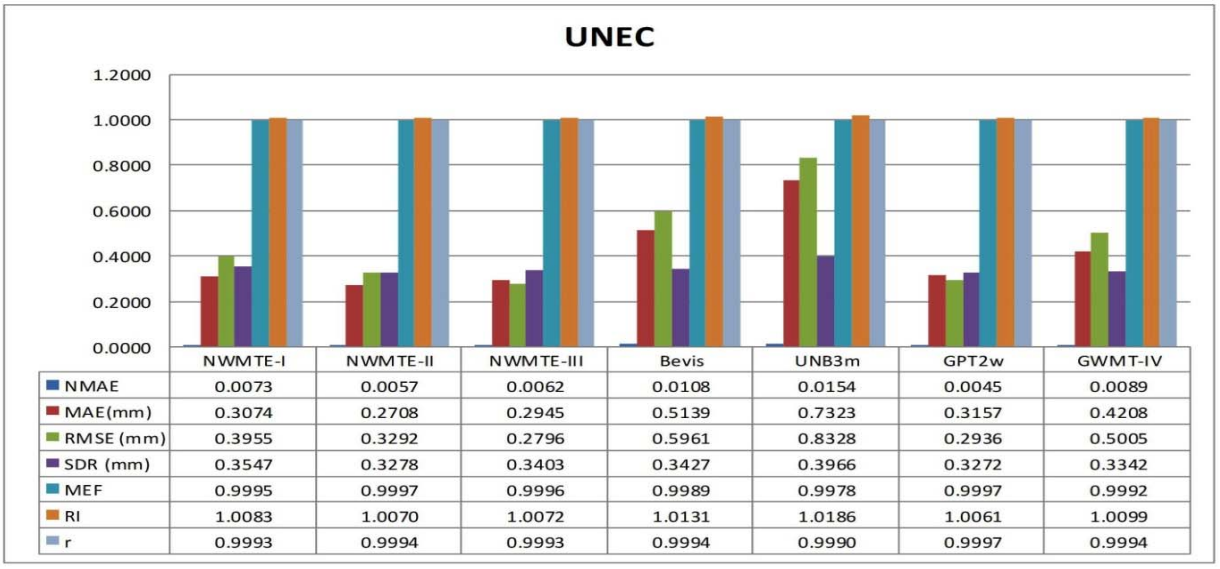

	NWMTE-I	NWMTE-II	NWMTE-III	Bevis	UNB3m	GPT2w	GWMT-IV
NMAE	0.0073	0.0057	0.0062	0.0108	0.0154	0.0045	0.0089
MAE(mm)	0.3074	0.2708	0.2945	0.5139	0.7323	0.3157	0.4208
RMSE (mm)	0.3955	0.3292	0.2796	0.5961	0.8328	0.2936	0.5005
SDR (mm)	0.3547	0.3278	0.3403	0.3427	0.3966	0.3272	0.3342
MEF	0.9995	0.9997	0.9996	0.9989	0.9978	0.9997	0.9992
RI	1.0083	1.0070	1.0072	1.0131	1.0186	1.0061	1.0099
r	0.9993	0.9994	0.9993	0.9994	0.9990	0.9997	0.9994

Figure 6.12: Performance of estimated PWV using T_m model based integration formula against the other models (NWMTE-I, NWMTE-II, NWMTE-III, Bevis, UNB3m, GPT2w, and GWMT-IV) at (a) 'ABUZ', (b) 'CLBR', (c) 'FUTY', (d), 'ULAG' and (e) 'UNEC' stations

The NMAE, MEF, RI, and r value in Figures 6.12 (a) - (e) at the different stations for all the models under consideration are indicative of the overall strength of the models in estimating PWV within acceptable accuracy limits. The MAE, SDR, and RMSE values for the UNB3m model are again larger at all the stations, which is suggestive of the weakness of the model. The MAE, SDR, and RMSE values for the NWMTE-I, NWMTE-II, and NWMTE-III models are lower than those of GMWT-IV and Bevis models. However, the MAE, SDR, and RMSE values for the GPT2w model of some of the stations outperform the NWMTE-I, NWMTE-II, and NWMTE-III. It evident from the SDR values at all the stations that the actual precision of estimating PWV from the different models does not exceed 1mm as oppose to the theoretical simulation shown earlier in the present paper (Section 6.4.1). Though in the previous simulation, the error limits were placed at maximum limits. The overall results presented in Figures 6.12 (a) - (e) are in very good agreement with discussions on Tables 6.5 and 6.6 of the preceding Sub-Section.

From the foregoing results and the rationales specified, it is concluded that the estimation of mean tropospheric temperature according to the UNB3m and GWMT-IV models is unsuitable for accurate PWV estimation in the region of this study. The performances of the Bevis model and GPT2w are acceptable choices in this region. Even though the GPT2w present itself as an excellent model, the fact remains that as a global blind model, abrupt changes in climatic characteristics cannot be accounted for by it and this singular condition reduces its suitability relative to linear models with direct dependence on measured atmospheric parameters at the GNSS sites. Also, the Bevis model is simple to use just like the NWMTE-I, NWMTE-II, and NWMTE-III models; these latter models come with additional advantages that are inherent in locally modified models, because they are better tailored to the geographical and climatic characteristics of the region and are consequently likely to produce better or more accurate estimate of PWV.

6.5 Concluding Remarks

This study addressed a fundamental issue in GNSS meteorology in the West African region, where little or no work has been previously carried out in modelling T_m. In this study, three models of T_m were developed based on data sets derived from the NCEP/NCAR reanalysis, radiosondes, and a combination thereof. The results of this study justify the need to model T_m accurately and demonstrate the importance of fine-tuning T_m to specific areas or regions of

the world. The precision of the new T_m models developed in the present study thus demonstrate their capacity to estimate PWV with a sufficient accuracy. Finally, the NWMTE-III $(T_m = 0.5245T_s + 132.12)$ is recommended for Nigerian users and NWMTE-II $(T_m = 0.5743T_s + 116.60)$ for users in the West African region.

Acknowledgement

This study was supported and funded by the Tertiary Education Trust Fund (TETFund) of Nigeria, Surveyor Registration council of Nigeria (SURCON), and University of Pretoria PhD Research Support grant to the first author. The authors would wish to express their profound gratitude to the numerous reviewers for their productive observations that helped to perk up the manuscript. The authors thank NCEP and IGRA for making meteorological data used in this study publicly available. We wish to thank the office of the Surveyor General of the Federal republic of Nigeria (OSGOF), University of New Brunswick and Vienna University of Technology for the GNSS data, the UNB3m and GPT2w models respectively. Finally, thanks also go to Changyong He for providing MATLAB script of the GWMT-IV model.

Chapter 7

Retrieval and Analysis of Precipitable Water Vapour based on GNSS, AIRS, and Reanalysis model over Nigeria **

"I seem to have been only like a boy playing on the seashore, and diverting myself in now and then finding a smoother pebble or a prettier shell than ordinary, whilst the great ocean of truth lay all undiscovered before me."
— Isaac Newton (1642-1727)

Précis

Precipitable water vapour (PWV) retrieved from ground-based global navigation satellite system (GNSS) stations over Nigeria from 2013 to 2014 is compared with PWV from a satellite remote sensing technique (Atmospheric Infrared Sounder (AIRS)), and a global reanalysis model (ERA-Interim) over Nigeria. The PWV for AIRS and ERA-Interim was obtained from the respective data providers. PWV estimates from the different techniques were grouped into daily estimates and were matched and re-grouped into monthly and seasonal averages. The performance of the PWV techniques was evaluated using recommended indices by the world meteorological organisation. All datasets gave a reasonable estimate of PWV when compared against GNSS at daily, monthly and seasonal scales, the agreement between the various techniques was better at monthly and seasonal scales. In terms of bias, precision, accuracy, fitness and reliability of measurement, ERA-Interim outperformed the other technique and could possibly be a complementary data source to GNSS PWV, though as a reanalysis it cannot be used for meteorology. The AIRS night time (or descending) retrieval was ranked next to the ERA-Interim; AIRS day-time (or ascending) retrieval agreed less with GNSS PWV, even when compared with ERA Interim and night time AIRS. These results indicate that GNSS PWV as observed over the study area represents a remarkable dataset for further evaluation studies and serves as a useful source of humidity information to improve the water cycle in numerical weather models for varying applications in the region.

*****This chapter consists of formatted text for one peer reviewed journal paper as follows:***

Isioye, O. A., Combrinck, L. & Botai O. J., 2017. Retrieval and Analysis of Precipitable Water Vapour based on GNSS, AIRS, and Reanalysis model over Nigeria, *International Journal of Remote Sensing* (***Revised***).

7.1 Introduction and background

The earth's atmosphere is critical to the environment and to life on earth. Studying the atmosphere plays an important role in many scientific areas, in particular meteorology. However, observing the atmosphere is a challenging task because of its variable nature and the complexity of its processes. Water vapour is one of the most variable constituents of the atmosphere and it plays an important role in the earth's weather and climate processes. It is the most abundant trace gas and represents up to 4% of the total volume of the atmosphere, mostly located closest to the surface in the troposphere (Melsheimer and Heygster, 2008). Because of its dipole molecular structure, water vapour effectively absorbs long-wave radiation emitted from the ground, whereas it transmits large amounts of incoming short-wave solar radiation and thus contributes to the greenhouse effect. It is actually the strongest greenhouse gas and also affects the climate through its capacity to transport large amounts of latent heat. Because of its radiative properties, water vapour contributes to a larger part of the atmosphere's radiation budget, and through precipitation and cloud and ice formation it affects most of the weather on earth (Melsheimer and Heygster, 2008; Soden and Held, 2006).

In view of the seasonal variability of water vapour and it significant role in analysing the global climate system, there is a need for more comprehensive data gathering and detailed knowledge of the global distribution of atmospheric water vapour in space and time to understand climate and weather patterns fully. Water vapour profiles have long been continuously measured by radiosondes at sparsely distributed stations around the world. The situation regarding available radiosondes is worse in Africa. The use of radiosondes is restricted by their low temporal resolution, high operational costs, decreasing sensor performance in cold, dry conditions and their poor coverage over oceans. Nevertheless, radiosondes play a vital role in operational meteorology, as many numerical weather prediction (NWP) schemes are largely trained on radiosonde ascent data, and they have for some time been one of the only sources of highly accurate upper air measurement. However, with the advent of modern remote satellites there are more options for upper air measurement. Because of the ability to achieve global measurement coverage, satellite remote sensing techniques have been very popular and many techniques have been developed during the last three decades, all with different advantages and drawbacks (Palm et al., 2010).

The ideal measurement of water vapour is in the form of a function of height (water vapour profiles). This is possible with in situ techniques such as radiosondes, but for remote sensing techniques it is a very demanding task. Such methods often instead result in an estimation of the vertically integrated column of water vapour from the ground to the top of the atmosphere, called precipitable water vapour (PWV). A PWV value lacks profile information but is a good measurement of the total water vapour content in the atmosphere. A relatively new method, using ground-based observations from the Global Navigation Satellite System (GNSS), can provide PWV estimates with high accuracy of about 1-2 mm under best scenarios (see, Bevis et al., 1994; Duan et al., 1996). The GNSS technique of sensing PWV was first put forward by Bevis et al. (1992, 1994) and Rocken et al. (1993, 1997) and offers the capability of handling large numbers of measurements, temporally and spatially, in all weather conditions. Moreover, the instrumentation does not require continual calibration as some sensors do for measurement drifts or biases, and runs automatically once installed. The accuracy and precision of GNSS-derived PWV has been widely reported (Hordyniec et al., 2015).

GNSS-derived PWV has been validated against independent data from radiosondes (Li et al., 2003; Wang and Zhang, 2008; Kwon et al., 2007*)*, NWP models (Bock et al., 2007a; Bock and Nuret, 2009; Qin et al., 2012; Kwon et al., 2010), very long baseline interferometry (Jin et al., 2009; Ning et al., 2012), water vapour radiometers (see, Ning et al., 2012), satellite retrieval (Raja et al., 2008; Bonafoni et al., 2013; Ning et al., 2015), sun photometers (Prasad et al., 2009; Pugnaghi et al., 2002; Pérez-Ramírez et al., 2014), the Fourier Transform infrared spectrometer (Mengistu Tsidu et al., 2015*),* microwave radiometers (Pacione et al., 2001; Bonafoni et al., 2013) and regional climate models (Vedel and Huang, 2004; Ning et al., 2013; Bollmeyer et al., 2015; Egova, 2015). These studies have all reported the good quality of GNSS-derived PWV estimates. Following these promising results, several meteorological studies using PWV derived from GNSS measurements have been conducted and have shown encouraging results in various fields of meteorology (Liang et al., 2015).

More recently, continuously operating ground-based GNSS networks have proven to be able to offer new information on PWV for the near real time application of weather forecasting and for different types of studies in climate research (Jerrett and Nash, 2001). In the latter case the time series of the water vapour content can be used for both climate monitoring and the evaluation of climate models (Nilsson and Elgered, 2008; Wang and

Zhang, 2009; Stoew and Elgered, 2004; Gradinarsky et al., 2002; see references in those publications). GNSS atmospheric products have also been assimilated into numerical mesoscale models (Falvey et al., 2002; Nakamura et al., 2004; Koizumi and Sato, 2004) and have shown good results in simulating different weather events (Shoji et al., 2002; Koizumi et al., 2005).

From the foregoing, it can be observed that most efforts to exploit the GNSS atmospheric sensing technique are well articulated in other parts of the world aside from Africa. In Africa GNSS networks are very sparse. In South Africa (Combrink et al., 2004), Ethiopia (Mengistu Tsidu et al., 2015), Morocco (Koulali et al., 2011), and Algeria (Boutiouta and Lahcene, 2013) efforts have been made to contribute to the understanding of water vapour accuracy from GNSS on the continent. Among others, the African Monsoon Multidisciplinary Analysis (AMMA) GPS project (1999-2007), which was a meteorological project aimed at West Africa using GPS as a supporting observing technique, initiated investigation of PWV in the West African region (Bock et al., 2007a & b). However, the AMMA GPS project did not collect any data from Nigeria in the investigation in the region. More recently, Nigeria established a network of GNSS stations to support positioning and navigation applications in the country and also as a contribution to the Africa Reference Frame (AFREF) programme. The use of these GNSS stations for GNSS meteorological applications is of substantial interest.

This paper reports an evaluation study comparing PWV measurements from GNSS to a satellite remote sensing technique (Atmospheric Infrared Sounder (AIRS)) and a global reanalysis model (ERA-Interim) over the precinct of Nigeria. This study takes advantage of currently operating permanent GNSS in Nigeria that are operated by the Office of the Surveyor General of Nigeria (OSGOF), and that have been established for positioning and navigation applications under the AFREF programme (Jatau et al., 2010), along with automatic weather stations that serve the Nigerian Meteorological Agency (NIMET). This adds significant extra value to existing (and future) infrastructure. This effort will also represent a first step towards a next generation observing system that could significantly improve numerical weather and storm prediction, as well as address climate study applications in Nigeria. The study presents the first analysis of PWV estimates in Nigeria from a ground-based GNSS network. Thus, the inter-comparison and analyses of GNSS PWV estimates as presented in this paper provide pioneering knowledge about the accuracy

of reanalysis and climate models over Nigeria, since they have not yet been assimilated and can also be viewed as independent data suitable for the valuation of these models.

The structure of the paper is as follows: first a description of all the measurement techniques and their corresponding datasets is presented in section 7.2. Section 7.3 explains the methods used in the comparisons. Section 7.4 describes the results and section 7.5 sums up the conclusion of the work.

7.2.0 Overview of Data Sets and PWV Retrieval Procedures

7.2.1 GNSS Observations

Currently, OSGOF operates and manages a network of 14 continuously operating GNSS reference stations (often referred to as the new Nigerian GNSS network (NIGNET)) in Nigeria (Jatau et al., 2010; Naibbi and Ibrahim, 2014). These stations are primarily for surveying and positioning applications in Nigeria and are the backbone of the proposed Nigerian geocentric data (Dodo et al., 2011; Nwilo et al., 2013). The NIGNET provides ample opportunities for Nigerian climate change modelling through the concept of GNSS meteorology and we therefore seek to demonstrate its potential in this study.

Radio signals from GNSS satellites suffer delay as they propagate through the atmosphere and this delay is largely driven by the water vapour content in the atmosphere. The zenith tropospheric (or total) delay (ZTD) is a widely accepted approach to expressing the total delay in the signal from all satellites and is a measure of the integrated tropospheric condition over a GNSS receiver station. In ZTD retrieval from GNSS observations, we used GAMIT/GLOBK software. GAMIT/GLOBK is a GNSS data analysis package developed at Massachusetts Institute of Technology and Scripps Institution of Oceanography. GAMIT is a modularized, open-source GNSS processing package, programmed mainly in FORTRAN language (Herring et al., 2006). It uses the GNSS broadcast carrier phase and pseudo-range observables to estimate three-dimensional relative positions of ground stations and satellite orbits, atmospheric zenith delays and earth orientation parameters. The software is designed to run under any UNIX operating system. GAMIT incorporates difference-operator algorithms that map the carrier beat phases into singly and doubly differenced phases. These algorithms extract the maximum relative positioning information from the phase data regardless of the number of data outages, and take into account the correlations that are introduced in the differencing process. In the presence of cycle slips, initial processing of phase data is often performed using triple difference or Doppler observations in order to

obtain a preliminary estimate of station or orbital parameters. GAMIT software uses triple differences in editing but not parameter estimation. Rather, it allows estimation of extra free bias parameters whenever an automatic editor flags an epoch as a possible cycle slip. It incorporates a weighted least-squares algorithm to estimate the relative positions of a set of stations, orbital and earth-rotation parameters, zenith delays and phase ambiguities by fitting the parameters to doubly differenced phase observations, since the functional (mathematical) model relating the observations and parameters is non-linear. The main advantage of the software is that it can be effectively used for real time analysis of the estimates of the parameters. The processing strategies and setting of the parameter have to be improved to obtain a more accurate estimation.

Thus, for processing we adopted a double difference ionospheric free (IF) combination at a 30 s sampling rate, with GNSS data down to an elevation cut-off of 10 degrees. For satellite orbits/earth rotation parameters, we used International GNSS service (IGS) final orbits (SP3) and IGS final earth rotation parameter products. The a priori tropospheric model employed is the Saastamoinen model (1972) + random-walk process based on meteorological sources from the global pressure temperature (GPT) model. The Vienna Mapping Function (Boehm et al., 2006) was used to calculate the zenith delay. Station displacement was accounted for using solid earth tide based on IERS03, and ocean tide loading correction based on FES2004. Station coordinates were heavily constrained to their ITRF 2008 values (Altamimi et al., 2011) and relative tropospheric constraints were set at 0.2 m, as it is recommended to set these loosely enough to encompass any error in wet delay (Herring et al., 2006). Satellite antenna phase centre offset and phase centre variation are based on AZEL for IGS absolute ANTEX files (Gendt and Schmid, 2005). The ZTD at each GNSS station was estimated two-hourly and daily within a 24-hour window session. Details of the strategy adopted for processing the GNSS data from the NIGNET stations have already been reported (Isioye et al., 2015, 2016a; Isioye, 2016).

In retrieving PWV estimates from GNSS-derived ZTDs, surface pressure and temperature are required. Ideally, each GNSS site is supposed to be collocated with a meteorological measuring unit. Unfortunately, the NIGNET GNSS sites are not equipped with these devices. However, several approaches to obtaining meteorological data (specifically, pressure and temperature) for GNSS meteorological applications in the absence of a collocated meteorological unit at GNSS sites have been put forward and applied (Bosy et al., 2010, 2012); Bai and Feng, 2003; Kwon et al., 2010; Musa et al., 2011; Hadas et al.,

2013;Fernandes et al., 2013; Sharifi et al., 2015; see references in those publications). In this study we adapted the approach described by Bai and Feng (2003) and Musa et al. (2011). Thus, surface temperature and pressure data from nearby weather stations were transferred to the GNSS sites as follows:

$$\left.\begin{aligned} T_{GNSS} &= T_{MSL} - 0.0065 \times H_{GNSS} \\ P_{GNSS} &= P_{MSL}\left(1 - 0.0000226 \times H_{GNSS}\right)^{5.225} \end{aligned}\right\} \qquad (7.1)$$

In Equation (7.1), T_{GNSS} and P_{GNSS} are reduced temperature and pressure at the GNSS site, T_{MSL} and $P_{MSL}\theta$ are the corresponding mean sea level values of temperature and pressure at the automatic weather observing station (AWOS) , respectively. Equation (7.1) takes into account the sensitivity of the variability of pressure and temperature at the GNSS antenna height $\left(H_{GNSS}\right)$. Figure 7.1 shows the location of some automatic weather stations and NIGNET GNSS sites in Nigeria. Table 7.1 contains information on the height of the respective GNSS and weather stations, and also the distances between them.

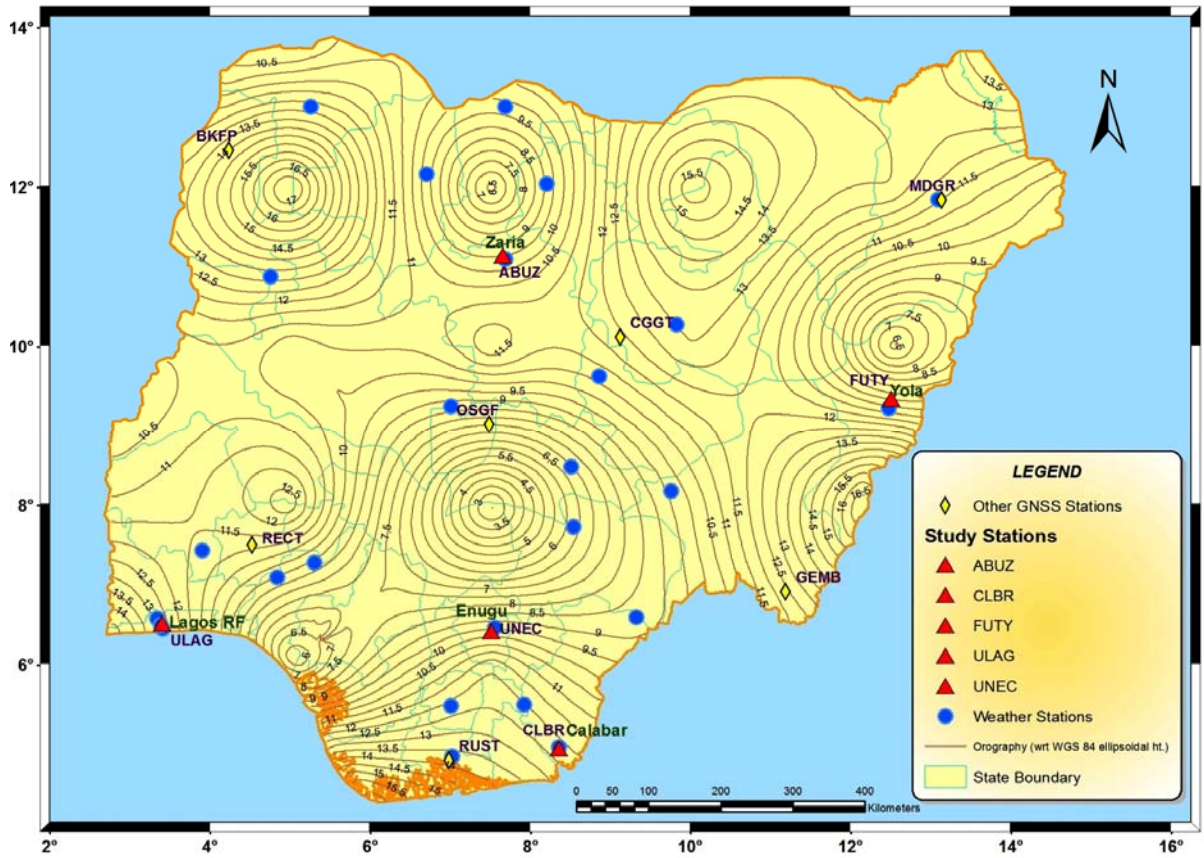

Figure 7. 1: Location of GNSS stations under the NIIGNET and weather stations in Nigeria; the GNSS stations highlighted with red triangular symbol were adopted for the current study based on their proximity to the weather stations

Table 7.1: GNSS stations in the NIGNET and corresponding nearest weather station

GNSS Station	GNSS Station Coordinate		AWOS Station	AWOS Station Coordinate		Station Height (m)		Geoidal Height at GNSS Stations (m)	Horizontal Distance (m)
	Lat (Deg)	*Long (Deg)*		*Lat (Deg)*	*Long (Deg)*	GNSS	AWOS		
abuz	11.15	7.65	Zaria	11.10	7.68	705.05	655.00	22.49	6855.03
clbr	4.95	8.35	Calabar	4.97	8.35	916.43	64.00	20.06	1822.22
futy	9.35	12.50	Yola	9.23	12.47	247.39	190.50	16.39	14391.76
ulag	6.52	3.40	Lagos RF	6.45	3.40	44.56	19.50	22.68	7447.34
unec	6.42	7.51	Enugu	6.47	7.55	254.39	137.00	22.16	6800.76

The ZTD comprises two major components, namely the zenith hydrostatic delay (ZHD) and zenith wet delay (ZWD). In GNSS meteorology it is useful to reduce the ZTD into its constituent parts. ZHD is responsible for the vast majority of the ZTD delay (typically around 90%) and is easily modelled if surface pressure and temperature are known, using empirical models. It is the ZWD that is of interest to meteorology, as it is this component that is related to humidity and can change rapidly, both spatially and temporally. Thus, according to Bevis et al. (1992, 1994), PWV is related to ZWD as follows:

$$PWV = \frac{10^6}{R_w \rho_w \left(k_2' + k_3/T_m\right)} \cdot \left(ZTD - ZHD\right) \quad . \tag{7.2}$$

The ZHD in Equation (7.2) for a given GNSS station can be calculated from the Saastamoinen formula, which is given as follows:

$$ZHD = 0.002277 \cdot \frac{P}{1 - 0.00266\cos\left(2\phi\right) - 0.28 \cdot 10^{-6} h} \quad , \tag{7.3}$$

where the surface pressure in hPa is indicated by P, the latitude ϕ is in radians and the height of the surface above the ellipsoid (in metres) is represented by h. Inserting Equation (7.3) into (7.2), we have:

$$\begin{aligned} PWV &= \frac{10^6}{R_w \rho_w \left(k_2' + k_3/T_m\right)} \cdot \left(ZTD - \frac{0.002277 P}{1 - 0.00266\cos\left(2\phi\right) - 0.28 \cdot 10^{-6} h} \right) \\ &= \frac{10^6}{R_w \rho_w \left(k_2' + k_3/T_m\right)} \cdot ZWD \quad . \end{aligned} \tag{7.4}$$

In Equation (7.4), PWV is the precipitable water vapour, ρ_w is the water density, $R_w = 461.525 \pm 0.003 \left[Jkg^{-1}K^{-1} \right]$ is the specific gas constant for water vapour, $k_2' = 22.1 \pm 2.2 Kmb^{-1}$ and $k_3 = 373900 \pm 0.012 K^2 mb^{-1}$ are refraction constants, and T_m is the weighted mean tropospheric temperature measured in Kelvin. We adopted the formula of Isioye et al. (2016a), which suggests the estimation of T_m from surface temperature T_s because of the strong correlation between the duo variables. Thus, according to Isioye et al., (2016a), T_m is represented as shown in Equation (7.5), and T_s in Kelvin is obtained from meteorological stations close to individual GNSS sites.

$$T_m = 0.5245 T_s + 132.12 \qquad (7.5)$$

Substituting the values of the constant into Equation (7.4), we derived a simplified expression for PWV as follows:

$$PWV = ZWD \cdot \left[\frac{132.12 + 0.5245 T_s}{1739.07624 + 0.053499 T_s} \right] . \qquad (7.6)$$

In Equation (7.6), ZWD is given in mm. If the polynomials (numerator and denominator) of Equation (7.6) are divided, we obtain a more simplified expression, as shown in Equation (7.7);

$$PWV = ZWD. \left[9.80392 - \frac{16917.64}{0.053499 T_s + 1739.07624} \right] . \qquad (7.7)$$

Equation (7.7) was used in this work and gives PWV in (mm) as well. The equation is suitable for users in Nigeria.

7.2.2 Atmospheric Infrared Sounder

The AIRS is a facility instrument on board the polar-orbiting earth-observing system Aqua satellite. It is the first in a new generation of high spectral resolution infrared sounder instruments flown aboard the Aqua research mission since its successful launch on May 4, 2002. AIRS and two microwave sounding radiometers (Advanced Microwave Sounding Unit-A (AMSU-A) and Humidity Sounder of Brazil (HSB)), are the three sensors on board Aqua. AIRS and HSB are capable of providing estimates of water vapour in the atmosphere, but the HSB instrument has malfunctioned since February 2003 (Parkinson, 2003; Divakarla et al., 2006).

The AIRS instrument is a high-resolution spectrometer with 2 378 bands in the thermal infrared region (3.74-15.4 μm) and four bands in the visible spectral region (0.4-1.0 μm). These ranges have been specifically selected to determine atmospheric temperature with an accuracy of 1 K per 1 km thick layer in the troposphere moisture profiles at an accuracy of 20% per 2 km thick layer in the lower troposphere (20% - 60% in the upper troposphere). Details of the AIRS instrumentation, inversion algorithm (i.e., calibration, microwave retrieval, cloud clearing, initial infrared retrieval, physical retrieval, bias correction and radiative transfer calculations) and accuracy standards can be found in Susskind et al. (2003), Divakarla et al. (2006) and Qin et al. (2012).

In this study we have used the Aqua AIRS (AIRS-only) level-3 daily standard physical retrieval product (AIRS3STD Version 006) available from Goddard Earth Sciences Data and Information Services Centre (http://acdisc.gesdisc.eosdis.nasa.gov/opendap/Aqua_AIRS_Level3/AIRX3STD.006/). The daily water vapour parameters are arranged in gridded files of 1 x 1 deg.

The AIRS team estimates the total column water vapour (TotH2OVap) from Level 3 standard specific humidity profiles. Specific humidity is expressed as level quantities (H2O_MMR) and as layer quantities (H2O_MMR_Lyr) (AIRS Science Team/Texeira, 2003). Both are given in units of g/kg of dry air. Using the TqJoint (ascending or descending) quantity, H2O_MMR_Lyr, which provides the average specific humidity in a layer bounded by two standard pressure levels, is more easily convertible to millimetres of PWV. Accordingly, each daily file includes the descending total column water vapour (TotH2OVap_D) (night-time @ 1.30 AM LT) and ascending (TotH2OVap_A) (daytime @1.30PM LT) orbits. TotH2OVap unit is in kg/m^2 and is equivalent to millimetres of precipitable water, since the density of water is $1gm/cm^3$. We used the TotH2OVap_D and TotH2OVap_A AIRS estimates for this study. For comparison of PWV estimates from AIRS, we interpolated the values by simply transferring the nearest grid node values to the particular GNSS site. The AIRS-derived PWV values were subsequently adjusted to the GNSS station height. Table 7.2 shows the coordinate of the GNSS stations in NGNET and corresponding nearest grid node of the AIRS model (note the AIRS were downloaded at 0.5 x 0.5 deg grid interval). The AIRS model topography was taken at 1000 mb (Equivalent 111m) and was assumed to be uniform.

Table 7.2: GNSS Stations in the NIGNET and corresponding grid node from AIRS model

GNSS Station	GNSS Station Coordinate		AIRS Grid coordinate		Station /Grid Height (m)		Horizontal Distance (m)
	Lat (Deg)	*Long (Deg)*	*Lat (Deg)*	*Long (Deg)*	GNSS	AIRS	
abuz	11.15	7.65	**11**	**7.5**	705.05	111	23356.82
clbr	4.95	8.35	**5**	**8.5**	916.43	111	17351.39
futy	9.35	12.50	**9.5**	**12.5**	247.39	111	16625.55
ulag	6.52	3.40	**6.5**	**3.5**	44.56	111	11486.58
unec	6.42	7.51	**6.5**	**7.5**	254.39	111	8334.62

7.2.3 ERA-Interim Reanalysis

Global atmospheric reanalysis products have played an important role in current climate assessments, diagnostic studies of climate features, seasonal prediction, and climate predictability. ERA-Interim Reanalysis (ERAI) is a global atmospheric reanalysis produced by the ECMWF. ERAI was originally planned as an 'interim' reanalysis in preparation for the next-generation extended reanalysis to replace ERA-40. It uses a newer version of the ECMWF Integrated Forecast Model (IFS Cy31r2), as opposed to ERA-40, which is based on IFS cycle 23r4. It originally covered dates from 1989 but an additional decade, from 1979, was added later. ERA-Interim is being continued in real time. ERAI comes with improvements on existing models and analysis techniques such as data selection, quality control, bias correction, performance monitoring and the use of a 12-hourly four-dimensional variational analysis (4D-Var) with adaptive estimation of biases in satellite radiance data (VarBC). See Dee et al. (2011*)* and the references in it for a full description of the ERA-Interim system. Both the ERAI and ERA-40 have been tested in the West African region in the AMMA project. They both show good agreement with GNSS PWV (Bock et al., 2007b and 2011).

For this study, we have used PWV from an ERAI reanalysis dataset available four times daily (at an interval of 6 hrs) for the entire globe at a spatial resolution of 0.5 deg. The long name of the dataset is "Total Column Water Vapour" and it was accessed at http://apps.ecmwf.int/datasets/data/interim-full-daily/. Since the dataset is of high resolution, we use the transferred value of PWV at the nearest horizontal grid point to the particular GNSS station, as recommended by Bock et al. (2005). Thereafter, the ERAI PWV values

were adjusted to the height of the respective GNSS station using the correction formula proposed by Bock et al. (2007a). Thus, we have

$$\delta_{PWV} = \rho_v \Delta h \left(1 - \frac{\rho_v \Delta h}{2PWV}\right) \tag{7.8}$$

In Equation (7.8), δ_{PWV} is the correction term, ρ_v is the water vapour density and Δh is the height difference between the nearest grid point and the respective GNSS station. The coordinates of the GNSS stations and their corresponding grid node from ERA-interim is presented in Table 7.3, The ERA-interim topography was obtained from the time- invariant geopotential number of each grid node and then converted to orthometric height unit by absolute value of gravity. Also, the respective geoid height was obtained from the global geiod model (EGM08) and was used to convert the GNSS ellipsoidal height to orthometric height units. The distance between the grid node from the respective model (AIRS and ERA-interim) and corresponding GNSS sites as contained in Tables 7.2 and 7.3 are within the spatial scale of the GNSS PWV. Characteristically, the GNSS PWV data is of a spatial scale of 20-50km in the troposphere (Bock et al., 2007b).

Table7. 3: GNSS Stations in the NIGNET and corresponding grid node from ERA-Interim model

GNSS Station	GNSS Station Coordinate		ERA-Interim Grid coordinate		Geoidal Height at GNSS Stations (m)	Station /Grid Height (m)		Horizontal Distance (m)
	Lat (Deg)	*Long (Deg)*	*Lat (Deg)*	*Long (Deg)*		GNSS	ERA-Interim	
abuz	11.15	7.65	**11**	**7.5**	22.49	705.05	615.76	23356.82
clbr	4.95	8.35	**5**	**8.5**	20.06	916.43	262.63	17351.39
futy	9.35	12.50	**9.5**	**12.5**	16.39	247.39	403.34	16625.55
ulag	6.52	3.40	**6.5**	**3.5**	22.68	44.56	44.52	11486.58
unec	6.42	7.51	**6.5**	**7.5**	22.16	254.39	143.48	8334.62

7.3.0 Methodology

The PWV estimates from ERAI, and AIRS (AIRS (**A**scending) and AIRS (Descending)) were interpolated to five GNSS stations (ABUZ, CLBR, FUTY, UNEC, and ULAG) in Nigeria, representing the different geo-spatial zones in the country. For broad assessment, the comparison between GNSS PWV and other techniques (AIRS, and ERAI) was accomplished at three temporal scales (i.e. daily, monthly and seasonally). The climate

over Nigeria is characterised by two distinct seasons, namely the wet (rain) and dry (Harmattan) seasons. The months of March, April, and May (MAM) are the hottest in the north, with little rain in the southern part of Nigeria. The peak of the wet season in all parts of Nigeria is in the months of June, July, and August (JJA). The months of September, October, and November (SON) signify the end of the wet season in the north, while in the south, it is a period often characterised by scanty rain and severe thunderstorms. The months of December, January, and February (DJF) are dry in the north with very low temperature because of the Harmattan, while the south is dry and humid. We have classified the PWV estimates into these four seasons (MAM, JJA, SON, and DJF) to study the seasonal dependency of PWV in Nigeria as recorded by the different techniques.

Next, we calculated the bias, precision, accuracy, fitness and reliability of the different PWV estimates from the different techniques (GNSS, AIRS (A), AIRS (D), and ERAI) with more emphasis on the GNSS PWV relations with other models. The bias (Wagner and Wildi, 2002), standard deviation of residuals (SDR) (WMO, 1992), model coefficient of variation (CV) (Cam et al., 2002), normalised root mean square error (NRMSE) (Walter and Moore, 2005), coefficient of determination (R^2), model efficiency (MEF))Murphy, 1998), and reliability index (RI) (Leggett and Williams, 1981) were used as performance indicators. The need to use different model indicators in evaluation of climate-related variables is recommended by the World Meteorological Organisation (WMO), since the different model performance indicators reveal different things about the models (Flato et al., 2013).The bias reflects the degree to which the PWV values are over- or underestimated between two techniques (or models). The SDR is an indicator of precision; it measures the dynamic correspondence between techniques and a near zero value indicating a close match. The RMSE is the square root of the variance of the residuals. It indicates how close the observed data points are to the model's predicted values. Scaling the RMSE by dividing with the time series of the reference model yields the NRMSE (or scaled root mean square error - SRMSE). The NRMSE is a unitless indicator and is expressed in percentage, a lower percentage indicating high accuracy. The CV is a normalised measure of precision for techniques or models with different means or simply the RMSE expressed as a percentage of the mean of the predicting model or technique. The model with the smaller CV has predicted values that are closer to the actual values. For a linear regression model, R^2 is basically the square of the correlation coefficient (or anomaly correlation coefficient (ACC)) (Jolliffe and Stephenson, 2003)) between two variables. It is interesting to note the differences between a

model's CV and R^2 values. Both are unitless measures that are indicative of model fit, but they define model fit in two different ways: CV evaluates the relative closeness of the predictions to the actual values while R^2 evaluates how much of the variability in the actual values is explained by the model. The MEF is an indicator of fitness that measures how one model forecasts the other relative to the average of the observation between both, with values varying between 0 and 1; an MEF value of 1 implies perfect agreement. The RI quantifies the average factor by which two measuring techniques differ from each other. A large RI value is indicative of large divergence between the techniques and thus less reliable. The formula of the performance indicators is illustrated as follows:

$$Bias = \frac{1}{N}\sum_{i=1}^{N}(O_i - P_i)\,, \tag{7.9}$$

$$SDR = \sqrt{\left[\frac{\sum_{i=1}^{N}(O-P)}{N} - \left(\bar{O}+\bar{P}\right)\right]^2}\,, \tag{7.10}$$

$$CV = \frac{1}{\bar{P}}\sqrt{\frac{\sum_{i=1}^{N}(O_i - P_i)^2}{N}}\cdot 100\%\,, \tag{7.11}$$

$$NRMSE = \frac{1}{O_i}\sqrt{\frac{\sum_{i=1}^{N}(O_i - P_i)^2}{N}}\cdot 100\%\,, \tag{7.12}$$

$$R^2 = \left[\frac{\sum_{i=1}^{N}(P_i-\bar{P})(O_i-\bar{O})}{\left[\sum_{i=1}^{N}(P_i-\bar{P})^2\cdot\sum_{i=1}^{N}(O_i-\bar{O})^2\right]^{1/2}}\right]^2\,, \tag{7.13}$$

$$MEF = 1 - \frac{\sum_{i=1}^{N}(Bias_i)^2}{\sum_{i=1}^{N}\left(\left|(P_i-\bar{O})\right| - \left|(O_i-\bar{O})\right|\right)^2}\,, \tag{7.14}$$

$$RI = \exp\sqrt{\frac{1}{N}\sum_{i=1}^{N}\left(\log\frac{O_i}{P_i}\right)^2}\,. \tag{7.15}$$

In Equations (7.9)-(7.15), O_i and P_i are respectively the time series of the reference (i.e., GNSS PWV) and the predicting (i.e., AIRS, and ERAI) models or techniques. The average of the reference and predicted model values is indicated by $\bar{O}$ and $\bar{P}$, respectively, and the number of observations is indicated by N.

7.4.0 Results and Discussions

This section discusses the results of the various evaluations. The emphasis is on the relation between GNSS PWV and other techniques (i.e. AIRS, and ERAI) at diurnal, monthly and seasonal scales.

7.4.1 Diurnal relations of GNSS PWV with other retrievals (AIRS and ERA-Interim)

The daily estimates of PWV from GNSS was matched (i.e. pairing of common days) with the relevant estimates from, AIRS (A), AIRS (D) and the ERAI. The differences and averages in PWV estimates from GNSS and other techniques were plotted against one another with the estimated confidence intervals around the bias and the individual differences as shown in Figure 7.2 at all the stations. The histogram plots of the differences between GNSS PWV estimates and those from the other techniques are shown in Figure 7.3 as well to test if they were normally distributed and formed the basis for computing the confidence interval of the differences. The distribution of the differences at all the stations for the different techniques follows the normal distribution closely but not perfectly. However, the best distribution could be seen between GNSS and ERAI, the distribution between GNSS and AIRS (A), and AIRS (D) spread out more on the left of the normal curve at most stations. This obviously signifies that GNSS PWV estimates are larger and those of other techniques been investigated in this study. From the agreement plots of Figure 7.2, one can again see that the ranges of confidence interval of the differences and biases for AIRS (A) are higher than those of the other techniques. The average daily bias for all the models at all the GNSS stations stood at --3.4 mm, -1.8 mm, and -1.2 mm for AIRS(A), AIRS(D), and ERAI, respectively.

Table 7.4 contains additional statistics on the performance of the different PWV techniques against GNSS. It can be seen from the SDR values that the precision of the daily PWV estimate is low, ranging between 4.3 mm to 7.3 across the stations for the different techniques. The average SDR value across all the different stations is estimated at 6.7 mm, 5.4 mm, and 4.6 mm for the , AIRS (A), AIRS (D), and ERAI, respectively.

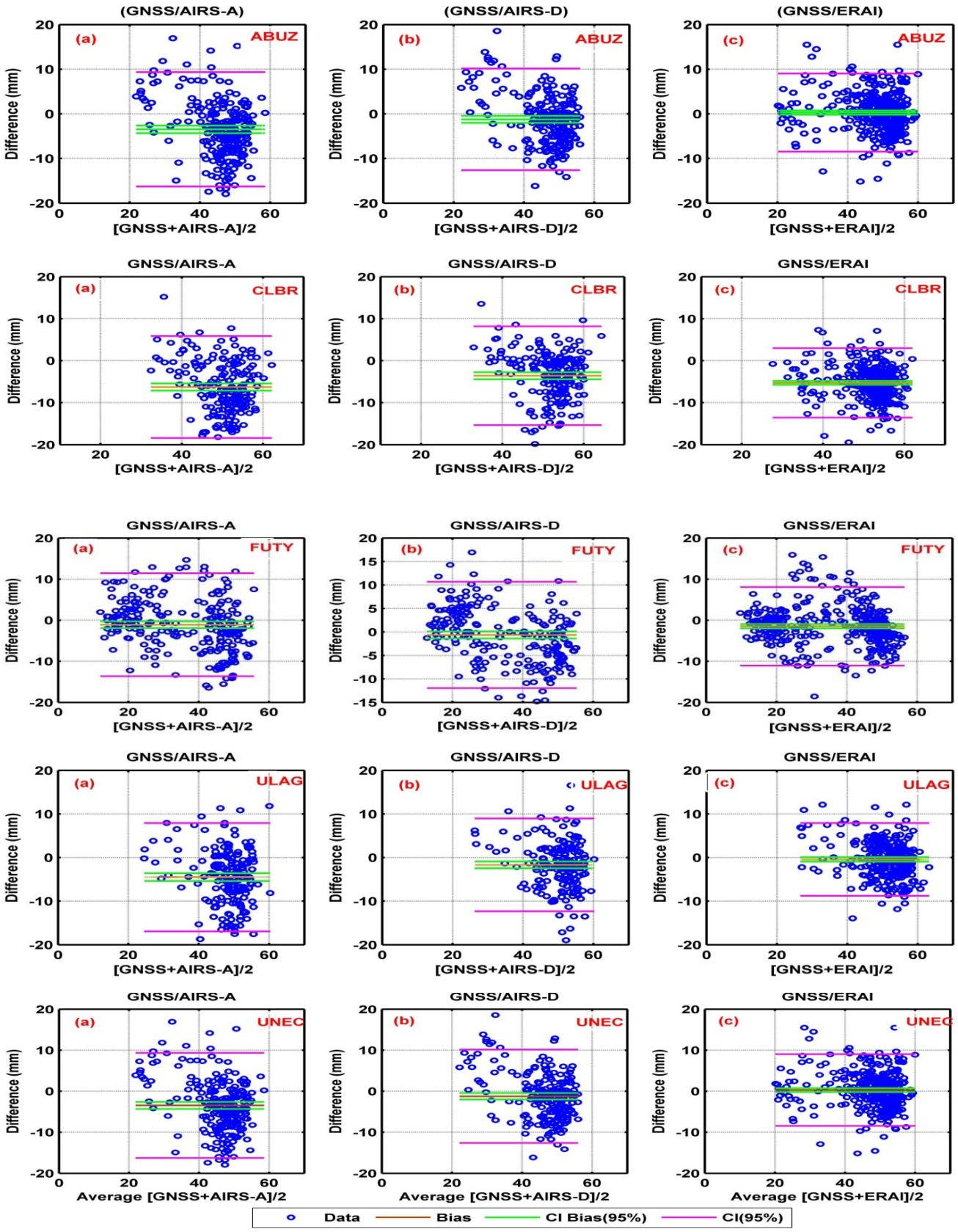

Figure7. 2: Images representing the agreement plots (or Bland and Altman plot) between GNSS PWV and (a) AIRS (Ascending) (b) AIRS (Descending) and (c) ERA (Interim) at the respective stations

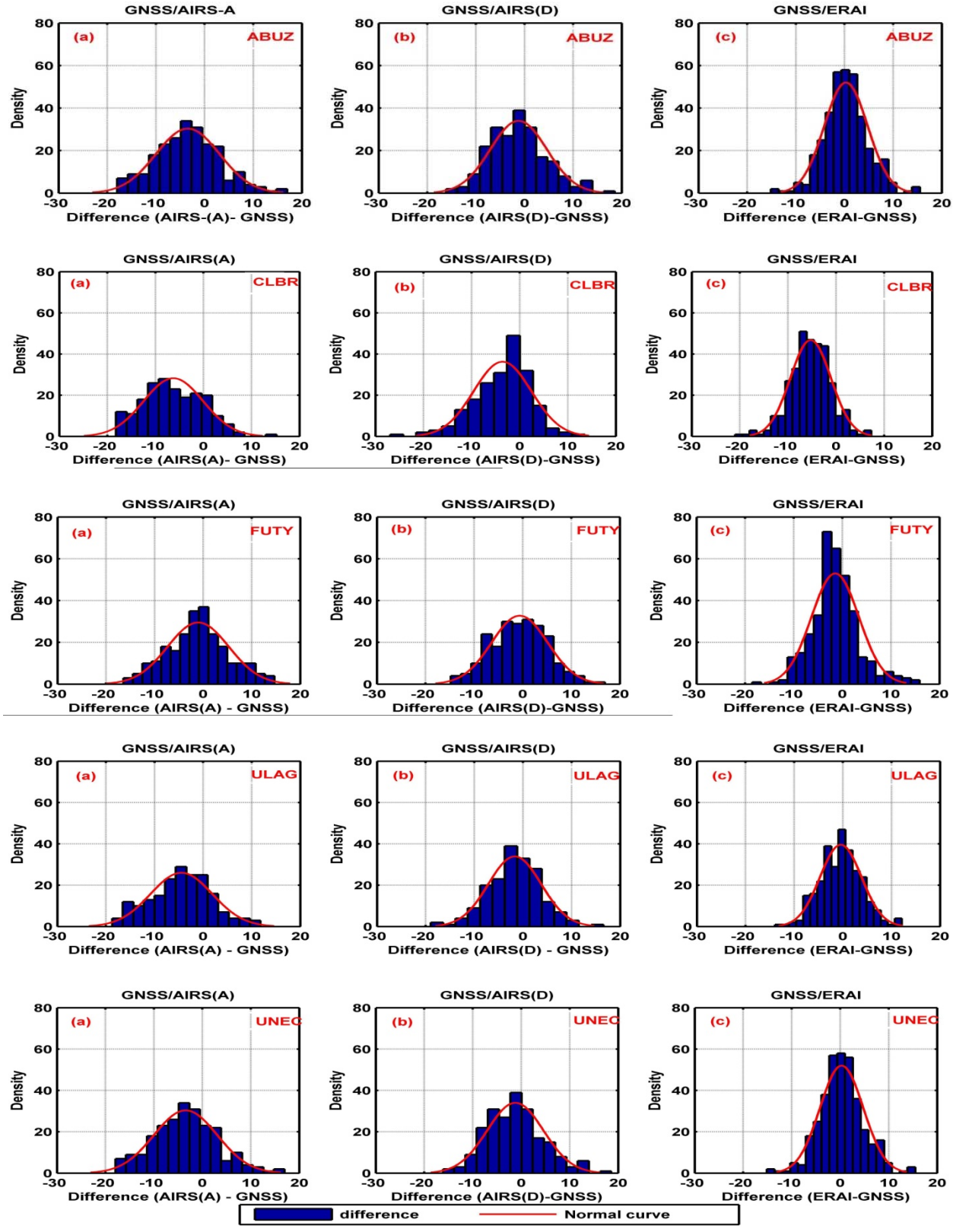

Figure 7. 3: Images representing the histogram of the differences between GNSS PWV and (a) AIRS (Ascending) (b) AIRS (Descending) and (c) ERA (Interim) at the respective stations

In Table 7.4, the NRMSE and CV values are shown to be less than 30% in all cases, which is an indication that the techniques are of good accuracy, since they yield less than 50%; the average values of the NRMSE across all stations stood at, 18.1%, 13.8%, and 11.8% for AIRS (A), AIRS (D), and ERAI. The CV follows the same trend with an average of 19.8%, 14.4%, and 11.8% in the same order. The fitness of the GNSS PWV against the other techniques as measured by R^2 recorded a minimum value of 0.2 and maximum value of 0.9 for AIRS (A) and AIRS (D) at CLBR and ABUZ, respectively. The average R^2 value across all stations was estimated at 0.5, 0.6, and 0.8 for AIRS (A), AIRS (D), and ERAI. The MEF, which also measures the fitness of GNSS with the other techniques, gives a slightly different result from R^2; in this case the fitness of all the models is above 0.5 (50%) with the average values ranging from 0.8 to 0.9 for all the techniques. The results thus far show that the ERAI and AIRS (D) are in better agreement with the GNSS techniques than with AIRS (A).

Table 7. 4: Statistics (diurnal and monthly) of relation between precipitable water from GNSS and other the techniques (AIRS and ERAI) at five GNSS stations over Nigeria from 2013 -2014

	ABUZ	*CLBR*	*FUTY*	*ULAG*	*UNEC*	*ABUZ*	*CLBR*	*FUTY*	*ULAG*	*UNEC*
	GNSS/AIRS-A (Daily)					***GNSS/AIRS-A (Monthly)***				
Bias (mm)	-1.4153	-6.2795	-1.1086	-4.4843	-3.4725	-1.7390	-8.1338	-1.2468	-4.8391	-3.8274
SDR (mm)	5.3835	7.3422	6.5112	7.2033	6.8962	2.5877	3.8877	2.6563	3.2262	3.0967
NRMSE (%)	18.5345	19.8029	18.0622	17.6322	16.6233	10.2273	16.7257	7.9500	12.7747	10.3909
CV (%)	19.5604	23.1170	18.6717	19.6840	18.0695	10.8460	19.6983	8.2344	14.2349	11.3040
R^2	0.8077	0.1619	0.7888	0.2366	0.4208	0.9527	0.3211	0.9776	0.9821	0.8454
MEF	0.9407	0.5524	0.9344	0.6517	0.7609	0.9767	0.5175	0.9847	0.9785	0.8344
	GNSS/AIRS-D (Daily)					***GNSS/AIRS-D (Monthly)***				
Bias (mm)	-1.9131	-3.5848	-0.6444	-1.6876	-1.2339	-2.0279	-4.5023	-0.9430	-1.5377	-1.2331
SDR (mm)	4.2907	5.9762	5.7617	5.4139	5.7921	1.6321	5.1107	2.9874	1.3063	2.7681
NRMSE (%)	15.7075	12.9999	16.5142	11.1899	12.6504	8.5024	12.5954	8.5491	4.4879	6.4073
CV (%)	16.7809	13.9315	16.8229	11.5754	12.9928	9.1055	13.7393	8.7749	4.6388	6.5788
R^2	0.8861	0.3428	0.8488	0.4614	0.5820	0.9832	0.1906	0.9854	0.9965	0.8476
MEF	0.9622	0.7244	0.9508	0.8081	0.8492	0.9687	0.8382	0.9459	0.8976	0.8904
	GNSS/ERAI (Daily)					***GNSS/ERAI (Monthly)***				
Bias (mm)	-0.0493	-5.2927	-1.4794	0.4328	0.2843	0.6352	-3.7053	-0.4692	-0.1518	1.3626
SDR (mm)	5.1302	4.2862	4.9339	4.2535	4.5127	2.5476	1.3323	2.2632	1.2421	1.2170
NRMSE (%)	16.9713	10.3851	13.3570	8.3650	9.9242	8.5980	7.2805	6.2700	2.9430	3.8535
CV (%)	16.4961	11.1290	13.5147	8.3728	9.6981	8.4229	7.8160	6.3508	2.9524	3.7458
R^2	0.8479	0.6307	0.8806	0.6751	0.7535	0.9573	0.9160	0.9707	0.9959	0.9665
MEF	0.9576	0.8322	0.9678	0.8985	0.9244	0.9866	0.8505	0.9918	0.9990	0.9809

Table 7.5 presents additional statistics on the interrelation among PWV estimates from AIRS (A), AIRS (D), and ERAI during 2103 and 2014. The results of the comparisons in Table 7.5 are suggestive of the strong interrelation among the techniques (or models). Comparing the average fitness ($R^2$and MEF) of the daily estimates of the models in Table 7.4 with those in Table 7.5, one can see that the variation in PWV from GNSS vs. ERAI is best accounted for with an average R^2 value of 0.8, when compared to the value of 0.61, 0.56, 0.63 for AIRS(A) vs. ERAI, AIRS(A) vs. AIRS(D) and AIRS(D) vs. ERAI, respectively.

Table 7.5: Daily precipitable water statistics of the interrelation between AIRS(A), AIRS(D) and ERAI models at five GNSS stations over Nigeria from 2013-2014

	ABUZ	*CLBR*	*FUTY*	*ULAG*	*UNEC*
	AIRS-A / AIRS-D(Daily)				
Bias (mm)	0.2068	-3.1416	-1.2344	-2.7749	-1.8686
SDR (mm)	4.5201	5.9079	5.1872	5.7049	4.9321
NRMSE (%)	15.9622	14.2371	16.5684	13.8628	12.0746
CV (%)	16.0795	13.3451	15.9564	13.0702	11.5792
R^2	0.8536	0.2393	0.8204	0.3419	0.5561
MEF	0.9598	0.6610	0.9480	0.7360	0.8448
	AIRS-D / ERAI(Daily)				
Bias (mm)	-1.7802	1.6684	0.9579	-1.5385	-1.6595
SDR (mm)	5.1059	5.6164	5.8571	4.3579	5.5435
NRMSE (%)	19.3149	11.7128	17.2213	9.4334	12.6954
CV (%)	18.1601	12.1169	17.7136	9.1461	12.2494
R^2	0.8395	0.3552	0.8117	0.5600	0.5971
MEF	0.9499	0.7511	0.9441	0.8502	0.8519
	AIRS-A / ERAI (Daily)				
Bias (mm)	-1.5884	-1.1516	0.3343	-4.2053	-3.7499
SDR (mm)	4.6814	6.1528	5.2033	5.3358	5.2711
NRMSE (%)	17.2582	13.3351	14.6911	14.8135	14.8020
CV (%)	16.3515	13.0158	14.8308	13.5693	13.6323
R^2	0.8666	0.2831	0.8487	0.4394	0.5938
MEF	0.9567	0.7240	0.9573	0.7435	0.8198

The MEF values followed the same pattern with the R^2 values for all the techniques, though the MEF reports stronger fitness among techniques than R^2 estimates. On average, the AIRS (A) estimates do not fit properly with GNSS, as both have R^2 value of less than 0.5. The weak correlation between the AIRS (daytime and night-time) retrievals and all the techniques at the coastal regions (ULAG, UNEC and CLBR) is also noticeable. These regions are known to be highly humid and cloudy. The amount of cloud in the atmosphere is also known to vary between day and night, so this may have a negative impact on AIRS retrievals and also be responsible for the variations in the AIRS daytime and night observations. The average SDR, NRMSE and CV of the relation between PWV estimates from the different techniques, as presented in Table 7.5, are (5.3 mm, 15.0%, 14.3%), (5.3

mm, 14.5%, 14.0%), (5.3 mm, 14.1%, 13.8772%) for ERAI vs. AIRS(A), AIRS(A) vs. AIRS(D), AIRS(D) vs. ERAI. These results are quite similar to earlier deductions in Table 7.4, thus the relation between GNSS and ERAI is presented as the most precise and accurate as indicated by the SDR, NRMSE and CV .

The measure of reliability among the PWV estimates from all the different techniques (GNNS, AIRS (A), AIRS (D), and ERAI) as revealed by the RI is shown in Figure 4. The average RI values for all the stations range from 1.15 to 1.21 for the different techniques. These values are indicative of the fact that the different techniques can forecast PWV within a tolerable average (or replicable) factor.

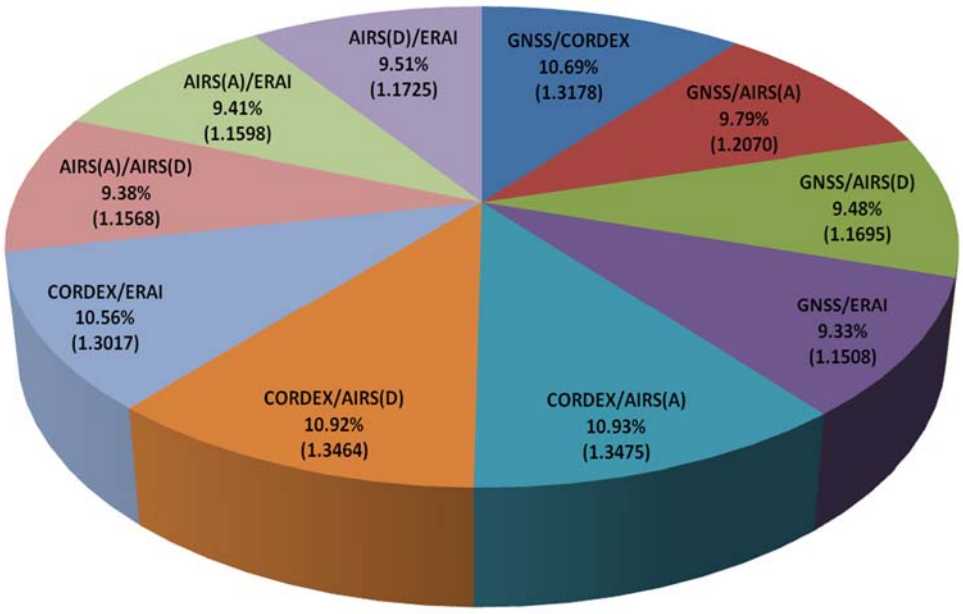

Figure 7.4: Chart depicting the reliability of the different PWV measuring techniques as determined by the RI. The average RI value for each pair of techniques across all five stations is shown, together with the percentage of divergence of each pair; lower percentages are indicative of better agreement between pairs

. 7.4.2 Monthly relations of GNSS PWV with other retrievals (AIRS and ERA-Interim)

The daily PWV estimates were aggregated into monthly PWV for the GNSS and the other techniques. The monthly PWV figures retrieved from satellite (AIRS), reanalysis model (ERAI) and GNSS were compared at five GNSS stations over Nigeria. Table 7.4 and Figure 7.5 show the monthly average statistics of the performance indicators, and plots for PWV from GNSS and other techniques. From Table 7.4 one can see that bias, SDR, NRMSE, and

CV show improvements on a monthly scale over the daily estimates for all the different techniques.

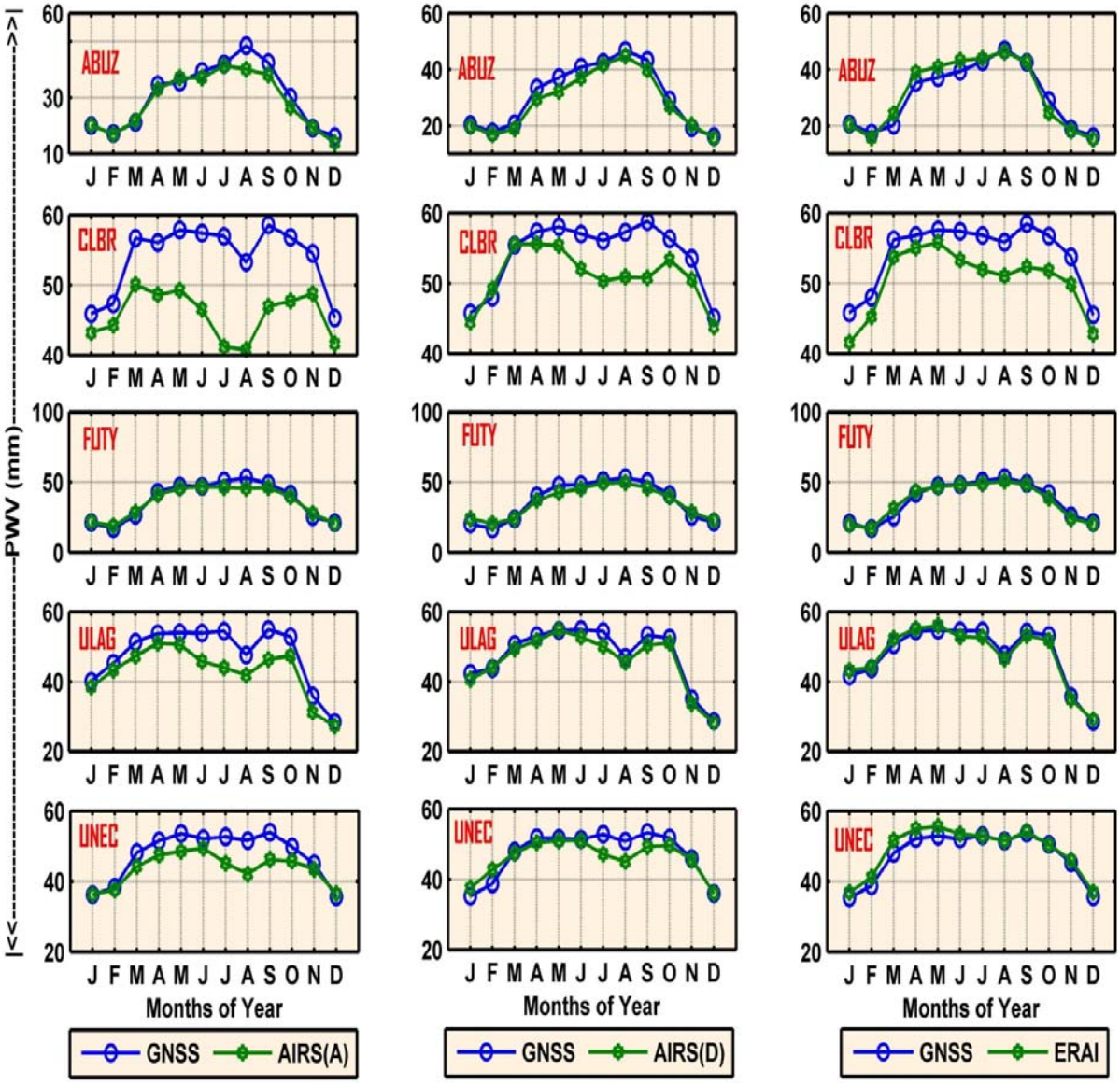

Figure 7.5: Plots of the monthly averages of PWV estimates at five GNSS station over Nigeria in 2013 and 2014. The GNSS and AIRS-Ascending, GNSS and AIRS-Descending, GNSS and ERAI relations at the respective stations are accordingly arranged in columns 1-3

The average monthly bias is negative for all the techniques, with a value of -4.0 for daytime AIRS, -2.0 for night-time AIRS observation and -0.5 for the reanalysis model, respectively. This result follows closely the trend in bias between daily GNSS PWV and the other techniques and we have already reported a larger estimation in the PWV quantity by

GNSS; a similar observation was reported by Mengistu Tsidu et al. (2015) for the Ethiopian territory. Good agreements with GNSS PWV were observed for all the techniques at the GNSS stations, with average R^2 of 0.82 for AIRS (A), 0.80for AIRS (D), and 0.96 for ERAI, respectively. The MEF follows in the same pattern and as previously, signifies stronger fitness among the different PWV estimates on a monthly scale.

The precision and accuracy measures for the different PWV estimates against GNSS showed very promising results with SDR, NRMSE, and CV of 3.1 mm, 11.6%, 12.9% for AIRS(A), 2.8 mm, 8.1%, 8.6% for AIRS(D), 1.7 mm, 5.8%, 5.9% for ERAI, respectively. The better precision and accuracy on a monthly scale than on a daily scale is attributable to the fact that the errors on the daily scale were nearly normally distributed (see Figure 7.3) and thus may perhaps negate each other after the summation. In terms of all the model performance indicators (Table 7.4), the GNSS/ERAI relation was adjudged the best on a monthly scale.

Figure 7.6 show statistics (bias (mm)) for the seasonal PWV variation of the model estimates with respect to GNSS measurement for 2013-2014 at all the GNSS stations. In Figure 7.6, the GNSS/AIRS (A) (sub-plots (a)-(d)), and GNSS/AIRS (D) (sub-plots (e)-(h)) relations exhibited large biases in the months of JJA; the months of DJF and MAM had the least bias for AIRS (A) and (D). The unsatisfactorily high biases in JJA and SON are possibly attributed to the performance of the cloud-clearing algorithm for the AIRS retrievals during these months, since the cloud amount is often high in JJA and SON because of rain. The GNSS/ERAI relation as shown in sub-plots (i)-(l) had the least bias for all the seasons at the different stations. The bias in the months of DJF again appears to show better relation between the GNSS and ERAI.

Figure 7.7 illustrates the NRMSE (%) for the seasonal PWV variation for the model-derived estimates with respect to GNSS measurement during 2013 and 2014 at ABUZ, CLBR, FUTY, ULAG and UNEC GNSS stations. The NRMSE is less than 50% for all stations and signifies the good accuracy of the different PWV observation techniques. Again, seasonal variations are seen in the accuracy of the different techniques as indicates by the NRMSE.

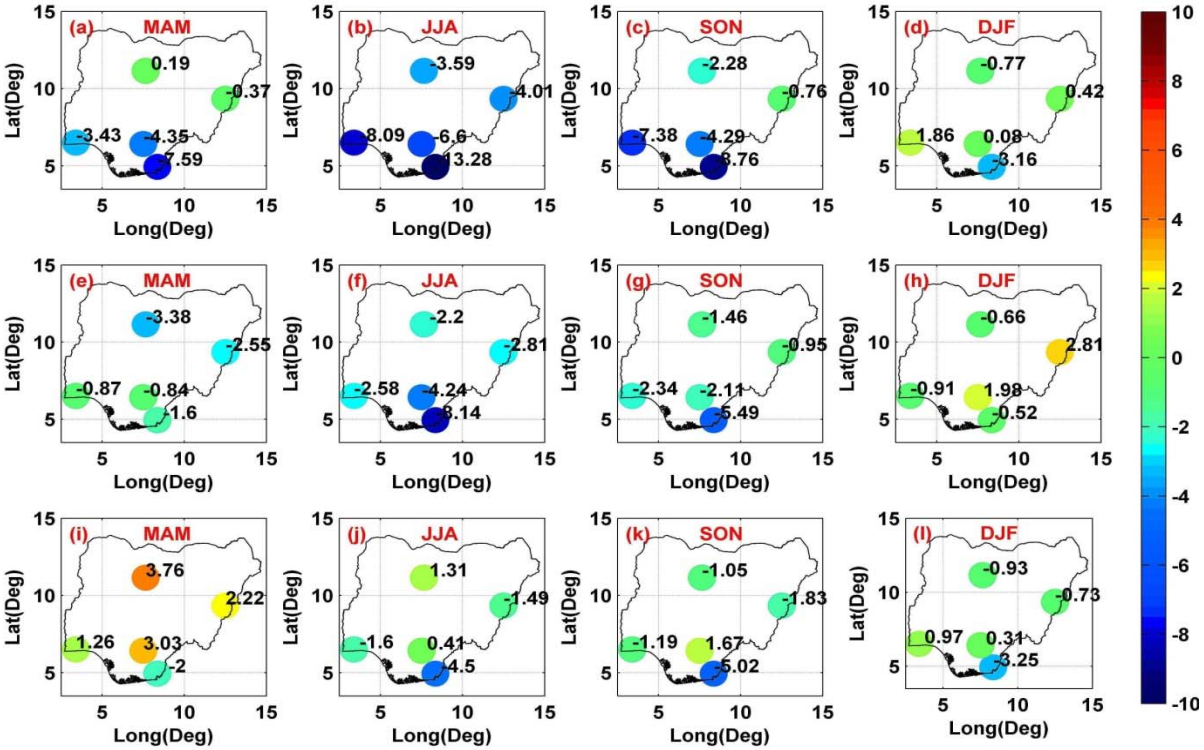

Figure 7.6: Plots of statistical bias (mm) across the seasonal for the relation between GNSS and AIRS-Ascending (a-d), GNSS and AIRS-Descending (e-h) and GNSS and ERAI (i-l)

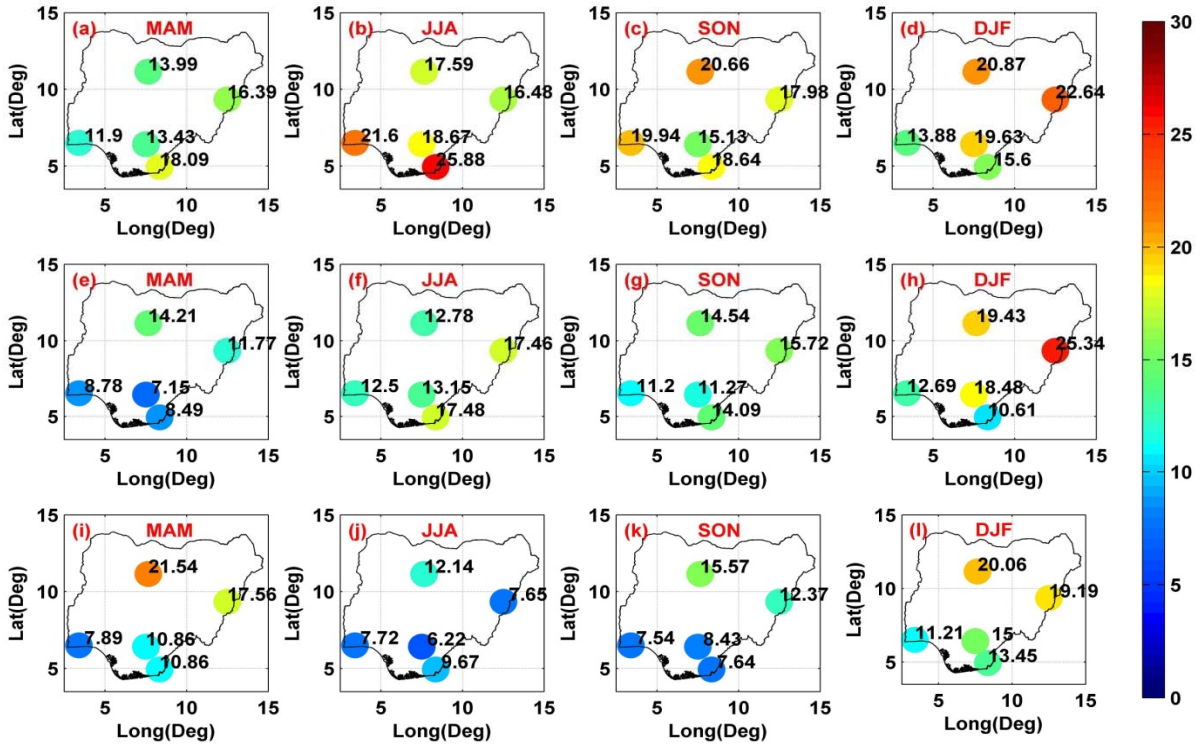

Figure 7.7: Plots of NRMSE (%) statistics across the seasons for the relation between GNSS and AIRS-Ascending (a-d), GNSS and AIRS-Descending (e-h) and GNSS and ERAI (i-l)

The accuracy of the PWV estimates from the different techniques reveals that the estimates from ERAI had the best estimate in the months of JJA. This coincides with high biases from the model and also high absolute value for PWV from the GNSS, and ERAI. The AIRS retrievals are more accurate during the MAM and SON periods, as shown in Figure 7.7.

Again similar to NRMSE, is the CV (%) error estimates shown in Figure 7.8. The CV is an atypical measure of the precision of the techniques. The same error pattern is seen in Figures 7.7 and 7.8 for the NRMSE and CV.

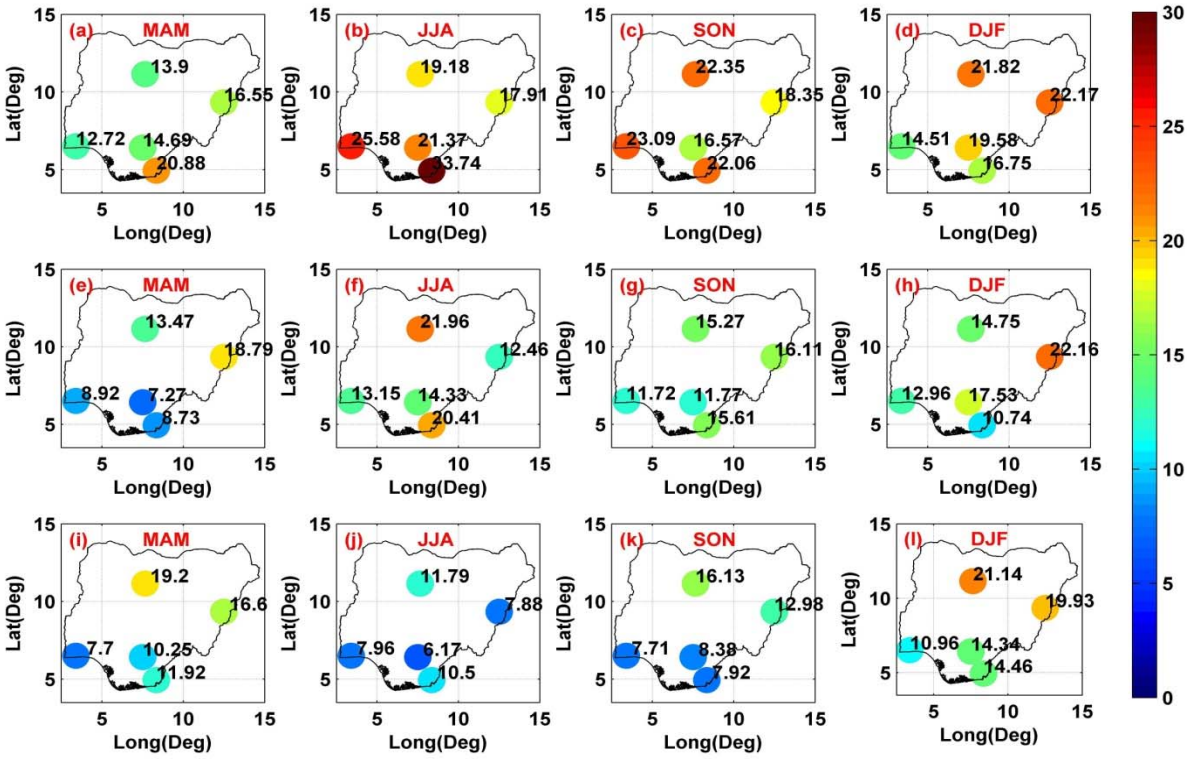

Figure 7.8: Plots of CV (%) statistics across the seasons for the relation between GNSS and AIRS-Ascending (a-d), GNSS and AIRS-Descending (e-h) and GNSS and ERAI (i-l)

Finally, the fitness of the models as indicated by the MEF in Figure 7.9 shows that the months of JJA had the least fit between GNSS PWV and the other techniques at all the stations, except at ULAG. The reason why ULAG behaved differently was not ascertained. This result is suggestive of the fact that all the techniques do not perform well during the months of JJA, which are the months associated with intense rainfall all over Nigeria. The MEF and R^2 indicators were unable to produce a clear distinction of fitness among the other seasons (MAM, SON, and DJF) at the different stations. However, on average ERAI again outpaced the other techniques with MEF values of 0.75, 0.65, 0.81, 0.88 for the months of

MAM, JJA, SON and DJF. AIRS (D) had 0.78, 0.54, 0.67, 0.85, and AIRS (A) had 0.66, 0.38, 0.57, 0.81 for the months of MAM, JJA, SON, and DJF, respectively.

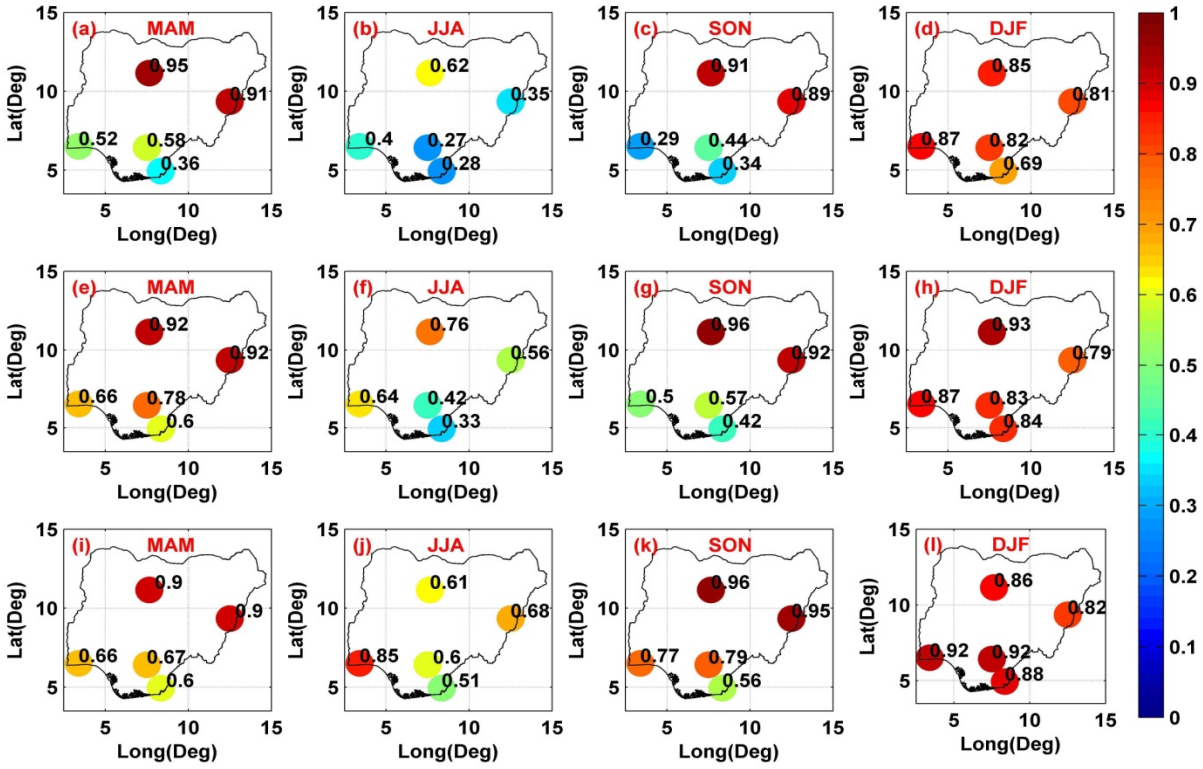

Figure 7.9: Plots of MEF across the seasons for the relation between GNSS and AIRS-Ascending (a-d), GNSS and AIRS-Descending (e-h) and GNSS and ERAI (i-l)

7.5.0 Concluding Remarks

In this study, the accuracy of AIRS and ERAI as instruments for measuring the PWV content of the atmosphere has been evaluated by comparison with concurrent observations from GNSS observational technique over the territory of Nigeria for the period of 2013-2014. The AIRS retrievals represent an infrared satellite measurement taken in the ascending and descending nodes on the satellites on board the Aqua. The ERAI represents a global reanalysis model. The daily PWV estimates from the different techniques were matched with their corresponding GNSS PWV estimates. The matched PWV estimates were further grouped into monthly and seasonal averages and standard indicators for model performances as recommended by the WMO were adopted for the comparison of the PWV estimates. All the different techniques performed reasonably well when compared to GNSS technique; the reliability of the techniques as measured by the RI indicates the GNSS/ERAI relation as the best, which was closely followed by the AIRS(A)/AIRS(D) relation. The GNSS/ERAI PWV relation was consistently outstanding among the different relations as shown by all the

indicators on daily, monthly and seasonal scales. The good correspondence found between GNSS and ERAI results is exceptionally promising; though, ERAI is a reanalysis model and therefore cannot be used for determining PWV for meteorology. They could possibly be used to calibrate each other and to improve or train other numeric models or validate each other, as the case might be. The results of this study consistently agree with previous studies in the region. Results that are relevant to the current study are those from the studies by Bock and Nuret (2009) and Acheampong et al. (2015). The satellite retrieval of PWV from the AIRS instrument shows good seasonal dependency, as indicated by the bias, accuracy, precision and fitness of the datasets. The effect of cloudy and moist atmospheric conditions often associated with the months of JJA was evident. The slight variations in the daytime and night-time (AIRS-A and AIRS-D) observation from the AIRS instrument could be associated with daily variations in cloud amount as well. The night-time AIRS (or AIRS (D)) observation agrees more with the GNSS in the study area. Finally, considering the high temporal resolution of GNSS measurement and its all-weather capability, the results of this study have demonstrated the great potential of the NIGNET as astounding PWV sensors over Nigeria. Moreover, this work confirms that the assimilation of GNSS data would be beneficial for improving the quality of water cycle in the various regional climate and reanalysis models, thus contributing immensely to the subject of weather and climate monitoring in Nigeria.

Acknowledgement

The authors thank the Swedish Meteorological and Hydrological Institute (SMHI), Goddard Earth Sciences Data and Information Services Centre (GESDISC), and the European centre for Medium-Range Weather Forecasts (ECMWF) for making CORDEX humidity profile files, AIRS PWV retrievals, ERA-Interim data used in this study publicly available. GAMIT/GLOBK GNSS processing software was also made unreservedly accessible by MIT through licence granted to HartRAO. Finally, our appreciation goes the office of the Surveyor General of the federal republic of Nigeria (OSGOF) for making available the GNSS data used in this study.

Chapter 8

Assessing the Meteorological Impact of Variations in Atmospheric Water Vapour Content over Nigeria from GNSS Measurements**

"The most incomprehensible thing about the world is that it is comprehensible."
— Albert Einstein (1879-1955)

Précis

This study analyses the meteorological impact of the variability of precipitable water vapour (PWV) retrieved from ground-based global navigation satellite system (GNSS) stations over Nigeria from 2013 to 2014; these measurements represent the foremost probe of GNSS PWV distribution and variability over Nigeria. In this study, GNSS PWV daily estimates were grouped into monthly and seasonal averages; the variations in the monthly and seasonal estimates of GNSS PWV were characterized and correlated with different weather events that are regarded as good climate change indicators. They were broadly classified into rainfall events [rainfall, relative humidity, daylight cloud amount and wind speed] and solar activity [temperature, sunspot number (SSN), total electron content (TEC), and total solar radiation (TSR)]. The results revealed that the spatiotemporal changes in PWV content are largely subjugated by the effects of latitude, topographical features, the seasons and the continental air masses. Our study shows that there is a very strong seasonal interplay among the GNSS PWV, relative humidity, rainfall and cloud estimates. Also, GNSS PWV and TEC estimates show an opposite relationship; the semi-diurnal relationship between GNSS PWV and TEC is stronger than the seasonal relationship. The seasonal relation among GNSS PWV, temperature and wind speed appears weak, while very strong interplay exists among the GNSS PWV, SSN and TSR estimates. Our results confirm that GNSS PWV is a good pointer for weather forecasting/monitoring and fit for climate monitoring if available on a longer time scale. Finally, we recommend the densification of the GNSS network in Nigeria, as this will enable 3D profiling of PWV, thereby providing more information on GNSS PWV time series, which is needed for long-term climatology.

*****This chapter consists of formatted text for one peer reviewed journal paper as follows:***

Isioye, O. A., Combrinck, L., Botai, O. J., Luhunga, P., & Moses, M. 2017. Assessing the Meteorological Impact of Variations in Atmospheric Water Vapour Content over Nigeria from GNSS Measurements, Advances *in Meteorology* (**Revised**).

8.1 Introduction and Background

Atmospheric water vapour is one of the crucial factors in the investigation of global climate systems, especially over low latitudes where water vapour exhibits significant seasonal changes (Musa et al., 2011). Lack of detailed understanding of the global distribution of atmospheric water vapour in space and time is the major limiting factor in the precise forecast of weather and climate using numerical models (Bokoye et al., 2003). Thus, more all-inclusive data sets are required to comprehend climate and weather patterns fully.

In recent years, it has been shown that ground-based global navigation satellite system (GNSS) receivers provide valuable information on precipitable water vapour (PWV) in the troposphere (e.g. Jin & Luo, 2009; Liang et al., 2015).This is achieved by calculating the approximate time changing zenith wet delay (ZWD), which is reclaimed by stochastic filtering of raw GNSS observations (e.g. Bevis et al., 1992; Rocken et al., 1995; Stoew and Elgered, 2004). GNSS has huge advantages over other systems for observing PWV, since it is a system that works in all weather conditions, with continuous unattended operation, good time resolution and a continual increase in the number of stations in many regions of the world (see Choy et al., 2015 and references in it).

Several feasibility studies have demonstrated the usefulness of the GNSS meteorology method; extensive experiments have so far shown that PWV can be obtained with an accuracy of better than 2 mm (or at the 5% level) from global positioning system (GPS)/GNSS observations (Rocken et al., 1995; Karabatic et al., 2011). Near-real-time (NRT) applications of zenith tropospheric delay (ZTD) and PWV have been investigated (see Gendt et al., 2004; Lu et al., 2015; Shi et al., 2015) and are shown to provide highly accurate results in NRT for forecasting models. Also, several studies have concluded that GNSS provides information that yields better prediction of extreme weather conditions, such as thunderstorms (e.g. Jerrett and Nash, 2001), lightning (e.g. Mazany et al., 2002, and references in it), typhoons (e.g. Song and Grejner-Brzezinska, 2009), night-time fog or intense precipitation (e.g. Liang et al., 2015; Benevides et al., 2015) and flooding (e.g. Katsougiannopoulos et al., 2015; Sharifi et al., 2015, and references therein). PWV derived GNSS observations have also been correlated with total electron content (TEC) from the same observation system to study the response of PWV to solar activities (see, Suparta et al., 2008; Suparta, 2014a&b).

Over the past few years, various government agencies around the world have launched projects to establish ground-based GPS/GNSS meteorological networks for

operational meteorology and many meteorological institutes all over the world have successfully assimilated ZTD and/or PWV data into numerical weather prediction (NWP) models. For example, the Forecasting System Laboratory of the National Oceanic and Atmospheric Administration in the USA has established a GPS precipitable water vapour (GPS-PWV) network, which currently produces PWV solutions on an hourly basis for operational weather-forecasting purposes (see Gutman et al., 2004 and references in it). In Japan, the Geospatial Information Authority of Japan is operating a nationwide GNSS network, called the GNSS Earth Observation Network System (GEONET), which has a mean horizontal spacing of approximately 20 km. The use of GEONET-derived water vapour data to support NWP models has been extensively tested by the Meteorological Research Institute and the Japanese Meteorological Agency (see Nakamura et al., 2004; Koizumi and Sato, 2004). In China, the China Meteorological Administration (CMA) has about 952 GNSS sites, which produce NRT water vapour for weather diagnoses and forecasting applications; PWV from CMA network has already been assimilated into the GRAPES_RAFS weather model (see Liang et al., 2015 and references in it). The Meteorological Office in the UK (Jerrett and Nash, 2001), MeteoSwiss in Switzerland (Guerova et al., 2006), the German Weather Service (Kopken, 2001), the Instituto Nacional de Meteorologia together with the institute of Space Studies of Catalonia in Spain (Cucurull et al., 2004) and many other agencies around the world have all assimilated GNSS atmospheric products into different NWP models for operational use. The situation in Africa appears quite different; there are no records of GNSS products being assimilated into NWP models by meteorological offices/agencies in the region.

Their application in climate research is in contrast to NRT applications of GNSS atmospheric products. For climate applications GNSS products are not required in NRT; instead highly accurate GNSS products are of the utmost importance. The spatial and long-term trends in water vapour content from GNSS have been useful in many studies focussed on climate monitoring in different regions around the world (e.g. Jin et al., 2007; Nilsson and Elgered, 2008; Jin and Luo, 2009). A further illustration of GNSS atmospheric products in climate research is the assessment of climate models (e.g. Ning et al., 2013).

In Nigeria, just like many other African countries, the application of the GNSS meteorology techniques for operational weather nowcasting and climate research is still unexploited. The Nigerian GNSS Network (NIGNET) is a network GNSS of 14 stations operated by the national mapping agency of Nigeria (or Office of the Surveyor General of the

Federation (OSGOF)) that became operational in 2010. At the moment, meteorological/climatic use of data from the NIGNET is still limited by the density of the network and the duration of available data from the NIGNET, which is considered relatively short compared to the time scale of observable changes due to climate change. Nevertheless, it still offers a unique, reliable, and consistent source of data, which can help in nowcasting/synoptic applications and understanding/monitoring changes in the climate over Nigeria. The goal of the present study is to show the potential of using the NIGNET as a novel and active tool for a variety of meteorological applications (i.e., monitoring of weather events and possibly climate monitoring when long-time records are available). To achieve this goal, attention is focussed on three major studies. Firstly, the monthly and seasonal variation/trends in GNSS PWV estimates are looked into to provide pioneering knowledge for weather studies in Nigeria from GNSS observations. Secondly, rainfall events (humidity, rainfall, amount of cloud and wind speed) are correlated with PWV estimates to demonstrate the potential of GNSS meteorology for weather monitoring further. Lastly, the relation between PWV and solar activity (i.e. temperature, sunspot number (SSN), radiation, and interaction between the upper atmosphere (ionosphere) and the lower atmosphere (troposphere) as explained by TEC and PWV) were investigated to explain interactions between terrestrial weather/climate changes and solar activity.

In this paper, the different data sets used in the study and procedures for estimation of TEC and PWV are presented in Section 8.2. In Section 8.3, the variability of GNSS-PWV over Nigeria is outlined. Section 8.4 investigates the relationship between GNSS-PWV and rainfall events over Nigeria. In Section 8.5, the relationship between GNSS-PWV and solar events over Nigeria is investigated. The summing up and concluding remarks are given in the final part.

8.2 Data and Methodology

Daily GNSS observation data files in RINEX format with a 30-seconds sampling rate were collected from seven stations representing the different climatic zones in Nigeria for the period 2013-2014 via file transfer protocol (ftp) from the NIGNET server (http://server.nignet.net/). The GNSS stations were carefully selected based on their proximity to automatic (synoptic) weather observing stations (AWOS), as shown in Figure 8.1. Data from the AWOS were obtained from the NIMET. The GAMIT/GLOBK software (Herring et al., 2006) was used to estimate the ZTD. It employs a forced batch least squares inversion process. The GAMIT/GLOBK software parameterises the ZTD as a stochastic

deviation of the uncomplicated representation of the Saastamoinen hydrostatic delay model (see Saastamoinen, 1972) with a Gauss–Markov power density of 2 $cm / hour^{1/2}$.

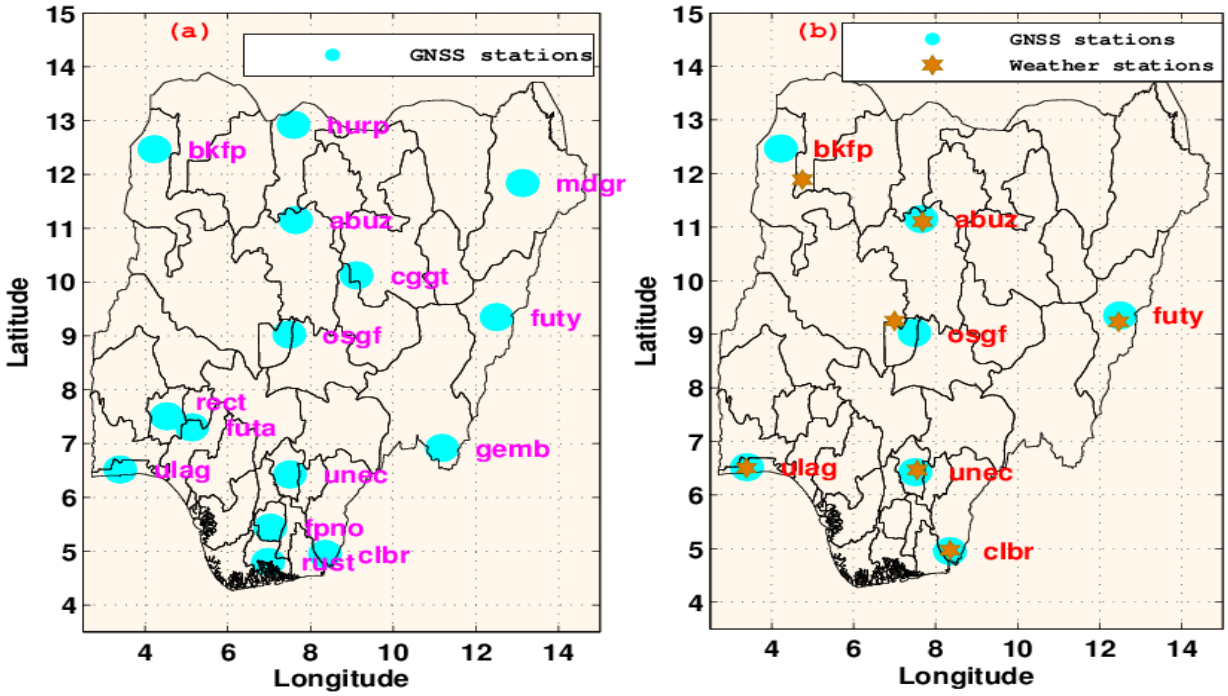

Figure 8.1: Location of GNSS sites in Nigeria (a) depicts all the stations in the new NIGNET under the management of the OSGOF (b) shows the seven chosen GNSS stations and matching AWOS sites at which PWV was estimated for this study

The ZTD at each GNSS station was estimated two-hourly and daily within a 24-hour window session. The International GNSS Service (IGS) final orbits (SP3) and IGS final ERP products were used. Satellite elevation cut-off was set to 10° during the data processing. Station coordinates were heavily constrained to their ITRF 2008 values (Altamimi et al., 2011). Solid earth tide based on the IERS03 and FES2004 models were used for solid earth tide and ocean tide loading corrections, respectively. The constraint used for zenith delay was 0.2 m, as it is recommended to set it loosely enough to encompass any error in wet delay (Herring et al., 2006). Satellite antenna phase centre offset and phase centre variation is based on AZEL for IGS absolute ANTEX files (Gendt and Schmid, 2005). The a priori tropospheric model used is the Saastamoinen model (1972) based on meteorological sources from the Global Pressure and Temperature (GPT) model. The Vienna Mapping Function (Boehm et al., 2006a) was used to calculate the zenith delay. To retrieve PWV estimates from GNSS-derived ZTDs, station temperature and pressure values are fundamental to separate the ZTD into its wet and dry components. Thus, surface temperature and pressure data from nearby AWOS (see Figure 8.1) were transferred to the GNSS sites employing the technique

demonstrated by Bai and Feng (2003), and Musa et al. (2011). The resultant ZWD component was transformed to PWV using the following relation (Bevis et al., 1992; Isioye et al., 2015a):

$$PWV = \frac{\left[ZTD_{GNSS} - ZHD\right]}{10^{-6} R_w \rho_w \left[k_2' + \frac{k_3}{T_m}\right]} = \Pi\left[ZTD_{GNSS} - ZHD\right] = \Pi \cdot ZWD \ . \qquad (8.1)$$

In Equation (8.1), $\rho_w = 1025\ kg/m^3$ is the density of liquid water, $R_w = 461.525 \pm 0.003\left(Jkg^{-1}K^{-1}\right)$ is the specific gas constant for water vapour. k_2' and k_3 are refraction constants, where $k_2' = 22.1 \pm 2.2\ K\ \text{hPa}^{-1}$ and $k_3 = 373900 \pm 0.012\ K^2 hPa^{-1}$ and T_m is the mean water vapour temperature of the atmosphere measured in Kelvin(K). The Nigeria Weighted Mean Temperature Equation (NWMTE) is, according to Isioye et al. (2016a), given as:

$$T_m = 0.5245 T_s + 132.12 \ . \qquad (8.2)$$

In Equation (8.2), T_s is the surface temperature at the individual GNSS sites in Kelvin. The T_m and T_s relationship and associated parameters in Equation (8.2) are based on the refinement of the Bevis formula (see Bevis et al., 1994), since the relation is geographic location dependent. Thus, substituting the value of the constants and T_m into Equation (8.1), we derived a simplified expression for PWV as follows:

$$PWV = ZWD.\left[9.80392 - \frac{16917.64}{0.053499 T_s + 1739.07624}\right] . \qquad (8.3)$$

Equation (8.3) is suggested to users as a handy formula to estimate PWV (in mm) in Nigeria using $T_s(K)$ and ZWD (mm) as inputs.

The TEC processing was carried out using the available GNSS observation data, satellite navigation data and the differential code bias (DCB) files by means of the free GPS-TEC analysis v2.2 software (http://seemala.blogspot.com), developed by Gopi Seemata at Boston College, USA. In this study, DCB for all satellites is obtained from the Centre for Orbit Determination in Europe, University of Bern, Switzerland (ftp://ftp.unibe.ch/~aiub/CODE) and DCBs for the ground GNSS station are estimated by the software. The TEC is a pointer of ionospheric inconsistency that is derived from the adapted GNSS signals

through free electrons; diverse epochs of ionospheric interactions can be considered by identifying and analysing the temporal variations in TEC. TEC is defined as the total number of electrons integrated along the path from the satellite to the receiver and can be written as (Zoundi et al., 2012):

$$TEC = \int_{\text{Receiver}}^{Satellite} N_e dh \ . \tag{8.4}$$

In Equation (8.4), N_e *is the* electron density down the ray paths from the satellite in space to the ground receiver. TEC is measured in units of 10^{16} electrons meter per square area, where 10^{16} $electron/m^2$ is equal to 1 TEC unit. As the TEC between the satellite and user receiver relies on the satellite elevation angle, the measure is the slant TEC. For practical applications the vertical TEC, which is free of elevation of the ray path, is often used and acquired from the slant TEC using the thin shell or single layer and mapping function of the simple layer model as follows (Norsuzila et al., 2009):

$$Vertical\ TEC = Slant\ TEC \times \cos\left[\sin^{-1}\left(\frac{R_e \cos\theta}{R_e + h_{\max}}\right)\right] . \tag{8.5}$$

In Equation (8.5), θ is the elevation angle at the ground station, $R_e = 6378\ km$ is the radius of the earth, and $h_{\max}$ is the maximum electron density height assumed in the model with a typical value of 350 km.

Quality-controlled monthly rainfall, relative humidity, wind speed and temperature (maximum and minimum) data over AWOS near GNSS sites in Nigeria were collected from the records of the NIMET, for a period of two years (2013-2014). Similarly, average monthly normal radiation and daylight cloud amount at the respective GNSS sites were obtained from the atmospheric science data centre of NASA (see https://eosweb.larc.nasa.gov/cgi-bin/sse/grid.cgi). Monthly predicted SSN for the period under investigation was obtained from the Solar Influence Data Analysis Centre, Royal Observatory of Belgium, Brussels (see http://www.sidc.be/SILSO/).

Similarly, GNSS PWV values were averaged into monthly values to correlate them with the other weather events (TEC, temperature, SSN, radiation, rainfall, humidity, wind speed and daylight cloud amount) and to understand the distribution of PWV by month. To investigate seasonal variations, data were divided into four seasonal groups. The months of March, April and May (MAM) are the hottest in the north, with few records of rain in the southern part of Nigeria. The peak of the wet season in all parts of Nigeria is in the months of

June, July and August (JJA). The months of September, October and November (SON) signify the end of the wet season in the north, while in the south, it is a period often characterised by scanty rains and severe thunderstorms. The months of December, January and February (DJF) are dry in the north, with very low temperature, because of the Harmattan, while the south is dry and humid.

8.3 Variability of GNSS-PWV over Nigeria

Figure 8.2 shows the monthly variation of PWV for the duration of our limited years of study (from 2013-2014) at seven GNSS station locations representing the different climate zones in Nigeria. The Nigerian climate is categorised largely by interaction between the trade winds and also by the ecological zones (which change from tropical rainforest along the coast to semi-arid zones in the northern outer reaches).

The lowest monthly PWV values at all the stations, as shown in Figure 8.2, were recorded in the months of December and January, with the northern stations (ABUZ, BKFP, FUTY, and OSGF) having lower PWV values than other stations (CLBR, ULAG and UNEC) in the southern part of Nigeria. The PWV values show an increasing trend from February until it reaches its maximum in July and August, then decreases toward December and January at all the stations. Again during the months with peak PWV values, stations in the southern part still have higher values of PWV compared to their counterparts in the north. From the foregoing it is obvious that the PWV values decrease from the south to the north of Nigeria or when moving from the stations in the coastal zones to the semi-arid zones. This pattern in the variability of PWV from the south to north may be attributed to the latitudinal dependence of PWV and/or the influence of the ocean on shorefronts. The stations (CLBR and ULAG) are located on the shorefront of the Atlantic Ocean around the coastal cities of Calabar and Lagos respectively. The PWV values at these GNSS stations when compared to the other stations are highest for all the months of the year. The high PWV values at CLBR and ULAG could in addition be attributed to the low elevation of the stations, which are at 57.13 m and 44.56 m respectively, compared to FUTY, BKFP, UNEC, OSGF and ABUZ at 247.39 m, 250 m, 254.39 m, 532.64 m, and 705.05 m respectively. There is a repetition of this trend at ABUZ; the monthly PWV value at ABUZ is lower than those of other northern stations, which are at higher latitude (i.e. BKFP) than ABUZ. Notably ABUZ has the highest station elevation among the GNSS stations and correspondingly the lowest PWV values for all the months. This is an indication that station elevation plays an important role in PWV estimates, as well the station latitude.

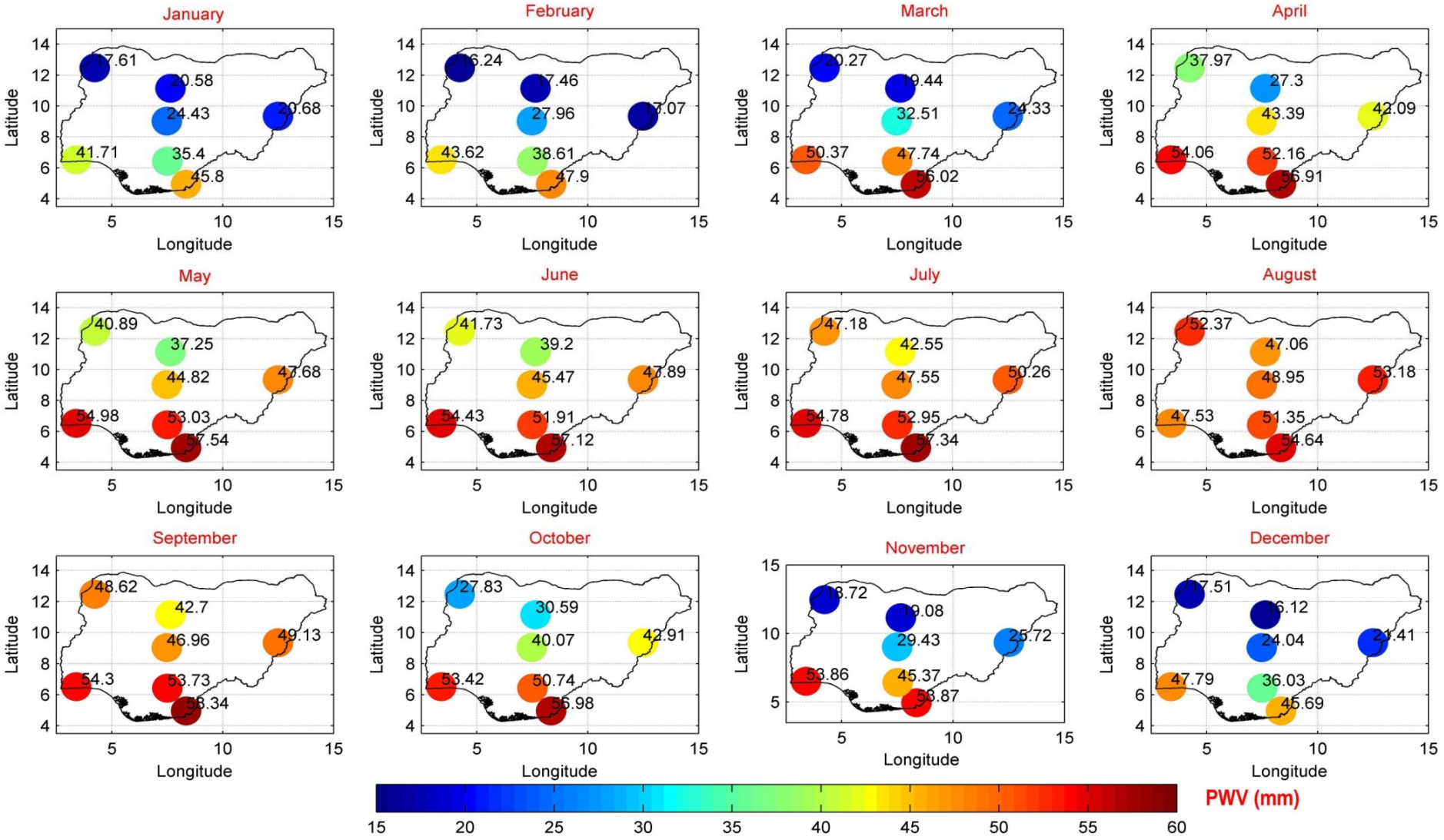

Figure 8.2: Monthly mean GNSS PWV (mm) for seven stations in different climatic regions of Nigeria from 2103 to 2014

Figure 8.3 presents the PWV values for the four seasons. According to Figure 8.3 the seasonal PWV confirms an apparent variation, with lower values in the dry season (DJF and MAM) and higher values in the wet season (JJA, SON), which reflects that in the wet (rainy) season, because of the strong moisture field (high water vapour pressure) the PWV magnitude is higher. PWV values at all the stations exhibit a recognised seasonal signal, which can be explained by a cosine function, as the increase to the maximum in the JJA season, which is the peak of the rainy season in both the north and south of Nigeria, and a decrease to the minimum in the months of DJF, the dry season in the south and the Harmattan in the north of Nigeria. There is little rain in the months of MAM and SON in the north and the temperature is high, while the south is not as dry as the north, thus the climate in the south is very humid and tends to keep the PWV values very high. PWVs vary spatially mainly according to altitude, though there is slight variation along both latitude and longitude over Nigeria. For instance, the magnitude of PWV is greater at all seasons along the shorefront of the Atlantic Ocean at CLBR and ULAG stations, which are in the lowlands.

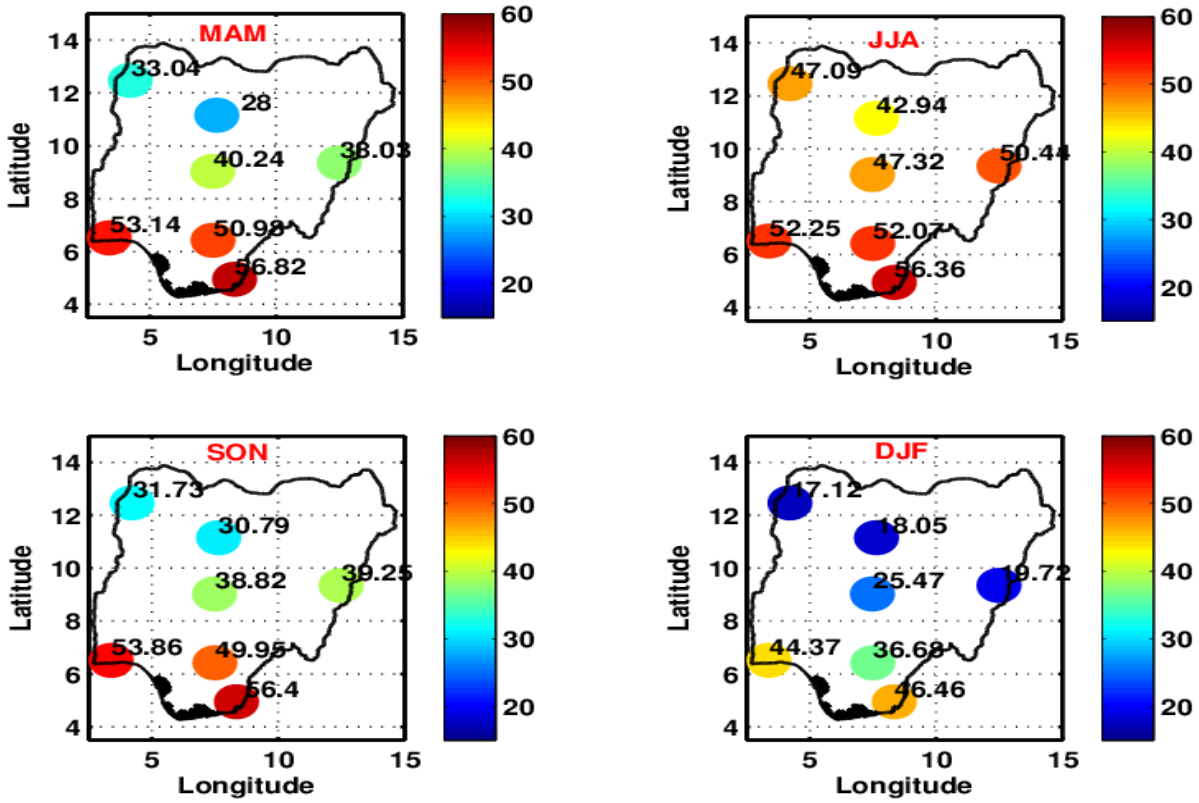

Figure 8.3: Seasonal mean GNSS PWV (mm) for MAM, JJA, SON, and DJF from 2013 to 2014

The seasonal range (i.e. difference between maximum and minimum seasonal values) of PWV at the different GNSS stations is 24.88 mm, 10.36 mm, 30.72 mm, 9.49 mm, 15.39 mm, 21.85 mm and 29.97 mm for ABUZ, CLBR, FUTY, ULAG, UNEC, OSGF, and BKFP, respectively. It is obvious that the range in PWV at most of the stations increases with latitude (i.e., movement from south to north). A sharp increase in the range values is seen at the location of GNSS stations (ABUZ, FUTY, OSGF, and BKFP) in the northern part of Nigeria. This is expected because of the extreme cold and hot weather during the dry season in the northern part of Nigeria, which often results in great variations in surface temperature.

The average annual PWV at ABUZ, CLBR, FUTY, ULAG, UNEC, OSGF, BKFP is 29.94 mm, 54.01 mm, 36.86 mm, 50. 90 mm, 47.42 mm, 37.96 mm and 32.25 mm, respectively. Again, the lowest mean annual average value of PWV was recorded at ABUZ and the highest recorded at the lowland (and coastal) stations of CLBR and ULAG. Clearly the PWV depends on the altitude and latitude. Figures 8.4 and 8. 5 show the scatter plots of annual PWV values with the latitude and elevation of the corresponding GNSS stations, respectively. Both plots had negative slopes as an indication of an inverse relation between dependent and independent variables. A stronger coefficient of determination (goodness of fit) was found between PWV and station latitude ($R^2 = 0.9648$), compared to the station elevation ($R^2 = 0.7916$). This result is indicative of the latitudinal dependence of PWV. The climate of Nigeria is also known to vary from the south to the north (i.e. latitudinally), and this shows that GNSS PWV has good potential for climate studies and monitoring.

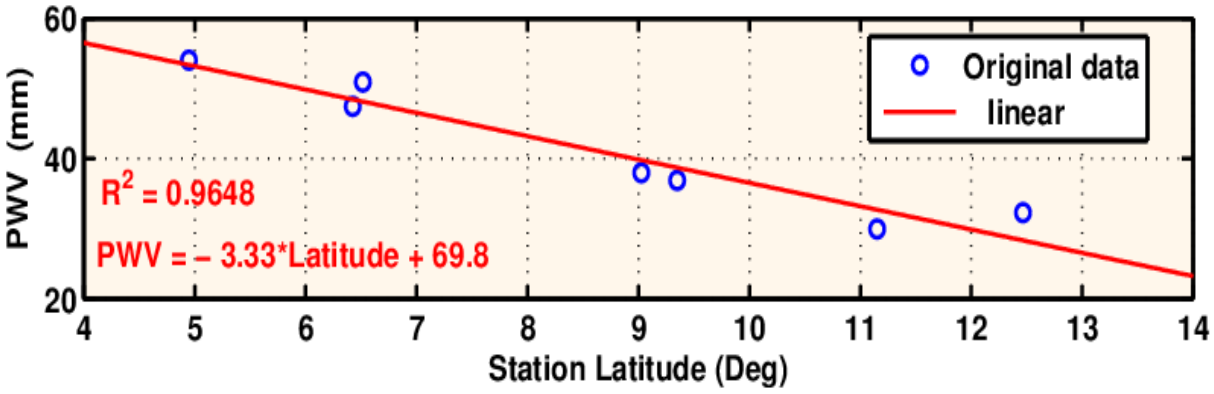

Figure 8.4: A scatter plot of the average PWV values at the different GNSS stations against the corresponding latitude of the GNSS station

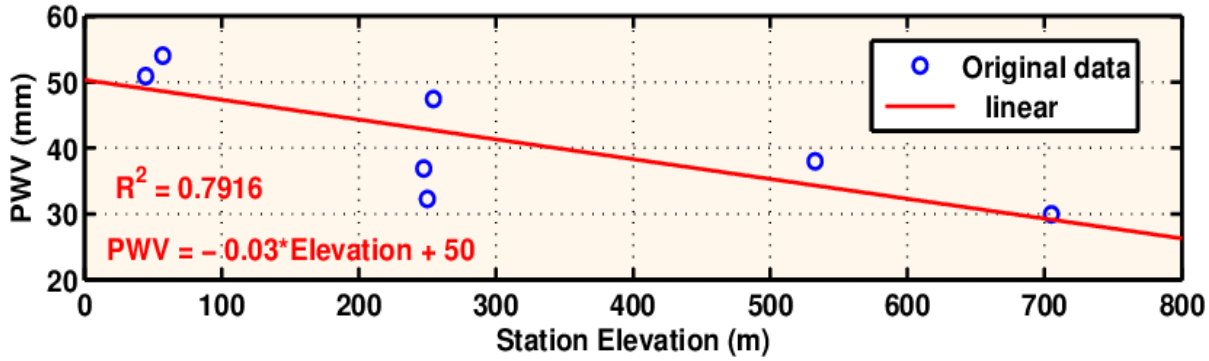

Figure8. 5: A scatter plot of the average PWV values at the different GNSS stations against the corresponding height of the GNSS station

In furthering earlier studies on the spatial dependence and temporal characteristics of GNSS-derived ZTD estimates in Nigeria as reported by Isioye et al. (2016b), it will be of great importance to determine the interrelationship between GNSS PWV and GNSS ZTD. From equation (1), one can see the relationship between PWV and ZWD after separation of the dry and wet components of the ZTD. The value of Π typically varies from about 0.16 to 0.17 across the different seasons in Nigeria; as shown in Table 1, Π contributes more to the absolute derivation of PWV and largely depends on the choice of the model of T_m and its ability to respond to varying weather conditions in the adapted geographic region. The importance of using locally adapted models of T_m rather than the global and Bevis models has been articulated in many publications (i.e., Song & Grejner-Brzezinska, 2009). Also, from Table 8.1, it is evident that the variation in ZHD is unaccounted for by PWV; it largely depends on the variation in atmospheric pressure at the GNSS stations.

Table 8.1: Average GNSS PWV and GNSS ZTD relationships over Nigeria from 2013 to 2014

Station	Π	**Coefficient of determination** (R^2)			**Regression** $PWV = a(ZWD) + b$	
		PWV-ZTD	PWV-ZHD	PWV-ZWD	Slope (a)	Intercept (b)
ABUZ	0.1647	0.9958	0.0041	0.9998	0.1639	0.1241
BKFP	0.1644	0.9945	0.0256	0.9998	0.1635	0.2458
CLBR	0.1643	0.9941	0.0825	0.9996	0.1635	0.2500
FUTY	0.1647	0.9978	0.0724	0.9999	0.1637	0.1830
OSGF	0.1645	0.9886	0.0392	0.9998	0.1636	0.1946
ULAG	0.1647	0.9895	0.0386	0.9995	0.1639	0.2353
UNEC	0.1644	0.9939	0.0473	0.9998	0.1636	0.2037

Owing to the small variations in T_m, it can be seen that the PWV is mainly responsible for the variation in ZWD, as presented in Table 8.1. The PWV and ZWD relationship is a perfect correlation, and it is logical to accept that PWV bears the same spatial and temporal characteristics with ZTD, since it is obviously the major driving force in the ZTD estimates.

The discussion on GNSS PWV can benefit from the study of Isioye et al. (2016b), which was based on a time series of two-hourly GNSS ZTD from 2010–2014 at 14 NIGNET stations. The study applied three spatial statistical models to the ZTD estimates, namely the ordinary least squares, spatial error model and spatial lag model. Diagnostic tests for independence of error terms, homogeneity of variance, normality and spatial dependence were performed for each model. Assumptions of all three models were not completely satisfactory and revealed weak spatial dependence among the stations (i.e. spatial autocorrelation was not obtained). This was attributed to the density of stations in the network; the GNSS PWV as estimated from the NIGNET over the same period is likely to follow suit. The diurnal and intra-seasonal variations of ZTD were also studied with GNSS measurements using the Mann-Kendall Trend test, Fisher's Kappa and Bartlett's Kolmogorov-Smirnov statistics. These were used to test for white noise in the ZTD estimates. The KPSS and Dickey-Fuller tests were used to test the stationarity of the ZTD time series. Tidal oscillations were noticed and reported at the GNSS stations. These oscillations were determined to have diurnal and semi-diurnal components. The diurnal components as seen from the ZTD were reported as the principal source of the oscillations. These outcomes can perhaps be ascribed to temporal variations in atmospheric water vapour on a diurnal scale. In addition, the diurnal ZTD cycles exhibited significant seasonal dependence, with larger amplitudes in the rainy (wet) season and smaller ones in the Harmattan (dry) season; the ZTD seasonal cycles are well in agreement with those PWVs observed in this study.

From the foregoing, it is evident that knowledge of the spatiotemporal changes of water vapour concentration may be of key significance to weather forecasting and monitoring and in the long term for climate research. It is important also to see how water vapour relates with other constituents of the atmosphere or weather events. In the preceding sections of this paper, discussions are focussed on the interaction between the variability of water vapour and other climate indices, which include rainfall events and solar activity.

8.4 Investigation of GNSS-PWV and Rainfall Events over Nigeria

The frequency and intensity of severe weather events are projected to increase in response to the effects of global warming and meteorological and hydrological hazards, such as sudden increases in river levels or floods, may be caused (see Adelekan, 2000; Atedhor et al., 2011). Torrential rainfall is becoming a serious problem in the urban areas of Nigeria because such events may develop suddenly making it difficult to issue timely warnings to the public (Adelekan, 2000). The accurate prediction of localised heavy rain on a horizontal scale of several kilometres is still a challenging task in current mesoscale numerical prediction models, partly because of the lack of a now-casting meteorological observation network with fine spatial resolution in many different regions of the world (Adam et al., 2011). Information on water vapour is a particularly important factor in improving the prediction of heavy rain. Note that weather radar can detect a cloud only after precipitation starts. It is necessary, therefore, to develop an observation system that can monitor the local in-homogeneities of water vapour distributions that could be associated with the formation of convective clouds before torrential rains occur. The rainfall process is influenced by numerous diverse micro- and mesoscale physical and dynamic circumstances (i.e. atmospheric steadiness, vertical velocity, humidity, cloud type, terrain) and many other circumstances, which include water vapour (Sharifi et al., 2015). Water vapour is an extremely changeable element of the atmosphere and its variability over Nigeria, based on observations from GNSS, has already been discussed in a previous section of this report. It is essential to the transport of energy in the atmosphere and in the development and circulation of weather (Pikridas, 2014). It is also the basis of rainfall and its latent heat is a significant element in the dynamics of most weather events (Suparta et al., 2008). Thus, in this section, monthly mean values of GNSS PWV are correlated with rainfall, relative humidity, daylight cloud amount and wind speed information to demonstrate the applicability of variability of GNSS PWV in climate studies.

Figures 8.6 (a and b), 8.7, 8.8 and 8.9 show the monthly variations of PWV with rainfall, relative humidity, daylight cloud amount and wind speed for the study period, respectively. In Figure 8.6 (a), the rainfall amount is seen to increase with monthly PWV estimates at all the stations. The variation in the rainfall between the driest and wettest month is higher at ABUZ and BKFP, which are in the north of the country. Similar variation is seen in PWV estimates at these stations, as already discussed in section 8.2 of this paper. The high amount of rainfall in the south, as observed at CLBR and ULAG, corresponds with the PWV values at these stations, which are also higher than those at ABUZ and BKFP. At station ABUZ, the highest amount of rainfall was recorded in August and was plotted against GNSS

PWV for the same period, as shown in Figure 8.6b; the PWV was estimated at two-hour intervals and the rainfall was recorded twice a day (i.e., from 06:00 -18:00 and 18:00 to 06:00). In Figure 8.6 (b) conspicuous peaks are seen in the GNSS PWV estimates hours before rainfall. However, because of the resolution of the rainfall records, the actual hours of rain corresponding to the peaks could not be ascertained. Similarly, depressions can be seen in Figure 8.6 (a) on days or intervals of no rain. This results further show that variability in PWV estimates as observed by GNSS is closely related to rainfall and confirms the efficiency of the GNSS meteorology technique in storm prediction and possibly also in improving future forecasting models in Nigeria, as already demonstrated in many other countries/regions of the world (Vedel et al 2004; Song & Grejner-Brzezinska, 2009; Katsougiannopoulos, 2015).

As seen from Figure 8.7, humidity is higher at CLBR and ULAG than at the other GNSS stations in the north of Nigeria. This obviously indicates that the coastal regions in the south are more humid (i.e. have a high amount of moist air) and have more potential capacity for rainfall. PWV, as observed from GNSS, has shown good agreement and interplay with rainfall amount and quantity of moisture in the air as indicated by the relative humidity. The higher the PWV content of the atmosphere, the more latent energy is available for the generation of storms. High temperatures in the north could also be attributed to the low amount of relative humidity and corresponding low PWV values. Daylight cloud amount, as shown in Figure 8.8, provides information on the visible mass of condensed watery vapour floating in the atmosphere. The cloud amount is high in the south and gradually decreases to the north with a wider range (difference between maximum and minimum value) from south to north. The cloud amount as depicted in Figure 8 is obviously in line with the GNSS-PWV trend at all the locations under investigation. Wind speed at 50 m, as shown in Figure 8.9, does not show any striking trend of variation at the GNSS stations in the different locations/regions in Nigeria, though an inverse relation is visible between the GNSS PWV values and the wind speed at each station.

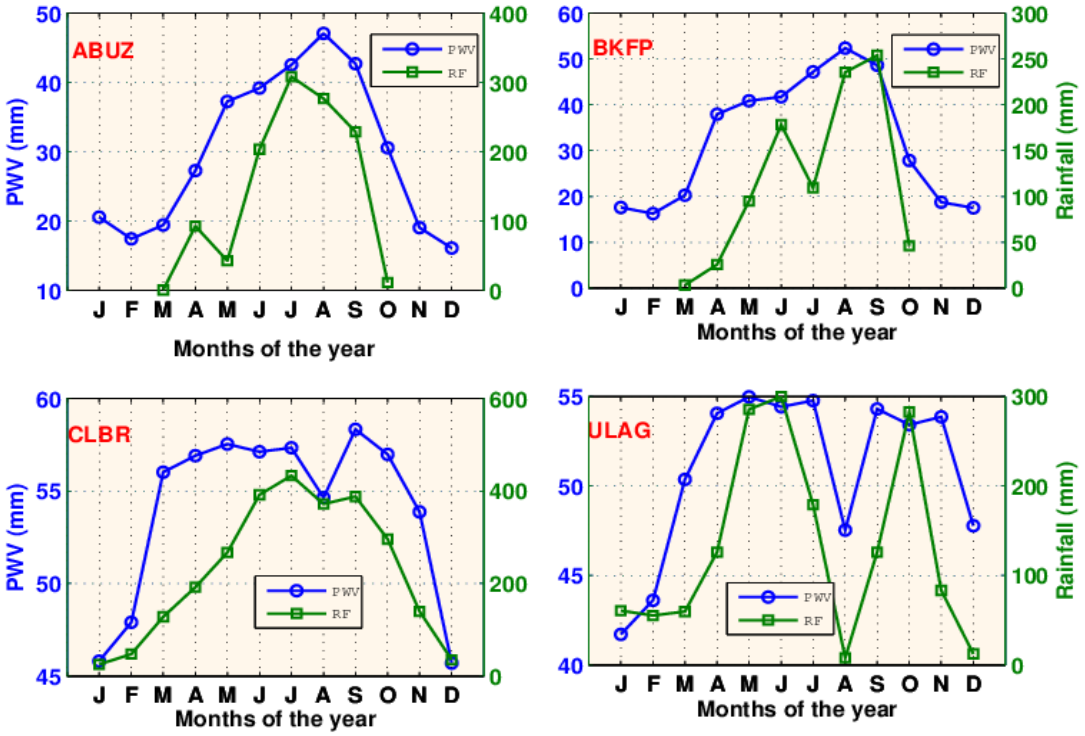

Figure8. 6a: Monthly distribution of PWV (in blue) and rainfall amount (in green) at four GNSS stations (ABUZ, BKFP, CLBR, and ULAG) in Nigeria

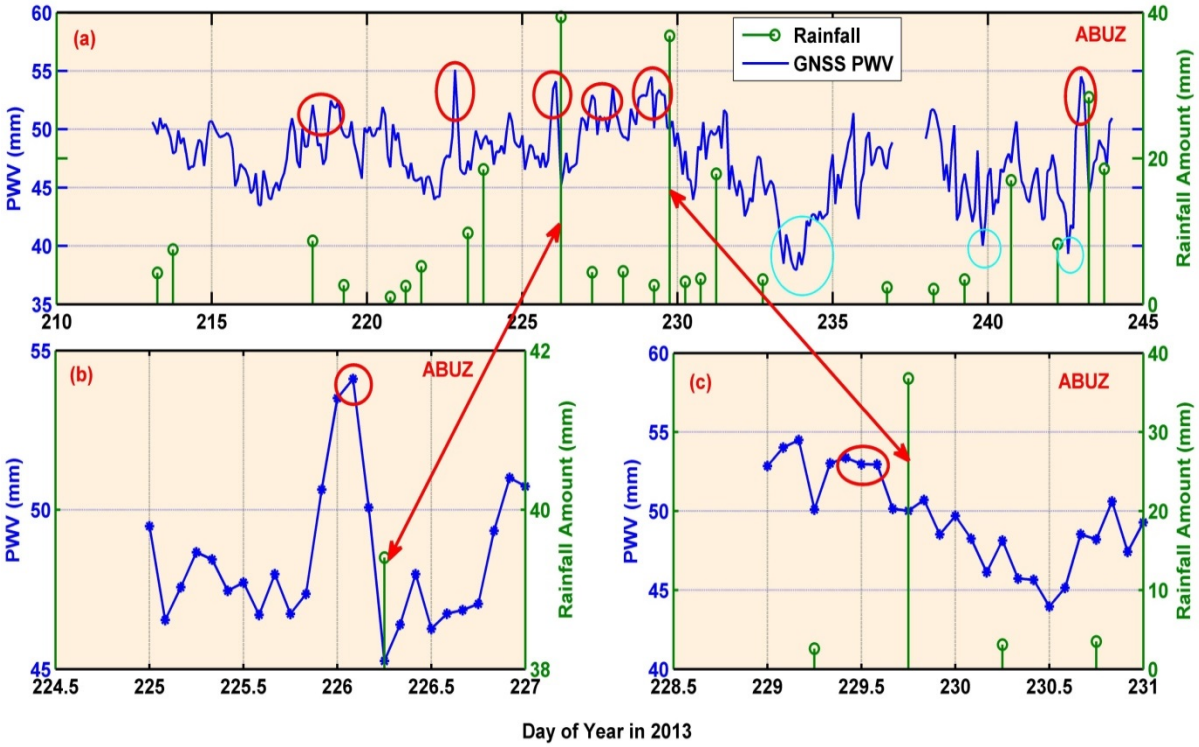

Figure8.6b: Distribution of PWV and rainfall in August 2013 at station ABUZ. The red circles indicate peaks in PWV estimates attributed to rainfall and cyan circles are tagged as depressions; (a) shows the distribution PWV alongside a 12-hourly record of rainfall, (b) is an exaggerated plot of the 14 August (DOY226) rainfall storm and (c) is an exaggerated plot of the 17 August (DOY 229) rainfall storm

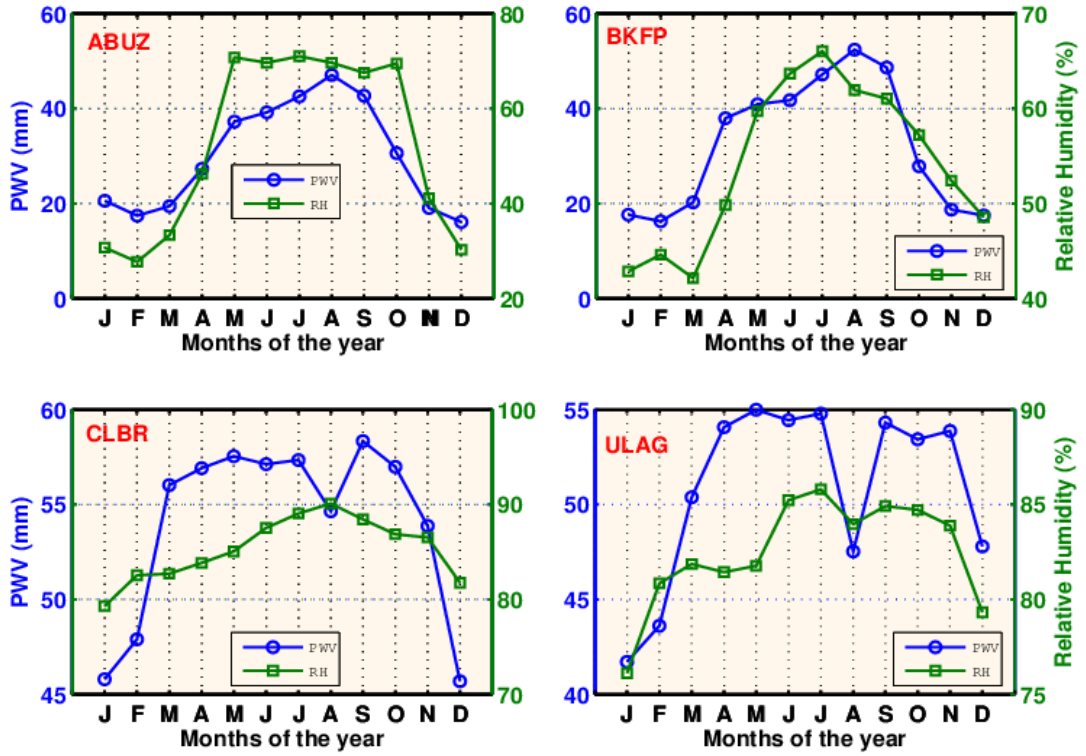

Figure8. 7: Monthly distribution of PWV (in blue) and relative humidity (in green) at four GNSS stations (ABUZ, BKFP, CLBR, and ULAG) in Nigeria

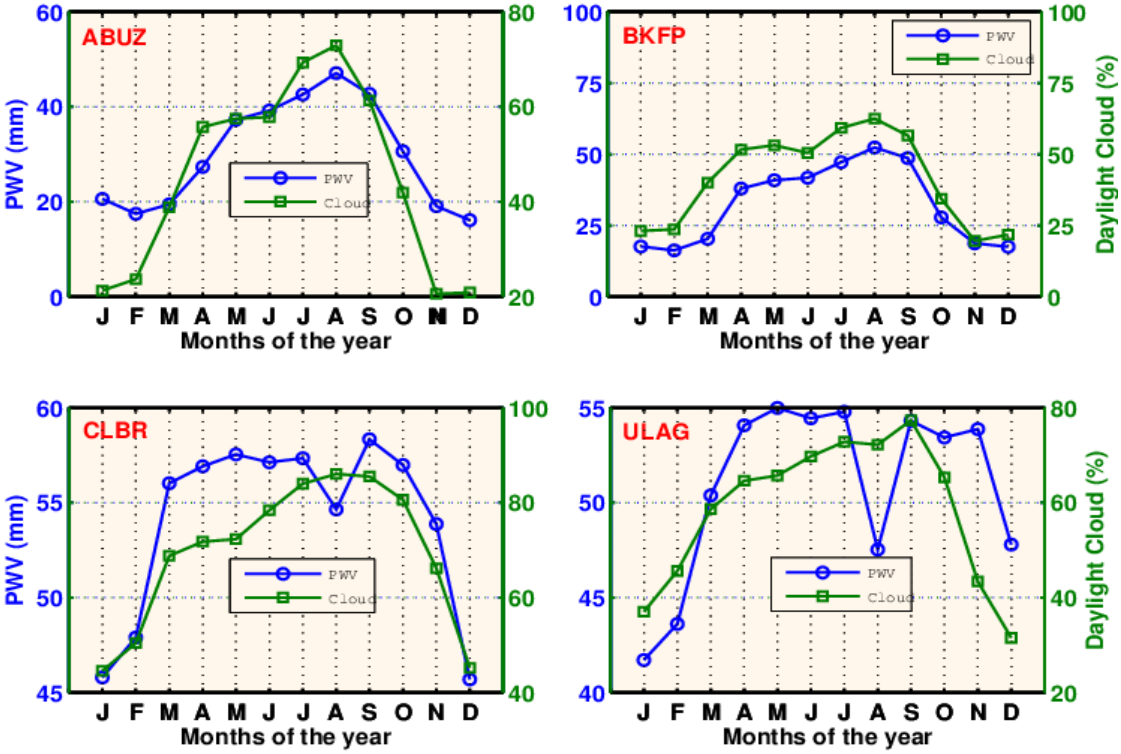

Figure 8.8: Monthly distribution of PWV (in blue) and daylight cloud amount (in green) at four GNSS stations (ABUZ, BKFP, CLBR, and ULAG) in Nigeria

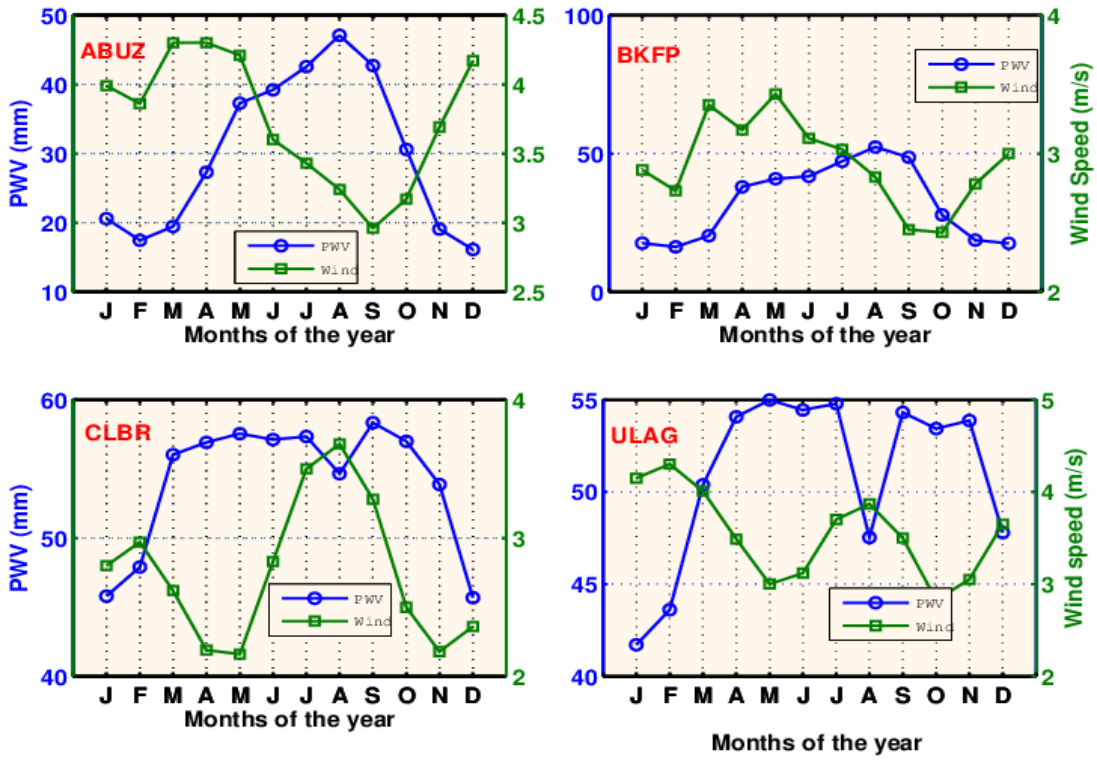

Figure 8.9: Monthly distribution of PWV (in blue) and wind speed (in green) at four GNSS stations (ABUZ, BKFP, CLBR, and ULAG) in Nigeria

To examine further how the climate indicators influence the study of weather/climate monitoring, it is ideal to describe the atmospheric system analytically and construct a general circulation model. However, this kind of model requires extensive data and massive numerical computations. Thus, we adopt a simple statistical approach of correlation analysis to further the interplay among the various climate indicators. The interplay among the different climate indicators as worked out from the Pearson's correlation coefficient test is presented in Table8. 2. GNSS PWV is seen to have a strong positive correlation with rainfall, humidity and the cloud amount at the different stations. Interestingly, the rainfall, relative humidity and cloud amount also exhibit a positive correlation among themselves because of their direct dependence on each other at the individual stations. The wind speed exhibits the weakest correlation with the GNSS PWV at the different stations, except at ULAG with a strong negative correlation of -0.7897. In addition, there is no statistically significant correlation (at 95% confidence level) between wind speed and the other climate indicators at most of the stations, as shown by entries in red in Table (8.2).

Table8. 2: *Pearson's correlation coefficient matrix for GNSS- PWV and the different rainfall events (rainfall, relative humidity (RH), wind, and daylight cloud amount) four GNSS locations in Nigeria*

Variables	GNSS- PWV	Rainfall	RH	Wind	Daylight cloud	GNSS- PWV	Rainfall	RH	Wind	Daylight cloud
			ABUZ					BKFP		
GNSS- PWV	1	0.8859	0.9269	-0.6356	0.9376	1	0.8848	0.8571	0.0235	0.9571
Rainfall		1	0.7146	-0.6044	0.8634		1	0.7916	-0.2195	0.7925
RH			1	-0.6310	0.8487			1	-0.1247	0.7314
Wind				1	-0.4264				1	0.2078
Daylight cloud					1					1
			CLBR					ULAG		
GNSS- PWV	1	0.8108	0.7273	0.0912	0.9172	1	0.6653	0.7544	-0.7897	0.6463
Rainfall		1	0.9119	0.5244	0.9378		1	0.6333	-0.5799	0.6879
RH			1	0.5152	0.9074			1	-0.5229	0.7713
Wind				1	0.4101				1	-0.3228
Daylight cloud					1					1

The coefficient of determination or goodness of fit $\left(R^2\right)$ between GNSS PWV and the other climate variables in the order of rainfall, humidity, wind speed and cloud amount at ABUZ is 0.7849, 0.8591, 0.4040, 0.8791, at BKFP it is 0.7829, 0.7349, 0.0006, 0.9161, at CLBR it is 0.6574, 0.5290, 0.0083, 0.8413, and at ULAG it is 0.4426, 0.5691, 0.6236, 0.4177, respectively. The R^2 values represented as percentages are shown in Figure 8.10; evidently, this result of the R^2 indicates that the variability in GNSS PWV can be adequately explained or predicted by similar variation in rainfall, humidity and cloud amount at the different GNSS locations under investigation. The predictability of GNSS PWV from wind speed observations as shown by the coefficient of determination still remains very weak at most of the stations or regions investigated. So, the relation as determined from the multivariate analysis between the different rain events (climate indicators) and GNSS PWV at the different regions can be given as follows:

$$\left.\begin{aligned} GNSSPWV_{abuz} &= 13.33 + 0.24 * Rainfall + 0.25 * RH - 1.93 * wind + 0.19 * cloud \\ GNSSPWV_{bkfp} &= 7.361 - 0.02 * Rainfall - 0.39 * RH + 2.47 * wind - 0.58 * cloud \\ GNSSPWV_{clbr} &= 81.96 + 0.004 * Rainfall - 0.58 * RH - 2.7 * wind + 0.40 * cloud \\ GNSSPWV_{ulag} &= 31.49 + 0.005 * Rainfall + 0.40 * RH - 5.14 * wind + 0.06 * cloud \end{aligned}\right\} . \quad (8.6)$$

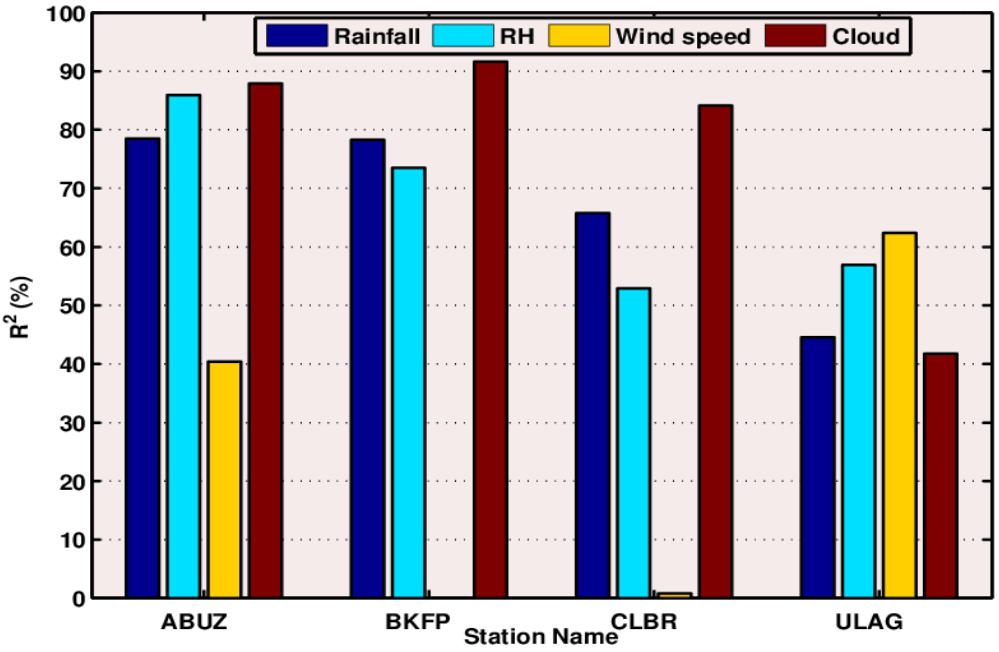

Figure 8.10: The coefficient of determination (R^2 in %) between GNSS PWV and the other climate variables at four GNSS stations (ABUZ, BKFP, CLBR, and ULAG) in Nigeria

From the foregoing GNSS, PWV can seen as a constituent of the atmosphere with very highly variable characteristics constituting a major factor in climate and weather analysis, as demonstrated in this study. GNSS PWV and the other climate indicators can be used in forecasting different weather events and analysing the climate. However, climate analysis requires a much longer observation period, so this study is mainly based on local weather conditions.

8.5 Investigation of GNSS-PWV and Solar Events over Nigeria

In this section, we investigate the effect that the variability of solar activity has on weather parameters, namely the water vapour. A comprehensible correlation between water vapour and solar activity can elucidate some physical systems of how solar activities affect earthly weather. Many forms of solar activity, such as TEC, solar radiation bursts and solar wind, are known to be the basis for radiation enrichment and plasma movement, which are directly or indirectly regarded as causing global climatological changes (Zhao et al., 2004). Many other studies in this region of the world have focussed on the relationsip between cosmic ray flux and the earth's cloud cover (Carslaw et al., 2002), SSN and precipitation (Zhao et al., 2004), SSN and PWV (Maghrabi & Al Dajani, 2014), PWV and temperature (Maghrabi & Al Dajani, 2014; Sharifi et al., 2015), PWV and TEC (Suparta et al., 2008; Suparta, 2014a&b), PWV and solar radiation intensity (Chen and Li, 2013). Different studies have reached different conclusions on the strength of the relationship linking the different

solar activity and weather parameters (climate indicators), though the results were inconclusive in most cases. Thus, the impact of solar activity on atmosphere dynamics and the physical mechanisms of the relations are still subject to further enquiry. In our contribution to the understanding of the effect that the variability of solar activity has on weather parameters, we explore the relationship between variation of GNSS PWV and four solar activity indicators (namely temperature, SSN, TEC and total solar radiation intensity (TSR)) over Nigeria.

Figures 8.11, 8.12, 8.13, and 8.14 illustrate the monthly variations of GNSS PWV with temperature, SSN, TSR, and TEC for the study period. In Figure 8.11, PWV increases with a decrease in temperature. The months of JJA register the minimum and maximum value for temperature and GNSS-PWV at all the stations from the south to the north of Nigeria. A reverse trend is seen in the months of MAM, when the temperature is at its maximum. The variation in the temperature between the coolest and hottest month is higher at ABUZ and BKFP, which are in the north of the country. A similar variation is seen in PWV estimates at these stations. The interplay between temperature and GNSS- PWV values is best explained by the movement of the tropical air masses. In the north during the months of DJF and MAM, the tropical continental air mass (or Sahara trade wind) from the Sahara tends to increase the temperature and lower humidity, which results in a corresponding decrease in PWV values. In the south, the air mass from the Atlantic Ocean (tropical maritime air mass) is responsible for high humidity and lower temperature in the south and correspondingly increases PWV. The ocean air masses overrun the southern part of Nigeria from February and spread northwards during JJA. The movement of the tropical air masses forces the continental air mass to retreat northward as a result of the sun's movement from the southern to the northern hemisphere (i.e. from the tropic of Capricorn to the tropic of Cancer). During the northward movement of the sun, it crosses the equator in March and is overhead throughout West Africa and thus responsible for the very high radiation and temperature recorded in the months of MAM. The SSNs, as presented in Figure 8.12, are disturbances (or spots) on the sun's surface that are characterised by severe magnetic activity (i.e. solar flares and hot gassy ejections from the sun's corona). The number of sunspots observable from the earth varies from daily to millennia cycles; the 11-year sunspot cycle remains the most eminent and well probed of these cycles. Over the past century, we have witnessed a warmer earth, at a time when the number of sunspots has also continually been rising. Thus, we may want to attribute the warming of the earth to the influence of solar activity on the global climate. Several climate scientists are of the opinion that sunspots could be playing a part in climate change (e.g. Friis-

Christensen and Lassen, 1991; Damon and Laut, 2004), while other assess it as quite negligible and ascribe the earths' warming principally to emissions from industrial activity. Figure 8.12 show that monthly SSN over the period display a similar pattern to the different GNSS-PWV values at all the stations. The sunspots are directly correlated with temperature on the earth and thus as the provider of nearly all the energy in the earths' climate, the sun has a formidable impact on climate.

The TSR amount as depicted in Figure 8.13 is obviously in an inverse relation with the GNSS-PWV trend at all the locations under investigation. The sun's principal impact on the earth's surface temperature is via inbound TSR. The global temperature change is as a result of energy imbalance attributed to variation in TSR through radiative forcing. TSR and SSN correlate strongly with the solar magnetic field (Wang et al., 2005). The relationship between the sun and the weather is further compounded by the variation in inbound radiation from the sun, which is a result of the balance between declines associated with sunspots and enhancements by faculae (dazzling areas), which surround sunspots. The probe of clouds, where they take place, and their features in relation to TSR play a crucial role in the comprehension of climate change (see Meehl et al., 2003). Low, dense clouds are a sign of solar radiation and cool the surface of the earth. High, weak clouds largely convey inward-bound solar radiation. Simultaneously, they ensnare some of the outward-bound infrared radiation released by the earth and release it back downward, thus heating up the surface of the earth. The results of the correlation between cloud amount, as shown in Figure 8.8, and TSR values (Figure 8.13) confirms the proposition of Meehl et al. (2003): an inverse relation is recorded between cloud amount and TSR at all the stations, with the R^2 values for ABUZ, BKFP and CLBR at 0.7639, 0.5528, and 0.9765, respectively. By comparing the TSR variability between seasons (Figure 8.13), it is seen that the months of JJA had the lowest record of TSR with a value of 4.56 and 5.24 $kWh/m^2/day$ at ABUZ and BKFP in the north, respectively. Also, in the south of Nigeria lower TSR values of 1.83 and 2.94 $kWh/m^2/day$ were obtained for JJA at CLBR and UNEC, respectively. In the months of DJF the value of TSR stood at its maximum with an increasing trend northwards. This further reflects the inverse relationship between TSR and GNSS PWV, and their dependence on latitudinal variation. GNSS PWV variation in Nigeria is evidently controlled by the surface radiation balance. This means that a more active season would result from more energy transferring from the related sun activities to the earth's surface through its atmospheric dynamics.

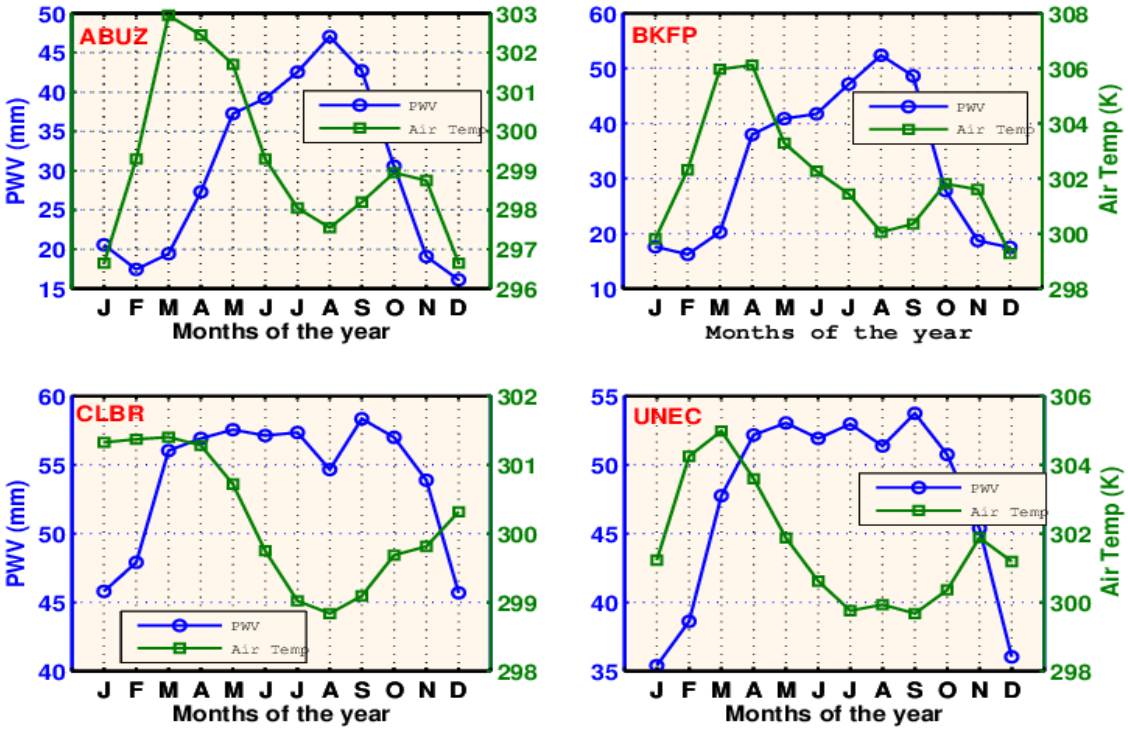

Figure 8.11: Monthly distribution of PWV (in blue) and temperature (in green) at four GNSS stations (ABUZ, BKFP, CLBR, and UNEC) in Nigeria

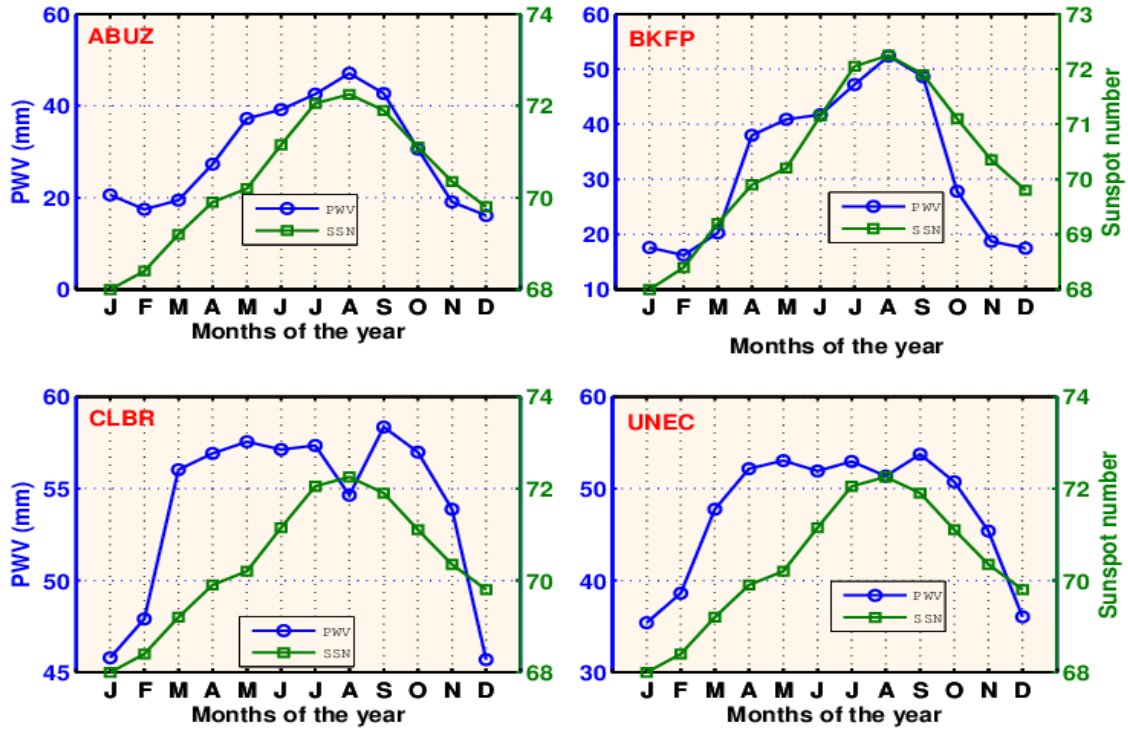

Figure 8.12: Monthly distribution of PWV (in blue) and SSN (in green) at four GNSS stations (ABUZ, BKFP, CLBR, and UNEC) in Nigeria

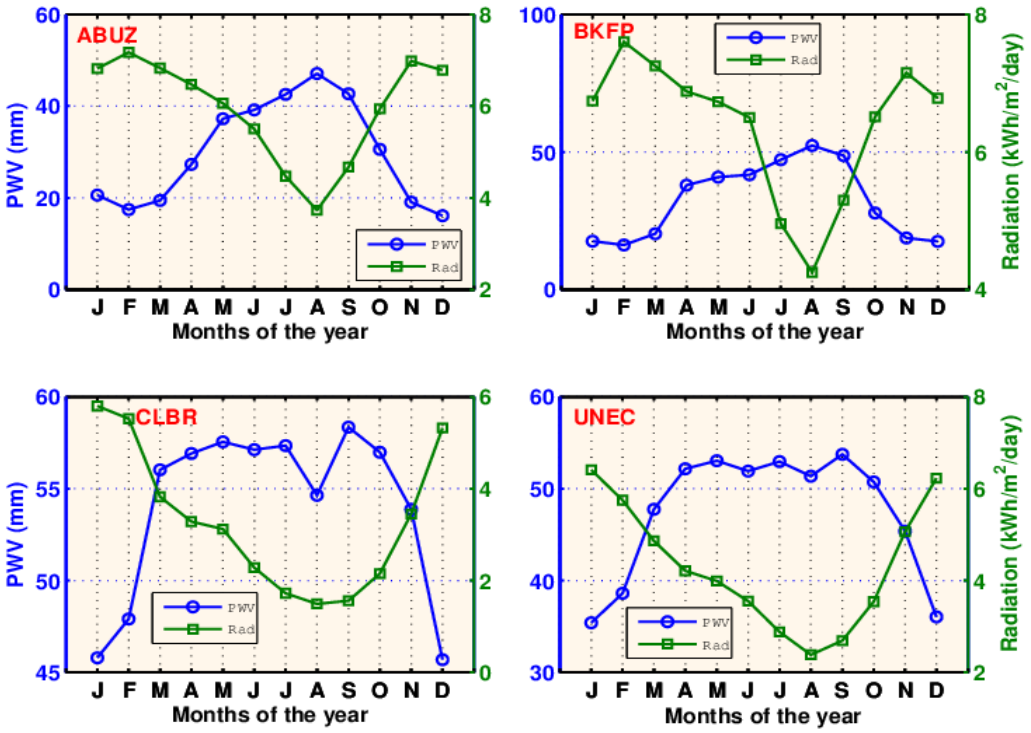

Figure 8.13: Daily distribution of PWV (in blue) and total solar radiation intensity (in green) at four GNSS stations (ABUZ, BKFP, CLBR, and UNEC) in Nigeria

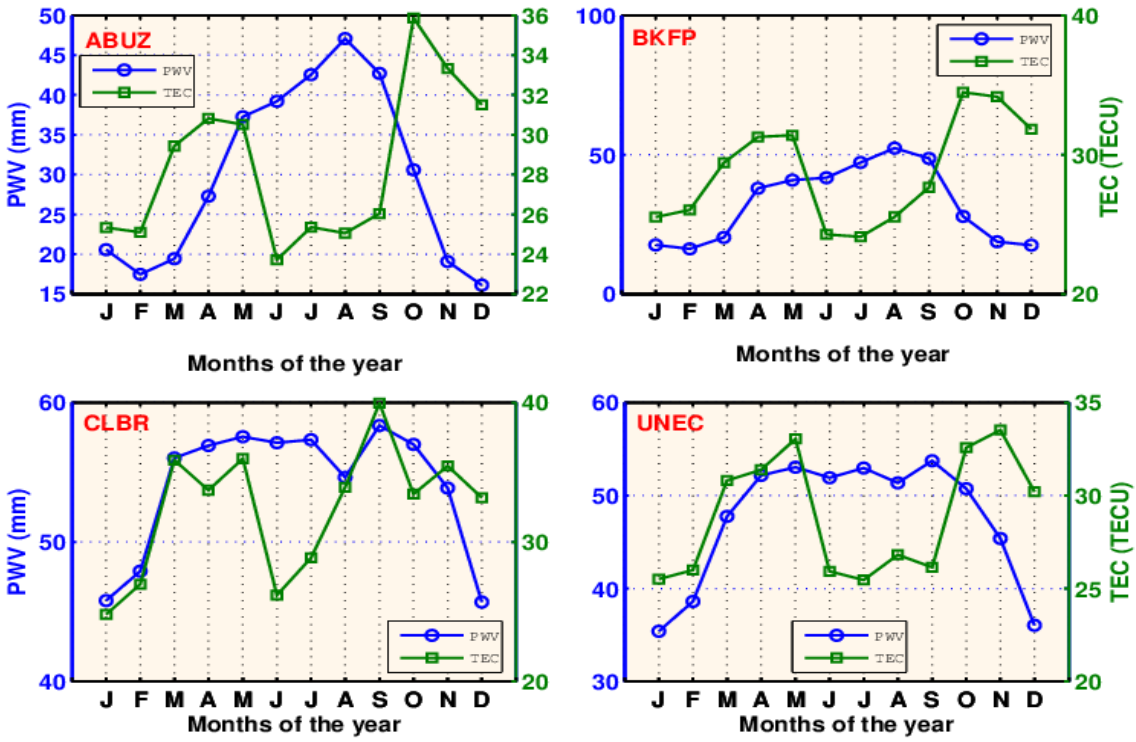

Figure 8.14: Monthly distribution of PWV (in blue) and TEC (in green) at four GNSS stations (ABUZ, BKFP, CLBR, and UNEC) in Nigeria

The TEC amount shown in Figure 8.14 is a key ionospheric parameter in monitoring ionospheric conditions and has features that are considerably influenced by the sun. TEC was generated alongside ZTD during the processing of GNSS observation files as described in section 8.2 of this report; the variation in ZTD is principally controlled by equivalent variations in PWV. The dynamics between the ionosphere and the lower atmosphere remains inadequately elucidated; a clear relationship between PWV and TEC can thus elucidate some of the physical processes through which solar activity affects terrestrial weather. According to Figure 8.14, average monthly TEC can be seen to exhibit an inverse relationship with PWV at the different stations. It can also be noticed that TEC values do show weak dependence on latitude and exhibit seasonal patterns with the lowest TEC values recorded in the months of JJA, which correspond to the peak PWV values at all the stations. Similarly, higher TEC values are seen in the months of SON, MAM and DJF, which are periods associated with lower PWV values. The variations in the ionosphere can have a regular or irregular pattern, depending on the geomagnetic activity level. Figure 8.15 shows the regular daily variation of TEC and PWV at four stations. The daily cycle reveals the difference in water vapour and TEC characteristics for 2013. In Figure 8.15 the seasonal variation pattern can be viewed from the day-to-day variations at the different stations.

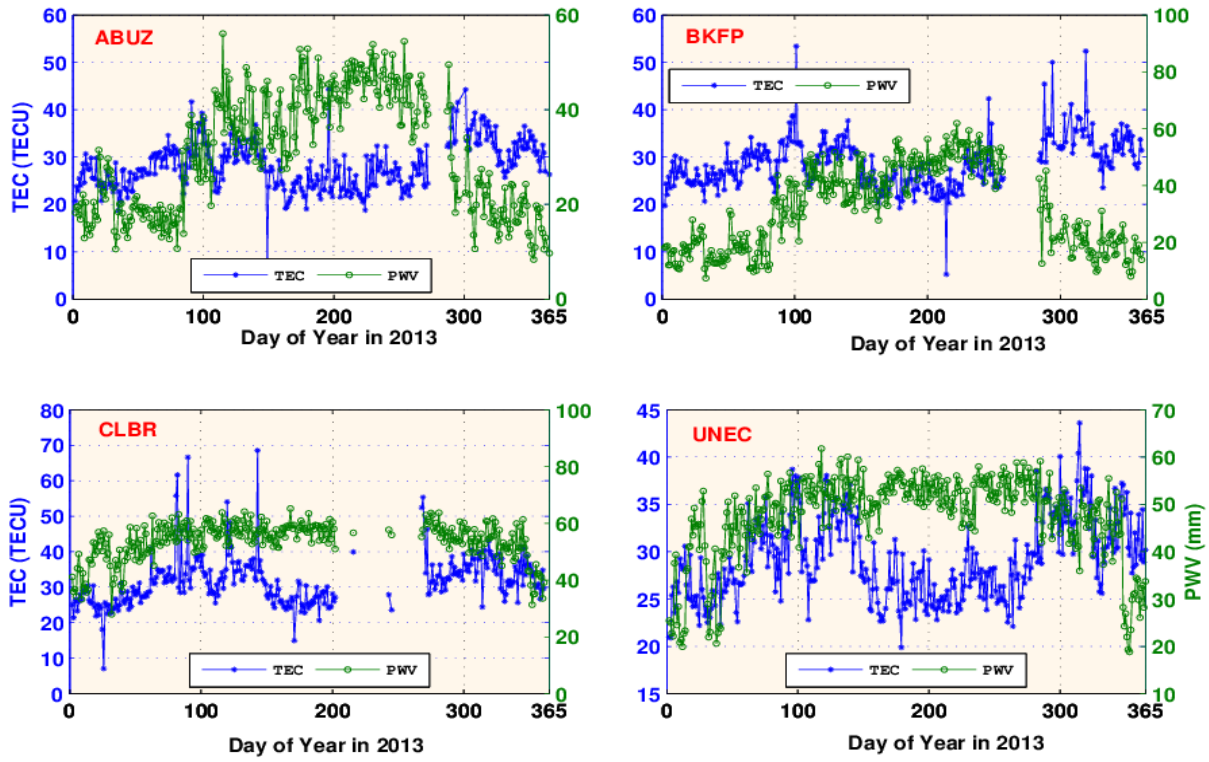

Figure 8.15: Daily average TEC (in blue) and PWV (in green) variations at four GNSS stations (ABUZ, BKFP, CLBR, and UNEC) for 2013

From the foregoing, it is clear that TEC is temporally and spatially variable. These variations during geomagnetic storms may become rapid and irregular and could cause significant bias in GNSS observation. Therefore, it is interesting to investigate how TEC estimated during an intense geomagnetic activity is linked to the lower atmosphere. Thus, we present results of two-hourly GNSS PWV and GNSS TEC measurement for two major solar/geomagnetic storms during the years 2013-2014. The solar flare records were obtained from solarham website (www.solarham.net). We consider the semi-diurnal cycles of the solar-24 top solar flares of classes X3.3 and X4.9, which occurred on the DOY 309 and 56 in November 2013 and February 2014, respectively. Data for one and a half days before and after the storm were analysed together to give a clear signature of the storm (see Figures 8.16 and 8.17). The R^2 values for the association between PWV and TEC before and after November 2013 at CLBR and UNEC are [0.5131 (51%) and 0.4783 (48%)] and [0.6092 (61%) and 0.3357 (34%)], respectively. During the storm (that is, between DOY 308.5 and 310.5), the R^2 value stood at 0.4816 (48%) and 0.7230 (72%) for CLBR and UNEC, respectively. Similarly, during the February 2014 storm, the R^2 values for the association between PWV and TEC before and after the storm at BKFP and UNEC were [0.7533 (75%) and 0.6162 (62%)] and [0.8672 (87%) and 0.3992 (40%)], respectively. During the storm (that is between DOY 55.5 and 57.5), the R^2 value stood at 0.7691 (77%) and 0.5641 (56%) for BKFP and UNEC, respectively. The strong R^2 values recorded during the period of the storms at the different GNSS stations indicate that the variation between PWV and TEC is largely accounted for during the occurrence of the geomagnetic storms. These results are, however, preliminary and are in good agreement with previous works that demonstrated the fact that the intensity of solar/geomagnetic activities is reflected in the PWV and TEC measurements at GNSS sites (Suparta et al., 2008).

In addition, in Figures 8.16 and 8.17, TEC is seen to exhibit a very conspicuous diurnal and semi-diurnal pattern (in contrast to PWV) with quite similar oscillatory patterns at the different stations; the semi-diurnal cycle for TEC reaches it maximum roughly around two hours after noon, and its minimum is reached before dawn.

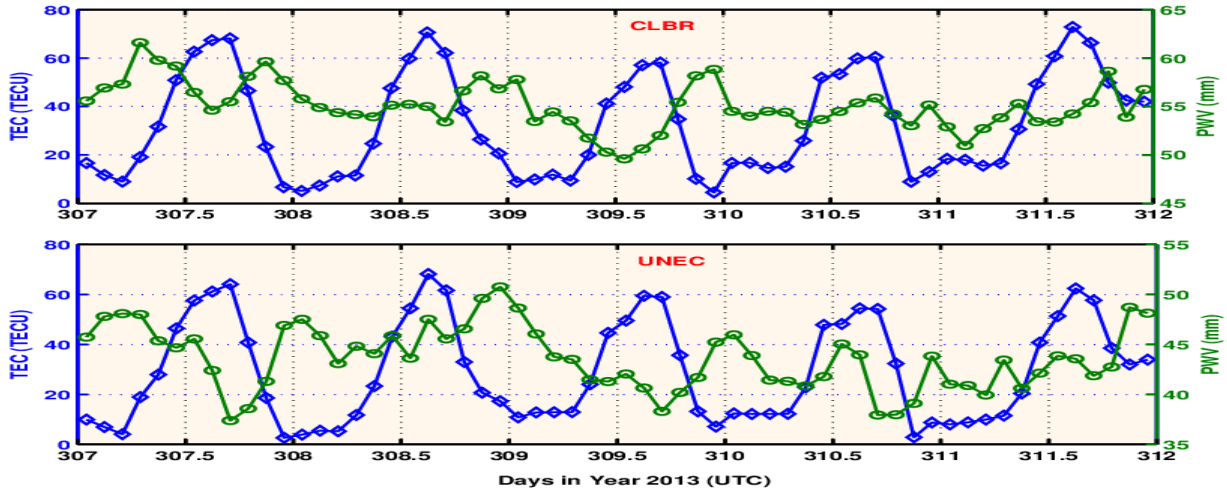

Figure 8.16: Plot of TEC and PWV at two GNSS stations (CLBR and UNEC) for DOY 307, 308, 309, 310 and 311 corresponding to November 2013 storm

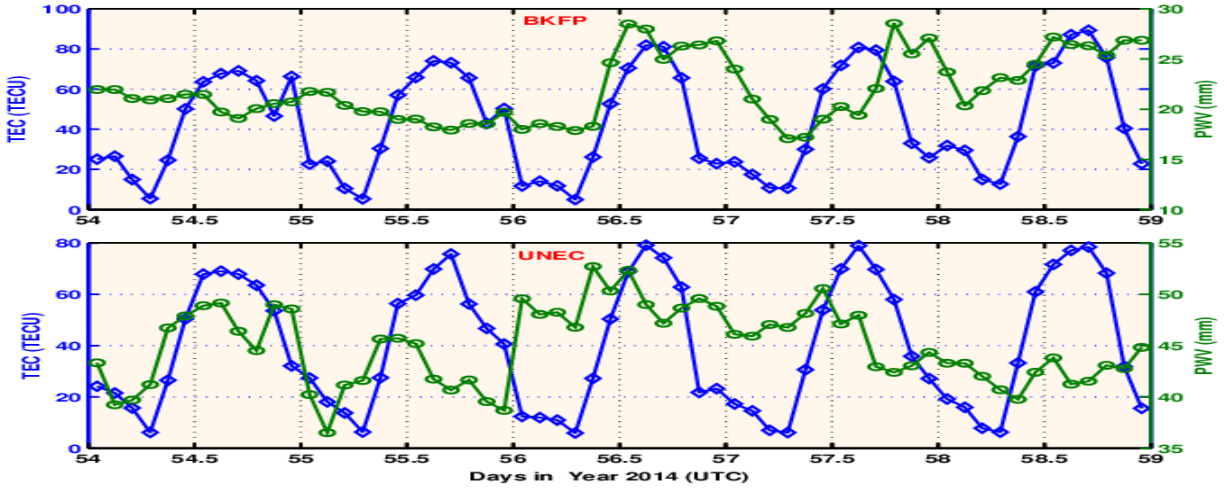

Figure 8.17: Plot of TEC and PWV at two GNSS stations (BKFP and UNEC) for DOY 54, 55, 56, 57 and 58 corresponding to February 2014 storm

The interplay among the different solar attributes as worked out from Pearson's correlation coefficient test is presented in Table 8.3. GNSS PWV is seen to have a strong positive correlation (significant at the 0.01 level) with SSN at the different stations. A strong negative correlation (significant at the 0.01 level) is also seen between GNSS PWV and total solar radiation. Interestingly, the correlation between GNSS PWV and the other attributes (temperature and TEC) is weak and insignificant. The SSN and radiation have very strong but negative agreement at all the stations. In addition, there is no statistically significant correlation (insignificant at the 0.01 level) between TEC and the other solar attributes at most of the stations, as shown by entries in red in Table8. 3.

Table8. 3: *Pearson's correlation coefficient matrix for GNSS- PWV and the different solar events (TEC, radiation, SSN, and temperature) at GNSS locations in Nigeria*

Variables	GNSS- PWV	Temp	SSN	TEC	Radiation	GNSS- PWV	Temp	SSN	TEC	Radiation
			ABUZ					BKFP		
GNSS- PWV	1	-0.0820	0.8487	-0.3928	-0.9417	1	-0.0332	0.8315	-0.3780	-0.8199
Temp		1	-0.1761	0.2561	0.2738		1	-0.2277	0.2241	0.4424
SSN			1	-0.0672	-0.8819			1	-0.1055	-0.8186
TEC				1	0.4181				1	0.4415
Radiation					1					1
			CLBR					UNEC		
GNSS- PWV	1	-0.4373	0.6877	0.4881	-0.8735	1	-0.2938	0.7655	0.1291	-0.9103
Temp		1	-0.9311	-0.2513	0.7955		1	-0.7260	0.3138	0.5438
SSN			1	0.3860	-0.9380			1	-0.0950	-0.9114
TEC				1	-0.4167				1	0.1424
Radiation					1					1

The R^2 (coefficient of determination) between GNSS PWV and the different solar attributes is shown in Figure 8.18. Evidently, this result of the coefficient of determination indicates that the variability in GNSS PWV can be adequately explained or predicted by a similar variation in SSN and TSR at the different GNSS locations under investigation. The predictability of GNSS PWV from TEC observations, as shown in Figure 8.18, is weak (less than 50%) at all the stations. This is in contrast to previous results from Figures 8.16 and 8.17, though it may imply that the diurnal relationship between GNSS PWV and TEC is stronger than the seasonal relationship. Notable, also from Figure 8.18, is the very weak variability accounted for in the monthly GNSS PWV and temperature relationship. This may imply that temperature does not play a major direct role in seasonal water vapour variation in the tropical region of West Africa where this study was conducted. The seasonal variability of water vapour is most probably dominated by that of humidity and the movement of the continental masses. This is contrary to the result of PWV and temperature seasonal relationship reported by some authors in other regions of the world, that suggests that an increase in temperature leads to a corresponding increase in the capacity of water vapour air masses, thus keeping the level away from saturation point and consequently preserving high PWV values (Maghrabi & Al Dajani, 2014; Suparta et al., 2008).

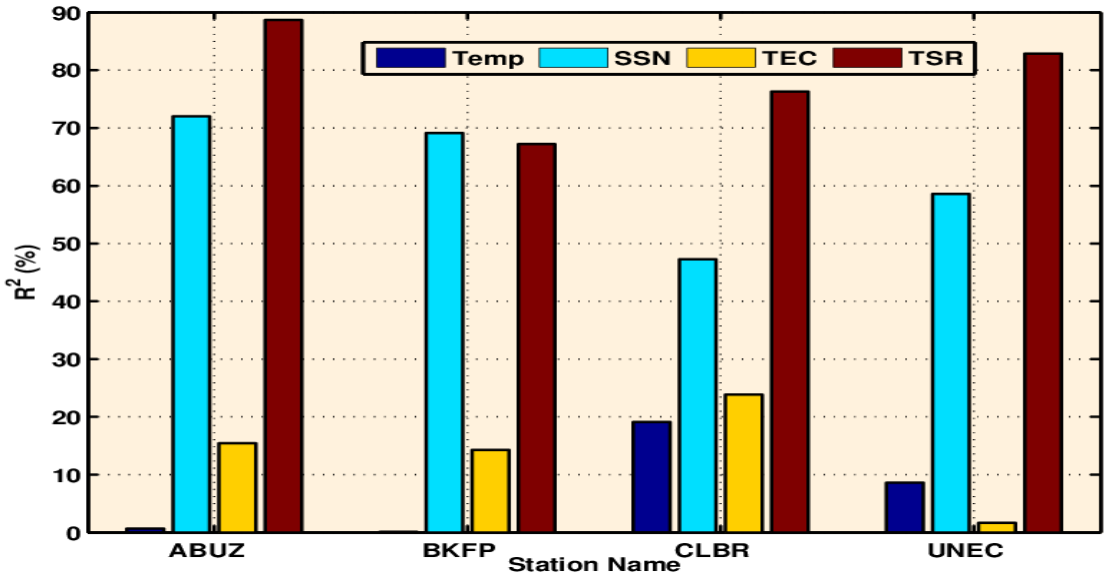

Figure 8.18: The coefficient of determination (R^2 in %) between GNSS PWV and the different solar attributes at four GNSS stations (ABUZ, BKFP, CLBR, and UNEC) in Nigeria

The relationship as determined from the multivariate analysis between the different solar activity and GNSS PWV at the different regions can be given as follows:

$$\left.\begin{aligned} GNSSPWV_{abuz} &= 302.02 - 1.04*Temp - 1.11*SSN + 0.24*TEC + 8.47*TSR \\ GNSSPWV_{bkfp} &= 888.64 + 2.10*Temp - 4.97*SSN + 0.70*TEC + 6.55*TSR \\ GNSSPWV_{clbr} &= 740.23 - 2.84*Temp + 0.64*SSN - 0.09*TEC + 4.50*TSR \\ GNSSPWV_{unec} &= 29.37 + 0.42*Temp - 1.39*SSN + 0.53*TEC - 6.36*TSR \end{aligned}\right\} . \qquad (8.7)$$

8.6 Concluding Remarks

In this paper, PWV was estimated from permanent GNSS stations within the new NIGNET with the objective of assessing the meteorological impact and possible applications of the variations in the atmospheric water content as estimated by GNSS. To achieve this objective, GNSS PWV daily estimates were grouped into monthly and seasonal averages; the variations in the monthly and seasonal estimates of GNSS PWV were characterised and correlated with different climate pointers. The climate pointers were broadly classified into rainfall events (rainfall, relative humidity, daylight cloud amount and wind speed) and solar activity (temperature, SSN, TEC, and TSR). The study of the relation or influence of the different rainfall events on predicting climate systems has received much attention from scientists around the world. Nevertheless, the impact of solar activity on the earth's atmospheric systems is still open for deliberation. This study is greatly restricted by the spatiotemporal resolution of ground meteorological data, which are needed in the retrieval of PWV from ZTD estimates and as such analysis was limited to GNSS stations with nearby

meteorological records at monthly and seasonal scales. This study represents a first step towards applying GNSS meteorology with regard to spatiotemporal variability, nowcasting/synoptic and climatic applications over Nigeria. Our main conclusions could be summarised as follows:

I. The analysis of the temporal variation of GNSS PWV over Nigeria for the period 2013-2014 reveals distinct seasonal cycles in the GNSS PWV estimates at all the GNSS stations investigated. The marked seasonal cycles are in the wet (rainy) season (during the months of JJA) with maximum PWV and in the dry/Harmattan season (during the months of DJF) with minimum PWV. The variation in PWV content between the period of maximum to minimum occurrence ranges from about 30 mm to 10 mm in the north and south of Nigeria respectively. This is an indication of the high variability in the nature of atmospheric dynamics and climate in the northern part of Nigeria.

II. Our result shows that GNSS PWV decreases with an increase in latitude, with an apparent distinction between southern and northern Nigeria. The average annual GNSS PWV estimate from the southernmost to the northernmost GNSS station stood at about 54.01 mm to 29.94 mm. The distribution patterns of GNSS PWV agree strongly with Nigeria's geographical locations and point toward the influence of the continental air masses (or trade winds).

III. Our study reveals a noticeable drop in the GNSS PWV content with increasing altitude. The R^2 value when the GNSS PWV was regressed with the individual station elevation was 0.7916 (79%), which is less than the 0.9648 (96%) when GNSS PWV estimates were regressed with station latitude. Thus the latitudinal dependence of GNSS PWV is stronger than that of the topography.

IV. Our study shows that there is a very strong seasonal interplay among the GNSS PWV, relative humidity, rainfall, and cloud estimates at all investigated GNSS locations in Nigeria; they are positively correlated to each other. The high R^2 values $\left(R^2 > 50\%\right)$ indicate that the variability in GNSS PWV can be adequately explained or predicted by a similar variation in rainfall, humidity and cloud amount or vice versa at the different locations in Nigeria. This result further justifies the need to assimilate GNSS products into regional models and Numerical Weather Prediction models, as such data could improve mid-term weather predictability, which is particularly useful for determining the likelihood of the onset of floods or the converse.

V. The correlation between GNSS PWV and wind speed observations is strongly negative at some stations and weakly positive at others. Also, it interplays with humidity and rainfall follows the same pattern at those stations. However, the correlation between wind speed and daylight cloud was insignificant at all stations.

VI. Our result reveals a weak seasonal and inverse relationship between GNSS PWV and temperature. This may imply that temperature does not play a major direct role in seasonal water vapour variation in the tropical region of West Africa where this study was conducted; the seasonal variability of GNSS PWV is thus most probably dominated by that of humidity and the movement of the continental masses.

VII. Our study shows that there is a very strong interplay among TSR, SSN and GNSS PWV. The TSR and SSN have an inverse and direct correlation with GNSS PWV, respectively. This result also reveals the strong influence of the sun on the earth's surface temperature through inward-bound TSR and so its effect is felt more strongly on GNSS PWV, as a weak relationship between GNSS PWV and temperature had been reported. .

VIII. Our study further affirms the relationship between clouds and TSR as described by Meehl et al. *(2003)*. The seasonal interplay among the GNSS PWV, clouds and TSR is very strong and together they can improve the predictability of each other and contribute to the subject of climate change and analysis.

IX. Our study shows that the TSR variability between seasons is converse to that of GNSS PWV, with maximum TSR occurring in seasons of minimum GNSS PWV and vice versa. Also, TSR exhibits an increasing trend northwards, in contrast to GNSS PWV, which decreases northwards. This further reflects the inverse relationship between TSR and GNSS PWV and their dependence on latitudinal variation. GNSS PWV variation in Nigeria is evidently controlled by the surface radiation balance. This means that a more active season would result from more energy transferring from the related sun activities to the earth's surface through its atmospheric dynamics.

X. Our study reveals from the results of the correlation between monthly GNSS PWV and the TEC estimate that an inverse relationship (though weak) exists between them. At diurnal scale, GNSS PWV and TEC measurement during two major solar storms during the years 2013-2014 revealed a strong diurnal trend between them. The R^2 values on the days of the respective storms were stronger than on the days before and after the storms. The reason for this remains unexplained. The results demonstrated the fact that the intensity of solar/geomagnetic activities is reflected in the GNSS

PWV and TEC measurements at GNSS sites, whereas the GNSS PWV and TEC estimates show an opposite relationship. The diurnal relationship between GNSS PWV and TEC is stronger than the seasonal relationship. The time series for both GNSS PWV and TEC reveals the seasonal dependence of both, and this demonstrates their applicability in operational meteorology and climate analysis. This analysis is a novel attempt at a possible characterisation of the nature of the upper and lower atmosphere in the region of the study and thus provides room for further investigation.

Undoubtedly, this study has demonstrated the viability of the GNSS meteorology technique over Nigeria as a new observational method with the potential of filling the existing gaps between current observational systems, based on its low cost, continuity, all-weather measuring capability and good spatiotemporal resolution. To explore the Nigerian weather and climate adequately, and to benefit optimally from the GNSS meteorology in Nigeria, further efforts are required. To obtain better correlation between GNSS PWV and meteorological events, it would probably be necessary to introduce the elaboration of slant water vapour contribution along the different lines of sight of GNSS receiver-satellites. If such a GNSS-based PWV measuring system were implemented, near-term/short-range weather forecasting and nowcasting would be possible, which may lead to a reduction in damage due to sudden severe weather conditions. In addition, such data could improve mid-term weather predictability, which is particularly useful for determining the likelihood of the onset of floods or the converse, severe drought. Also, the densification of the NIGNET, which should include the provision of meteorological sensors for PWV retrieval from ZTDs, is suggested. A dense network will contribute valuable water vapour field data for initialisation, setting boundary limits or substantiating NWPs and high resolution regional climate models.

The results of our study is preliminary in the sense that more complex statistical tests and a longer time period are required to validate the correlation between the different weather events/climate indices that were investigated properly. Long-term climatology would also benefit from the GNSS-derived water vapour time series if this should be made available. However, our results are in good agreement with previous studies around the world (Jin et al., 2008; Suparta, 2011) and provide the needed background for further study on the subject of climatic application of GNSS atmospheric products in Nigeria.

Acknowledgement

This study was supported and funded by the Tertiary Education Trust Fund (TETFund) of Nigeria, Surveyor Registration council of Nigeria (SURCON), and University of Pretoria PhD Research Support grant to the first author. The authors would wish to express their profound gratitude to the numerous reviewers for their productive observations that helped to perk up the manuscript. The authors thank CODE, SILSO, and the atmospheric science data centre of NASA for making the DCBs files, sunspot number and solar radiation data used in this study publicly available. We wish to thank the office of the Surveyor General of the Federal republic of Nigeria (OSGOF) for the GNSS data. Finally, thanks also go to Gopi Seemata for providing the GPS TEC analysis software.

Chapter 9

Conclusion, Outlook and Recommendations

"We are just an advanced breed of monkeys on a minor planet of a very average star. But we can understand the Universe. That makes us something very special."
— Stephen Hawking

The development, investigation and analysis of the use of atmospheric PWV derived from GNSS observations for operational meteorology and climate monitoring in Nigeria are the major goals of this research. This thesis presents the first comprehensive PhD study conducted in Nigeria on the GNSS remote sensing technique. This final chapter summarizes the results presented in this thesis in terms of the research objectives identified in the introductory chapter. Recommendations for future work on GNSS meteorology in Nigeria are also included.

9.1 Summary

Water vapour in the atmosphere plays an important role in meteorological applications. Monitoring the earth's atmosphere effectively and efficiently is one of the most significant and most complicated tasks in meteorology in view of the variability in water vapour content. The GNSS remote sensing technique has been proven to be an important alternative to the current atmospheric observation methods and can provide high quality and high resolution PWV observations at local, regional and global scales. It has the potential to revolutionise meteorological research and practice in the future. This thesis is a study on the application of GNSS for meteorology in Nigeria. The study is intended to address important questions and practical issues that are confronted by Nigeria in using GNSS atmospheric products for better meteorological services and climate monitoring. It is pertinent to note that the problem of climate change was indirectly addressed in this research, because the time period of the study (2010-2014) is relatively short compared to the time scale of observable changes due to climate change. Nevertheless, it has laid the foundation for future studies because the amount of water vapour in the atmosphere is of great significance to climate change.

The significant contributions of this research can be summarised as follows:

- Previous attempts by the AMMA GPS project (1999-2007), which was a meteorological project aimed at West Africa using GPS as a supporting observing

technique, did not collect any data from Nigeria (Bock et al., 2007; Walpersdorf, et al., 2007). AMMA remains the most comprehensive GPS meteorology project in the region of West Africa. Therefore, this research presents the first analysis of PWV estimates in Nigeria from a ground-based GNSS atmospheric sensing technique. Thus, the short-time variation and long-term trends in ZTD estimates as analysed in this thesis provide pioneering knowledge for weather and climatic studies in Nigeria based on GNSS.

- This research brings together data from currently operating GNSS CORS and AWOS in Nigeria. The GNSS CORS are operated by OSGOF and are established for positioning and navigation applications under the AFREF programme, while the AWOS serves the NIMET in operational meteorological services. This synergy adds significant extra value to this existing (and future) infrastructure. This effort also represents a first step towards the integration of a next-generation observing system that could significantly improve numerical weather and storm prediction, as well as address climate study applications in Nigeria.

- This research compares the statistical properties of surface variables (atmospheric pressure, temperature and humidity) from global reanalysis models (NCEP/NCAR and ERAI) with observations at AWOS over Nigeria. The results of the validation provide significant insight into the accuracy of the reanalysis models over Nigeria and thus serve as guide for GNSS users on the scale of variability and applicability of the models over Nigeria.

- A methodology for modelling meteorological parameters (atmospheric pressure, temperature and humidity) in a local GNSS network where no meteorological sensors have been installed has been achieved. Computer programs for the modelling of meteorological parameters in a local GNSS network have been developed.

- For the first time in Nigeria, the Nigerian weighted mean temperature equation has been determined from the fusion of radiosonde and reanalysis datasets. This is expected to be a significant tool for future retrieval of PWV from GNSS observation in Nigeria.

- The research correlates and gives insight into the interaction between the upper atmosphere (ionosphere) and the lower atmosphere (troposphere) over Nigeria, as

indicated by total electron content (TEC) and PWV estimates, respectively. Furthermore, precipitation events and PWV are related to each other in order to study the behaviour of PWV and its contribution to climate monitoring further.

9.2 Conclusions

The respective chapters of this thesis addressed the different objectives of the research. Accordingly, the conclusion will now be presented with respect to the research reflected in the chapters.

— ***The Potential of Observing African Weather with GNSS Remote Sensing***

This chapter addressed the first and second objectives of this thesis as outlined in the introductory chapter. It provided a background discussion on the theory of water vapour estimation from GNSS. It highlighted the operational requirements and standards for GNSS meteorology. A short review on the status of the African GNSS network was provided as well. This review work proved that the GNSS remote sensing technique can provide benchmark atmospheric data for future atmospheric studies. Nigerian meteorology can benefit significantly from the GNSS meteorology technique as well. Based on the existing and expected GNSS CORS in Africa, steps to improve GNSS meteorology were put forward for practical application of GNSS meteorology on the continent.

— ***Evaluation of Spatial and Temporal Characteristics of GNSS-Derived ZTD Estimates in Nigeria***

In this chapter the spatial and temporal variations of GNSS-derived ZTD were examined using data from the NIGNET. GNSS data from the NIGNET are available from 2010 onwards at a sampling rate of 30 sec. The time series of two-hourly GNSS ZTD from 2010–2014 on the NIGNET provided a unique and important dataset to evaluate the spatial dependence of ZTD estimates based on the NIGNET stations and also their temporal variations. The ZTD estimates showed weak spatial dependence among the stations, though this was attributed to the density of stations in the network. Tidal oscillations were noticed at the GNSS stations. These oscillations concerned the diurnal and semi-diurnal components. The diurnal components as seen from the ZTD were the principal source of the oscillations. These outcomes could perhaps be ascribed to temporal variations in atmospheric water vapour on a diurnal scale. In addition, the diurnal ZTD cycles exhibited noteworthy seasonal dependence, with larger amplitudes in the rainy (wet) season and smaller ones in the Harmattan (dry) season. Remarkably, the stations in the northern part of

the country reached very high amplitudes in the months of JJA at the peak of the wet season, characterised by very high rainfall. This emphasised that with the small amount of atmospheric water vapour in the atmosphere, usually around 10%, its variations greatly influence the corresponding diurnal and seasonal discrepancies of ZTD. This study affirmed the prospective relevance of ground-based GNSS data for atmospheric studies.

— ***Performance Evaluation of Blind Tropospheric Delay Correction Models over Africa***

In this chapter a comparative analysis to understand the accuracy of blind tropospheric models in the estimation of ZTD over Africa as a whole was presented. The chapter partly addressed the fourth objective of this research work. The study evaluated the accuracies of the UNB3m and GPT2w tropospheric correction models over Africa by using the ZTD time series from the global IGS GNSS network in Africa, and the Saastamoinen formula based on measured meteorological parameters. The GPT2w represents an excellent model for ZHD estimation owing to its highly accurate pressure estimates. The GPT2w model showed very good signatures of seasonal ZTD trends but weak daily variations, but in both cases better than the UNB3m model. The Saastamoinen model performed poorly with the use of standard atmospheric parameters and thus failed to address the peculiarities of the African GNSS network, which is characterised by a lack of sensors for measuring meteorological data. Thus, better estimates of ZTD from GNSS can be obtained with the GPT2w model without actual field measurements. Finally, there was better agreement between the GPT2w and IGS estimates at all stations. The results from this chapter clearly demonstrated the potential of blind tropospheric models in estimating tropospheric variables.

— ***Evaluation of Surface Variables from Global Reanalysis Models and their Application in Precipitable Water Vapour Retrieval from GNSS Observations over Nigeria***

This chapter investigated the usefulness of global reanalysis models (NCEP/NCAR and ERAI) and the GPT2 empirical model in GNSS meteorology. It also addressed the fourth objective of this research work. Surface variables (temperature, pressure, and relative humidity) from two reanalysis models (ERAI and NCEP/NCEP2) were evaluated against AWOS during a three-year period (2010-2012) over Nigeria for the purpose of ascertaining the suitability of reanalysis models in the retrieval of atmospheric PWV from GNSS observation. The study further introduced the GPT2 empirical meteorological model, whose

climatological datasets are based on ERAI reanalysis and which has been specifically developed for GNSS and other geodetic applications. For the two reanalysis datasets studied and for the sample stations chosen, NCEP/NCAR offered the greatest serial correlation with perfect coincidence with AWOS observations and the greatest internal consistency over the period 2010-2012 for the three surface variables (temperature, pressure, and relative humidity). In estimating relative humidity, the reanalysis models appeared not to be good predictors. Relative humidity varied widely at the stations, with RMSE ranging from 17.520 to 8.031% for ERAI and 38.162 to 9.125% for NCEP/NCAR. There was perfect agreement between the theoretically simulated precision of PWV estimated from ERAI and NCEP and that based on actual or practical formulations and data. Both estimates showed that PWV can be retrieved to a precision of about 1 mm, provided that GNSS ZTD is of high precision. The GPT model presented itself as a very promising model for the estimation of PWV, as it had the strongest correlation with the AWOS values in the estimation of ZHD, T_m, and PWV. The major shortfall of the model is that it can only be used in diurnal or annual estimation PWV, although it does give sub-daily meteorological parameters obtainable from its own source of climatological data. It must also be noted that large weather changes at synoptic time scales are not accounted for in the model and thus abrupt changes in PWV may not be adequately accounted for. The results from this chapter undoubtedly demonstrated the accuracy of the reanalysis models and the efficacy of the models in GNSS meteorology over Nigeria.

— ***Modelling Weighted Mean Temperature in West African Region: Implication for GNSS Meteorology***

This chapter addressed the fifth objective of this research work. Tropospheric weighted mean temperature (T_m) is a critical parameter in the estimation of PWV from ground-based GNSS receivers. In this chapter, models for the tropospheric weighted mean temperature were presented based on radiosonde and reanalysis data in the West African region. The performances of the models that were developed were promising compared with the global models, justifying the need to use measured meteorological parameters when estimating and fine-tuning the models to specific areas or regions. The results from this chapter demonstrated the usefulness of local models of weighted mean temperature in retrieving PWV from GNSS ZTD. The models presented in this chapter are expected to

serve as important parameters in future GNSS meteorological activities in the West African region.

— ***Retrieval and Analysis of Precipitable Water Vapour based on GNSS, AIRS, Reanalysis Models and CORDEX-Africa RCM Ensemble over Nigeria***

In this chapter, PWV retrieved from the NIGNET from 2013 to 2014 were compared with PWV from a regional climate model (CORDEX in the Africa domain), a satellite remote sensing technique (AIRS), and global reanalysis model (ERA-Interim) over Nigeria. All datasets gave a reasonable estimate of PWV at daily, monthly and seasonal scales, though the statistics were better at monthly and seasonal scales. The ERA-Interim outperformed the other techniques and could possibly be a complementary data source to GNSS PWV. The AIRS daytime (or ascending) retrieval was ranked next to the ERA-Interim, AIRS night-time (or descending) retrieval and CORDEX-RCM showed some discrepancies with GNSS PWV, even when compared with ERA-Interim and daytime AIRS. These results indicated that GNSS PWV as observed over the study area represented a remarkable dataset for further evaluation and could serve as a useful source of humidity information to improve the water cycle in numerical weather models for varying applications in the region. The results of this chapter provided an important source of information on the possible application of GNSS meteorology and helped addressed the sixth objective of the research.

— ***Assessing the Meteorological Impact of Variations in Atmospheric Water Vapour Content over Nigeria from GNSS Measurements***

In this chapter the variability in water vapour over Nigeria as observed by GNSS was evaluated. Noticeable seasonal trends were observed in the GNSS PWV estimates, as was a clear distinction in the distribution of water vapour from the south to the north of Nigeria. The trend in GNSS PWV distribution correlated well with other weather events over Nigeria. The study demonstrated the practicability of the GNSS meteorology technique over Nigeria as a new observational method with the potential of filling the existing gaps between current observational systems, based on its low cost, continuity, all-weather measuring capability and good spatiotemporal resolution. The chapter addressed the last objective of the research and thus provided the required background for further study on the subject of weather and climatic application of GNSS atmospheric products in Nigeria.

9.3 Outlook and Recommendations

Further studies need to be carried out on GNSS meteorology in Nigeria to improve the technique and usability of the retrievals. Some suggestions and recommendations are given below:

- A major drawback of ground-based GNSS meteorology is that it does not provide atmospheric profile information. In order to obtain information on the atmospheric profile, GNSS slant observation should be combined in tomographic analysis. This approach is expected to be a gateway into future 3D water vapour estimates at high resolution, pending the densification of the GNSS CORS in Nigeria.

- The exploration of the spaced-based atmospheric profile from the GNSS radio occultation technique (GNSS-RO) should be undertaken. A low earth orbit satellite receives GNSS signals during an occultation event, can determine the atmospheric bending angle that can be used to derive the vertical refractivity profile in the stratosphere and upper troposphere, and may thus improve the numerical weather models.

- Assimilation of GNSS atmospheric products into mesoscale NWP/RCMs for the development and improvement of local models for effective operational meteorological service and climate monitoring is required. Assimilation of GNSS atmospheric products into mesoscale models would require data from a dense GNSS network; thus there is a need for the densification of the NIGNET.

- As a step towards attaining an operational GNSS meteorology service in Nigeria, there is a need for clear policies on data sharing and collaboration among the different organisations that operate GNSS stations in the country. The idea of collaboration is to effect the densification of the GNSS network in Nigeria, since the budgetary allocation of OSGOF alone may not be able to provide the much needed number of GNSS stations for the country in coming years. Also, as already demonstrated in this thesis, there is a need for synergy between NIMET and OSGOF or any other organisation charged with the management of GNSS CORS in Nigeria, since the GNSS stations are not equipped with meteorological sensors. Such synergy will enable real time logging of meteorological data to enable NRT estimation of GNSS atmospheric conditions for effective operational meteorology.

In summary, this thesis presented a series of studies on the GNSS atmospheric sensing technique for Nigeria. The GNSS meteorology technique is a significant development in atmospheric monitoring and adopting the technique is a major landmark. Ever since the first GNSS atmospheric sensing results were presented in 1992, the improvement and recognition of the technique have been gaining momentum and have brought significant advantages to the meteorological community. The improvement of the technique will continue to provide robust solutions for earth's atmospheric monitoring. Nigeria should continue its investigations into GNSS meteorology for better meteorological services and also for better response to climate change monitoring and analysis.

References

1. Acheampong, A.A., Fosu, C., Amekudzi, L.K., & Kaas, E. 2015.Comparison of Precipitable Water over Ghana using GPS Signals and Reanalysis Products. *J.Geod. Sci*., 5, 163-170, doi: 10.1515/jogs-2015-0016.

2. Adamowski, J. & Prokoph, A. 2013. Assessing the Impacts of the Urban Heat Island Effect on Streamflow Patterns in Ottawa, Canada. *Journal of Hydrology*, 496(2013):225–237, http://dx.doi.org/10.1016/j.jhydrol.2013.05.032.

3. Adams, D.K., Fernandes, R.M.S., Kursinski, E.R., Maia, J.M., Sapucci, L.F., Machado, L.A.T., Vitorello, I., Monico, J.F.G., Kirk L., Holub, K.L., Seth, I., Gutman, S.I., Filizola, N., Richard, A. & Bennett, R.A. 2011. A Dense GNSS Meteorological Network for Observing Deep Convection in the Amazon. *Atmos. Sci. Let*, 12:207−212, doi:10.1002/asl.312.

4. Adelekan, I.O. 2000. A Survey of Rainstorms as Weather Hazards in Southern Nigeria, *Environmentalist*, Vol.20, Issue1, 33-39.

5. Ahmed F, Hunegnaw A, Teferle FN, and Bingley R (2015) Analysis of global climate variability from homogenously reprocessed ground-based GNSS measurements, Geophysical Research Abstracts Vol. 17, EGU2015-8981, 2015 EGU General Assembly.

6. AIRS Science Team/Joao Texeira. 2003. Aqua AIRS Level 3 Daily Standard Physical Retrieval (AIRS-Only), Version 006, Greenbelt, MD, USA: NASA Goddard Earth Science Data and Information Services Centre (GES DISC), Accessed 25/12/2015, doi: 10.5067/AQUA/AIRS/DATA303.

7. Alessi, M., & Egenhofer, C. 2011. *Space Observation Systems: An Underused Asset in EU and Global Climate Change Policy* [Online]. Report of the Centre for European Policy Studies (CEPS). Available: www.ceps.eu [2011, August 12].

8. Allen, R.M., & Ziv, A. 2011. Application of Real-Time GPS to Earthquake Early Warning. *Geophysical Research Letters*, 38(L16310), doi: 10.1029/2011GL047947.

9. Altamimi, Z., Collilieux, X. & Métivier, L. 2011. ITRF2008: An Improved Solution of the International Terrestrial Reference Frame. *J Geod*., 85:457–473, doi: 10.1007/S00190-011-0444-4.

10. Altamimi, Z., Sillard, P., & Boucher, C. 2002. ITRF2000: A New Release of the International Terrestrial Reference Frame for Earth Science Application. *Journal of Geophysical Research*, 107(B10):2214, doi: 10.1029/2001JB000561.

11. Altiner, Y., Bruyninx, C., Ihde, J., Mervant, L., Sohne, W & Weber, G. 2010. Development of the EUREF GNSS Services and Reference Networks. In *Workshop on the Application of GNSS.* Chisinau: Moldovia: 17-21.

12. Alves, D.B.M., Sapucci, L.F., Marques, H.A., De Souza, E.M., Gouveia, T.A.F. & Magario, J.A. 2015. Using a Regional Numerical Weather Prediction Model for GNSS Positioning over Brazil. *GPS Solutions*, doi:10.1007/S10291-015-0477-X.

13. American Geophysical Union (AGU), AIAA, NOAA, U.S.ATC, Washington, DC & Spilker, J.J. 1996. Tropospheric Effects on GPS; In: Spilker and Parkinson, *GPS Theory and Applications*, Progress In Astronautics and Aeronautics, 1(163):517.

14. Andrei, C.O. & Chen, R. 2009. Assessment of Time-Series of Troposphere Zenith Delays Derived from the Global Data Assimilation System Numerical Weather Model. *GPS Solutions*, 13(2):109, doi: 10.1007/s10291-008-0104-1.

15. Anselin L. 2003. *Geoda 0.9 User's Guide.* Centre for the Spatial Integration of Social Sciences and Spatial Analysis Laboratory. Urbana-Champaign, IL: Department Of Geography, University of Illinois. [Online], Available: http://www.sal.agecon.uinc/edu/csiss/pdf/Geoda093.Pdf.

16. Anselin L. 2005. *Exploring Spatial Data with Geoda™: A Workbook Geoda0.9 User's Guide.* Centre for the Spatial Integration of Social Sciences and Spatial Analysis Laboratory Urbana-Champaign, IL: Department of Geography, University of Illinois. [Online], Available: http://Geodacenter.Asu.Edu/System/Files/Geodaworkbook.Pdf.

17. Anselin, L. 1992. *Spatial Data Analysis with GIS: An Introduction to Application in the Social Sciences* [Online]. Santa Barbara, CA: National Centre for Geographic Information and Analysis, University Of California. Report 92-10:1-53. Available: http://www.ncgia.ucsb.edu/Technical-Reports/PDF/92-10.Pdf.

18. Anthes, R.A. 2011. Exploring Earth's Atmosphere With Radio Occultation: Contributions to Weather, Climate and Space Weather, *Atmos. Meas. Tech*, 4:1077−1103, doi: 10.5194/Amt-4-1077-2011.

19. Anthes, R.A., Bernhardt, P.A., Chen, Y., Cucurull, L., Dymond, K.F., Ector, D., Healy, S.B., Ho, S.P., Hunt, D.C., Kuo, Y.H., Liu, H., Manning, K., Mccleese, D.J., Meehan, T.K., Randel, W.J., Rocken, C., Schrener, W.S., Sokolovskiy, S.V., Thompson, D.C., Ternberth, K.E., Wee, T.K., Yen, N.L. & Zeng, Z. 2008. The COSMIC/FORMOST-3 Mission: Early Results. *Bulletin of the American Meteorological Society,* 89:313-333, doi:10.1175/BAMS-89-3-313, 2008.

20. Anthes, R.A., Rocken, C. & Kuo, Y.H. 2000. Applications of COSMIC To Meteorology and Climate. *Terrestrial, Atmospheric and Oceanic Sciences*, *Special Issue on COSMIC*, 11:115-156.

21. Aoki, K. & Kutsuwada, K. 2008. Verification of the Wind Driven Transport in the North Pacific Subtropical Gyre Using Gridded Wind Stress Products. *J. Oceanogr*, 64:49-60.

22. Aquila, A.D., Lucarini, V., Ruti, P.M. & Calmanti, S. 2005. Hayashi Spectra of the Northern Hemisphere Mid-Latitude Atmospheric Variability in the NCEP-NCAR and ECMWF Reanalyses. *Clim Dyn*, 25:639-652, doi: 10.1007/S00382-005-0048-X.

23. Askne, J. & Nordius, H. 1987. Estimation of Tropospheric Delay for Microwaves from Surface Weather Data. *Radio Science*, 22(3):379-386.

24. Atedhor, G.O., Odjugo, P.A.O. & Uriri, A.E. 2011. Changing Rainfall and Anthropogenic – Induced Flooding: Impacts and Adaptation Strategies in Benin City, Nigeria. *Journal of Geography and Regional Planning,* Vol.4 (1), Pp.42-52.

25. Awange, W.L. & Grafarend, E.W. 2005. Solving Algebraic Computational Problems in Geodesy and Geoinformatics, *Springer:* 344.

26. Awange, W.L., Grafarend, E.W., Palancz, B. & Zaletnyik. P. 2010. *Solving Algebraic Computational Problems in Geodesy and Geoinformatics*. Springer.

27. Bai, Z. & Feng, Y. 2003. GPS Water Vapour Estimation using Interpolated Surface Meteorological Data from the Australian Automatic Weather Stations, *Journal of Global Positioning Systems*, 2(2):83-89.

28. Bai, Z. 2004. Near-Real-Time GPS Sensing of Atmospheric Water Vapour. Doctoral Thesis. Australia: Queensland University Of Technology: 148.

29. Barkhuus, L. & Dey, A.K. 2003. Location-Based Services for Mobile Telephony: A Study of Users' Privacy Concerns. In *INTERACT*, 3:702-712.

30. Batisani, N. 2011. Spatio-temporal ephemeral stream flow as influenced by climate variability in Botswana, *J. Geogr. Sci*, 2011, **21**(3): 417-428, doi:10.1007/s11442-011-0854-5.

31. Bender, M., Dick, G., Wickert, J., Ramatschi, M., Ge, M., Gendt, G., Rothacher, M., Raabe, A. & Tetzlaff, G. 2009. Estimates of the Information Provided by GPS Slant Data Observed in Germany Regarding Tomographic Applications. *J. Geophys. Res.* 114(D06303).

32. Benevides, P., Catalao, J. & Miranda, P.M.A. 2015. On the Inclusion of GPS Precipitable Water Vapour in the Nowcasting of Rainfall, *Nat. Hazards Earth Syst. Sci.*, 15:2605–2616, doi:10.5194/Nhess-15-2605-2015.

33. Bennitt, G.V. & Jupp, A. 2012. Operational Assimilation of GPS Zenith Total Delay Observations into the UK Met Office Numerical Weather Prediction Models, *Mon. Weather Rev.,* 140:2706-2719, doi: 10.1175/MWR-D-11-00156.1.

34. Beranger, K., Barnier, B., Gulev, S. & Crepon, M. 2006. Comparing 20 Years of Precipitation Estimates from Different Sources over the World's Ocean. *Ocean Dynam*, 56:104-138, doi: 10.1007/s10236-006-0065-2.

35. Berman, A.L. 1976. *The Prediction of Zenith Range Refraction from Surface Measurements of Meteorological Parameters*. National Aeronautics and Space Administration Technical Report 32–1602:40. Pasadena, California: Jet Propulsion Laboratory, California Institute of Technology.

36. Beutler, G., Mueller, I.I. & Neilan, R.E. 1994. The International GPS Service for Geodynamics: Development and Start of Official Service on 1 January 1994. *Bulletin of Geodesique,* 68:39–70.

37. Bevis, M., Businger, S., Chiswell, S., Herring, T.A., Anthes, R.A., Rocken, C. & Ware, R.H. 1994. GPS Meteorology: Mapping Zenith Wet Delays onto Precipitable Water. *J. Appl. Meteorol.*, 33:79–386, doi:10.1175/1520- 0450.

38. Bevis, M., Businger, S., Herring, T.A., Rocken, C., Anthes, R.A. & Ware, R.H. 1992. GPS Meteorology: Remote Sensing of Atmospheric Water Vapour using the Global Positioning System. *J. Geophys. Res*., 97:15787–15801, doi: 10.1029/92JD01517.

39. Black, H.D. & Eisner, A. 1984. Correcting Satellite Doppler Data for Tropospheric Effects, *J.Geophys. Res*., 89(D2):2616-2626.

40. Blewitt, G. (Ed.). 2015. *GPS and Space-Based Geodetic Methods, In Treatise on Geophysics (Second Edition)* [Online]. Oxford: Elsevier. ISBN 9780444538031, http://dx.doi.org/10.1016/B978-0-444-53802-4.00060-9.

41. Bock, O. & Nuret, M. 2009. Verification of NWP Model Analyses and Radiosonde Humidity Data with GPS Precipitable Water Vapour Estimates During AMMA, *American Meteorological Society*, Special Collection:1085-1101, doi: 10.1175/2009 WAF 2222239.1.

42. Bock, O., Bouin, M.N., Walpersdorf, A., Lafore, J. P., Janicot, S., Guichard, F. & Agusti-Panareda, A. 2007a. Comparison of Ground-Based GPS Precipitable Water Vapour to Independent Observations and NWP Model Reanalyses Over Africa, *Q. J. R. Meteorol. Soc*, 133:2011-2027, doi:10.1002/qj.185.

43. Bock, O., Guichard, F., Janicot, S., Lafore, J.B., Bouin, M.N. & Sultan, B. 2007b. Multiscale Analysis of Precipitable Water Vapour over Africa from GPS Data and ECMWF Analyses. *Geophys. Res Lett*., 34(L09705), doi:10.1029/2006GL028039.

44. Bock, O., Guichard, F., Meynadier, R., Gervois, S., Agusti-Panareda, A., Beljaars, A., Boone, A., Nuret, M., Redelsperger, J.L. & Roucou, P. 2011.The Large-Scale Water Cycle of the West African Monsoon. *Atmosph. Sci. Lett*., 12:51–57, doi:10.1002/asl.288.

45. Bock, O., Keil, C., Richard, E., Flamant, C. & Bouin, M.N. 2005. Validation of Precipitable Water from ECMWF Model Analyses with GPS and Radiosonde Data during the MAP SOP. *Q. J. Roy. Meteorol. Soc*., 131:3013–3036, doi:10.1256/qj.05.27, 2005.

46. Bock, O., Willis, P., Lacarra, M. & Bosser, P. 2010. An Inter-Comparison of Zenith Tropospheric Delay Derived from DORIS and GPS Data, In DORIS Special Issue: Precise Orbit Determination and Application to the Earth Sciences, P.Willis (Ed.), *Advances in Space Research*, 46(12):1648-1660. doi: 10.1016/j.asr.2010.05.018.

47. Boehm, J., Heinkelmann, R. & Schuh, H. 2007. Short Note: A Global Model of Pressure and Temperature for Geodetic Applications. *Journal of Geodesy*, 81(10):679-683, doi: 10.1007/s00190-007-0135-3.

48. Boehm, J., Möller, G., Schindelegger, M., Pain, G. & Weber, R. 2014. Development of an Improved Blind Model for Slant Delays in the Troposphere (GPT2w). *GPS Solutions*. doi: 10.1007/s10291-014-0403-7.

49. Boehm, J., Niell, A., Tregoning, P. & Schuh, H. 2006b. Global Mapping Function (GMF): A New Empirical Mapping Function Based on Data from Numerical Weather Model Data. *Geophysical Research Letters*, 33(L07304), doi: 10.1029/2005GL025546.

50. Boehm, J., Werl, B. & Schuh, H. 2006a.Troposphere Mapping Functions For GPS and Very Long Baseline Interferometry from European Centre for Medium-Range Weather Forecasts Operational Analysis Data. *J. Geophys. Res.*, *111*(B02406), Doi: 10.1029/2005JB003629.

51. Bokoye, A.I., Royer, A., O'Neill, N.T., Cliche, P., Mcarthur, L.J.B., Teillet, P.M., Fedosejevs, G., & Theriault, J.-M. 2003. Multisensor Analysis of Integrated Atmospheric Water Vapour over Canada and Alaska. *J. Geophy. Res.: Atmospheres*, 108(D15):1984-2012.

52. Bollmeyer, C., Keller, J., Ohlwein, C., Bentzien, S., Crewell, S., Friedrichs, P., Hense, A., Keune, J., Kneifel, S., Pscheidt, I., Redl, S. & Steinke, S. 2015. Towards A High Resolution Regional Reanalysis for the European CORDEX Domain. *Q. J. Roy. Meteorol. Soc*., 141:1-15, Doi:10.1002/Qj.2486.

53. Bonafoni, S., Mazzoni, A., Cimini, D., Montopoli, M., Pierdicca, N., Basili, P., Ciotti, P. & Carlesimo, G. 2013. Assessment of Water Vapour Retrievals from A GPS Receiver Network. *GPS Solutions*, 17:475-484.

54. Bordi, I., Fraedrich, K., Petitta, M. & Sutera, A. 2006. Large Scale Assessment of Drought Variability Based on NCEP-NCAR and ERA-40 Reanalyses. *Water Resour Manag*, 20:899-915, doi: 10.1007/s11269-005-9013-Z.

55. Bosilovich, M.G., Kennedy, J., Dee, D., Allan, R. & O'Neill, A. 2013. On the Reprocessing and Reanalysis of Observations for Climate. In Asrar, G. and Hurrell, J. W. (Eds.). *Climate Science for Serving Society: Research, Modelling and Prediction Priorities*: 51–71. Netherlands: Springer.

56. Bosy, J., Kaplon, J., Rohm, W., Sierny, J. & Hadas, T. 2012. Near Real Time Estimation of Water Vapour in the Troposphere using Ground GNSS and the Meteorological Data. *Ann. Geophys.*, 30:1379-1391, doi:10.5194/Angeo-30-1379-2012.

57. Bosy, J., Rohm, W., Borkowski, A., Kroszczynski, K. & Figurski, M. 2010. Integration and Verification of Meteorological Observations and NWP Model Data for the Local GNSS Tomography. *Atmospheric Research,* 96:522-530, doi: 10.1016/J.Atmosres.2009.12.012.

58. Boutiouta, S. & Lahcene A. 2013. Preliminary Study of GNSS Meteorology Techniques in Algeria. *International Journal of Remote Sensing*, 34(14):5105-5118, doi:10.1080/01431161.2013.786850.

59. Bozzano, R., Siccardi, A., Schiano, M.E., Borghimi, M. & Castellari, S. 2004. Comparison of ECMWF Surface Meteorology and Buoy Observations in the Ligurian Sea. *Annales Geophysicae*, 22:317-330, doi:10.5194/Angeo-22-317-2004.

60. Braun, J.J., Mattioli, G., Calais, D.C.E., Jackson, M., Kursinski, R., Miller, M. & Pandya, R. 2012. Multi-Disciplinary Natural Hazards Research Initiative Begins Across Caribbean Basin. *EOS. Trans. AGU*, 93(9):89–90, doi:10.1029/2012EO090001.

61. Breusch, T. & Pagan, A. 1979. A Simple Test of Heteroskedascity and Random Coefficient Variation. *Econometrica,* 47:1287-1294.

62. Byun, S.H. & Bar-Sever, Y.E. 2009. A New Type of Troposphere Zenith Path Delay Product of the International GNSS Service. *J Geod*, 83:367-373. doi: 10.1007/S00190-008-0288-8.

63. Cam, E. *Et Al*. 2002. On the Estimation of Species Richness based on the Accumulation of Previously Unrecorded Species. *Ecography,* 25:102-108.

64. Cao, Y., Zheng, F., Xie, Y. & Bi, Y. 2008. Impact of the Weighted Mean Temperature on the Estimation of GPS Precipitable Water Vapour. In *ICMMT 2008 Proceedings*, Nanjing, China. [21-24 April].

65. Carslaw, K.S., Harrison, R.G. & Kirkby, J. 2002. Cosmic Rays, Clouds, and Climate, *Science*, 298(5599), 1732-1737.

66. Carter, B.A., Zhang, K., Norman, R., Kumar, V.V. & Kumar, S. 2013. On the Occurrence of Equatorial F-Region Irregularities during Solar Minimum using Radio Occultation Measurements, *J. Geophys. Res. Space Physics*, 118:892−904, doi:10.1002/Jgra.50089.

67. Chen, J. & Li, G. 2013. Diurnal Variations of Ground-Based GPS-PWV under Different Solar Radiation Intensity in the Chengdu Plain. *Journal of Geodynamics*, 72:81-95, http://dx.doi.org/10.1016/J.jog.2013.08.002.

68. Chen, P., Yao, W. & Zhu, X. 2014. Realization of Global Empirical Model for Mapping Zenith Wet Delays onto Precipitable Water Using NCEP Re-Analysis Data. *Geophys. J. Int.,* 198(3):1748-1757, doi: 10.1093/gji/ggu223.

69. Chen, Q., Song, S., Heise, S., Liou, Y.-A, Zhu, W. & Zhao, J. 2011. Assessment of ZTD Derived from ECMWF/NCEP Data with GPS ZTD over China*, GPS Solution*, doi: 10.1007/S10291-010-0200-X.

70. Choy, S., Wang, C.-S., Yeh, T.-K., Dawson, J., Jia, M. & Kuleshov, Y. 2015. Precipitable Water Vapour Estimates in the Australian Region from Ground Based GPS Observations. *Advances in Meteorology*, 2015:1-14, http://dx.doi.org/10.1155/2015/956481.

71. Cliff, A.D. & Ord, J.K. 1975. The Choice of a Test for Spatial Autocorrelation. In Davies, J.C. & Mccullagh, M.J. (Eds.). *Display and Analysis of Spatial Data*. London: John Wiley And Sons: 54-77.

72. Cliff, A.D. & Ord, J.K. 1981. S*patial Processes - Models and Applications.* London: Pion.

73. COESA. 1966. *U.S. Standard Atmosphere Supplements, 1966*. U.S. Committee on Extension to the Standard Atmosphere. Sponsored by Environmental Science Services Administration, National Aeronautics and Space Administration, United States Air Force and Published by the Superintendent of Documents, U.S. Government Printing Office, Washington, D.C.

74. Collins, J.P. & Langley, R.B. 1997. A Tropospheric Delay Model for the user of the Wide Area Augmentation System. *Final Contract Report for Nav Canada, Department of Geodesy and Geomatics Engineering*. Technical Report No. 187, Fredericton, Canada: University of New Brunswick.

75. Collins, J.P. & Langley, R.B. 1998. The Residual Tropospheric Propagation Delay: How Bad Can It Get? In *Proceedings of ION GPS-98, 11th International Technical Meeting of the Satellite Division.* Nashville, TN: The Institute of Navigation: 729-738. [15-18 September].

76. Collins, J.P. & Langley, R.B. 1999, *Nominal and Extreme Error Performance of the UNB3 Tropospheric Delay Model. Final Contract Report for Nav Canada, Department of Geodesy and Geomatics Engineering.* Technical Report No. 204, Fredericton, Canada: University of New Brunswick.

77. Combrinck, W.L. & Chin, M. 2001. IGS Stations: Station and Regional Issues, *Phys. Chem. Earth (A)*, 26(6-8):539-544.

78. Combrinck, W.L. & Chin, M. 2000. IGS Stations: Station and Regional Issues. In H.P. Plag, S. Barlag, M. Caissey, L. Combrinck, G. Elgered, A. Moore & H Van Der Marel. (Eds.). *Proceedings of the First COST Action 716 Workshop "Towards Operational GPS Meteorology" And the Second Network Workshop of the International GPS Service (IGS).* Norway: Oslo. [2000, July].

79. Combrink, A.Z.A., Combrinck, W.L. & Moraal, H. 2004. Near Real-Time Detection of Atmospheric Water Vapour using the SADC GPS Network. *South African Journal of Science*, 100(9-10):436–442.

80. Combrinck, L. 2013. General Relativity and Space Geodesy, "Sciences of Geodesy II", Editor Guochang Xu, Sciences of Geodesy - II , p. 53-95, Springer Berlin Heidelberg DOI: 10.1007/978-3-642- 28000-9_2.

81. Connolley, W.M. & Harangozo, S.A. 2001. A Comparison of Five Numerical Weather Prediction Analysis Climatologies in Southern High Latitudes. *J. Climate*, 14:30-44.

82. Cucurull, L. & Derber, J.C. 2008. Operational Implementation of COSMIC Observations into NCEP's Global Data Assimilation System. *Weather Forecasting*, 23:702−711, doi:10.1175/2008WAF2007070.1.

83. Cucurull, L., Derber, J. C. & Laparta, W. 2012. Assessing the Benefits of Assimilating GPS RO Profiles into Global Numerical Weather Prediction Models. *WMO Workshop,* [22-25 May]. Sedona, Arizona. [Online], Available: http://www.wmo.int/pages/prog/www/OSY~/meetings/~NWP5-sedona2012/ib5-cucurull.pdf.

84. Cucurull, L., Vandenberghe, F., Barker, D., Vilaclara, E., & Rius. 2004. Three-Dimensional Variational Data *Assimilation* of Groundbased GPS ZTD and Meteorological Observations during the 14 December 2001 Storm Event over the Western Mediterranean Sea. *Mon. Weather Rev.*, 132:749–763.

85. Cui, M.C., Feng, M. & Lian, S.M. 2000. Evaluation of Daily Precipitation in China from ECMWF and NCEP Reanalyses. *Chin J Oceanol and Limn.* 18(1):35-41.

86. Damon, P. E., and Laut , P.20 04.Pattern of strange errors plagues solar activity and terrestrial climate data, *Eos Trans. AGU*, 85(39), 370–374, doi:10.1029/2004EO390005.

87. Davis, J.L., Herring, T.A., Shapiro, I., Rogers, A.E. & Elgered, G. 1985. Geodesy by Interferometry: Effects of Atmospheric Modelling Errors on Estimates of Base Line Length. *Radio Sci.*, 20:1593–1607.

88. De Haan, S. 2006. National/Regional Operational Procedures of GPS Water Vapour Networks and Agreed International Procedures. *WMO: Instruments And Observing Methods*, 92: WMO/TD-No1340.

89. De Haan, S. 2008. Meteorological Applications of a Surface Network of Global Positioning System Receivers [Online]. Doctoral Thesis. Wageningen: Wageningen University. Available: www.radiometrics.com/data/uploads/2012/…/dehaan_doctoral-thesis-2008.pdf.

90. De Haan, S. 2013. Assimilation of GNSS ZTD and Radar Radial Velocity For The Benefit Of Very-Short-Range Regional Weather Forecasts. *Q.J.R. Meteorol. Soc.*, 139:2097-2107. http://dx.doi.org/10.1002/qj.2087.

91. De Haan, S., Holleman, I. & Holtslag, A.A.M. 2009. Real-Time Water Vapor Maps from A GPS Surface Network: Construction, Validation, and Applications. *J. Appl. Meteorol. Climatol.,* 48:1302-1316, doi: 10.1175/2008JAMC2024.1.

92. Dee, D. P., Balmaseda, M., Balsamo, G., Engelen, R., Simmons, A. J. & Thepaut, J.N. 2014. Towards A Consistent Reanalysis of the Climate System. *B. Am. Meteorol.* Soc., 95:1235–1248, doi:10.1175/BAMS-D-13-00043.1.

93. Dee, D.P. & Uppala, S. 2009. Variational Bias Correction of Satellite Radiance Data in the ERA-Interim Reanalysis. *Quart. J. R. Meteorol. Soc.*, 135:1830-1841, doi: 10.1002/qj.493.

94. Dee, D.P., Uppala, S. M., Simmons, A. J., Berrisford, P., Poli, P., Kobayashi, S., Andrae, U., Balmaseda, M. A., Balsamo, G., Bauer, P., Bechtold, P., Beljaars, A. C. M., Van De Berg, L., Bidlot, J., Bormann, N., Delsol, C., Dragani, R., Fuentes, M., Geer, A. J., Haimberger, L., Healy, S. B., Hersbach, H., Hólm, E. V., Isaksen, L., Kållberg, P., Köhler, M., Matricardi, M., Mcnally, A. P., Monge-Sanz, B. M., Morcrette, J.-J., Park, B.-K., Peubey, C., De Rosnay, P., Tavolato, C., Thépaut, J.-N. & Vitart, F. 2011. The ERA-Interim Reanalysis: Configuration and Performance of the Data Assimilation System. *Quart. J. R. Meteorol. Soc.*, 137:553-597, doi: 10.1002/qj.828.

95. Dick, G., Gendt, G. & Reigber, C. 2001. First Experience With Near Real Time Water Vapour Estimation in a German GPS Network. *Journal of Atmospheric and Solar-Terrestrial Physics*, 63(12):1295-1304.

96. Dickey, D.A. & Fuller, W.A. 1979. Distribution of the Estimators for Autoregressive Time Series with a Unit Root. *Journal of the American Statistical Association,* 74(366):427–431. JSTOR 2286348.

97. Divakarla, M.G., Barnet, C.D., Goldberg, M.D., Mcmillin, L.M., Maddy, E., Wolf, W., Zhou, L. & Liu, X. 2006. Validation of Atmospheric Infrared Sounder Temperature and Water Vapour Retrievals with Matched Radiosonde Measurements and Forecast. *J. Geophy. Res.,* 111(D09S15), doi: 10.1029/2005/JD00616.

98. Dodo, J.D. & Idowu, T.O. 2009. *Regional Assessment of the GPS Tropospheric Delay Models on the African GNSS Network.* Presented at the 3rd International Academy of Astronautics (IAA) African Regional Conference. Nigeria: Abuja. [2009, November 24-26].

99. Dodo, J.D. & Idowu, T.O. 2010. Regional Assessment of the GPS Tropospheric Delay Models on the African GNSS Network. *Journal of Emerging Trends in Engineering and Applied Sciences (JETEAS),* 1(1):113-121.

100. Dodo, J.D., Yakubu, T.A., Usifoh, E.S. & Bojude, A.M. 2011. ITRF 2008 Realization of the Nigerian Geocentric Datum (GDN2012): Preliminary Results. *Journal of Emerging Trends in Engineering and Applied Sciences (JETEAS)*. 2(6):978-986. UK: Scholarlink Research Institute Journals, 2011 (ISSN: 2141-7016).

101. Dodson, A.H., Chen, W., Baker, H.C., Penna, N.T., Roberts, G.W., Westbrook, J. & Jeans, R. 1999. Assessment of EGNOS Tropospheric Correction Model. In *proceedings of ION GPS-99, 12th International Technical Meeting of the Satellite Division.* Nashville, TN: The Institute of Navigation: 1401-1407. [14-17 September].

102. Dousa, J. & Vaclavovic P. 2014. Real-Time Zenith Tropospheric Delays in Support of Numerical Weather Prediction Applications. *Advances in Space Research*, 53(9):1347-1358, doi:10.1016/j.asr.2014.02.021.

103. Dow, J.M., Neilan, R.E. & Rizos, C. 2009. The International GNSS Service in a Changing Landscape of Global Navigation Satellite Systems. *J Geod*, 83:191-198. doi: 10.1007/s00190-008-0300-3.

104. Durre, I., Russell, S., Vose, R.S. & Wuertz, D.B. 2006. Overview of the Integrated Global Radiosonde Archive. *J. Climate*, 19:53–68, doi: http://dx.doi.org/10.1175/JCLI3594.1.

105. Egova, E.S. 2015. Integrated Water Vapour Comparison from GNSS and WRF Model for Bulgaria in 2013. Unpublished Master's Thesis. Bulgaria: Department of Meteorology and Geophysics, Sofia University.

106. Elgered, G., Plag, H.P., van der Marel, H., Barlag, S. & Nash, J. (Eds.) 2005. EUR 21639- COST action 716- Expoitation of Ground-Based GPS for Operational Numerical Weather Prediction and Climate Applications. *Final Report.* 18(2005):234.

107. Elliott, W.P. & Gaffen, D.J. 1991. On the Utility of Radiosonde Humidity Archives for Climate Studies. *Bull. Amer. Meteor. Soc*., 72:1507–1520.

108. Emardson, T.R., Elegered, T.R. & Johansson, J.M. 1998. Three Months of Continuous Monitoring of Atmospheric Water Vapour with a Network of Global Positioning System Receiver. *J Geophys Res.,* 103:1807-1820, doi: 10.1029/97JD03015.

109. ESA Galileo Programme. 2012. *Galileo Reference Troposphere Model for the User Receiver*, ESA-APPNG-REF/00621-AM, ver. 2.7.

110. Essen, L. & Froome, K.D. 1951. The Refractive Indices and Dielectric Constants of Air and its Principal Constituents at 24,000 Mc/s. *Proc. Phys. Soc. B.*, 64(10):862-875. [Online], Available: http://iopscience.iop.org/0370-1301/64/10/303.

111. Falvey, M. & John Beavan, J. 2002. The Impact of GPS Precipitable Water Assimilation on Mesoscale Model Retrievals of Orographic Rainfall during SALPEX'96. *Monthly Weather Review*, 30:2874-2887.

112. Fan, K. & Wang, H.J. 2004. Antarctic Oscillation and Dust Weather Frequency in North China, *Geophys. Res. Lett.*, 31(L10201).

113. Farah, A. 2011. Assessment of UNB3M Neutral Atmosphere Model and EGNOS Model for Near Equatorial Tropospheric Delay Correction. *Journal of Geomatics*, 5(2):67-72.

114. Feng, Y., Bai, Z., Fang, P. & Williams, A. 2001. GPS Water Vapour Experimental Results from Observations of the Australian Regional GPS Network (ARGN). In *2001: A Spatial Odyssey*. 42nd Australian Surveyors Congress.

115. Fernandez, L.I., Salio, P., Natali, M.P. & Meza, A.M. 2010. Estimation of Precipitable Water Vapour from GPS Measurements in Argentina: Validation and Qualitative analysis of Results. *Advances in Space Research,* 46(2010):879-894, doi: 10.1016/j.asr.2010.05.012.

116. Fernandes, M.J., Pires, N., Lazaro, C., & Nunes, A.L. 2013.Tropospheric Delays from GNSS for Application in Coastal Altimetry. Advances in Space Research, 51(8), doi:10.1016/j.asr.2012.04.025

117. Flato, G., Marotzke, J., Abiodun, B., Braconnot, P., Chou, S.C., Collins, W., Cox, P., Driouech, F., Emori, S. , Eyring, V., Forest, C., Gleckler, P. , Guilyardi, E. , Jakob, C., Kattsov, V., Reason, C., & Rummukainen, M. 2013. *Evaluation of Climate Models. In: Climate Change 2013: The Physical Science Basis.* Contribution of Working Group I to the Fifth Assessment Report of the Intergovernmental Panel on Climate Change [Stocker, T.F., D. Qin, G.-K. Plattner, M. Tignor, S.K. Allen, J. Boschung, A. Nauels, Y. Xia, V. Bex and P.M. Midgley (eds.)]. Cambridge University Press, Cambridge, United Kingdom and New York, NY, USA.

118. Flores, A., Ruffini, G. & Rius, A. 2000. 4D Tropospheric Tomography using GPS Slant Wet Delay. *Ann. Geophys*. 18:223–234.

119. Foelsche, U., Scherllin-Pirscher, B., Ladstädter, F., Steiner, A.K. & Kirchengast, G. 2011. Refractivity and Temperature Climate Records from Multiple Radio Occultation Satellites Consistent within 0.05%. *Atmos. Meas. Tech*, 4:2007−2018, doi: 10.5194/amt-4-2007-2011.

120. Friis Christensen, E., & Lassen, K. 1991. Length of the Solar Cycle: An Indicator of Solar Activity Closely Associated with Climate. *Science*, 254(698700).

121. Fu, E. 2011. *An Investigation of GNSS Radio Occultation Atmosphere Sounding Techniques for Australian Meteorology*. Doctoral thesis. Australia: RMIT University: 163.

122. Fund, F., Morel, L., Mocquet, A. & Boehm, J. 2011. Assessment of ECMWF Derived Tropospheric Delay Models within the EUREF Permanent Network. *GPS Solution*, 15:39-48, doi: 10.1007/s/10291-010--0166-8.

123. Gaylard, M.J., Bietenholz, M.F., Combrinck, L., Booth, R.S., Buchner, S.J., Fanaroff, B.L., MacLeod, G.C., Nicolson, G.D., Quick, J.F.H., Stronkhorst, P. & Venkatasubramani, T.L. 2011. An African VLBI Network of radio telescopes, In Basson, I. & Botha, A.E. (Eds.). *Proceedings of SAIP2011, the 56th Annual Conference of the South African Institute of Physics*. [Online]. Pretoria: University of South Africa: 473-478, ISBN: 978-1-86888-688-3. Available: http://www.saip.org.za.

124. GCOS. 2006. Systematic Observation Requirements for Satellite-based Products for Climate - Supplemental Details to the Satellite-Based Component of the 'Implementation Plan for the Global Observing System for Climate. In *Support of the UNFCCC', GCOS-107*.

125. Geary, R. 1954. The Contiguity Ratio and Statistical Mapping. *The Incorporated Statistician*, 5:115–145.

126. Gendt, G. & Schmid, R. 2005. Planned Changes to IGS Antenna Calibrations. *IGSMAIL-5189, IGS Ce*ntral Bureau. Avialable at http://igscb.jpl.nasa.gov/mail/igs.

127. Gendt, G., Dick, G., Reigber, C., Tomassini, M., Liu, Y. & Ramatschi, M. 2004. Near Real-Time GPS Water Vapour Monitoring for Numerical Weather Prediction in Germany. *Journal of the Meteorological Society of Japan,* 82:361–370.

128. Gendt, G., Reigber, C. & Dick, G. 2001. Near Real Time Water Vapour Estimation in a German Network - First Results from the Ground Program of the HGF GASP Project, *Physics and Chemistry of the Earth*, 26(6-8):413-416.

129. Geng, T., Xie, X., Fang, R., Su, X., Zhao, Q., Liu, G., Li, H., Shi, C. & Liu, J. 2015. Real-Time Capture of Seismic Waves using High-Rate Multi-GNSS Observations: Application to the 2015 Mw 7.8 Nepal Earthquake. *Geophys. Res. Lett.*, 42, doi:10.1002/2015GL067044.

130. Giorgi, F. 2006. Regional Climate Modeling: Status and Perspectives. *Journal de Physique IV (Proceedings)*, 139(1):101-118, DOI 10.1051/jp4:2006139008.

131. Gleisner, H., Thejll, P., Stendel, M., Kaas, E. & Machenhauer, B. 2005. Solar Signals in Tropospheric Re-analysis Data Comparing NCEP-NCAR and ERA-40. *J Atmos Sol-Terr Phy*, 67:785-791.

132. Goosse, H., Barriat, P.Y., Lefebvre, W., M.F. Loutre, M.F. & Zunz, V. 2010. *Introduction to Climate Dynamics and Climate Modeling*. Online Textbook Available at http://www.climate.be/textbook.

133. Gradinarsky, L.P., Johansson, J.M., Bouma, H. R., Scherneck, H.G. & Elgered, G. 2002. Climate Monitoring using GPS. *Phys. Chem. Earth*, 27:225-340, doi: 10.1016/s1474-7065(02)00009-8.

134. Gregow, H., Poli, P., Mäkelä, H.M., Jylhä, K., Kaiser-Weiss, A.K., Obregon, A., Tan, D. G.H., Kekki, S. & Kaspar, F. 2015. User Awareness Concerning Feedback Data and Input Observations used in Reanalysis Systems, *Adv. Sci. Res*., 12:63–67, doi:10.5194/asr-12-63-2015.

135. Grody, N., Zhao, J., Ferraro, R., Weng, F. & Biers, R. 2001. Determination of Precipitable Water and Cloud Liquid Water over Oceans from NOAA 15 Advanced Microwaves Sounding Unit. *Journal of Geophysical Research*, 106(D3):2943-2953.

136. Grody, N.C. (ed.). 1993. *Remote Sensing of the Atmosphere from Satellites using Microwave Radiometry, in Atmospheric Remote Sensing by Microwave Radiometry.* New Jersey: John Wiley, Hoboken.

137. Grotijahn, R. 2008. Different Data, Different Circulations: A comparison of Selected Fields in NCEP/DOE AMIP-II and ECMWF ERA-40 Reanalyses. *Dynam Atmos Oceans,* 44:108-142.

138. Gruteser, M. & Grunwald, D. 2003. Anonymous Usage of Location-Based Services through Spatial and Temporal Cloaking. In *Proceedings of the 1st International Conference on Mobile Systems, Applications and Services*, 31-42. ACM.

139. Guerova, G., Bettems, J.-M., Brockmann, E. & Matzler, C. 2006. Assimilation of COST 716 Near-Real Time GPS Data in the Non-hydrostatic Limited Area Model used at MeteoSwiss. *Meteorol. Atmos. Phys*., 91:149-164, doi: 10.1007/s00703-005-0110-6.

140. Gutman, S., Sahm, R., Benjamin, G., Schwartz, E., Holub, L., Stewart, Q. & Smith, L. 2004. Rapid Retrieval and Assimilation of Ground Based GPS-Met Observations at the NOAA Forecast Systems Laboratory: Impact on Weather Forecasts. *Journal of the Meteorological Society of Japan*, 82:351–360.

141. Haase, J., Vedel, H., Ge, M. & Calais, E. 2000. Radiosonde and GPS Zenith Tropospheric Delay (ZTD) Variability in the Mediterranean. Presented at *COST Action 716 Workshop*, Oslo.

142. Hadas, T., Kaplon, T., Bosy, J., Sierny, J. & Wilgan, K. 2013. Near-Real-Time Regional Troposphere Models for the GNSS Precise Point Positioning Technique. *Meas. Sci. Tech.* 24(2013, 055003):12, doi: 10.1088/0957-0233/24/5/055003.

143. Hagan, M.E., Forbes, J.M. & Richmond, A. 2003. *Atmospheric Tides*. Encyclopaedia of Atmospheric Sciences.

144. Haining, R.P. 2003. *Spatial Data Analysis: Theory and Practice*. Cambridge: University of Cambridge Press.

145. Hammond, W.C. 2005. The Ghost of an Earthquake. *Science,* 310:1440–1442.

146. Hanning, R.P. 1990. *Spatial Data Analysis in the Social and Environmental Sciences*. Cambridge: University of Cambridge Press.

147. Hanson, C.E., Palutikof, J.P. & Davies, T.D. 2004. Objective Cyclone Climatologies of the North Atlantic: A Comaprison between the ECMWF and NCEP Reanalyses. *Clim Dyn* 22:757-769, doi: 10.1007/s00382-004-0415-z.

148. Hartmann, D.L., Klein Tank, A.M.G., Rusticucci, M., Alexander, L.V., Brönnimann, S., Charabi, Y., Dentener, F.J., Dlugokencky, E.J., Easterling, D.R., Kaplan, A., Soden, B.J., Thorne, P.W., Wild, M. & Zhai, P.M. 2013. Observations: Atmosphere and surface. In *Climate Change 2013: The Physical Science Basis*. Contribution of Working Group I to the Fifth Assessment Report of the Intergovernmental Panel on Climate Change. Cambridge: Cambridge University Press and New York: Cambridge University Press.

149. He, C., Y, Y., Zhao, D., Li, K. & Qian, C. 2013. GWMT Global Atmospheric Weighted Mean Temperature Models: Development and Refinement. In J. Sun et al. (eds.), *China Satellite Navigation Conference (CSNC) 2013 Proceedings*, Lecture Notes in Electrical Engineering: 244, doi: 10.1007/978-3-642-37404-3_40.

150. Herring, T.A., King, R.W. & McClusky, S.C. 2006. *Introduction to GAMIT/GLOBK, Release 10.3*, Massachusetts: Department of Earth, Atmospheric and Planetary Sciences, Massachusetts Institute of Technology, Cambridge.

151. Higazi, S.F., Abdel-Hady, D.H. & Al-Oulfi, S.A. 2013 Application of Spatial Regression Models to Income Poverty Ratios in Middle Delta Contiguous Counties in Egypt. *Pak.j.stat.oper.res.,* 10(1):93-110.

152. Hobiger, T., Shimadab, S., Shimizub, S., Ichikawa, R., Koyamaa, Y. & Kondoa, T. 2010. Improving GPS Positioning Estimates during Extreme Weather Situations by the Help of Fine Mesh Numerical Models. *J. Atmos Solar Terr Phys*, 72:262-270, doi; 10.1016/j.jastp.2009.11.018.

153. Hoffmann-Wellenhof, B., Lichtenegger, B. & Wasle, E. 2008. *GNSS – Global Navigation Satellite Systems; GPS, GLONASS, Galileo, and more.* New York: Springer-Verlag.

154. Hopfield, H.S. 1969. Two Quartic Tropospheric Refractive Profiles for Correcting Satellite Data. *J. Geophys. Res.*, 74(18):4487-4499.

155. Hordyniec, P., Bosy, J. & Rohm, W. 2015. Assessment of Errors in Precipitable Water Data Derived from Global Navigation Satellite System Observations. *Journal of Atmospheric and Solar-Terrestrial Physics*, 129(2015):69-77, http://dx.doi.org/10.1016/j.jastp.2015.04.012.

156. Humphreys, T.E., Kelley, M.C., Huber, N. & Kintner, J.M. 2005. The Semidiurnal Variation in GPS-Derived Zenith Neutral Delay. *Geophysical Research Letters*, 32(24):1–4, doi: 10.1029/2005GL024207.

157. ICAO. 1996. International Standards and Recommended Practices: Aeronautical Telecommunications (5th ed.). *Radio Navigation Aids*, 1(10).

158. Ifadis, I.I. 1986. The Atmospheric Delay of Radio Waves: Modeling the Elevation Dependence on a Global Scale. *Technical Report 38L.* Goteborg, Sweden: Chalmers University of Technology.

159. Ihde, J. 2008. Developments of the EUREF GNSS Services and Reference Networks. A Paper Presented at ICG-03 meeting. 8-12 December, USA: Pasaden.

160. Immler, F.J., Dykema, J., Gardiner, T., Whiteman, D.N., Thorne, P.W. & Vome, H. 2010. Reference Quality Upper-air Measurements: Guidance for Developing GRUAN Data Products. *Atmos. Meas. Tech*., 3:1217-1231, doi:10.5194/amt-3-1217-2010.

161. IPCC. 2001a. Climate Change 2001: The Scientific Basis. Contribution of Working IPCC. The Scientific Basis. *Contribution of Working Group I to the Third Assessment Report of the Intergovernmental Panel on Climate Change.* Cambridge: Cambridge University Press, UK.

162. IPCC. 2001b. Climate Change 2001: Impacts, Adaptation, and Vulnerability. *IPCC. Report of the Intergovernmental Panel on Climate Change.* Cambridge: Cambridge University Press, UK.

163. IPCC. 2007. Summary for Policymakers. In Solomon, S., Qin, D., Manning, M., Chen, Z., Marquis, M., Averyt, K.B., Tignor, M. & Miller, H.L. (Eds.). *Climate Change 2007: The Physical Science Basis. Contribution of Working Group I to the Fourth Assessment Report of the Intergovernmental Panel on Climate Change.* Cambridge: Cambridge University Press.

164. Isioye, O.A. 2011. Towards An Operational Near Real Time Meteorology on the African GNSS Network: Challenges and Benefits. *Nigerian Journal of Scientific Research,* 9&10:90–98. Nigeria: Ahmadu Bello University, available at njsr.abu.edu.ng/publications/2011_12.pdf.

165. Isioye, O.A., Combrinck, L., Botai, J.O. & Munghemezulu, C. 2015a. The Potential of Observing African Weather with GNSS Remote Sensing. *Advances in Meteorology*, 2015(723071):1-16, http://dx.doi.org/10/1155/2015/723071.

166. Isioye, O.A., Combrinck, L. & Botai, J.O. 2015b. Performance evaluation of the GPT2w and UNB3m Tropospheric Delay Correction Models over Africa [Online]. *A Presentation at the United Nations/Russian Federation Workshop on the Application of Global Navigation Satellite Systems.* Russia Federation: Krasnoyarsk. [2015, May 18-22]. Available: *http://www.unoosa.org/oosa/en/SAP/act2015/russia-gnss/2015workshop-gnss.html*

167. Isioye, O.A., Combrinck, L. & Botai, J.O. 2015c. Performance Evaluation of Blind Tropospheric Delay Correction Models over Africa. *South African Journal of Geomatics*, 4(4), 502-525, doi: http://dx.doi.org/10.4314/sajg.v4i4.8.

168. Isioye, O.A., Combrinck, L. & Botai, J.O. 2016a. Modelling Weighted Mean Temperature in the West African Region: Implications for GNSS Meteorology. *Meteorological Applications*, volume 23, issue 4, 614-632, http://dx.doi.org/10.1002/met.1584.

169. Isioye, O.A., Combrinck, L. & Botai, J.O. 2016b. Evaluation of Spatial and Temporal Characteristics of GNSS-Derived ZTD Estimates in Nigeria. *Theoretical and Applied Climatology* (Revised).

170. Isioye O. A. 2016.Evaluation of Surface Variables from Global Reanalysis Models and their application in Precipitable Water Vapour Retrieval from GNSS Observations over Nigeria. Proceedings of the 29th International Technical Meeting of the satellite division of the Institute of Navigation (ION GNSS + 2016), Portland, Oregon, USA, pp.1617-1641, September 12-16, 2016. https://www.ion.org/publications/abstract.cfm?~ jp=p&articleID=14723.

171. Isioye, O.A., Combrinck, L. & Botai, J.O. 2014. Modelling of Atmospheric Parameters over Nigeria based on GNSS Data. *A Presentation at the United Nations/Abdus Salam International Centre for Theoretical Physics Workshop on the use of Global Navigation Satellite Systems for*

Scientific Applications, Trieste, Italy. [1-5 December]. [Online], Available: http://www.unoosa.org/pdf/sap/2014/trieste-gnss/23.pdf.

172. Jade, S. & Vijayan, M.S.M. 2008. GPS- Based Atmospheric Precipitable Water Vapour Estimation using Meteorological Parameters Interpolated from NCEP Global Reanalysis Data. *J.Geophys. Res*., 113(D03106), doi: 10.1029/2007JD008758.

173. Jade, S., Vijayan, M.S.M., Gaur, V.K., Prabhu, T.P. & Sahu, S.C. 2005. Estimates of Precipitable Water Vapour from GPS Data over the Indian Subcontinent. *Journal of Atmospheric and Solar-Terrestrial Physics,* 67(2005):623-635, doi: 10.1016/j.jastp.2004.12.010.

174. Jakobson, E., Vihma, T., Palo, T., Jakobson, L., Keernik, H. & Jaagus, J. 2012. Validation of Atmospheric Reanalyses over the Central Arctic Ocean. *Geophys. Res. Lett*., 39(L10802), doi:10.1029/2012GL051591.

175. Jatau, B., Rui, M., Adeyemi, A. & Nuno, G. 2010. NIGNET: The New Permanent GNSS Network of Nigeria. *FIG Congress 2010: Facing the Challenges – Building the Capacity,* Sydney: Australia. [Online], Available: http://fig.net/pub/fig2010/papers/fs02h%5Cfs02h_jatau_fernandes_et_al_4549.pdf. [April 11-16].

176. Jerrett, D. & Nash, J. 2001. Potential uses of Surface Based GPS Water Vapour Measurements for Meteorological Purposes. *Phys. Chem. Earth (A)*, 26(6-8):457-461, PII: S1464-1895(01)00083-7.

177. Jin, S., Feng, G.P. & Gleason, S. 2011. Remote Sensing using GNSS Signals: Current Status and Future Directions. *Advances in Space Research,* 47(2011):1691-1703, doi: 10.1016/j.asr.2010.10.028.

178. Jin, S., Luo, O.F. & Cho, J. 2009a. Systematic Errors between VLBI and GPS Precipitable Water Vapour Estimations from 5-year Co-located Measurements. *J. Atmos. Solar–Terr. Phys*., 71:264–272, doi:10.1016/j.jastp.2008.11.018.

179. Jin, S., Luo, O.F. & Gleason, S. 2009b. Characterization of Diurnal Cycles in ZTD from a Decade of Global GPS Observations. *J. Geod,* 83(2009):537-545, doi:10.1007/s00190-008-0264-3.

180. Jin, S.G**.** & Luo, O.F. 2009c. Variability and Climatology of PWV from Global 13-year GPS Observations. *IEEE Trans. Geosci. Remote Sensing*, 47(7):1918-1924, doi: 10.1109/TGRS.2008.2010401.

181. Jin, S.G., Li, Z. & Cho, J. 2008. Integrated Water Vapour Field and Multiscale Variations over China from GPS Measurements. *Journal of Applied Meteorology and Climatology*, 47:3008-3015, doi:10.1175/2008JAMC1920.1.

182. Jin, S.G**.**, Park, J., Cho, J. & Park, P. 2007. Seasonal Variability of GPS-Derived Zenith Tropospheric Delay (1994-2006) and Climate Implications. *J. Geophys. Res.*, 112(D09110), doi: 10.1029/2006JD007772.

183. Jolliffe, I.T. & Stephenson, D.B. (Eds.). 2003. *Forecast Verification: A Practitioner's Guide in Atmospheric Science*. Chichester: John Wiley and Sons: 240.

184. Jones, J. 2010. *An Assessment of the Quality of GPS Water Vapour Estimates and their use in Operational Meteorology and Climate monitoring* [Online]. Doctoral thesis, University of Nottingham, United Kingdom. Available: http://eprint.nottingham.ac.uk/~11287/1/JJ_Thesis_Final.pdf.

185. Jupp, S.M., Powe, J., Owen, J. & Butcher, X. 2003. Use of Numerical Weather Prediction Fields for the Improvement of Tropospheric Corrections in Global Positioning Applications. *Proc. ION GPS 2003*. Portland: Institute of Navigation: 377-389. [9-12 September].

186. Kaiser-Weiss, A.K., Kaspar, F., Heene, V., Borsche, M., Tan, D.G.H., Poli, P., Obregon, A. & Gregow, H. 2015. Comparison of Regional and Global Reanalysis near Surface Winds with Station Observations over Germany. *Adv. Sci. Res.,* 12:187-198, doi: 10.5194/asr-12-187-2015.

187. Kalnay, E., Kanamitsu, M., Kistler, R., Collins, W., Deaven, D., Gandin, L., Iredell, M., Saha, S., White, G., Woollen, J., Zhu, Y., Leetmaa, A., Reynolds, R., Chelliah, M., Ebisuzaki, W. Higgins, W., Janowiak, J., Mo, K.C., Ropelewski, C., Wang, J., Jenne, R., Joseph, D. 1996. The NCEP/NCAR 40-Year Reanalysis Project. *Bull. Amer. Meteor. Soc*., 77:437-470, doi: 10.1175/1520-0477(1996)077<0437:TNYRP>2.0.CO;2.

188. Karabatic, A., Weber, R. & Haiden, T. 2011. Near Real Time Estimation of Troposheric Water Vapour Content from Ground Based GNSS Data and its Potential Contribution to Weather Now-casting in Austria. *Advances in Space Research*, 47(2011):1691-1703, doi:10.1016/j.asr.2010.10.028.

189. Karmeshu, M. 2012. *Trend Detection in Annual Temperature & Precipitation using the Mann Kendall Test – A Case Study to Assess Climate Change on Select States in the North Eastern United States*. Master's Thesis. Pennsylvania: University of Pennsylvania Scholarly Commons. Available: http://repository.upenn.edu/cgi/viewcontent.cgi?article=1045&context=mes~_capstones.

190. Katsougiannopoulos, S., Pikridas, C., Zinas, N., Chatzinikos, M. & Bitharis, S. 2015. Analysis of Precipitable Water Estimates using Permanent GPS Station Data during the Athens Heavy Rainfall on February 22th 2013. *International Association of Geodesy Symposia*, doi:10.1007/1345_2015_16.

191. Kendall, M.G. 1975. *Rank Correlation Measures*. London: Charles Griffin.

192. Kennish, M. J. 2001. *Practical Handbook of Marine Science* (3rd ed.). USA: Boca Raton, CRC Press.

193. Kishore, P., VenkatRatnam, M., Mamboothiri, S.P., Velicogna, I., Basha, G., Jiang, J.H., Igarashi, K., Rao, S.V.B. & Sivakumar, V. 2011. Global (50S - 50N) Distribution of Water Vapour observed by COSMIC GPS RO: Comparison with GPS Radiosonde, NCEP, ERA-Interim & IRA-25 Reanalysis Data Sets. *Journal of Atmospheric and Solar Terrestrial Physics,* 73(2011):1849-1860, doi:10.1016/j.astp.2011.04.017.

194. Kistler, R., Collins, W., Saha, S., White, G., Woollen, J., Kalnay, E., Chelliah, M., Ebisuzaki, W., Kanamitsu, M., Kousky, V., van den Dool, H., Jenne, R. & Fiorino, M. 2001. The NCEP–NCAR 50–Year Reanalysis: Monthly Means CD–ROM and Documentation. *Bull. Amer. Meteor. Soc.*, 82:247-267, doi:10.1175/1520-0477(2001)082<0247:TNNYRM>2.3.CO;2.

195. Kleijer, F. 2004. *Troposphere Modelling and Filtering for Precise GPS Levelling*. Doctoral Thesis. Kluyverweg: Delft University of Technology: 260.

196. Koizumi, K. & Sato, Y. 2004. Impact of GPS and TMI Precipitable Water Data on Mesoscale Numerical Weather Prediction Model Forecasts. *J. Meteor. Soc. Japan.*, 82:453-457.

197. Koizumi, K., Ishikawa, Y. & Tsuyuki, T. 2005. Assimilation of Precipitation Data to the JMA Mesoscale Model with a Four-Dimensional Variational Method and its Impact on Precipitation Forecasts. *SOLA*, 1:45-48.

198. Kopken, C. 2001. Validation of Integrated Water Vapour from Numerical Models using Ground – Based GPS, SSM/I, and Water Vapour Radiometer Measurements. *J. Appl. Meteorol.*, 40:1105-1117.

199. Kouba, J. 1998. IGS Analysis Activities, 1998. *IGS Annual Report, IGS Central Bureau.* Pasadena: Jet Propulsion Laboratory: 13-17.

200. Kouba, J. 2003. Measuring Seismic Waves Induced by Large Earthquakes with GPS. *Studia Geophysica et Geodaetica,* 47(4):741–755. doi:10.1023/A:1026390618355.

201. Koulali, A., Ouazor, D., Bock, O. & Fadil, A. 2011. Study of Seasonal-Scale Atmospheric Water Cycle with Ground-Based GPS Receivers, Radiosondes and NWP Models over Morocco. *Atmos. Res.,* 104-105:273-291, doi:10.1016/j.atmosres.2011.11.002.

202. Kuo, Y.H., Hsiao, L.F., Chen, D.S., Guo, Y.R., Yeh, T.C., Hong, J.S., Fong, C.T. & Lee, C.S. 2012. Application of WRF 3DVAR to Operational Typhoon Prediction in Taiwan: Impact of Outer Loop and Partial Cycling Approaches. *Weather Forecasting*, 27:1249–1263, doi:10.1175/WAF-D-11-00131.1.

203. Küpper, A., 2005. *Location-Based Services: Fundamentals and Operation*. John Wiley & Sons.

204. Kursinski, E.R., Ward, D., Otarola, A., Frehlich, R., Groppi, C., Albanna, S., Shein, M., Bertiger, W., Pickett, H. & Ross, M. 2009. The Active Temperature, Ozone and Moisture Microwave Spectrometer (ATOMMS). In Steiner, A., Pirscher, B., Foelsche, U. & Kirchengast, G., Springer (Eds.). *New Horizons in Occultation Research Studies in Atmosphere and Climate*: 315.

205. Kwiatkowski, D., Phillips, P.C.B., Schmidt, P. & Shin, Y. 1992. Testing the Null Hypothesis of Stationarity against Alternative of a Unit Root. *Journal of Econometrics*, 54:159-178.

206. Kwon, H.T., Iwabuchi, T. & Lim, G.H. 2007. Comparison of Precipitable Water Derived from Ground-Based GPS Measurements with Radiosonde Observation over the Korean Peninsula. *J. Meteor. Soc. Japan*, 85:733-746.

207. Kwon, H.T., Jung, E.H. & Lim, G.H. 2010. A Comparison of GPS- and NWP-Derived PW Data over the Korean Peninsula. *Adv. Atmos. Sci.*, 27(4):871-882, doi: 10.1007/s00376-009-9069-4.

208. Lagler, K., Schindelegger, M., Böhm, J., Krásná, H. & Nilsson, T. 2013. GPT2: Empirical Slant Delay Model for Radio Space Geodetic Techniques. *Geophys. Res. Lett.*, 40:1069–1073, doi:10.1002/grl.50288.

209. Larson, K., Bodin, P., & Gomberg, J. 2003. Using 1Hz GPS Data to Measure Deformations caused by the Denali Fault Earthquake. *Science,* 300:1421–1424.

210. Larson, K.M. 2009. GPS Seismology. *Journal of Geodesy*, 83:227–233, doi: 10.1007/s00190-008-0233-x.

211. Larson, K.M., Löfgren, J.S. & Rüdiger. 2012. Coastal Sea Level Measurements using a Single Geodetic GPS Receiver. *Adv. Space. Res*., doi: org/10.1016/j.asr.2012.04.017.

212. Larson, K.M., Ray, R.D., Nievinski, F.G. & Freymueller, J.T. 2013. The Accidental Tide Gauge: A GPS Reflection Case Study from Kachemak Bay, Alaska. *IEEE Geosci. Remote Sens. Lett.* 10:1200–1204, doi:10.1109/lgrs.2012.2236075.

213. Leandro, R.F., Langley, R.B. & Santos, M.C. 2008. UNB3m_Pack: A Neural Atmosphere Delay Package for Radiometric Space Techniques. *GPS Solutions*, 12(1):65-70, doi: 10.1007/s10291-007-0077-5.

214. Leandro, R.F., Santos, M.C. & Langley, R.B. 2006. UNB Neural Atmosphere Models: Development and Performance. In *proceedings of ION NTM 2006:* 564-573, Monterey, California, USA.

215. Legates, D.R. & McCabe Jr, G.J. 1999. Evaluating the use of "goodness-of-fit" Measures in Hydrologic and Hydro-Climatic Model Validation. *Water Resources Research*, 35:233-241.

216. Leggett, R.W. & Williams, L.R. 1981. A Reliability Index for Models. *Ecological Modelling,* (13):303-312.

217. Leuning, R., Dunin, F.X. & Wang, Y.P. 1998. A Two-leaf Model for Canopy Conductance, Photosynthesis and Partitioning of Available Energy II: Comparison with Measurements. *Agric for Meteorol*. 91:113-125.

218. Levine, J. 1999. Time Transfer using Multi-Channel GPS Receivers. *IEEE Trans Ultrason Ferroelectr Freq Control.* 46(2):392-398, doi: 10.1109/58.753028.

219. Li, Y. 2013. *A New Dynamic Approach for Statistical Optimization of GNSS Radio Occultation Bending Angles*. Doctoral thesis. Australia: RMIT University, Australia, 154p.

220. Li, Z., Muller, J.P. & Cross, P. 2003. Comparison of Precipitable Water Vapour Derived from Radiosonde, GPS and Moderate-Resolution Imaging Spectroradiometer. *J. Geophys. Res.,* 108(D20):4651, doi:10.1029/2003JD003372.

221. Liang, H., Cao, Y., Wan, X., Xu, Z., Wang, H. & Hu, H. 2015. Meteorological Applications of Precipitable Water Vapour Measurements Retrieved by the National GNSS Network of China. *Geodesy and geodynamics,* 2015, http://dx.doi.org/10.1016/j.geog.2015.03.001.

222. Lilong, L., Chaolong, Y. & Hongyan, W. 2012. Empirical T_m Modelling in the Region of Guangxi. *Geodesy and Geodynamics*, 3(4):47-52, doi: 10.3724/SP.J. 1246.2012.00047.

223. Liou, Y., & Huang, C. 2000. GPS Observations of PW during the Passage of a Typhoon. *Earth Planets Space*, 52:709.

224. Liou, Y.A., Pavelyev, A.G., Liu, S.F., Pavelyev, A.A., Yen, N., Huang, C.Y. & Fong, C.J. 2007. FORMOSAT-3/COSMIC GPS Radio Occultation Mission: Preliminary Results. *IEEE Trans. on Geoscience and Remote Sensing*, 45(2007):14.

225. Liu, Z., Xu, Z., Yao, Z. & Huang, H. 2012. Comparison of Surface Variables from ERA and NCEP Reanalysis with Station Data over Eastern China. *Theor. Appl. Climatol*., 107:611-621, doi: 10.1007/s00704-011-0501-1.

226. Löfgren J.S., Haas, R., Scherneck, H.G. & Bos, M.S. 2011b. Three Months of Local Sea Level Derived from Reflected GNSS Signals. *Radio Sci.,* 46(RS0C05), doi:10.1029/2011rs004693.

227. Löfgren, J.S., Haas, R. & Johansson, J.M. 2010. High-rate Local Sea Level monitoring with a GNSS-Based Tide Gauge. In *Proceeding of Geoscience and Remote Sensing Symposium (IGARSS)*, doi: 10.1109/ IGARSS.2010.5652888.

228. Löfgren, J.S., Haas, R. & Johansson, J.M. 2011a. Monitoring Coastal Sea Level using Reflected GNSS Signals. *Adv. Space Res.* 47:213–220, doi:10.1016/j.asr.2010.08.015.

229. Lombardi, M.A., Nelson, L.M., Novick, A.N. & Zhang, V.S. 2001. Time and Frequency Measurements using the Global Positioning System. *Cal Lab: International Journal of Metrology*, *8*(3):26-33.

230. Lu, C., Li, X., Ge, M., Heinkelmann, R., Nilsson, T., Soja, B., Dick, G. & Schuh, H. 2015. Estimation and Evaluation of Real-Time Precipitable Water Vapour from GLONASS and GPS, *GPS Solution*, doi: 10.1007/s10291-015-0479-8.

231. Lutgens, F.K. & Tarbuck, E.J. 2004. *The Atmosphere: An Introduction to Meteorology*. New Jersey: Pearson Education, Inc. p508.

232. MacKinnon, J.G. 1996. Numerical Distribution Functions for Unit Root and Co-integration Tests. *Journal of Applied Econometrics*, 11:601–618.

233. Maghrabi, A.H. & Al Dajani, H.M. 2014. Time Distribution of the Precipitable Water Vapour in Central Saudi Arabia and its Relationship to Solar Activity. *Advances in Space Research*, 53:1169-1179, http://dx.doi.org/10.1016/j.asr.2014.02.006.

234. Marc, T., Alain, G., Donat, P., Hans-Gert, K., Daniel, L. & Elman, B. 2007. GPS Tomography for Meteorology. In *the Proceedings of the 20th International Technical Meeting of the Satellite Division of the Institute of Navigation*, Fort worth, TX, USA: 2861-2869. [25-28 September, 2007].

235. Marques, C.A.F., Rocha, A. & Corte-Real, J. 2010. Comparative Energetics of ERA-40, JRA-25, and NCEP-R2 Reanalysis, in the Wave Number Domain. *Dynam Atmos Oceans*, 50:375-399.

236. Marques, C.A.F., Rocha, A., Corte-Real, J., Castanheira, J.M., Ferreira, J. & Melo-Goncalves, P. 2009. Global Atmospheric Energetics from NCEP Reanalysis 2 and ECMWF-ERA 40 Reanalysis. *Int Climatol* 29:159-174, doi: 10.1002/joc.1704.

237. Mason, N., Hughes, P., McMullan, P., Reynolds, R., Simmonds, L. & Twidell, J. 2001. *Introduction to Environmental Physics: Planet Earth, Life and Climate*, London: Tylor & Francis.

238. Mason, P. 2010. A Review of the 2010 update of the Implementation Plan for the Global Observing System for Climate in Support of the UNFCCC. *GCOS SC*, 18(13). [July 31].

239. Mazany, A., Businger, S., Gutman, S.I. & Roeder, W. 2002. A Lightning Prediction Index that utilizes GPS Integrated Precipitable Water Vapour. *Weather Forecast*, 17(5):1034-1047.

240. Mazinga, G. 2006. Patterns of Satisfaction with Health Services in Malawi: Analysis using Geographic Information Technology. In *GSDI-9 Conference Proceedings*, [November 6-10], Santiago: Chile. [Online], Available: www.gsdidocs.org/gsdiconf/GSDI-9/papers/TS58.2paper.pdf.

241. McCarthy, D.D. & Petit, G. 2004. IERS Conventions (2003). *IERS Technical Note 32*. Verlag des undesamts für Kartographie und Geodäsie, Frankfurt am Main.

242. Meehl, G.A., Washington, W.M., Wigley, T.M.L., Arblaster, J.M. & Dai, A. 2003. Solar and Greenhouse Gas Forcing and Climate Response in the Twentieth Century. *Journal of Climate*, 16(426444).

243. Melsheimer, C. & Heygster, G. 2008. Improved Retrival of Total Water Vapour over Polar Regions from AMSU-B Microwave Radiometer Data. *IEEE T. Geosci. Remote*, 46:2307-2322, doi:10.1109/TGRS.2008.918013.

244. Mengistu Tsidu, G., Blumenstock, T. & Hase, F. 2015. Observations of Precipitable Water Vapour over Complex Topography of Ethiopia from Ground-Based GPS, FTIR, Radiosonde and ERA-Interim Reanalysis. *Atmos. Meas. Tech*., 8:3277-3295, doi: 10.5194/amt-8-3277-2015.

245. Michelsen, M.W. 1998. GPS "Noise" Benefits Weather Forecasting [Online]. *Earth Observation Magazine.* Available: http://www.eomonline.com/Common/Archives/1998oct/98oct_michael.html.

246. Mithell, J.M., Dzerdzeevskii, B. & Flohn, et al. 1966. *Climate Change* (Report of a working group of the commission for climatology), WMO Technical Note **No. 79**, World Meteorological Organization.

247. Miyazaki, S., Iwabuchi, T., Heki, K. & Naito, I. 2003. An Impact of Estimating Tropospheric Delay Gradients on Precise Positioning in the Summer using the Japanese Nationwide GPS Array, *J. Geophys. Res*., 108(B7):2335, doi: 10.1029/2000JB000113.

248. Moller, G., Weber, R. & Boehm, J. 2013. Improved Troposphere Blind Models based on Numerical Weather Data. In *the Proceedings of the 26th International Technical Meeting of the ION satellite Division*, ION GNSS + 2013, Nashville: Tennessee. [16-20 September].

249. Moran, P.A.P. 1950. Notes on Continuous Stochastic Phenomena. *Biometrika,* 37:17–23.

250. Murphy, A.H. 1988. Skill Scores based on the Mean Square Error and their Relationship to the Correlation Coefficient. *Mon. Weather Rev.,* 116:2417-2424.

251. Musa, T.A., Amir, S., Othman, R., Ses, S., Omar, K., Abdullah, K., Samsung, L. & Rizos, C. 2011. GPS Meteorology in a Low Latitude Region: Remote Sensing of Atmospheric Water Vapour over Malaysian Peninsula. *Journal of Atmospheric and Solar Terrestrial Physics*, 73:2410-2422, doi: 10.1016/j.jastp.2011.08.014.

252. Naibbi, A.I. & Ibrahim, S.S. 2014. An Assessment of the Existing Continuously Operating Reference Stations (CORS) in Nigeria: An Exploration using Geographical Information System (GIS). *American Journal of Geographic Information Systems*, 3(4):147–157, doi:10.5923//j.ajgis.20140304.01.

253. Nakamura, H., Koizumi, K. & Mannoji, N. 2004. Data Assimilation of GPS Precipitable Water Vapour into the JMA Mesoscale Numerical Weather Prediction Model and its Impact on Rainfall Forecast. *Journal of the Meteorological Society of Japan*, 82(2004):441-452.

254. Nash, J., Orliac, E.J., Dodson, A.H., Bingley, R.M., Jones, J. & Tererle, F.N. 2006. On the use of Near Real Time GPS Inferred Humidity Fields for Monitoring Thunders Storm Activity, *EOS Transactions,* 87(52): AIIE-08.

255. Nash, J.E. & Sutcliffe, J.V. 1970. River Flow Forecasting through Conceptual Models Part I- A Discussion of Principles. *Journal of Hydrology*, 10(3):282-290.

256. Neilan, R. & Wonnacott, R. 2002. *Establishing a Continental Reference System in Africa: AFREF*. Proposal to International Council for Science on behalf of International Union of Geodesy and Geophysics/International Association of Geodesy, International GPS Service/International Earth Rotation Service and International Society of Photogrammetry and Remote Sensing.

257. Niell, A., Coster, A., Solheim, F., Menders, V., Toor, P., Langley, R. & Upham, C. 2001. Comparison of Measurements of Atmospheric Wet Delay by Radiosonde, Water Vapour Radiometer, GPS, and VLBI. *J. Atmos. Oceanic Technol,* 18(6):830–850.

258. Niell, A.E. 1996. Global Mapping Functions for the Atmosphere Delay at Radio Wavelengths. *Journal of Geophysical Research*, 101(B2):3227-3246.

259. Nilsson, T. & Elgered, G. 2008. Long-Term Trends in the Atmospheric Water Vapour Content Estimated from Ground-Based GPS Data. *J. Geophys. Res.,* 113(D19101), doi: 10.1029/2008JD010110.

260. Nilsson, T. & Gradinarsky, L. 2006. Water Vapour Tomography using GPS Phase Observations: Simulation Results. *Geoscience and Remote Sensing, IEEE Transactions.* 44(10 Part 2):2927–2941.

261. Ning, L., Trenberth, K.E., Qin, J., Yang, K. & Yao, L. 2015. Detecting Long Term Trends in Precipitable Water over the Tibetan Plateau by Synthesis of Station and MODIS Observations. *J. Climate,* 28:1707-1722, doi:10.1175/JCLI-D-14-00301.1.

262. Ning, T., Elgered, G., Willen, U. & Johansson, J.M. 2013. Evaluation of the Atmospheric Water Vapour Content in a Regional Climate Model using Ground-Based GPS Measurements. *J. Geophys. Res. Atmos*., 118:329-339, doi: 10.1029/2012JD018053.

263. Ning, T., Haas, R., Elgered, G. & Willen, U.2012. Multi-technique Comparisons of Ten Years of Wet Delay Estimates on the West Coast of Sweden. *Journal of Geodesy,* 87(7), doi:10.1007/s00190-011-0527-2.

264. Norsuliza, Y., Abdullahi, M., Ismail, M. & Zaharim, A. 2009. A Model Validation for Total Electron Content (TEC) at an Equatorial Region. *European Journal of Scientific Research*, 28(4):642-648.

265. Nwilo, P., Dodo, J., Edozie, R. & Adebohehin, A. 2013. The Nigerian Geocentric Datum (NGD2012): Preliminary Results. In *FIG Working Week 2013: Environment for Sustainability*, [May6–10]. Abuja: Nigeria. [Online], Available: www.fig.net/pub/fig2013/papers/.../TS01B_nwilo_dodo_et_al_6524.pdf.

266. Odijk, D. 2002. *Fast Precise GPS Positioning in the Presence of Ionospheric Delays*. Doctoral Thesis. Delft: Delft University of Technology.

267. Oginni, A. & Adebamowo, M. 2013. An Evaluation of the Socio-cultural Effects of Climate Change on Vulnerable Africa: Making a Case for Urgent Action towards Adaptation in Nigeria. *British Journal of Arts and Social Sciences*, 11(2). ISSN: 2046-9578. [Online], Available: http://www.bjournal.co.uk/BJASS.aspx.

268. Orliac, E. 2002. *Troposphere Delay Models for Satellite Navigation Applications*. Diploma Thesis. Lausanne: École Polytechnique Fédérale de Lausanne.

269. Pacione, R., Sciarretta, C., Vespe, F., Faccani, C., Ferretti, R., Fionda, E., Ferraro, C. & Nardi, A. 2001. GPS Meteorology: Validation and Comparisons with Ground-Based Microwave Radiometer and Mesoscale Model for the Italian GPS Permanent Stations. *Phys. Chem. Earth*, 26A:139–145.

270. Pałm, M., Melsheimer, C., Noël, S., Heise, S., Notholt, J., Burrows, J. & Schrems, O. 2010. Integrated Water Vapour above Ny Ålesund, Spitsbergen: A Multi-Sensor Intercomparison. *Atmos. Chem. Phys.,* 10:1215–1226, doi:10.5194/acp-10-1215-2010.

271. Pany, T., Pesec, P. & Stangl, G. 2001. Elimination of Tropospheric Path Delays in GPS Observations with the ECMWF Numerical Weather Model. *Phys Chem Earth A: Solid Earth Geodesy* 26(6-8):487-492.

272. Paun, M., Chen, T., & Nassar, R .2009. Spectral analysis on Tripolar Laplacian Electrocardiagram, *Romanian Journal of Information Science and Technology*, **vol.,12**, no.1, 91-100.

273. Parkinson, C.L. 2003. Aqua: An Earth-Observing Satellite Mission to Examine Water and other Climate Variables. *IEEE Trans. Geosci. Remote Sens.,* 41:173-183, doi:10.1109/TGRS.2002.808319.

274. Pauly, K., Koch, O., Bertrand-Noel, V. 2015. Galileo FOC – Design, Production, Early Operations after 1st Launch, and Project Status, *Proceedings of the 66th International Astronautical Congress (IAC 2015*), Jerusalem, Israel, Oct.12-16, 2015, paper: IAC-15-B2.2.1.

275. Penna, N., Dodson, A. & Chen, W. 2001. Assessment of EGNOS Tropospheric Correction Model. *Journal of Navigation*, 54(1):37-55.

276. Pérez-Ramírez, D., Whiteman, D.N., Smirnov, A., Lyamani, H., Holben, B.N., Pinker, R., Andrade, M. & AladosArboledas, L. 2014. Evaluation of AERONET Precipitable Water Vapour versus Microwave Radiometry, GPS and Radiosondes at ARM Sites. *J. Geophys. Res. Atmos.,* 119:9596–9613, doi:10.1002/2014JD021730.

277. Pikridas, C. 2014. Monitoring Climate Changes on Small Scale Networks using Ground Based GPS and Meteorological Data. *Artificial satellites*, 49(3), doi:10.2478/arsa-2014-0010.

278. Pirscher, B., Foelsche, U., Borsche, M., Kirchengast, G. & Kuo, Y.H. 2010. Analysis of Migrating Diurnal Tides Detected in FORMOSAT-3/COSMIC Temperature Data, *J. Geophys. Res*, 115(D14), doi: 10.1029/2009JD013008.

279. Plag, H.P., Juttner, H.U. & Rautenberg, V. 1996. On the Possibility of Global and Regional Inversion of Exogenic Deformations for Mechanical Properties of the Earth's Interior. *Journal of Geodynamics,* 21:287–309.

280. Poli, P. 2006. Assimilation of GNSS Radio Occultation Data into Numerical Weather Prediction. *Atmosphere and Climate*: 195-204, doi: 10.1007/3-540-34121-8-17.

281. Prasad, A.K. & Singh, R.P. 2009. Validation of MODDIS Terra, AIRS, NCEP/DOE AMIP-II Reanalysis-2, and AERONET Sun Photometer Derived Integrated Water Vapour using Ground-Based GPS Receivers over India. *J. Geophys. Res.*, 114(D05107), doi:10.1029/2008JD011230.

282. Provost, C. & Escoffier, C. 1998. Surface Forcing over South West Atlantic According to NCEP and ECMWF Reanalysis over the Period 1979-1990. *Phys Chem Earth*, 23(56):537-542.

283. Pugnaghi, S., Boccolari, M., Fazlagic, S., Pacione, R., Santangelo, R., Vedel, H. & Vespe, F. 2002. Comparison of Independent Integrated Water Vapour Estimates from GPS and Sun Photometer Measurements and a Meteorological Model. *Physics and Chemistry of the Earth,* 27:355-362.

284. Qin, J., Yang, K., Koike, T., Lu, H., Yaoming, M.A. & Xu, X. 2012. Evaluation of AIRS Precipitable Water Vapour against Ground-Based GPS Measurements over the Tibetan Plateau and its Surroundings. *Journal of the Meteorological Society of Japan*, 90C:87-98, doi: 10.2151/jmsj.2012-C06.

285. Raja, M.K.V., Gutman, S.I., Yoe, J.G., McMillin, L.M. & Zhao, J. 2008. The Validation of AIRS Retrievals of Integrated Precipitable Water Vapour using Measurements from a Network of Ground-Based GPS Receivers over the Contiguous United States. *J. Atmos. Ocean Tech.*, 25:416-428.

286. Raju, C.S., Saha, K. & Parameswaran, K. 2009. Signature of Atmospheric Oscillation in GPS Measured Tropospheric Delay. *Journal of Atmospheric and Solar-Terrestrial Physics,* 71(17):1784-1793, doi: 10.1016/j.jastp.2009.06.011.

287. Raju, C.S., Saha, K., Thampi, B.V. & Parameswaran, K. 2007. Empirical Model for the Mean Temperature of the Indian Zone and Precipitable Water Vapour from Ground Based GPS Measurements. *Ann. Geophs*, 25:1935-1948. [Online], Available: www.ann-geophy.net/25/1935/2007/.

288. Reigber, C., Gendt, G., Dick, G., & Tomassini, M. 2002. Near-Real-Time Water Vapour Monitoring for Weather Forecasts, *GPS World* (2002, January 18).

289. Rocken, C., Van Hove, T. & Ware, R. 1997. Near Real-Time Sensing of Atmospheric Water Vapour. *Geophys. Res. Lett.*, 24:3221–3224, doi:10.1029/97GL03312.

290. Rocken, C., Van Hove, T., Johnson, J., Solheim, F., Ware, R.H., Bevis, M., Businger, S. & Chiswell, S. 1995. GPS/STORM - GPS Sensing of Atmospheric Water Vapour for Meteorology. *Journal of Atmos. and Ocean. Tech.,* 12(3):468-478.

291. Rocken, C., Ware, R., Van hove, T., Solheim, F., Alber, C., Jhonson, J., Bevis, M. & Businger, S. 1993. Sensing Atmospheric Water Vapour with Global Positioning System. *Geophys. Res. Lett.,* 20:2631-2634.

292. Ross, R.J. & Rosenfeld, S. 1997. Estimating Mean Weighted Temperature of the Atmosphere for Global Positioning System Applications. *J. Geophys. Res*., 102(D18): 21719–21730.

293. RTCA, Inc. 2001. *DO-229C, Minimum Operational Performance Standards for Global Positioning System/Wide Area Augmentation System Airborne Equipment*, SC-169. Washington, D.C.: RTCA, Inc.

294. Saastamoinen, J. 1972. Atmospheric Correction for Troposphere and Stratosphere in Radio Ranging of Satellites. The Use of Artificial Satellites for Geodesy. In Henriksen, S.W., Mancini, A. & Chovitz, B.H. (Eds.). *Papers Presented at the Third International Symposium on the use of Artificial Satellites for Geodesy.* Washington, D. C.: AGU, AIAA, NOAA, U.S.ATC, American Geophysical Union, Geophysical Monograph: 247 – 252. [1971, April 15-17].

295. Santamaría-Gómez, A., Gravelle, M., Collilieux, X., Guichard, M., Míguez, B.M., Tiphaneau, P. & Wöppelmann, G. 2012. Mitigating the Effects of Vertical Land Motion in Tide Gauge Records using a State-of-the-art GPS Velocity Field. *Glob. Planet. Change,* 98&99:6–17, doi:10.1016/j.gloplacha.2012.07.007.

296. Sapucci, L.F. 2014. Evaluation of Modelling Water Vapour Weighted Mean Tropospheric Temperature for GNSS-Integrated Water Vapour Estimates in Brazil. *American Meteorological Society*, 53:715-730, doi:10.1175/JAMC-D-13-048.1.

297. Sarazin, M.S., Graham, E., Beniston, M. & Riemer, M. 2003. New Tools for a Global Survey of Potential Sites for the Future Giant Telescopes. In *Proceedings of SPIE 4840, Future Giant Telescopes*: 291, http://dx.doi.org/10.1117/12.459984.

298. Schiller, J. & Voisard, A. 2004. *Location-Based Services*, Morgan Kaufmann/Elsevier, London, UK, 255p.

299. Schingelegger, M., Moller, G., Boehm, J., Weber, R. & Pain, G. 2014, Troposphere Delay Models in Blind Mode: Towards Improved Predictions of the Wet Component. Vienna: *EGU General Assembly*. [27 April- 2 May].

300. Schueler, T., Posfay, A.G., Hein, G.W. & Biberger, R. 2001. A Global Analysis of the Mean Atmospheric Temperature for GPS Water Vapour Estimation. Reprints, *14th IONGNSS Int. Tech. Meeting*, Salt Lake City, UT: Institute of Navigation.

301. Seaman, M.A., Levin, J.R. & Serlin, R.C. 1991. New Developments in Pair Wise Multiple Comparisons: Some Powerful and Practicable Procedures. *Psychological Bulletin*, 110:577-586.

302. Sharifi, M.A., Khanniani, A.S. & Joghataei, M. 2015. Comparison of GPS Precipitable Water Vapour and Meteorological Parameters during Rainfalls in Tehran. *Meteorol Atmos Phys,* 127(2015):701-710, doi:10.1007/s00703-015-0383-3.

303. Shcherbakov, M.V., Brebels, A., Shcherbakova, N.L., Tyukov, A.P., Janovsky, T.A. & Kamaev, V.A. 2013. A Survey of Forecast Error Measures. *World Applied Sciences Journal*, 24:171-176, doi:10.5829/idosi.wasj.2013.24.itimes.80032.

304. Shi, C., Lou, Y., Zhang, H., Zhao, Q., Geng, J., Wang, R., Fang, R. & Liu, J. 2010. Seismic Deformation of the Mw 8.0 Wenchuan Earthquake from High-Rate GPS Observations. *Advances in Space Research*, 46(2):228–235. doi:10.1016/j.asr.2010.03.006.

305. Shi, J., Xu, C., Guo, J. & Gao, Y. 2015. Real-time GPS Precise Point Positioning-Based Precipitable Water Vapour Estimation for Rainfall Monitoring and Forecasting. *IEEE Trans Geosci Remote Sens*. 53(6):3452–3459. doi:10.1109/TGRS.2014.2377041.

306. Shi, P., Ma, X., Chen, X., Qu, S. & Zhang, Z. 2013. Analysis of Variation Trends in Precipitation in an Upstream Catchment of Huai River. *Mathematical Problems in Engineering*, 2013(929383):11, doi:10.1155/2013/929383.

307. Shoji, Y., Seko, H., Iwabuchi, T. & Nakamura, H. 2002. A Case Study of Water Vapour Variation in a Severe Thunderstorm in Tokyo by using Dense Network of GPS. In *proceedings of International Conference on Mesoscale Convective Systems and Heavy Rain in East Asia Tokyo*.

308. Shrestha, S. & Singh, P. 2014. Global Climate System, Energy balance, and the Hydrological Cycle. *CRC Press*, 1-30, doi: 10.1201/b16969-2.

309. Simeonov, T., Sidorov, D., Teferle, N., Guerova, G., Egova, E., Vassileva, K., Milev, I. & Milev, G. 2015. Sofia University GNSS Analysis Center (SUGAC). In *Proceedings of FIG Working Week 2015*, Sofia, Bulgaria. [17-21 May].

310. Simmons, A.J. et al. 2014. Estimating Low-Frequency Variability and Trends in Atmospheric Temperature using ERA-Interim. *Quart. J. R. Meteorol. Soc.*, doi: 10.1002/qj.2317.

311. Simmons, A.J., Willett, K.M., Jones, P.D., Thorne, P.W. & Dee, D.P. 2010. Low-Frequency Variations in Surface Atmospheric Humidity, Temperature and Precipitation: Inferences from Reanalyses and Monthly Gridded Observational Datasets. *J. Geophys. Res.*, 115(D01110), doi:10.1029/2009JD012442.

312. Singh, D., Ghosh, J.K. & Kashyap, D. 2013. Weighted Mean Temperature Model for Extra Tropical Region of India. *Journal of Atmospheric and solar-Terrestrial Physics*, 107(2014):48-53. http://dx.doi.org/10.1016/j.astp.2013.10.016.

313. Sobolev, S.V., Babeyko, A.Y., Wang, R., Hoechner, A. & Galas, R. 2007. Tsunami Early Warning using GPS-Shield Arrays. *Journal of Geophysical Research,* 112:B08415. doi: 10.1029/2006JB004640.

314. Soden, B.J. & Held, I.M. 2006. An Assessment of Climate Feedbacks in Coupled Ocean-Atmosphere Models. *J. Climate*, 19:3354–3360, doi:10.1175/JCLI3799.1, 2006.

315. Sokolovskiy, S., Kuo, Y.H., Rocken, C., Schreiner, W.S., Hunt, D. & Anthes, R.A. 2006. Monitoring the Atmospheric Boundary Layer by GPS Radio Occultation Signals Recorded in the Open-Loop Mode, *Geophys. Res. Lett*, 33, doi: 10.1029/2006GL025955.

316. Song, D.S. & Grejner-Brzezinska, D.A. 2009. Remote Sensing of Atmospheric Water Vapour Variation from GPS Measurements during a Severe Weather Event, *Earth Planets Space*, 61:1117-1125.

317. Steigenberger, P., Rothacher, M., Dietrich, R., Fritsche, M., Rulke, A. & Vey, S, 2006. Reprocessing of a Global GPS Network. *Journal of Geophysical Research,* 111:B05402, doi: 10.1029/2005JB003747.

318. Stoew, B. & Elgered, G. 2004. Characterization of Atmospheric Parameter using a Ground Based GPS Network in North Europe. *Journal of the Meteorological Society of Japan*, 82(1B):587-596.

319. Sultan, B. Janicot, S. & Drobinski, P.2007. Characterization of the Diurnal Cycle of the West African Monsoon around the Monsoon Onset. *Journal of Climate*, 20:4014-4032, doi:10.1175/JCL14218.1.

320. Sun, J.Q., Wang, H.J. & Yuan, W. 2008. A Possible Mechanism for the Co-variability of the Boreal Spring Antarctic Oscillation and the Yangtze River Valley Summer Rainfall. *International Journal of Climatology*, 29:1276–1284, doi: 10.1002/joc.1773.

321. Suparta, W. & Iskandar, A. 2013. Modelling of Weighted Mean Temperature over the Western Pacific Region to Estimate GPS PWV. In *the proceeding of the 2013 IEEE International Conference on Space Science and Communication (Icon Space)* [2013, July 1-3], Melaka, Malaysia.

322. Suparta, W. 2011. Variability of GPS-Based Precipitable Water vapour over Antarctica: Comparison between Observations and Predictions. *World Applied Sciences Journal*, 12(9): 1597-1604.

323. Suparta, W. 2014a. Sensing the Upper and Lower Levels of the Atmosphere during the 2009 Equinoxes using GPS Measurements. *Annals of Geophysics*, 57(2), A0215, doi: 10.4401/ag-6320.

324. Suparta, W. and Fraser, G.J. 2014b. A Case Study of Relationship between GPS PWV and Solar Variability during the Declining Phase of Solar Cycle. *23 Acta Geophysica*, 62(1):220-240, DOI: 10.2478/s11600-013-0146-9.

325. Suparta, W., Abdul Rashid, Z.A., Mohd. Ali, M.A., Yatim, B. & Fraser, G.J. 2008. Observations of Antarctic Precipitable Water Vapour and its Response to the Solar Activity Based on GPS Sensing, *Journal of Atmospheric and Solar-Terrestrial Physics*, 70:1419-1447, doi:10.1016/j.jastp.2008.04.006.

326. Susskind, J., Barnet, C.D. & Blaisdell, J.M. 2003. Retrival of Atmsopheric and Surface Parameters form AIRS/AMSU/HSB Data in Presence of Clouds. *IEEE Trans. Geosci. Remote Sens.*, 41:390-409.

327. Tao, W. 2008. Near Real Time GPS Inferred Water Vapour System Development and Evaluation, MSC Thesis, Department of Geomatics Engineeering, University of Calgary, UCGE Reports no: 20275, 171p.

328. Tastula, E.M., Vihma, T., Andreas, E.L. & Galperin, B. 2013. Validation of the Diurnal Cycles in Atmospheric Reanalyses over Antarctic Sea Ice. *J. Geophys. Res. Atmos.*, 118:4194–4204, doi:10.1002/jgrd.50336.

329. Teke, K., Bohm, J., Nilsson, T., Schuh, H., Steigeberger, P., Dach, P., Heinkelman, R., Willis, P., Haas, R., Garcia-Espada, S., Hobiger, T., Pchikawa, R., Shimizu, S. 2011. Multi-technique Comparison of Troposphere Zenith Delays and Gradients during CONT08. *Journal of Geodesy*, 85(7):395-493, doi: 10.1007/s00190-010-0434-y.

330. Teng, H., Zhou Shi, Z., Ma, Z. & Li, Y. 2014. Estimating Spatially Downscaled Rainfall by Regression Kriging using TRMM Precipitation and Elevation in Zhejiang Province, Southeast

China. *International Journal of Remote Sensing*, 35(22):7775-7794, doi:0.1080/01431161.2014.976888.

331. Tian, J. & Fernandez, G.C.J. 1999. Seasonal Trend Analysis of Monthly Water Quality Data. In *Proceedings of the 7th Annual Western users of SAS Software Regional users Group*: 229-234. [Online], Available: www.ag.unr.edu/gf/pdf/joyce.pdf.

332. Torre, A.D.L., Alexander, P., Llamedo, P., Schmidt, T. & Wickert, J. 2009. Recent Advances in Gravity Wave Analysis from Long Term Global GPS Radio Occultation Observations. In Steiner, A., Pirscher, B., Foelsche, U. & Kirchengast, G. (Eds.). *New Horizons in Occultation Research Studies in Atmosphere and Climate*. Springer: 315.

333. Trambauer, P., Dutra, E., Maskey, S., Werner, M., Pappenberger, F., van Beck, L.P.H. & Uhlenbrook, S. 2014. Comparison of Different Evaporation Estimates over the African Continent. *Hydrol. Earth Syst. Sci*., 18:193-212, doi: 10.5194/hess-18-193-2014.

334. Trenberth, K.E., Fasullo, J. & Smith, L. 2005. Trends and Variability in Column-Integrated Atmospheric Water Vapour. *Clim Dyn*., 24:741-758.

335. Troller, M., Geiger, A., Brockmann, E., Bettems, J.M., Burki, B. & Kahle, H.G. 2006. Tomographic Determination of the Spatial Distribution of Water Vapour using GPS Observations. *Adv. Space Res*., 37:2211–2217.

336. Tuka, A. & El-Mowafy, A. 2013. Performance Evaluation of Different Troposphere Delay Models and Mapping Functions. *Measurement*, 46(2013):928-937. http://dx.doi.org/10.1016/j.measurement.2012.10.015 .

337. Uppala, S., Kfallberg, S.P., Simmons, P.K.A., Andrae, U., Bechtold, V., Fiorino, M., Gibson, J., Haseler, J., Hernandez, A. & Kelly, G. 2005. The ERA-40 Reanalysis. *Q.J.R. Meteorol. Soc.,* 131(612):2961-3012.

338. Van der Marel, H. 2004. COST-716 Demonostration Project for the Near Real Time Estimation of Integrated Water Vapour from GPS. *Physics and Chemistry of the Earth,* Parts A/B/C(29):187-199, doi: 10.1016/j.pce.2004.01.001.

339. Van Malderen, R., Brenot, H., Pottiaux, E., Beirle, S., Hermans, C., De Maziere, M., Wagner, T. & De Backen, H. 2014. A Multi-site Inter-comparison of Integrated Water Vapour Observations for Climate Change Analysis. *Atmos. Meas Tech*, 7:2487-2512. doi: 10.5194/amt-7-2487-2014.

340. Vedel, H. & Huang, X.Y. 2004. Impact of Ground based GPS Data on Numerical Weather Prediction. Journal of the Meteorological Society of Japan. 82(1B):459-472.

341. Vedel, H., Mogensen, K. & Huang, X.Y. 2001. Calculation of Delays from Meteorological Data: Comparison of NWP Model and Observed Delays. *Physics and Chemistry of the Earth*, 26:497-502.

342. Vey, S., Dietrich, R., Fritsche, M., Rulke, A., Steigenberger, P. & Rothacher, M. 2009. On the Homogeneity and Interpretation of Precipitable Water Time Series Derived from Global GPS Observations. *J. Geophys.Res*., 114(D10101), doi: 10.1029/2008JD010415.

343. Wagner, H.H. & Wildi, O. 2002. Realistic Simulation of the effects of Abundance Distribution and Spatial Heterogeneity on Non-parametric Estimators of Species Richness. *Ecoscience*, 9:241-250.

344. Walpersdorf, A., Bouin, M. N., Bock, O. & Doerflinger, E. 2007. Assessment of GPS Data for Meteorological Applications over Africa: Study of Error Sources and Analysis of Positioning Accuracy. *Journal of Atmospheric and Solar Terrestrial Physics*, 69: 1312-1330, doi: 10.1016/j.astp.2007.64.008.

345. Walther, B.A. & Moore, J.L. 2005. The Concepts of Bias, Precision and Accuracy, and their use in testing the Performance of Species Richness Estimators, with a Literature Review of Estimator Performance. *Ecography,* 28:815-829, doi: 10.1111/j.2005.0906-7590.04112.x.

346. Wang, J. & Zhang, L. 2007. Systematic Errors in Global Radiosonde Precipitable Water Data from Comparisons with Ground-Based GPS Measurements. *Journal of Climate,* 21(10):2218-2138, doi: 10.1175/2007/JCLI1944.1.

347. Wang, J. & Zhang, L. 2009. Climate Applications of Global 2-hourly Atmospheric Precipitable Water Dataset from IGS Gound-Based GPS Measurement. *J. Geod.,* 83:209-217, doi: 10.1007/s00190-008-0238-5.

348. Wang, J. 2013. Global Navigation Satellite System (GNSS, Climate and GRUAN). *Presentation at the GRUAN ICM-5 Meeting*, Netherlands: De Bilt. [February 25 - March 1].

349. Wang, J., Zhang, L. & Dai, A. 2005. Global Estimates of Water Vapour Weighted Mean Temperature of the Atmosphere for GPS Applications. *J.Geophys.Res*, 110(D21), doi: 10.1029/2005JD006215.

350. Wang, X., Song, L. & Cao, Y. 2012. Analysis of the Weighted Mean Temperature of China Based on Sounding and ECMWF Reanalysis Data. *Acta Meteor. Sinica*, 26(5):642-652, doi: 10.1007/s13351-012-0508-2.

351. Wang, Y.M., Lean, J.L. & Sheeley, N.R., Jr. 2005. Modelling the Sun's Magnetic Field and Irradiance since 1713. *The Astrophysical Journal*, 625(522538).

352. Ware, R., Braun, J., Ha, Y.S., Hunt, D., Kuo, Y.H., Rocken, C., Sleziak, M., Van Hove, T., Weber, J. & Anthes, R. 2003. Real Time Water Vapour Sensing with SUOMINET- Today and Tomorrow. *International GPS meteorology workshop, Tsukuba, Japan,* [2003, January 14-16].

353. Ware, R., Fulker, D., Stein, S., Anderson, D., Avery, S., Clark, R., Droegemeier, K., Kuettner, J., Minster, J. & Sorooshian, S. 2000. SuomiNet: A Real-time National GPS Network for Atmospheric Research and Education. *Bulletin of the American Meteorological Society*, 81:677.

354. Weber, R., Ray, J. & Kouba, J. 2002. Review of IGS Analysis Products. [Online]. In *Proceedings of IGS Network, Data and Analysis Center Workshop*. Canada: Ottawa. [April 8-11]. Available: http://www.igs.org/overview/pubs/ottawa_ws.html.

355. Wickert, J., Beyerle, G., Kfonig, R., Heise, S., Grunwaldt, L., Michalak, G., Reigber, C. & Schmidt, T. 2005. GPS Radio Occultation with CHAMP and GRACE: A First Look at a New and Promising Satellite Configuration for Global Atmospheric Sounding, *Ann. Geophysicae*, 23:653–658.

356. Wickert, J., Michalak, G., Schmidt, T., Beyerle, G., Cheng, C., Healy, S., Heise, S., Huang, C., Jakowski, N., Kohler, W., Mayer, C., Offiler, D., Ozawa, E., Pavelyev, A. G., Rothacher, M., Tapley, B. & Arras, C. 2009. GPS Radio Occultation: Results from CHAMP, GRACE and FORMOSAT-3/COSMIC. *Terrestrial Atmospheric and Ocenic Sciences.* 20:35-50, doi: 10.3319/TAO.2007.12.26.01(F3C).

357. Wickert, J., Rannat, K., Wang, J., Braun, J., Dick, G., Elgerd, G., Gutman, S., Joned, J., Liu, Z., Shoji, Y. 2012. GRUAN GNSS Precipitable Water Task Team. *IGS workshop*. Poland: Olsztyn.

358. Wilgan, K., Rohm, W. & Bosy, J. 2015. Multi-observation Meteorological and GNSS Data Comparison with Numerical Weather Prediction Model. *Atmospheric Research,* 156:29-42, doi:10.1016/j.atmosres.2014.12.011.

359. Willmott, C.J., Robeson, S.M. & Matsuura, K. 2012. Short Communication: A Refined Index of Model Performance. *International Journal of Climatology*, 32:2088-2094, doi:10.1002/joc.2419.

360. WMO. 2002. *Standardised Verification System (SVS) for Long Range Forecast*. Manual on the GDPS, 1(485).

361. WMO.1992. *Manual on the Global Data Processing System*. WMO Technical Document No.485, II.7-36-II.7-39.

362. WMO. 1957. Meteorology - A Three-dimensional Science: Second Session of the Commission for Aerology. *WMO Bulletin,* 4(4):134-138.

363. Wolfe, D.E. & Gutman, S. I. 2000. Developing an Operational, Surface-based, GPS, Water Vapour Observing System for NOAA: Network Design and Results. *Journal of Atmospheric and Oceanic Technology*, 17:426.

364. Won, J., Park, K.D., Ha, J. & Cho, J. 2010. Effects of Tropospheric Mapping Functions on GPS Data Processing. *J. Aston. Space Sci*., 27(1):21-30, doi: 10.5140/JASS.2010.27.1.021.

365. Wonnacott, R. 2005. AFREF: Background and Progress towards a Unified Reference System for Africa. *A paper presented at the FIG working week/GSDI-8 Conference*. Cairo: Egypt. [2005, April 16-17]. [Online], Available: http://www.fig.net/pub/monthly_articles/June_2005/June_2005_wonnacott.pdf.

366. Xu, X., Luo, J. & Zhang, K. 2011. An Analysis Structure and Variation of the Tropopause over China with GPS Radio Occultation Data. *The Journal of Navigation*, 64:S103−S111, doi: 10.1017/S0373463311000336.

367. Yanxin, T., Lilong, L. & Chaolong, Y. 2013. Empirical Model for Mean Temperature and Assessment of Precipitable Water Vapour Derived from GPS. *Geodesy and Geodynamics*, 4(4):51-56, doi: 10.3724/SP.J.1246.2013.04051.

368. Yao, Y., Zhu, S. & Yue, S. 2012. A Globally Applicable Season Specific Model for Estimating the Weighted Mean Temperature of the Atmosphere. *J.Geod,* 86:1125-1135, doi: 10.1007/s00190-012-0568-1.

369. You, Q.L., Kang, S.C., Pepin, N., Flugel, W.A., Yan, Y.P., Behrawan, H. & Huang, J. 2010. Relationship between Temperature Trend Magnitude, Elevation and Mean Temperature in the Tibetan Plateau from Homogenized Surface Stations and Reanalysis Data. *Global Planet Change,* 71:124-133.

370. Yu, L., Zhang, Z., Zhou, M., Zhong, S., Lenschow, D., Hsu, H., Wu, H. & Sun, B. 2010. Validation of ECMWF and NCEP-NCAR Reanalysis Data in Antarctica. *Adv. Atmos. Sci*., 27(5):1151-1168, doi: 10.1007/s00376-010-9140-1.

371. Yu, X., Zha, T., Pang, Z., Wu, B., Wang, X., Chen, G., Li, C., Cao, J., Jia, G., Li, X. & Wu, H. 2011. Response of Soil Respiration to Soil Temperature in a 50-year-old Oriental Arborvitae Plantation in China. *PLOS ONE*, 6(12):e28397, doi: 10.1371/journal.pone.0028397.

372. Yue, X. & Wang, H.J. 2008. The Springtime North Asia Cyclone Activity Index and the Southern Annular Mode. *Adv. Atmos. Sci*., 25(4):673-679.

373. Zhang, J., Zhang, K., Grenfell, R. & Deakin, R. 2006. Short Note: On the Relativistic Doppler effect for Precise Velocity Determination using GPS. *Journal of Geodesy*, 80(2):104-110.

374. Zhang, K., Fu, E., Silcock, D., Wang, Y. & Kuleshov, Y. 2011. An Investigation of Atmospheric Temperature Profiles in the Australian Region using Collocated GPS Radio Occultation Data and Radiosonde Data. *Atmos. Meas. Tech*, 4:2087−2092, doi:10.5194/amt-4-2087-2011.

375. Zhao, J., Han, Y.B & Li, Z.A. 2004. The Effect of Solar Activity on the Annual Precipitation in the Beijing Area, *Chin. J. Astron. Astrophs*., 4:189-197.

376. Zhao, T. B. & Fu, C.B. 2009. Inter-comparison of the Summertime Subtropical High from the ERA-40 and NCEP-NCAR Reanalysis over East Eurasia and Western North pacific. *Adv Atmos Sci*., 26(1):119-131.

377. Zhao, T.B. & Fu, C.B. 2006. Comparison of Products from ERA-40, NCEP-2, and CRU with Station Data for Summer Precipitation over China. *Adv Atmos Sci*., 23(4):593-604.

378. Zheng, Y. 2006. Generation of Network-Based Differential Corrections for Regional GNSS Service [Online]. Doctoral Dissertation. Queensland University of Technology, Australia. Available at http://www.eprint.qut.edu.au/16359/1/Yi-Zheng_Thesis.pdf.

379. Zhu, Y.L. 2009. The Antarctic Oscillation-East Asian Summer Monsoon Connections in NCEP1 and ERA-40. *Adv. Atmos. Sci.*, 26(4):707-716, doi: 10.1007/s00376-009-8196-2.

380. Zoundi, C., Ouattarra, F., Fleury, R., Amory-Mazaudien, C. & Duchesne, L.P. 2012. Seasonal TEC Variability in West Africa Equatorial Anomaly Region, *Journal of Scientific Research, EuroJournals*, 77(3):309-319, <hal-00968583>.

381. Zus, F., Dick, G., Dousa, J. & Wickert, J. 2015. Systematic Errors of Mapping Functions which are based on the VMF1 Concept. *GPS Solutions*, 19(2):277-286, doi: 10.1007/s10291-014-0386-4.